

**PHOTOACOUSTIC INVESTIGATION OF THE OPTICAL
AND THERMAL PROPERTIES OF SELECTED
AMORPHOUS CHALCOGENIDE SEMICONDUCTORS**

K N. MADHUSOODANAN

**THESIS SUBMITTED
IN PARTIAL FULFILMENT OF THE REQUIREMENTS
FOR THE DEGREE OF
DOCTOR OF PHILOSOPHY**

**DEPARTMENT OF PHYSICS
COCHIN UNIVERSITY OF SCIENCE AND TECHNOLOGY
COCHIN - 682 022
INDIA**

NOVEMBER 1988

CERTIFICATE

Certified that the work presented in this thesis is based on the bona fide work done by K.N.Madhusoodanan, Research Scholar, under my guidance in the Department of Physics, Cochin University of Science and Technology, and has not been included in any other thesis submitted previously for the award of any degree.

Cochin 682 022
November 28, 1988



Dr. Jacob Philip
Supervising Teacher

DECLARATION

Certified that the work presented in this thesis is based on the original work done by me under the guidance of Dr. Jacob Philip, Reader, Department of Physics, Cochin University of Science and Technology, and has not been included in any other thesis submitted previously for the award of any degree.

Cochin 682 022
November 28, 1988



K.N.Madhusoodanan

PREFACE

The study of non-crystalline materials is one of the active areas of research in solid state physics in recent years. One of the main reasons for this is the technological importance of these materials. These materials are also important from the point of view of fundamental physics. The potentials of these materials for technological application is yet to be completely explored for which a thorough understanding of their properties is essential.

Our aim has been to investigate systematically the optical and thermal properties of selected semiconducting chalcogenide glasses using one of the modern analytical tools viz. the photoacoustic technique. We have concentrated our investigations on $A^{IV}B^{VI}$ and A^VB^{VI} type binary chalcogenides where A^{IV} is a group IV element such as Ge or Si, A^V is a group V element such as As and B^{VI} is a chalcogen atom such as Se or Te. The results of the systematic investigations carried out on the optical absorption and thermal transport properties and their composition

and temperature dependences in a few selected $A_x^{IV}B_{1-x}^{VI}$ and $A_x^{V}B_{1-x}^{VI}$ glasses, in the glass forming range, are presented in this thesis.

The thesis is presented in eight chapters. The first chapter is bifurcated into two parts, part-A being devoted to a review of the status of amorphous semiconductor research and part-B to a review of photoacoustic and photoacoustic spectroscopy of condensed matter. Chemical bond approach, band models and states in the gap of amorphous semiconductors are outlined and discussed in part A. The classification and preparation methods of different types of amorphous semiconductors are briefly reviewed. A brief discussion on the structural, electrical, optical and thermal properties of these materials is also included. The principle of the photoacoustic effect, its use as an analytical tool and its various applications are presented in part-B. Necessary theory of the photoacoustic effect, with particular reference to signal generation from condensed matter, is briefly outlined.

Chapter 2 is devoted to the description of instrumentation and the experimental set up used in the work. A brief description of the different modules namely, the

Xenon lamp, monochromator, light beam chopper and lock-in amplifier of the spectrometer set up by us is given. Design considerations and calibration of the room temperature and the high temperature PA cells used in the experiments are discussed in detail in this chapter.

Chapter 3 deals with the optical absorption studies on $A_x^{IV}B_{1-x}^{VI}$ binary glassy systems using photoacoustic technique. Photoacoustic spectra, recorded by plotting the normalized photoacoustic signal as a function of incident wavelength, are reported for Ge_xTe_{1-x} , Si_xTe_{1-x} and Ge_xSe_{1-x} glasses. The features of the PA spectra are discussed in detail. The variation of the optical energy gap, determined from the photoacoustic spectra, with the composition parameter x is presented and discussed for all these systems.

Another system of glass whose optical absorption characteristics has been investigated is the As_xSe_{1-x} system which belongs to the $A_x^{V}B_{1-x}^{VI}$ family of chalcogenide glasses. In chapter 4 the photoacoustic spectra of these samples are presented and the results are discussed. An explanation for the variation of the optical energy gap

with composition is given on the basis of the chemical bonding between atoms in the network.

The details of the thermal diffusivity measurements on $\text{Ge}_x\text{Te}_{1-x}$, $\text{Si}_x\text{Te}_{1-x}$, $\text{Ge}_x\text{Se}_{1-x}$, $\text{As}_x\text{Se}_{1-x}$ and $\text{As}_x\text{Te}_{1-x}$ glasses are presented in chapter 5. The necessary theory for thermal diffusivity measurements also has been outlined. Thermal diffusivity has been determined by studying the variation of the photoacoustic signal amplitude and phase with chopping frequency using samples of appropriate thickness. The variation of thermal diffusivity with composition is presented for all the five groups of samples. The results give evidence for the existence of critical composition at which the average coordination number $m = 2.4$ in all these systems.

In chapter 6 a theoretical explanation for the existence of the critical composition in chalcogenide glasses, as evidenced by the results on thermal diffusivity measurements presented in chapter 5 is given on the basis of constraints theory and the idea of rigidity percolation in random networks.

The results of the optical absorption and thermal conduction studies on $\text{As}_x\text{Se}_{1-x}$ and $\text{Ge}_x\text{Se}_{1-x}$ glasses at high temperatures are presented in chapter 7. It is demonstrated that it is possible to determine the transition temperature by measuring the variation of the photoacoustic signal amplitude and phase with temperature. The variation of glass transition temperature with composition for both the systems are discussed. Details of the determination of the temperature dependence of optical absorption, optical energy gap and thermal diffusivity are presented in this chapter. The features of the temperature dependent variation of these properties are discussed in detail.

Chapter 8 incorporates the summary and conclusions of the work presented in earlier chapters.

Most of the results presented in this thesis have been published/accepted for publication/communicated in the form of the following papers:

1. Optical absorption and thermal diffusivity in $\text{Ge}_x\text{Te}_{100-x}$ glasses by the photoacoustic technique.
Philos.Mag.B 58 123 (1988).

2. Photoacoustic investigation of the optical absorption and thermal diffusivity in $\text{Si}_x\text{Te}_{100-x}$ glasses.
J.Non-Cryst.Solids (in press).
3. Optical energy gap and thermal diffusivity of Ge-Se semiconducting glasses.
Phys.Stat.Solidi (a) (~~in press~~). 108 775 (1988)
4. Percolation threshold of thermal conduction in $\text{A}_x^{\text{IV}}\text{B}_{1-x}^{\text{VI}}$ chalcogenide semiconducting glasses.
Phys.Rev.B 38 4127 (1988).
5. An evidence for threshold percolation of rigidity in $\text{A}_x^{\text{IV}}\text{B}_{1-x}^{\text{VI}}$ glassy networks.
Indian J.Phys. (in press).
6. Thermal diffusivity of $\text{As}_x\text{Te}_{1-x}$ glasses measured using photoacoustic technique.
J.Mater.Sci.Lett. (in press).
7. Composition dependence of the energy gap and thermal diffusivity in bulk As-Se glasses.
J.Mater.Sci. (communicated).

8. Thermal transport near glass transition in bulk As-Se glasses.

Phys.Rev.B (in press).

9. Thermal diffusion near glass transition in Ge-Se glasses measured by photoacoustics.

Pramana (communicated).

In addition, the following papers also have been published during the course of this work:

1. Photoacoustic measurements of the thermal conductivity of some bulk polymer samples.

J.Appl.Phys. 62 1162 (1987).

2. A sensitive electret microphone for the detection of photoacoustic signals.

J.Acoust.Soc.India 14 125 (1986).

ACKNOWLEDGEMENTS

The investigations presented in this thesis have been carried out under the able and inspiring guidance of Dr. Jacob Philip, Reader, Department of Physics, Cochin University of Science and Technology. I express my deep sense of gratitude to him for his invaluable guidance.

I am thankful to Prof. K. Babu Joseph, Head of the Department of Physics, Cochin University of Science and Technology, and Prof. M. G. Krishna Pillai, former Head of the Department, for providing necessary facilities to carry out this work.

I am extremely thankful to Prof. E. S. R. Gopal, Dr. S. Asokan and Dr. G. Parthasarathy, Department of Physics, Indian Institute of Science, Bangalore for their help and interest in the work.

I would like to thank my colleagues Mr. Johny Isaac, Mr. L. Godfrey, Mr. K. Nandakumar and Mr. R. Sreekumar for their help and cooperation.

I thank the staff of the University Science Instrumentation Centre, Cochin University of Science and Technology for their assistance in fabrication works.

I gratefully acknowledge the financial support provided by DAE (Govt. of India), UGC (Govt. of India) and CSIR (Govt. of India) in the form of research fellowships.

I would like to thank Mr. Sasi for neatly typing the manuscript.

K. N. MADHUSOODANAN.

CONTENTS

	<u>Page</u>
PREFACE	.. i
ACKNOWLEDGEMENTS	.. viii
Chapter 1 INTRODUCTION	
PART-A AMORPHOUS SEMICONDUCTOR RESEARCH-- AN INTRODUCTION	
1.1 Opening Remarks	.. 1
1.2 Chemical Approach	.. 4
1.3 Energy Band Models	.. 7
1.4 Classification of Amorphous Semiconductors	11
1.5 Preparation of Amorphous Semiconductors	.. 13
1.6 Defects and States in the Gap	.. 17
1.7 Structural, Electrical, Optical and Thermal Properties	.. 23
 PART-B PHOTOACOUSTIC SPECTROSCOPY OF SOLIDS	
1.8 Introduction	.. 37
1.9 The Photoacoustic Effect	.. 39
1.10 Theory of Photoacoustic Effect in Solids	.. 41
1.11 Applications of the Photoacoustic Effect	.. 54
Chapter 2 THE EXPERIMENTAL SET UP	
2.1 A Photoacoustic Spectrometer: General Considerations	.. 62
2.2 Details of Our Photoacoustic Spectrometer	.. 72
2.3 Design, Fabrication and Calibration of Photoacoustic Cells	.. 76

Chapter 3	COMPOSITION DEPENDENCE OF THE OPTICAL ENERGY GAP IN $A^{IV}B^{VI}$ GLASSES		
3.1	Introduction	..	90
3.2	Experimental Details	..	92
3.3	Photoacoustic Spectra of $A_x^{IV}B_{1-x}^{VI}$ Glasses	..	94
3.4	Optical Energy Gap of $A^{IV}B^{VI}$ Systems	..	105
Chapter 4	COMPOSITION DEPENDENCE OF ENERGY GAP IN As-Se GLASSES		
4.1	Introduction	..	123
4.2	Photoacoustic Spectra of As_xSe_{1-x} Glasses	..	125
4.3	Variation of E_o with Composition	..	129
Chapter 5	COMPOSITION DEPENDENCE OF THERMAL DIFFUSIVITY IN $A_x^{IV}B_{1-x}^{VI}$ AND $A_x^VB_{1-x}^{VI}$ SYSTEMS		
5.1	Introduction	..	138
5.2	Outline of the Theory	..	142
5.3	Experimental Procedure	..	147
5.4	Variation of Thermal Diffusivity with Composition	..	162
Chapter 6	RIGIDITY PERCOLATION AND THRESHOLD THERMAL CONDUCTION IN BINARY CHALCOGENIDE RANDOM NETWORKS		
6.1	Introduction	..	171
6.2	Topological Description of the Glass Network	..	175
6.3	Threshold Behaviour and Constraints in the Glass Network	..	178

Chapter 7	GLASS TRANSITION AND TEMPERATURE DEPENDENCE OF THERMAL DIFFUSIVITY AND ENERGY GAP IN SELECTED $A_x^{IV}B_{1-x}^{VI}$ AND $A_x^V B_{1-x}^{VI}$ GLASSES INVESTIGATED USING PHOTOACOUSTIC TECHNIQUE		
7.1	Introduction	..	187
7.2	Determination of Glass Transition Temperature	..	190
7.3	Variation of Thermal Diffusivity with Temperature	..	202
7.4	Variation of Optical Energy Gap with Temperature	..	214
Chapter 8	SUMMARY AND CONCLUSIONS	..	221
REFERENCES	228

Chapter 1

INTRODUCTION

PART-A

AMORPHOUS SEMICONDUCTOR RESEARCH - AN INTRODUCTION

1.1 OPENING REMARKS

Even though glasses have a long history of over ten thousand years very little had been known about the physics of amorphous materials until recently. During the last 3-4 decades interest in both fundamental and applied aspects of amorphous materials has grown rapidly because of several new applications of these materials like electrophotographic copying, memory and switching elements, energy conversion devices such as solar cells etc. Research in the fascinating area of amorphous semiconductors started gaining momentum in 1950's with the discovery by Kolomiets that chalcogenide glasses behave like intrinsic semiconductors and that their electrical conductivity cannot be increased by adding dopants [1]. Spear's report [2] on the drift mobility measurements in amorphous selenium in 1957 and Tauc's studies [3] on amorphous germanium in 1960's were important developments in

this area. Ovshinsky's paper [4] on the switching and memory effects in chalcogenide glasses was a turning point which attracted several scientists to the field of amorphous materials. The important discoveries made on the optical memory effects, imaging, photodoping, reversible photostructural changes etc. suggested possibilities for new applications for non-crystalline semiconductors. Also the developments in the field of amorphous silicon which started in 1960's [5,6] promised its applications as cheap, efficient and large area photovoltaic and photothermal devices. The discovery by Spear and Lecomber [7], that the electronic properties of a-Si and a-Ge could be controlled by substitutional doping was another milestone. This led to the fabrication of thin film a-Si p-n junctions, thin film transistors and photovoltaic devices [8-10]. All these developments resulted in making the field of amorphous semiconductors a frontier area of research.

Remarkable progress in our understanding of the physics of crystalline solids has been made during the past 50 to 60 years. This was achieved mostly by the application of the principles of quantum mechanics to explain microscopic phenomena in solids and subsequently by the development of band theory which turned out to be very

successful in explaining most of the properties of crystalline materials. This was possible because of the mathematical simplification resulting from the periodicity of the lattice [11,12]. On the other hand proper theoretical understanding of disordered systems was largely undeveloped mainly because of the mathematical complexity in dealing with non-periodic systems. An important theoretical study on this subject was presented by Anderson [13]. In interpreting the transport properties of amorphous semiconductors the concept of Anderson localization has often played a key role. According to him if we think of the center of the band of states produced by a simple Hamiltonian, disorder in the network can localize the eigen states. Above a critical strength of disorder all states are localized. The goal of several of the theoretical formulations developed later was directed towards locating the critical strength of disorder for Anderson transition. Several analytical and numerical work have been reported in this context [14-20]. Scaling theories and the ideas of localization and percolation has been exploited by several authors to solve problems associated with disordered systems [21-23]. Pioneering work done by Mott on the various theoretical aspects of the problem [24] made significant contributions to our understanding of the amorphous state.

1.2 CHEMICAL APPROACH

Solid state theory developed on the basis of crystal symmetry and long-range order led us to think that periodicity is vital to understand the electronic properties of materials. But the existence of several materials in the amorphous form with same order of electrical and optical characteristics as crystalline materials projects the importance of short-range order and the chemistry of the constituent atoms [25]. The chemical approach makes use of tight binding approximations [26] and it emphasises the importance of short-range order. It has been very successful in explaining the semiconducting property of amorphous materials and in characterising various kinds of disorder describing the structural properties.

Earlier it was believed that energy gap is a consequence of the long-range periodicity in crystals. After the experimental observation of semiconducting property in amorphous materials the existence of bands and band gaps were established in materials having only short-range order on the basis of chemical bond formation. Combinations of atoms form stable molecules provided the energy of molecular combination is lower than that of the combined atoms. In molecules held together by covalent bonds the

outer electrons of two adjacent atoms become spread out over both of them. Whenever any two atoms are close enough for their outer electrons to interact, the energies of their states get shifted by the interaction. This gives rise to bonding states with reduced energy and an equal number of antibonding states with increased energy. States that are unshifted in energy are called nonbonding states. Since the separation in energy between s and p states is usually of the same order of magnitude as the bonding energy it is possible to promote one of the paired s electrons to a p state and then to form two covalent bonds. This can be done very conveniently in group IV elements in which the configuration sp^3 gives maximum possible number of s-p bonds, namely four. In group V elements it is no longer energetically favourable to promote one of the s electrons, because there are already three unpaired p electrons without the promotion and therefore no additional bonds can form. The s electrons remain paired and only three p bonds are possible. The group VI elements ordinarily have a p lone pair in addition to the s lone pair, so that the lowest energy configuration involves only two p bonds. When a solid is formed these bonding, antibonding and non-bonding states form bands with a separation in energy. This is illustrated in Fig.1.1 for silicon and selenium.

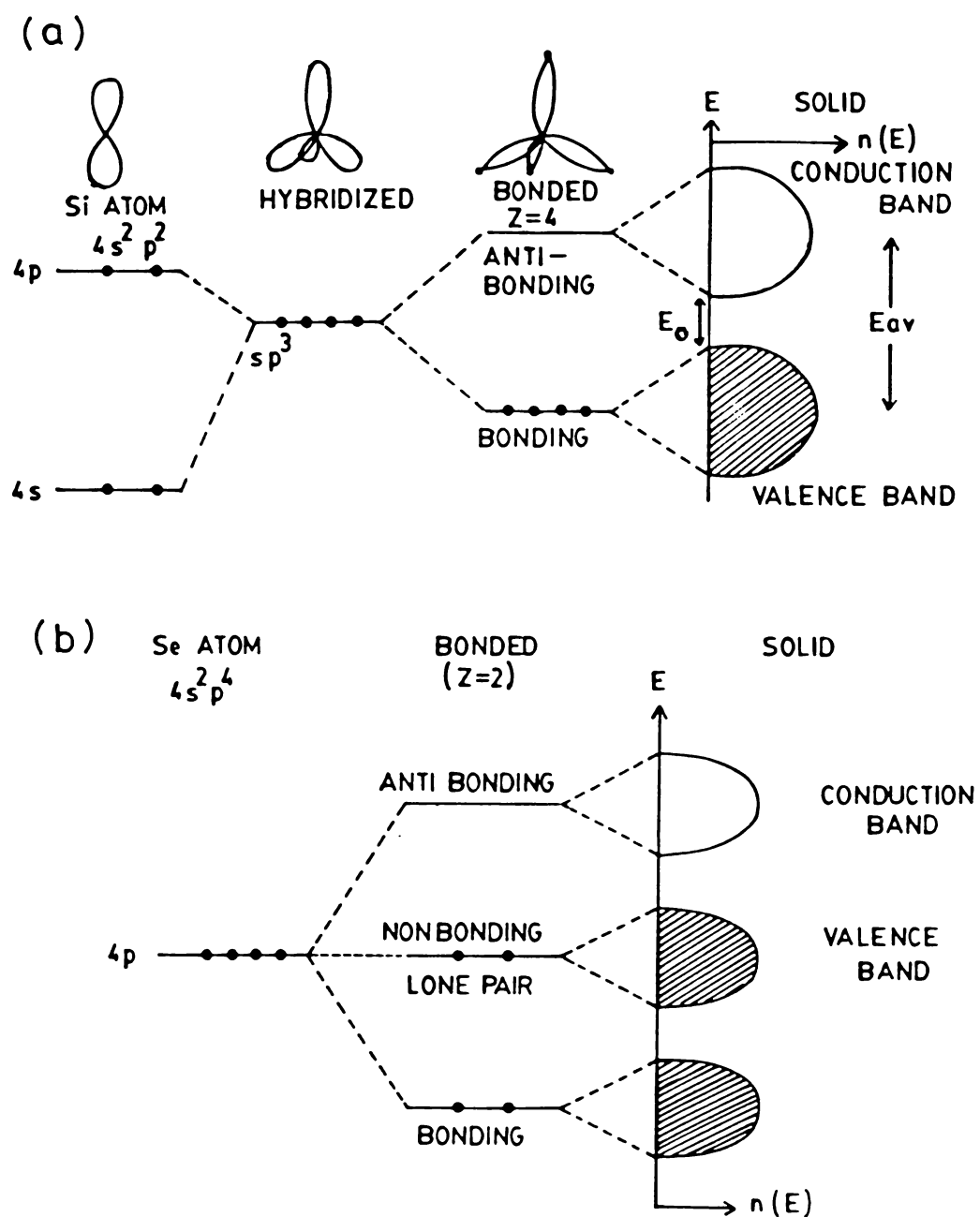


Fig.1.1 Bonding schematic for the electronic structure of (a) silicon and (b) selenium.

In Si the conduction band originates from antibonding levels and valence band from bonding levels with a band gap E_0 between them. In Se, in addition to the bonding and antibonding bands, nonbonding band which originates from lone pair p electrons is also present. This nonbonding band constitutes the valence band while the conduction band is constituted by antibonding band.

1.3 ENERGY BAND MODELS

Making use of the long-range periodicity, band theory of solids effectively explains the main features of crystalline semiconductors such as the existence of conduction band and valence band with sharp edges in density of states and well defined forbidden gap. The concept of the density of states can also be applied to amorphous solids where the long-range order is destroyed. The first step in generalizing the theory of crystalline semiconductors to amorphous ones was taken by Mott [24,27]. Based on Anderson theory, Mott argued that the spatial fluctuations in the potential caused by the configurational disorder in amorphous materials may lead to the formation of localized states which do not occupy all the different energies in the band, but form a tail above and below the normal band. These states are called localized

in the sense that an electron placed in a region will not diffuse at zero temperature to other regions with corresponding potential fluctuations. Mott further suggested that there is a particular density of electronic states above which the states in amorphous solid become extended. This leads to the existence of critical energies in each band where there is a sharp jump in mobility, from negligible values to finite ones, takes place. These critical energies are called the mobility edges and play the same role in amorphous solids that band edges play in crystalline solids. The energy difference between mobility edges of the valence band and those of the conduction band is the mobility gap.

Cohen-Fritzsche-Ovshinsky (CFO) model [28] for band structure in amorphous semiconductors was an extension of Mott's model and is based on four principles. (1) Amorphous materials have band tails whose exact nature depends on the extent of the deviations from perfect periodicity. (2) There are sharp mobility edges separating localized and extended states in each band. (3) The localized band tails overlap in the mobility gap resulting in a finite density of states at the Fermi level. (4) Since amorphous solids do not have the rigid constraints of a crystalline structure, each atom ordinarily can be expected

to fulfill its proper valence requirements locally; thus eliminating any sharp structure in the density of localized states in the gap. The CFO model was specifically proposed for multicomponent chalcogenide glasses used in switching devices. A consequence of band overlapping is that there are states in the valence band, ordinarily filled, that have higher energies than states in the conduction band that are ordinarily unfilled. A redistribution of the electrons takes place, forming filled states in the conduction band tail which are negatively charged and empty states in valence band which are positively charged. This model therefore ensures self compensation, and pins the Fermi level close to the middle of the gap; a feature required to explain the electrical properties of these materials. The high transparency of the amorphous chalcogenides below a well defined absorption edge suggests that the extent of tailing in chalcogenides may not be as large as described by CFO model.

The model due to Davis and Mott [29] proposes rather narrow tails of localized states which extend a few tenths of an eV into the forbidden gap. Furthermore they proposed the existence of a band of compensated levels near the middle of the gap, originating from defects in the random network such as dangling bonds, vacancies etc.

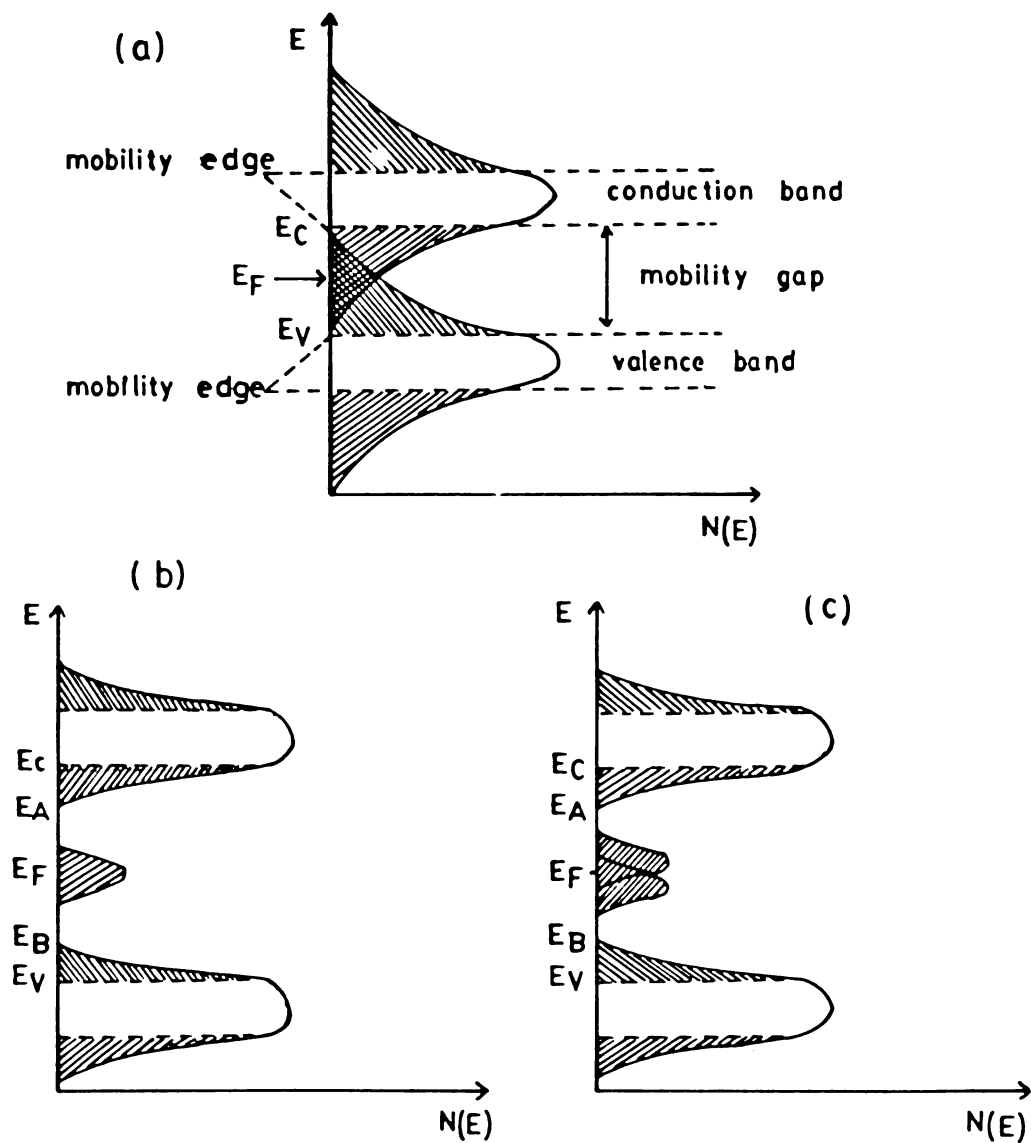


Fig.1.2 Schematic density of states diagrams for amorphous semiconductors. (a) CFO model, (b) Davis-Mott model, (c) modified Davis-Mott model.

The interval between the energies E_c and E_v , which separates the ranges where the states are localized and extended, acts as a pseudogap and is defined as the mobility gap. The center of the band may be split into donor and acceptor band, which will also pin the Fermi level. Recent experimental evidences from luminescence, photoconductivity and drift mobility measurements establish the existence of localized gap states located at well defined energy levels in the gap.

Schematic diagrams of the density of electronic states in amorphous semiconductors based on CFO model, Davis-Mott model and modified Davis-Mott model are shown in Fig.1.2.

1.4 CLASSIFICATION OF AMORPHOUS SEMICONDUCTORS

Amorphous semiconductors can be divided into two subfields as tetrahedrally coordinated silicon like materials and chalcogenide glasses. The distinction between these two classes can be well accounted for on the basis of chemical considerations. The four-fold coordination in Si leads to symmetrical bonding and the formation of rigid structures. In this case a continuous random network with tetrahedral bonds can be constructed with negligible density deficit and very little possibility for local

reorganisation of atoms. On the other hand two fold coordination in Se is very asymmetrical and the structure gives rise to greater degree of flexibility. A major distinction comes from the fact that in Se, but not in Si, the uppermost valence band is formed from nonbonding lone pair p electrons. It is very important when we consider the defect chemistry and various properties that differentiate it from Si like materials.

Some of the distinctive properties from which we can determine to which class a material belongs are presence of paramagnetic centers, photoinduced ESR, luminescence, variable range hopping conduction etc. The Si-type materials have large density of dangling bonds. The density of paramagnetic centers is normally found to be between 10^{19} and 10^{20} cm^{-3} . Contrary to this the density of paramagnetic centers is negligible in Se and chalcogenide glasses. However in these materials it is possible to create paramagnetic centers by illuminating with radiation of energy close to that of the band gap, while no such photoinduced effect is found in Si-type materials. Following excitation with radiation in the wavelength range identical to that giving rise to photoinduced ESR, luminescence occurs in Se type materials with a large stokes

shift which suggest strong electron-phonon coupling. Si-type materials do not show such effects with the exception of a-Si:H. At low temperatures Si-type materials show variable range hopping conduction with a $T^{-\frac{1}{4}}$ dependence amongst localized states at the Fermi level. But in the case of Se and chalcogenides the conductivity is temperature activated in an Arrhenius manner with an energy close to one half the optical band gap. Apart from the extreme classes of Si-type and Se-type materials we can think of an intermediate class consisting of arsenic and III-V semiconductors having properties characteristic of two extremes.

1.5 PREPARATION OF AMORPHOUS SEMICONDUCTORS

Amorphous solids are usually prepared by two different methods viz. vapour condensation technique and melt quenching technique. Vapour condensation technique gives rise to thin films while bulk glasses, having a well defined glass transition temperature, are prepared by melt quenching technique.

Out of the two classes of materials described, Se and chalcogenides can be prepared in the form of bulk glasses by melt quenching technique. They can also be prepared in the thin film form; but a direct comparison of the properties of thin films and bulk glasses may not

be possible. Stable glasses (eg. As_2Se_3) may undergo a second order phase transition at the glass transition temperature T_g which marks the onset of softening of the network and is accompanied by an increase in heat capacity and thermal expansion coefficient. Less stable glasses may on heating undergo phase separation and crystallization. In order to prepare such glasses rather fast quenching rate is needed to avoid crystallization as in the case of As_2Te_3 . Therefore quenching rate is an important parameter in the preparation of glasses by supercooling the liquid [30].

The Si-type materials cannot often be prepared in the glassy form by melt quenching. These materials are usually prepared in the thin film form by deposition on a substrate [31]. Several techniques such as vacuum evaporation, sputtering, electrolytic deposition, glow discharge deposition, chemical vapour deposition etc. are employed for preparing the material in the thin film form.

The reason why some of the materials can only be prepared in the thin film form whereas others can be prepared in the form of bulk glasses as well can be explained by considering the nature of chemical bonds. This

difference has its origin in the mismatch between constraints and the number of degrees of freedom in three dimensions and in the flexibility required to accommodate the mismatch. The flexibility of covalent bond angles is largest for the two-fold coordinated Se-type materials and least for the tetrahedrally coordinated Si-type materials. The reason for this is the greater variety of admixture from other atomic orbitals to the covalent bond when the coordination number is less than the number of valence electrons. In SiO_2 glasses the oxygen atoms bridging the Si tetrahedra provide the essential flexibility which is needed to form a random covalent network without much strain. Covalent random network of a-Si without the flexing bridges of group VI elements is highly overconstrained and no longer forms glass. Therefore based on chemical considerations and average coordination number m a classification of non-crystalline solids can be made as shown in Fig.1.3. According to this, glasses are restricted to $3 > m \geq 2$. Materials with higher connectivity viz., $4 \geq m \geq 3$ are overconstrained amorphous while those with $m < 2$ are under crosslinked amorphous. The average coordination $m = 4$ separates non-crystalline metals from semiconductors or insulators.

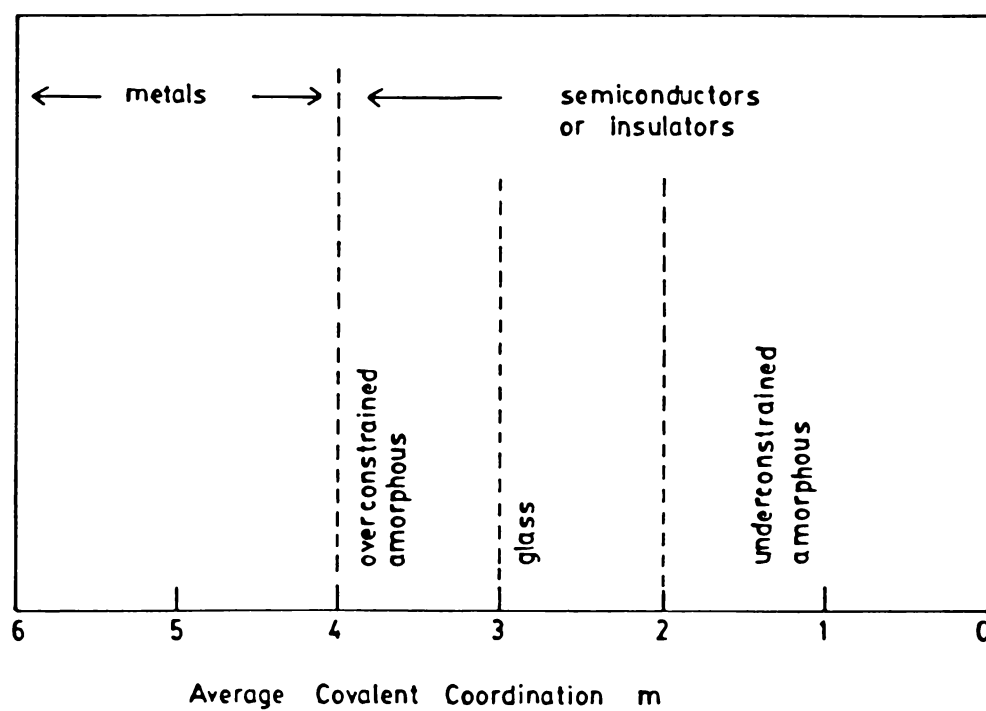


Fig.1.3 Classification scheme for non-crystalline solids based on average coordination number.

1.6 DEFECTS AND STATES IN THE GAP

In amorphous semiconductors the potential fluctuations due to disorder associated with the bond length, bond angle, dihedral angle etc. result in the tailing of the valence band and conduction band. Also, the experimental results obtained from structural, electrical and optical properties give evidence for the existence of density of states in the mobility gap. These states are associated with various kinds of defects which are different in nature for tetrahedrally coordinated semiconductors and chalcogenides.

Early models for gap states were developed to explain the experimentally observed features such as the insensitivity to doping, pinning of the Fermi level near midgap, general similarity of the overall distribution of the density of states in the valence band and conduction band to that of the crystalline phase etc. The CFO model and Davis-Mott model met with success to a large extent in explaining the gap states as evidenced by the experimental results obtained from drift mobility, field effect, photoconductivity, luminescence etc. Another model due to Phillips [32] suggests that the structure of an

amorphous material might relax energetically so as to cause the expulsion of states from the gap. According to him the bonding states associated with long or short bonds or with defects lower their energy towards the valence band while antibonding states of these configurations are pushed up into the conduction band. Anderson put forward a model [33] in which gap is essentially free of one-electron states, but a pseudogap containing a continuum of two-electron states exists. Here the strong coupling between electrons and phonons leads to a negative term in the energy which compensates for the Colom b repulsive force between electrons at the same site.

Amorphous Si and related alloys possess large defect concentrations. Strains introduced during deposition give rise to structural features such as cracks and microvoids as well as local imperfections like distorted bonds and defect centres. Apart from bond angle and bond length deviations, coordination variations can also be present. Such defects include three-fold coordinated Si atom called dangling bond and two fold coordinated Si atom [34]. By introducing hydrogen into a-Si film, it is possible to reduce the density of dangling bond states.

Since amorphous chalcogens and chalcogenide alloys are not ordinarily overconstrained we can expect that these materials are devoid of considerable amount of strain related defects. But many experimental evidences related to optical and electrical properties suggest the existence of well defined defects in chalcogenides [35]. Elaborate studies have been done by Street and his coworkers [36,37] on the nature of defects in chalcogenides. They made use of Anderson's concept of effective negative correlation energy U_{eff} [33] to sepcific defects to explain the defect structure of chalcogenides. These authors considered two dangling bonds at the ends of the Se chain. When they each contain a single electron, the defects are neutral and can be designated as D° . The reaction $2D^{\circ} \rightarrow D^{+} + D^{-}$, representing the creation of two charged defects D^{+} and D^{-} by the transfer of an electron from one chain end to the other, is exothermic with necessary lowering in energy arising from local lattice distortions. The positive correlation energy associated with the two electrons at D^{-} in the absence of configurational changes become negative U_{eff} after lattice relaxation [38]. The coordination of Se atoms at D^{+} is three, and at D^{-} it is one whereas at a normally bonded Se atom it is two.

A chemical bond description of the defects in chalcogens has been given by Kastner et al [39,40]. They designated the charged states of the defect as C_1^- and C_3^+ where C stands for chalcogenide and the subscript indicate the atomic coordination. The neutral center is labelled C_3^0 because an extra electron placed on C_3^+ is shared equally between the three bonds of the atom which therefore remains three-fold coordinated and the normal bonding configuration is represented by C_2^0 . Other possible defect states are C_3^- and C_1^0 . The structures and energies of these bonding configurations has been given by Kastner et al [39,40]. In their notation the reaction which creates triply coordinated and singly coordinated charged defects can be represented as $2C_3^0 \rightarrow C_3^+ + C_1^-$. These charged defects C_3^+ and C_1^- are also called valence alternation pair (VAP) and their creation starting from a fully bonded network in which all atoms are in the C_2^0 configuration can be described by $2C_2^0 \rightarrow C_3^+ + C_1^-$. The energy to create VAP may be reduced, if they form close to each other because of Coulomb energy of attraction. Such bond pairs are called intimate valence alternation pairs (IVAP). The formation of VAP for a-Se and a-As₂Se₃ are shown in Fig.1.4. The lowest energy defect in a-As₂Se₃ or a-As₂Te₃ is a $C_3^+ - P_2^-$ pair where P stands for pnictogen and this defect is a valence alternation pair. The reason for the low creation energy of VAP's

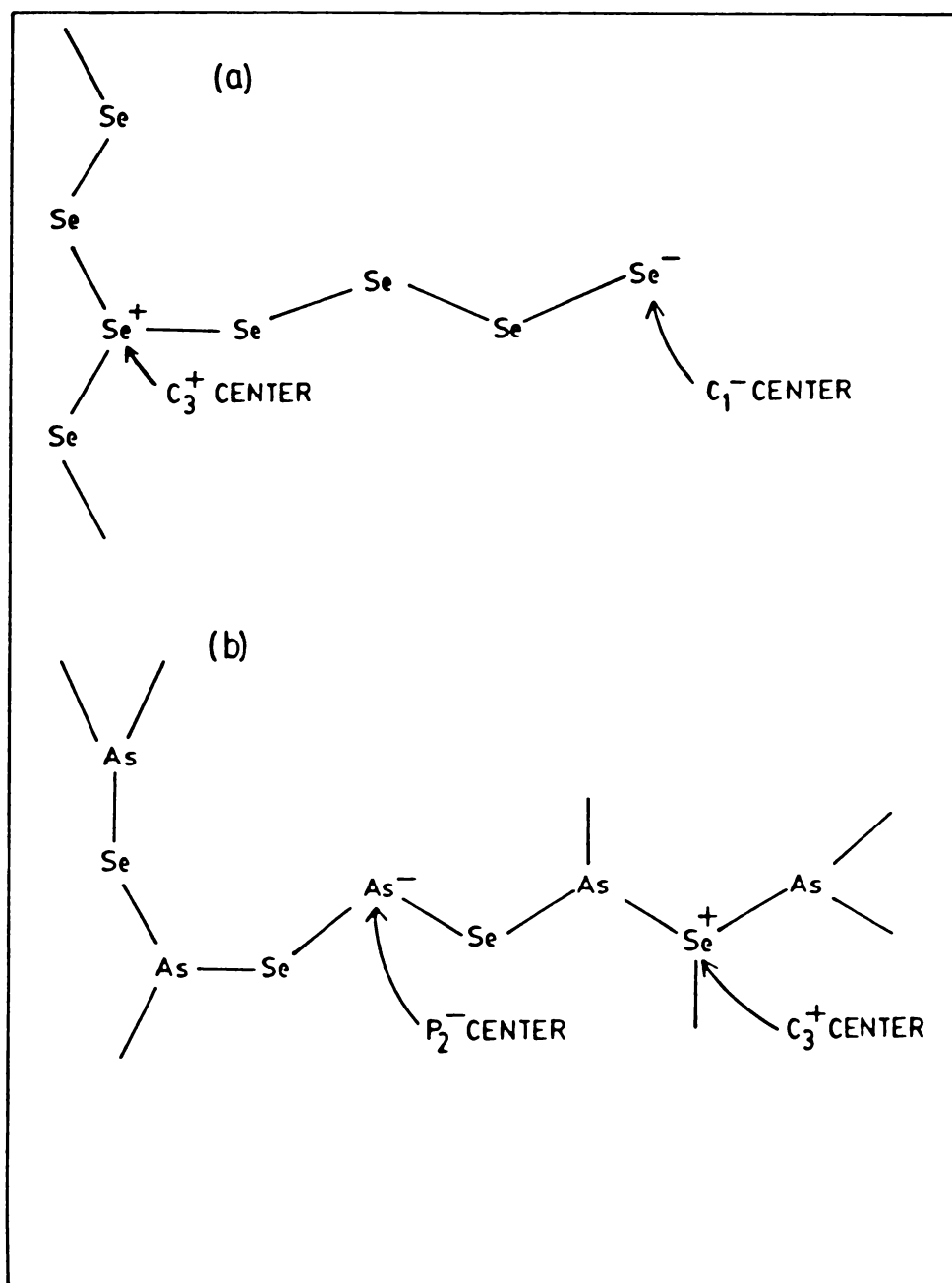


Fig.1.4 Examples of valence alternation pairs.
 (a) $a\text{-Se}$, (b) $a\text{-As}_2\text{Se}_3$.

is that the total number of bonds is the same as when both atoms are in their ground state configurations. The VAP's are spinless defects since both centers are optimally coordinated for their particular electronic configurations.

Several experimental techniques have been developed in the past to study the tail states and gap states. These include the conventional optical absorption and electrical conduction measurements. Optical absorption methods bring out the gross features of the density of states because it always yield the product of the initial and the final state density of states. Different experimental techniques are required to measure absorption coefficient which span a very wide range. Recent advances include the use of photoconductivity [41] to measure absorption coefficient in the band tail region and the development of the technique of photothermal deflection spectroscopy [42] to determine absorption coefficient even in regions of localized-to-localized excitations. A completely different technique for determining density of states in the band tail region is the transient spectroscopy [43]. Here excess carriers are excited by a pulse of light and the responses such as photoconductivity, optical absorption, luminescence etc. are measured as a function of time. More detailed information about the distribution in energy of

defect states deep in the gap is obtained from a variety of techniques such as field effect measurements [44], deep level transient spectroscopy [45], tunneling spectroscopy [46], isothermal capacitance transient spectroscopy [47], capacitance-voltage measurements [48], transient voltage spectroscopy [49], space-charge limited-current experiments [50], thermally stimulated current measurements [51] etc.

1.7 STRUCTURAL, ELECTRICAL, OPTICAL AND THERMAL PROPERTIES

1.7a Structural properties

The structure of amorphous semiconductors is developed by the repetition of one or more basic molecular units in a way that cannot be identified topologically with any known crystalline structure or with any infinite periodic array. But the atomic order within a molecular unit might be similar within small bond angle distortions in both crystalline and amorphous phases. This reveals the importance of short range order in describing structural behaviour of a non-periodic network. There have been many discussions on the types of structural models that can be used to describe amorphous solids [52]. The main point in describing the structure is the specification of the short range order and the topological rules which determine it. Given the short range order, with three parameters viz., the number of bonds Z , the bond length a and the

bond angle θ having well-determined values in a narrow range, it is possible to construct a model for the structure which does not have any long range crystalline periodicity. Such models are called random networks. Zachariasen [53] was the first to model an amorphous solid by a random network of atoms with near-perfect short range order, with particular reference to oxide glasses. Mott [54] utilized this type of structural models based on continuous random networks to explain dark d.c. conductivity in chalcogenide glasses.

The random network model that applies to tetrahedrally bonded amorphous semiconductors have been constructed by Polk [55]. Models for a network of three-fold coordinated atoms have been constructed by Greaves and Davis [56] and for a network of two-fold coordinated atoms by Long et al [57]. Locally the network topology is three dimensional for a random network of four-fold coordinated atoms while for three-fold and two-fold coordinations the local topologies are respectively two and one dimensional. It should be mentioned that discrete molecular species, arising out of the lower coordination which allows deviation from a completely interconnected network have been identified in amorphous Se as Se_8 ring molecules, in amorphous As as As_4 pyramidal molecules and in S rich As-S and Ge-S glasses as S_8 ring molecules. Some of the experimental

results suggests that the structure of the stoichiometric melt quenched network glasses is not all that random. The presence of a very sharp first peak in the diffraction spectra observed in GeSe_2 and As_2Se_3 type glasses suggests medium range order of the scale $15\text{-}30\text{\AA}$ [58]. On the basis of the results from Raman [59] and Mössbauer [60] experiments, new structural models based on the formation of molecular clusters have been proposed for these systems [61,62].

The experimental methods used to determine the structure fall under four major categories namely diffraction method [63], vibrational spectroscopy [64], photoemission spectroscopy [65] and hyperfine interactions [66,67]. The diffraction technique mainly depends on X-ray diffraction experiments. In the radial distribution function, obtained by a Fourier inversion of the angular dependence of scattered radiation, amorphous semiconductors give evidence for short range order. Extended X-ray absorption fine structure (EXAFS) is an important technique for structural studies which can determine the local atomic arrangement about each type of atoms separately [68]. Vibrational spectra, obtained by infrared absorption or reflection and Raman scattering, are very useful for structural studies. Information about the ring statistics of

network can be obtained from X-ray and UV photoemission techniques. The local bonding chemistry which is very important in the structural investigations, can be studied by hyperfine interaction methods. These include nuclear quadrupole resonance, nuclear magnetic resonance, Mössbauer effect etc. Structural changes in an amorphous solid as a function of temperature can be detected by differential thermal analysis [69].

7.1b Electrical properties

The presence of localized states at the band edges and in the energy gap play an important role in determining the electrical transport properties of amorphous semiconductors. The vanishing of conductivity as temperature $T \rightarrow 0$ for states with density of states $n(E)$ at energy E serves as a definition for localized states. All eigen functions of the one electron Schrodinger equation decays exponentially in space outside regions in which the eigenfunctions are localized. The disorder can be introduced by the addition of a random potential energy, which is a measure of disorder, to the potential wells corresponding to crystalline lattice. This results in the random variations in the sign of the electron wave function γ from well to well. When the strength of the

disorder is very large the wavefunction for each isolated well would fall off exponentially with distance. Anderson [13] found that localization of states is brought in with no diffusion of electrons at absolute zero temperature if strength of disorder is greater than a critical value that depends upon the coordination number.

Pioneering work on Anderson localization and on the transport properties of amorphous semiconductors have been done by Mott [54,27,70]. According to him conductivity can have finite value for values of energy E in the middle of the band, but may be zero towards its extremities if the density of states drops there. Here a critical energy E_c separates the two regions as illustrated in Fig.1.5 for a density of states resulting from the Anderson potential, where energies E_c and E_c' separate localized and non-localized states. For values of E slightly less than E_c the wavefunction on any well will have random signs and amplitudes but its envelope fall off exponentially as $E \rightarrow E_c$. The states with energy less than E_c are thus localized. If states are localized an electron can move only by hopping from one state to another, exchanging energy with a phonon in the process. For values of E slightly greater than E_c the wavefunctions on each well is random but the wavefunctions extend through the

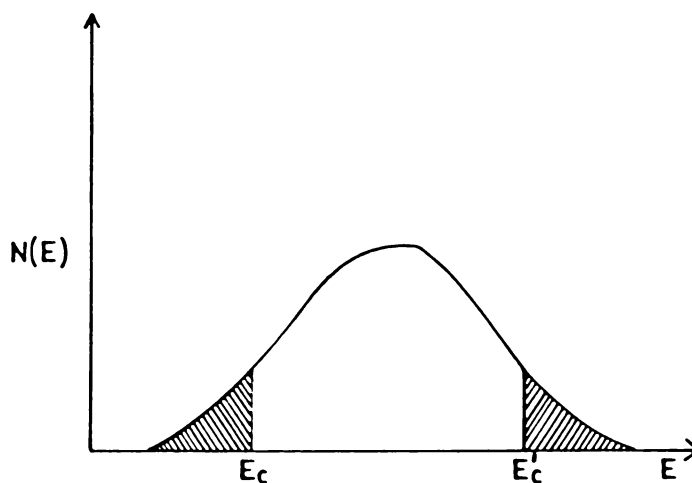


Fig.1.5 Density of states in the Anderson model, when states are non-localized in the center of the band. Localized states are shown shaded.

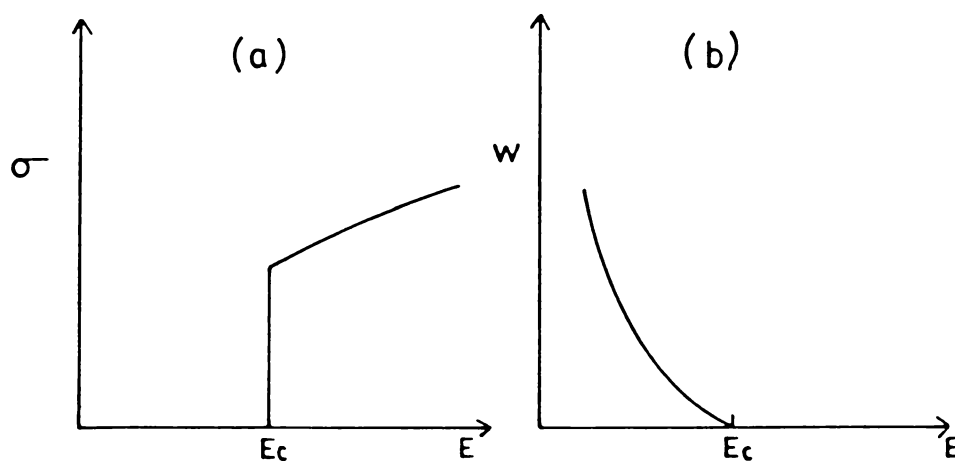


Fig.1.6 (a) The conductivity as a function of E when $T = 0$ in Anderson model.
 (b) The hopping activation energy as a function of E .

lattice. Therefore there will be a discontinuous change in d.c. conductivity at E_c when $T \rightarrow 0$ and the activation energy for hopping $W \rightarrow 0$ as shown in Fig.1.6. The minimum metallic conductivity when E just exceeds E_c is given by $\sigma_0 = 0.06 \frac{e^2}{\hbar a}$ where a is the atomic separation. The energy E_c of this kind exists in the conduction band of amorphous semiconductors and corresponding energy E_v for the valence band, as has been explained by the band models [28,29].

One of the interesting properties of amorphous semiconductors is the variable range hopping conduction occurring at sufficiently low temperature where the logarithm of conductivity varies as $T^{-\frac{1}{2}}$. This is a consequence of hopping conduction which involves more distant centers. When current is carried by charge carriers excited into the conduction band and valence band, the localized and non-localized states in the bands contribute to the conductivity. The conductivity due to carriers excited into the extended states of the conduction band can be written as

$$\sigma = \sigma_0 \exp\left[-(E_c - E_F)/kT\right] \quad (1.1)$$

where σ_0 is minimum metallic conductivity. For $E \leq E_c$ conduction will be by phonon assisted hopping. The mobility

decreases by a factor $\sim 10^3$ as the energy E goes through the value E_c for conduction band or E_v for valence band. This drop in mobility is called the mobility shoulder [24]. Hopping conduction also occurs as a result of carriers hopping between localized states near the Fermi energy.

A.C. conductivity also shows difference in behaviour depending on whether the conductivity is by carriers in the extended states or by hopping in localized states. When carriers are excited across the mobility edges into the extended states, the conductivity does not depend on frequency in the electrical range of frequencies. The a.c. conductivity due to carriers excited into localized states [71] at the band edge of valence band or conduction band and that near the Fermi level are by phonon assisted hopping and it varies approximately as $\omega^{0.8}$. The Hall coefficient and thermopower also exhibit features of the density of states in amorphous semiconductors [72]. In most of the chalcogenides the Hall coefficient is negative in contrast to the thermopower which shows a positive sign. Another important transport property of highly disordered solids is the dispersive transport [30,73] observed in transient photoconductivity experiments.

1.7c Optical properties

The fundamental optical spectra of crystals, both vibrational and electronic, are characterized by sharp structural features. This is a consequence of long range periodicity of crystalline lattices. In amorphous semiconductors the sharp structural features of corresponding crystalline state disappear while there is a similarity in the broad features of the spectra. Many crystals are optically anisotropic and display polarization dependent spectra whereas amorphous solids are optically isotropic. However, macroscopic inhomogeneity results in small variations in the refractive index in these materials. The existence of a transition window between the electronic and vibrational transitions, with very low absorption level makes the glasses suitable for optical fibres. The minimum of the absorption constant in SiO_2 can be as low as 10^{-6} cm^{-1} in the range of 0.7 to 1.1 μm in very pure glasses. Since the non-oxide chalcogenide glasses are composed of heavier atoms than oxide glasses, the vibration frequencies are shifted further into the infrared region. At the same time the absorption edge shifts towards smaller energies so that transparency range is deeper in the infrared.

Infrared and Raman spectroscopy, associated with strong absorption process due to vibrational excitations, are being effectively used for the study of amorphous materials. In amorphous materials, since the k vector conservation in photon-phonon interactions is no longer valid, all phonons can take part in first order interactions with light. Thus the entire phonon density of states appear in the infrared and Raman spectra which results in broad band instead of line spectrum as in crystalline solids.

Electronic transitions between the valence and conduction bands in the crystal starts at the absorption edge which corresponds to the minimum energy difference between the lowest minimum of the conduction band and the highest maximum of the valence band. In amorphous materials the absorption edge may be shifted either towards higher energies or towards lower energies. In fully coordinated systems the short range order is responsible for establishing the band widths, which explains the similarity of the optical band gaps of amorphous and crystalline phases. The features of density of states are determined by [74] topological disorder, ring statistics of the network and the nature of molecular units. The potential fluctuations

due to disorder lead to strong electron scattering and a short coherence length for the wavefunctions. The momentum selection rule breaks down in optical transitions when the coherence length is of the order of lattice spacing and the uncertainty in the wave vector becomes of the order of the wave vector itself. But the probability of optical transitions between filled and empty tail states is limited by disorder induced localization of electron states near the band edges. Transitions are allowed therefore to the extent that there is a spatial overlap of the localized wavefunctions whereas the transitions between localized and delocalized states beyond the mobility edges are strongly allowed.

The absorption edge in amorphous semiconductors can generally be separated into three regions [75] with absorption coefficient $\beta \geq 10^4 \text{ cm}^{-1}$, $1 \text{ cm}^{-1} < \beta < 10^4 \text{ cm}^{-1}$ and $\beta \leq 1 \text{ cm}^{-1}$. The first two regions are created by transitions within a fully coordinated system perturbed by defects while the third region arises from transition involving the defect states directly. In the high absorption region the absorption is governed by a power law of the type

$$\beta = \text{Const.} \times (h\nu - E_0)^p \quad (1.2)$$

For most of the amorphous semiconductors $p = 2$ where the band edges are both parabolic. Exception to this quadratic frequency dependence has been observed in a-Se and in some multicomponent glasses. On the basis of the above relation an empirical definition of the optical energy gap E_o can be made. In a crystal, photon of energy $h\nu$ can induce a transition from a filled state of energy E to an empty state of energy $(E + h\nu)$ only if the wave vector is conserved. Thus, among all pairs of electronic states separated by energy $h\nu$, only very few contribute to optical absorption. Since in amorphous semiconductors the selection rule is relaxed, all pairs of extended states with energy difference $h\nu$ can contribute to optical absorption. A plot of $\beta^{1/2}$ vs. $h\nu$ yields a straight line and the extrapolated $h\nu$ at which $\beta^{1/2} \rightarrow 0$ gives the value of optical energy gap E_o .

In the intermediate range of absorption coefficient there is an exponential tail in β associated with the intrinsic disorder. This behaviour is observed in all amorphous semiconductors but the precise origin of this is still being debated. It has been suggested that the origin of the phenomenon is disorder induced potential fluctuations [76,77]. Tauc [75] considered the origin of the potential fluctuations as deriving from longitudinal

optical phonons frozen in at the glass transition temperature. Strong electron-phonon interaction has also been suggested as a possible reason for exponential absorption [78]. In tetrahedrally coordinated materials, the defects called voids formed as a result of the strain release mechanism, provide a possible explanation for absorption tails and for the origin of the potential fluctuations that induce the exponential absorption. In chalcogenide glasses defects due to coordination variation explains several optical properties. In the weak absorption region the strength and the shape of the absorption tail are found to depend on the preparation, purity and thermal history of the material [79].

Amorphous semiconductors, absorb strongly above the fundamental absorption edge. The measurement of reflectivity and subsequent Kramers-Kronig analysis give information about the optical properties in this high photon energy region. In crystalline materials it gives sharp features related to the structure in the density of states of both valence and conduction bands. The sharp structure is lost in amorphous semiconductors again due to the relaxation in k conservation. The overall shape of the band is similar for crystals and glasses because the short range order is more or less same. The double peak feature observed in the ultraviolet spectra of chalcogenides, but not

in tetrahedrally coordinated materials, is attributed to the nonbonding-bonding division within the valence band density of states in these materials.

1.7d Thermal properties

The phonon mean free path of highly disordered and non-crystalline solids is considerably shorter than that in crystals and correspondingly thermal conductivity is less. The measurements of thermal, acoustic and dielectric properties of disordered solids below 50 K show a number of unusual features which have no counterparts in crystals [80]. In low temperature region the thermal conductivity decreases slowly with decreasing temperature. Near ≈ 10 K the thermal conductivity is only weakly temperature dependent, thus showing a 'plateau' region. At still lower temperatures the thermal conductivity decreases roughly as T^2 for amorphous solids. Recently Alexander et al [81] have attempted to explain the variations in thermal conductivity with temperature using phonon-fracton anharmonic interaction model.

The elastic and dielectric behaviour of amorphous solids at low temperatures also differ considerably from that of crystalline solids. For example, the acoustic

and dielectric absorption is strongly enhanced compared to crystals and large absorption peak is found around liquid nitrogen temperature in many glasses. Below liquid helium temperature a number of anomalous effects were observed which can be attributed to low energy excitations closely related to the amorphous state. These excitations are not only responsible for the anomalously high specific heat but also determine the elastic and dielectric properties.

PART-B

PHOTOACOUSTIC SPECTROSCOPY OF SOLIDS

1.8 INTRODUCTION

Optical spectroscopy, which is based on the interaction of radiation with matter, is one of the most effective means employed to study the physical properties of matter. Almost all the conventional optical spectroscopic methods are either transmission type, which involves the measurement of the intensity of radiation transmitted through the medium, or reflection type which involves the measurement of the intensity of radiation scattered or reflected from the material. Optical spectroscopy has been very successful in the case of a variety of materials.

At the same time there are situations in which it often fails to give good results. Such situations arise when we try to make measurements on weakly absorbing materials, highly light scattering materials such as powders, amorphous solids, gels, smears and suspensions, optically opaque materials etc. Several techniques such as diffuse reflectance [82], attenuated total reflection and internal reflection spectroscopy [83], Raman scattering [84] etc. have been in use in such situations. But the application of these techniques are limited to a relatively small category of materials and wavelength ranges and the data obtained are often difficult to interpret. Recently the photoacoustic spectroscopy (PAS) has developed into a powerful analytical tool which is devoid of these limitations. This becomes possible because in this technique the interaction of radiation with the medium is studied through the direct measure of the energy absorbed by the material and not through the detection and analysis of outgoing photons.

The photoacoustic (PA) effect which is the underlying principle of PAS was discovered by Alexander Graham Bell in 1880 [85,86]. The PA effect has developed as a technique to study infrared light absorption in gases,

to evaluate concentrations of gaseous species in gas mixtures and to study deexcitation and energy transfer processes in gases during the 1930's and 40's [87-92]. Even though the PA effect was used for gas analysis and in infrared spectroscopy for many decades, the full potential of the effect has not been explored until recently. The recent developments owe mainly to the pioneering work by Rosencwaig and co-workers [93-96] which has resulted in great uprise in interest in PA effect. Equipped with powerful light sources such as lasers and high power lamps and sophisticated signal detection, processing and data acquisition systems, the PA techniques has of late entered various branches of science and technology as a powerful analytical technique.

1.9 THE PHOTOACOUSTIC EFFECT

Bell [85,86] was of the view that PA effect was due to the periodic expulsion of air from the pores of the sample caused by periodic heating and cooling produced when the sample is illuminated with an intensity modulated light beam. However in the case of membrane or disc type solid samples he agreed with Rayleigh's idea [97] that the primary source of the acoustic signal was the mechanical

vibration of the disc. Another explanation put forward was that PA signal is due to vibrating movement produced in the gaseous layer adhering to the solid surface due to alternate heating and cooling. The present understanding based on experimental and theoretical considerations suggests that in a gas-microphone PA system, the primary source of acoustic signal from a non-gaseous sample arises from the periodic heat flow from the sample to the surrounding gas as the sample is cyclically heated by the incident radiation. In the PA method first we illuminate the sample contained in an enclosed cell, which also contains a microphone to detect the signal, with a chopped light beam. The absorption of the incident photons by the sample excites its internal energy levels. Upon subsequent deexcitation, all or part of the absorbed photon energy is transformed into heat energy through nonradiative deexcitation processes. In a gas this heat energy appears as kinetic energy of the gas molecules whereas in a solid or liquid, it appears as vibrational energy of ions or atoms. The periodic heat thus produced causes pressure fluctuations in a gas medium surrounding the sample which is detected by a sensitive microphone. In this way PAS is a combination of calorimetry and optical spectroscopy. It is also

possible to use piezoelectric detectors in PA studies of liquids and solids. Here the detector placed in intimate contact with the sample detects the pressure or stress variations in the sample itself produced by heating.

Being a photocalorimetric technique PA effect has got wide ranging applications in determining the properties related to optical and thermal characteristics of all forms of matter. Since this technique does not involve detection of photons it can be effectively used with equal success for the study of weakly absorbing samples as well as highly light scattering and optically opaque materials. This unique capability of the PA technique resulting from the fact that only the absorbed light contributes to acoustic signal is one of the important advantages of this technique over other spectroscopic techniques. Also since the sample itself constitutes the radiation detector, no photoelectronic device is necessary and thus studies over a wide range of wavelengths are possible without the need to change the detection system.

1.10 THEORY OF PHOTOACOUSTIC EFFECT IN SOLIDS

As has already been pointed out, several theoretical explanations have been put forward for explaining

the PA effect in the 19th century itself. But satisfactory quantitative theories began to evolve only recently. First among them was the theory by Parker which appeared in 1973 [98]. He developed a theory to give a quantitative explanation for the PA signal emanating from cell windows while performing PA experiments on gases. Later a more general theory of the PA effect in solid samples was put forward by Rosencwaig and Gersho [95,99]. Rosencwaig-Gersho (RG) theory predicts that the PA signal depends both on the generation of an acoustic pressure disturbance at the sample-gas interface and on the transport of this disturbance through the gas to the microphone. The generation of the surface pressure disturbance depends in turn on the periodic temperature at the sample-gas interface. RG theory gives an exact equation for the magnitude and phase of the PA signal as a function of the optical, thermal and geometrical properties of the sample, the cell and the gas within the cell. Since this theory was found to be very successful in interpreting most of the experimental results, it is briefly outlined below. Moreover, we have used the RG theory extensively for interpreting our experimental findings.

RG theory is a one dimensional analysis of the production of PA signal, based on equations for thermal diffusion in the sample, the backing material and surrounding gas, in a cylindrical cell as shown in Fig.1.7. The PA cell has a diameter D and length L . It is assumed that the length L is small compared to the wavelength of the acoustic signal and the microphone detects the average pressure produced in the cell. The sample, considered to be in the form of a disc having diameter D and thickness l_s is mounted on a poor thermal conductor of thickness l_b . The length of the gas column in the cell is l_g . It is assumed that the gas and backing material do not absorb radiation.

The following physical parameters of the sample, backing and gas enter in the theoretical considerations.

k , the thermal conductivity (cal/cm-sec- $^{\circ}$ C)

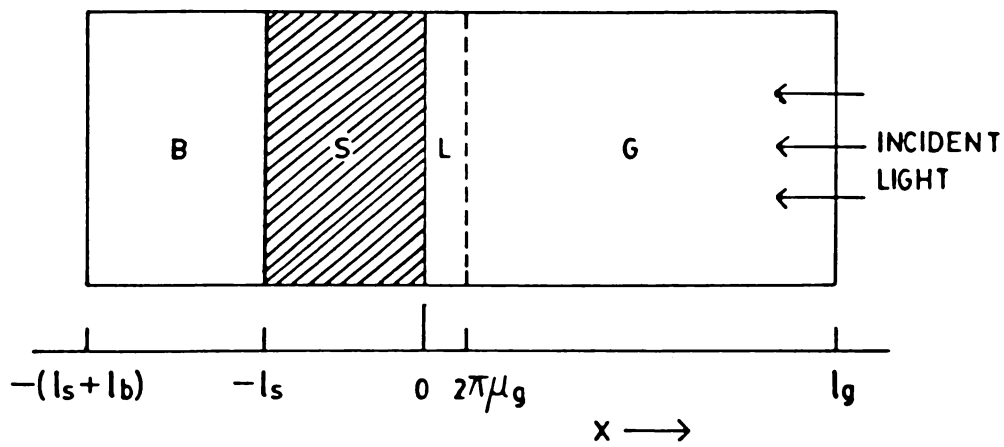
ρ , the density (g/cm 3)

c , the specific heat (cal/g- $^{\circ}$ C)

α , = $\frac{k}{\rho c}$, thermal diffusivity (cm 2 /sec.)

a = $(\frac{\omega}{2\alpha})^{\frac{1}{2}}$ the thermal diffusion coefficient (cm $^{-1}$)

μ = $\frac{1}{a}$, the thermal diffusion length (cm).



- B — BACKING MATERIAL
- S — SAMPLE
- L — BOUNDARY LAYER OF GAS
- G — GAS MEDIUM

Fig.1.7 Cross-sectional view of a simple cylindrical photoacoustic cell.

The suffixes s, b and g refer to the sample, backing and gas respectively.

The intensity of the sinusoidally chopped monochromatic light with wavelength λ incident on the sample can be written as

$$I = \frac{1}{2} I_0 (1 + \cos \omega t) \quad (1.3)$$

where I_0 is the incident light flux (W/cm^2) and ω is the chopping frequency in radians/sec. The density of heat produced at any point x due to light absorbed at this point in the solid is given by

$$H = \frac{1}{2} I_0 \beta e^{\beta x} (1 + \cos \omega t) \quad (1.4)$$

where β is the optical absorption coefficient of the solid sample and x is negative (see Fig.1.7). The thermal diffusion equation in the solid taking into account distributed heat source can be written as

$$\frac{\partial^2 \theta}{\partial x^2} = \frac{1}{\alpha_s} \frac{\partial \theta}{\partial t} - A e^{\beta x} (1 + e^{i\omega t}) \text{ for } -l_s \leq x \leq 0 \quad (1.5)$$

where $A = \frac{\beta I_0 \eta}{2k_s}$, θ is the temperature and η is the efficiency with which the absorbed light is converted into

heat by nonradiative deexcitation processes and is assumed to be one. For backing and gas, the thermal diffusion equations are respectively given by

$$\frac{\partial^2 \theta}{\partial x^2} = \frac{1}{\alpha_b} \frac{\partial \theta}{\partial t} \quad , \quad \text{for } -l_b - l_s \leq x \leq -l_s \quad (1.6)$$

$$\frac{\partial^2 \theta}{\partial x^2} = \frac{1}{\alpha_g} \frac{\partial \theta}{\partial t} \quad , \quad \text{for } 0 \leq x \leq l_g \quad (1.7)$$

The real part of the complex valued function $\theta(x,t)$ is the solution of physical interest and represents the temperature in the cell relative to ambient temperature as a function of position and time. The general solution for $\theta(x,t)$ in the cell neglecting transients can be written as

$$\theta(x,t) = \begin{cases} \frac{1}{l_b}(x + l_s + l_b)W_0 + W e^{\sigma_b(x+l_s)} e^{i\omega t} & \text{for } -l_s - l_b \leq x \leq -l_s \\ b_1 + b_2 x + b_3 e^{\beta x} + (U e^{\sigma_s x} + V e^{-\sigma_s x} - E e^{\beta x}) e^{i\omega t} & \text{for } -l_s \leq x \leq 0 \\ (1 - \frac{x}{l_g})F + \theta_0 e^{-\sigma_g x} e^{i\omega t} & \text{for } 0 \leq x \leq l_g \end{cases} \quad (1.8)$$

where W , U , V , E and θ_0 are complex valued constants, b_1 , b_2 , b_3 , W_0 and F are real valued constants and $\sigma = (1 + i)a$. θ_0 and W represent the complex amplitude

of periodic temperatures at the sample-gas and sample-backing boundaries respectively. The d.c. component at these boundaries are given by F and W_0 . b_3 and E , determined by the forcing function in equation (1.5), are given by

$$b_3 = -\frac{A}{\beta^2} \quad (1.9)$$

$$E = \frac{A}{(\beta^2 - \sigma_s^2)} = \frac{\beta I_0}{2k_s(\beta^2 - \sigma_s^2)} \quad (1.10)$$

By applying the boundary conditions obtained from the requirement of temperature and heat flux continuity at the boundaries $x = 0$ and $x = -l_s$ and the constraints that the temperature at the cell walls $x = +l_g$ and $x = (-l_s - l_b)$ is at ambient, all the constants in equation (1.8) and thus the a.c. and d.c. components of the solution can be obtained. The explicit solution of θ_0 , the complex amplitude of the periodic temperature at the solid-gas boundary ($x = 0$) is given by

$$\theta_0 = \frac{\beta I_0}{2k_s(\beta^2 - \sigma_s^2)} \left[\frac{(r-1)(b+1)e^{\sigma_s l_s} - (r+1)(b-1)e^{-\sigma_s l_s} + 2(b-r)e^{-\beta l_s}}{(g+1)(b+1)e^{\sigma_s l_s} - (g-1)(b-1)e^{-\sigma_s l_s}} \right] \quad (1.11)$$

$$\text{where } b = \frac{k_b a_b}{k_s a_s}, \quad g = \frac{k_g a_g}{k_s a_s}, \quad \gamma = (1-i) \frac{\beta}{2a_s} \quad (1.12)$$

The periodic heat flow from the solid to the surrounding gas produces a periodic temperature variation in the gas which can be represented by

$$\theta_{a.c.}(x,t) = \theta_0 e^{-\sigma_g x} e^{i\omega t} \quad (1.13)$$

Since the periodic temperature variation in the gas is effectively fully damped out at distance of $2\pi\mu_g$ only the boundary layer of the gas having thickness $2\pi\mu_g$ is capable of responding thermally to the periodic temperature at the surface of the sample. This boundary layer of gas expands and contracts periodically thus acting as an acoustic piston. The displacement of this gas piston can be written as

$$\delta x(t) = 2\pi\mu_g \frac{\bar{\theta}(t)}{T_0} = \frac{\theta_0 \mu_g}{\sqrt{2} T_0} e^{i(\omega t - \pi/4)} \quad (1.14)$$

Here $\bar{\theta}(t)$ is the spatially averaged temperature of the gas within the boundary layer given by

$$\bar{\theta}(t) = \frac{1}{2\pi\mu_g} \int_0^{2\pi\mu_g} \theta_{a.c.}(x,t) dx \simeq \frac{1}{2\sqrt{2}\pi} \theta_0 e^{i(\omega t - \pi/4)} \quad (1.15)$$

If we assume that the gas responds to the action of this piston adiabatically, then the acoustic pressure in the cell due to the displacement of this gas piston is derived from the adiabatic gas law

$$PV^\gamma = \text{Constant}. \quad (1.16)$$

where P is the pressure, V is the gas volume in the cell and γ is the ratio of specific heats. Thus the incremental pressure is

$$\delta P(t) = \frac{\gamma P_0}{V_0} \delta V = \frac{\gamma P_0}{l_g} \delta x(t) \quad (1.17)$$

where P_0 and V_0 are ambient pressure and volume respectively and $-\delta V$ is the incremental volume. Then substituting for $\delta x(t)$ from equation (1.14)

$$\delta P(t) = Q e^{i(\omega t - \pi/4)} \quad (1.18)$$

where

$$Q = \frac{\gamma P_0 \theta_0}{\sqrt{2} l_g a_g T_0} \quad (1.19)$$

Q may be specified as the complex envelope of the sinusoidal pressure variation. Substituting for θ_0 from

equation (1.11)

$$Q = \frac{\beta I_0 \gamma P_0}{2\sqrt{2} T_0 k_s l_g a_g (\beta^2 - \sigma_s^2)} \left[\frac{(\gamma-1)(b+1)e^{\sigma_s l_s} - (\gamma+1)(b-1)e^{-\sigma_s l_s} + 2(b-\gamma)e^{-\beta l_s}}{(g+1)(b+1)e^{\sigma_s l_s} - (g-1)(b-1)e^{-\sigma_s l_s}} \right] \quad (1.20)$$

Special cases;

The complicated expression given above can be made simple considering some special cases. These cases may be examined on the basis of three length parameters namely optical absorption length $l_p = \frac{1}{\beta}$, thermal diffusion length μ_s and the physical length l_s of the sample. It is assumed that $k_g a_g < k_b a_b$ and $k_b a_b \approx k_s a_s$. It is convenient to define

$$Y = \frac{\gamma P_0 I_0}{2\sqrt{2} T_0 l_g} \quad (1.21)$$

Case 1: Optically transparent solids ($l_p > l_s$).

In this case the light is absorbed throughout the length of the sample and some light is transmitted through the sample. Here, depending upon thermal diffusion length three cases can be visualized as follows:

Case 1a: Thermally thin solids ($\mu_s \gg l_s; \mu_s > l_p$)

Here setting

$$e^{-\beta l_s} \approx 1 - \beta l_s, \quad e^{\pm \sigma_s l_s} \approx 1 \quad \text{and } |\gamma| > 1$$

we get

$$Q = \frac{(1-i)\beta l_s}{2a_g} \left(\frac{\mu_b}{k_b} \right) \gamma \quad (1.22)$$

The acoustic signal is proportional to βl_s and it has an ω^{-1} dependence.

Case 1b: Thermally thin solids ($\mu_s > l_s; \mu_s < l_\beta$)

This sets $e^{-\beta l_s} \simeq (1 - \beta l_s)$, $e^{\pm \sigma_s l_s} \simeq (1 \pm \sigma_s l_s)$ and $|\gamma| < 1$

$$\text{Then } Q = \frac{(1-i)\beta l_s}{2a_g} \left(\frac{\mu_b}{k_b} \right) \gamma \quad (1.23)$$

Here also the signal is proportional to βl_s and has ω^{-1} dependence.

Case 1c: Thermally thick solids ($\mu_s < l_s; \mu_s \ll l_\beta$)

Setting $e^{-\beta l_s} \simeq (1 - \beta l_s)$, $e^{-\sigma_s l_s} \simeq 0$ and $|\gamma| \ll 1$

$$Q = \frac{-i\beta \mu_s}{2a_g} \left(\frac{\mu_s}{k_s} \right) \gamma \quad (1.24)$$

Here the signal is proportional to $\beta \mu_s$ and therefore only the light absorbed within the first thermal diffusion length contribute to the signal. The signal has got an $\omega^{-3/2}$ frequency dependence.

Case 2: Optically opaque solids ($l_p \ll l_s$)

In this case most of the light is absorbed within a distance that is small compared to l_s . Here also, depending upon the thermal diffusion length, three cases can be considered.

Case 2a: Thermally thin solids ($\mu_s \gg l_s; \mu_s \gg l_p$)

Here setting $e^{-\beta l_s} \approx 0$, $e^{\pm \sigma_s l_s} \approx 1$ and $|\gamma| \gg 1$

we obtain

$$Q = \frac{(1-i)}{2a_g} \left(\frac{\mu_b}{k_b} \right) \gamma \quad (1.25)$$

The singal is independent of the absorption coefficient and varies as ω^{-1} . This would be the case for a good absorber such as carbon black.

Case 2b: Thermally thick solids ($\mu_s < l_s; \mu_s > l_p$)

This sets $e^{-\beta l_s} \approx 0$, $e^{-\sigma_s l_s} \approx 0$ and $|\gamma| > 1$

Then

$$Q = \frac{(1-i)}{2a_g} \left(\frac{\mu_s}{k_s} \right) \gamma \quad (1.26)$$

Here also the acoustic signal is independent of β and varies as ω^{-1} .

Case 2c: Thermally thick solids ($\mu_s \ll l_s; \mu_s < l_\beta$)

Setting $e^{-\beta l_s} \approx 0, e^{-\sigma_s l_s} \approx 0$ and $|r| < 1$, we get

$$Q = -\frac{i\beta\mu_s}{2a_g} \left(\frac{\mu_s}{k_s}\right) Y \quad (1.27)$$

The interesting point to note here is that even though the sample is optically opaque the PA signal is proportional to β if $\mu_s < l_\beta$. The signal varies as $\omega^{-3/2}$ in this case.

The RG theory discussed above could successfully explain most of the experimental results as has been verified by several authors [96,100-103]. After the formulation of RG theory several refinements to it have been made treating the transport of acoustic disturbances in the gas more exactly with Navier-Stokes equations [104-107]. McDonald and Wetsel [106] included in the theory, the contribution to the signal from thermally induced vibrations in the sample. These modifications to the theory of PA effect

could account for observed deviations from the RG theory at very low frequencies.

1.11 APPLICATIONS OF THE PHOTOACOUSTIC EFFECT

Wide ranging applications of the PA effect in various fields of physics, chemistry, biology, engineering and medicine have been reported in the last few years. The applications of the PA effect in the study of properties of materials fall into four general classes namely: (a) photoacoustic spectroscopy, (b) photoacoustic monitoring of deexcitation processes, (c) photoacoustic probing of thermoelastic and relative properties of materials, and (d) depth profiling and microscopy.

1.11a Photoacoustic spectroscopy

In this class of applications the PA signal is measured for a range of optical excitation wavelengths producing a PA spectrum. PA signal gives spectroscopic information over a wide range of absorption coefficients, ranging from weakly absorbing materials to opaque materials. The sensitivity of laser PA system has advanced to an absorption measurement capability of $\approx 10^{-10} \text{ cm}^{-1}$ [108] which is several orders higher than conventional techniques.

Such a high sensitivity of the PA technique has found use in detecting weak absorptions that are forbidden by the dipole selection rule or by spin conservation and weak absorption due to strong absorption line of a trace constituent. This finds applications in overtone spectroscopy, trace analysis and pollution monitoring [109-113].

PA monitoring of weak absorption in solids with a detection sensitivity of $\approx 10^{-5} \text{ cm}^{-1}$ using piezoelectric detection has been reported on highly transparent solids like CaF_2 , SrF_2 , etc. [114]. The high sensitivity of the technique makes it very suitable for monitoring absorptions in thin films because weak absorption may be caused by a low absorption coefficient for the optical wavelength or may be caused by a short path length. This has immense applications in thin film optical coatings like laser mirrors, absorption by glass surfaces, thin layer chromatography, surface chemistry, surface catalysis etc. PAS can be used effectively for studying adsorbed or chemisorbed molecular species and compounds, surface passivation and surface oxidation or reduction studies on metals, semiconductors and insulators.

PAS is found to be very useful to study insulator, semiconductor and metallic systems that cannot be studied

readily by conventional techniques. In the case of insulators PA spectra give direct information about the optical absorption bands in the material [93]. One of the important applications is that optical absorption characteristics of highly opaque samples can be obtained using high chopping frequency so that $\mu_s < l_p$. If $\mu_s > l_p$, with optically opaque sample it is possible to get the power spectrum of the excitation source. Thus a power meter which can be used over a very wide wavelength range can be constructed with a black sample very easily. In the case of semiconductors PAS can be used to study both direct and indirect transitions [94,115]. In addition it can also be used to study Urbach tail, excitons and other fine structures in crystalline, powder and amorphous semiconductors [116, 117] and thus aids to investigate the effects of impurities, dopants and electromagnetic fields etc.

1.11b Photoacoustic monitoring of deexcitation processes

In this class of applications the thermal decay branch is monitored to provide information about the deexcitation mechanism of the material. After optical excitation four decay branches are generally possible. They are luminescence, photochemical reaction, photoelectric phenomenon and generation of heat by energy transfer

processes. The selective sensitivity of the PA technique to heat producing deexcitation channel can be used to study fluorescent and photosensitive properties of materials. If there are only two competing branches, for example luminescence and generations of heat, then by PA monitoring of the heat branch, the quantum efficiency of luminescence under various conditions can be deduced. Determination of luminescence quantum efficiency by PA effect has been reported by several authors [118-121]. When a major contribution to the deexcitation of excited level is by radiative relaxation then acoustic signal produced will be weak. PA effect has been effectively utilized for deexcitation studies in rare earth oxides and in doped crystals [122, 123]. It gives information about the life times of various states and deexcitation channels. A combination of conventional fluorescent spectroscopy and PAS can provide information about the relative strengths of the radiative and nonradiative deexcitation processes in solids.

When the channel of deexcitation for absorbed light energy is through photochemical processes PAS enables one to obtain the activation energy spectrum by comparing the PA spectrum with the conventional absorption spectrum. From the phase measurements of the PA signal information about photochemical reaction rates can be obtained.

In materials where photovoltaic processes occur, the PA signal depends upon the energy conversion efficiency for this process. Therefore in order to study the photovoltaic deexcitation processes in semiconductors PA technique is very useful. When part of the light energy is converted into electrical energy, the thermal energy produced will be correspondingly reduced. First demonstration of PA monitoring of photoelectrical effects was reported by Cahen in 1978 [124]. He measured the photoelectrical generation efficiency of silicon solar cells as a function of load resistance. Tam [125] successfully used the PA method to determine the photoconductive quantum efficiency of a thin organic dye film. Another important work was done by Thielemann and Neumann [126] in which they used PA technique to determine the photocarrier generation quantum efficiency of a Schottky diode. There has been report about the investigation of nonradiative states in GaAs and InP using PAS [127]. It has been effectively used for the study of regions above the fundamental absorption edge in Si, Ge, InSb, GaAs and GaP [128]. The use of PA method to investigate laser annealing of semiconductor surfaces, to monitor dopant concentration and their diffusions, to know degree of recrystallization and to detect possible damage associated with the intense radiation have

been demonstrated [129,130]. Since the PA signal also depends upon the transport properties it can be used to study recombination processes in semiconductor along with photoconductivity study [131,132].

1.11c Photoacoustic method of probing thermoelastic and related properties

The optical generation of thermal and acoustic waves can be used to gather informations such as sound velocity, elasticity, flow velocity, specific heat, thermal diffusivity, thickness of thin films, sub-surface defects and so on. This is because the PA process depends not only on the optical properties of the sample but also on its thermal, geometrical and elastic properties. Ever since the report of thermal diffusivity measurements by Adams and Kirkbright using PA technique [133], it has been used to measure the thermal conductivity and thermal diffusivity of a wide variety of samples. Changes in the thermal parameters can be used to monitor changes within a material as they generally undergo a change when the material undergoes a transition. Monitoring the variations in the PA signal as a function of temperature provide information about the occurrence of phase transitions. There has been several reports on the investigation of both first and

second order phase transitions [134]. The application of PA effect to phase transition studies should contribute a useful complementary technique to the conventional calorimetric methods.

1.11d Depth profiling and microscopy

One of the unique applications of PA technique is that by changing the chopping frequency, it is possible to obtain a depth profile analysis of the optical and thermal properties of a material. At high chopping frequencies information about the sample near the surface is obtained, while at low frequencies data comes from deeper regions within the sample. Such applications are very useful in thin films, layered and optically opaque samples etc. Depth profiling is also important in the study of doped semiconducting materials, laser windows whose surfaces have absorption properties different from that of bulk and biological tissues.

The PA technique has been successfully used in imaging applications. The PA signal for a sample monitored over a range of excitation location provides PA imaging of the sample. The best optical excitation source for PA microscopy is a laser beam, at a wavelength that is strongly absorbed by the sample and at an intensity below

the damage threshold of the sample, well focused to a small spot on the sample. The scanning can be done by moving either the sample or the light beam. PA images are obtained due to spatial variations in the optical and thermal properties of the sample. Both gas-microphone and piezoelectric methods have been used for this powerful non-destructive testing technique. PA microscopy is a quickly expanding area of research because of its potential applications in thin film technology, chemical engineering, biology and medicine, semiconductor industry etc. Coupled with depth profiling capability it provides a unique method for obtaining subsurface images of irregularities, flaws, doping concentrations etc. In semiconductor industry PA microscopy can be employed in semiconductor fabrication line to monitor the presence of electrical shorts or leak in integrated circuits. It can also be used for on-line study of patterns and structures that are below the surface and to perform localized thin film thickness measurements.

Chapter 2

THE EXPERIMENTAL SET UP

In this chapter we give the details of experimental set up we have used in this work.

2.1 A PHOTOACOUSTIC SPECTROMETER: GENERAL CONSIDERATIONS

In order to carry out photoacoustic studies on any kind of sample, an efficient PA spectrometer has to be set up. The essential parts of a PA spectrometer are: (a) light source in the spectral region of interest, (b) means for intensity modulation of light, (c) PA cell in which the sample is situated, (d) means for detecting the generated acoustic signal, and (e) signal processing equipments. The overall performance of a PA spectrometer depends on the quality of these modules. The basic experimental set up for a gas microphone PA spectrometer is shown in Fig.2.1. Now we will consider each component of the system separately.

2.1a Light source

In PA studies, depending upon its nature, different light sources can be used for irradiating the sample.

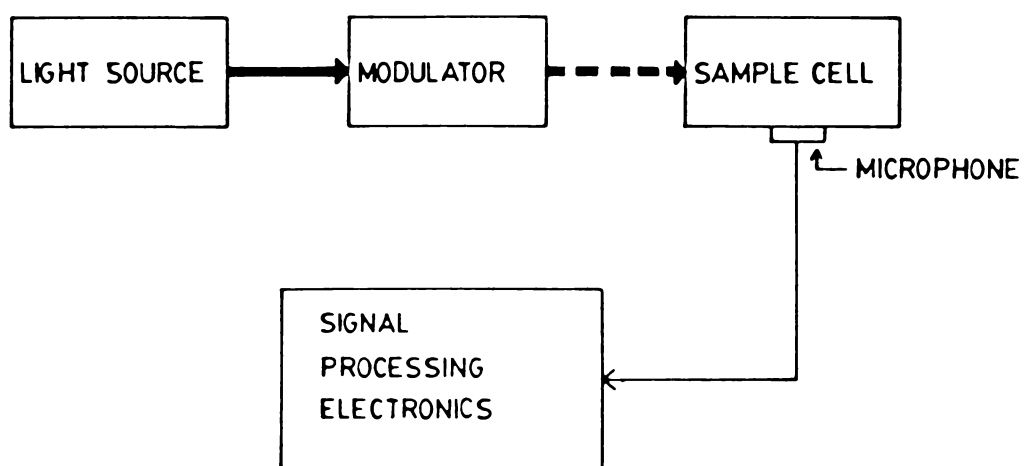


Fig.2.1 The basic experimental set up for a gas-microphone PA spectrometer.

Both incoherent and coherent sources are widely used. The important parameters for the selection of a light source are available power per usable bandwidth, the wavelength range, tunability and ease of intensity modulation.

Incoherent sources such as arc lamps, filament lamps etc. along with monochromators can be used to cover broad spectral ranges from ultraviolet to far infrared. The optical sources should have a high spectral radiance because the strength of PA signal is directly proportional to the intensity of the radiation. Incoherent sources commonly in use are carbon arc lamps, high pressure mercury lamps, high pressure Xenon lamps, tungsten lamps, Nerst glowers etc. In combination with suitable optical systems monochromatic radiation having bandwidth $10\text{-}100\text{\AA}$ can be obtained with reasonable intensity. Most monochromators utilize either a prism or a diffraction grating as the dispersive element. For low resolution it is sufficient to use an optical filter in place of the monochromator.

Lasers are widely accepted light sources in PA experiments, especially for measuring weak absorption. This is mainly because of their high spectral radiance resulting from the extremely narrow linewidths and high

collimation. Because of the spectral purity, lasers can be effectively used for high resolution PA spectroscopy experiments. The main drawback of the laser sources is their limited tuning range. However, tunable dye lasers [135] are widely used nowadays.

2.1b Modulation

The modulation of the incident light beam is essential for the generation of PA signal. Either amplitude or frequency of the radiation can be modulated. One of the inexpensive, efficient and common method to accomplish amplitude modulation is to use a mechanical chopper. The depth of modulation in this case is $\approx 100\%$. The chopper wheel must be properly housed to eliminate chopper induced noise transmitting directly to the microphone detector. In the case of electrical CW lasers, modulation can be achieved by varying the discharge tube current. Electro-optic modulation involves changing the plane of the polarization of an incoming polarized laser beam in a nonlinear crystal (ADP or KDP) under the application of a modulated electric field. In the acousto-optic technique the modulation is accomplished by diffraction of light by sound waves in crystals generated by a transducer excited by a radio frequency signal. Frequency modulation can also

be utilized for PA signal generation. In dye lasers rapid frequency change can be accomplished by using an electro-optic tuner in place of a birefringent filter. Frequency modulation is well suited for narrow linewidth absorbers.

2.1c The photoacoustic cell

The PA cell which contains the sample and the microphone can be considered as the heart of a PA spectrometer. Some of the important criteria governing the construction of a PA cell are given below.

(1) The cell should be acoustically isolated from the outside world. For this the cell should be designed with good acoustic seals and with walls of sufficient thickness to form a good acoustic barrier. The thermal mass of the cell walls should be large.

(2) In some cases the PA signal arising due to absorption in cell windows causes serious problems. In order to minimize this, windows should be as transparent as possible for the wavelength region of interest. Extraneous signals may also be produced due to the interaction of light beam with the walls of the cell and with the microphone diaphragm. Therefore the cell geometry should be

such that the scattering and reflection of light towards cell walls and microphone are avoided. The cell body may be constructed out of polished aluminium or stainless steel. Although aluminium or stainless steel walls absorb some of the incident and scattered radiation the resultant PA signal will be negligible as long as the thermal mass of these walls is large. Also, the inside surface of the cell should be free from contaminants.

(3) Since the PA signal varies inversely with the cell volume, the cell dimensions should be so chosen that the volume is minimum. However, care must be taken to avoid the appreciable dissipation of acoustic signal produced, to the cell windows and walls before reaching the microphone. Also for all chopping frequencies of interest the gas column length l_g in the cell should be greater than the thermal diffusion length μ_g of the gas, since it is this boundary layer of gas that acts as an acoustic piston generating the signal in the cell. Tam [136] has suggested the optimum gas column length to be $l_g \approx 1.8\mu_g$. Another important parameter to be considered in the design of a PA cell is the thermoviscous damping, because this could be a source of signal dissipation at the cell boundaries. Thermoviscous damping coefficient varies as $\omega^{1/2}$

and becomes important at high frequencies whereas thermal diffusion length which varies as $\omega^{-\frac{1}{2}}$ is predominant at low frequencies. Considering all these effects the distance between the sample and window can be chosen to be 1-3 mm [137].

Depending upon the nature of the investigations to be carried out, various cell designs have appeared in literature [138,139]. The most common cell design adopts cylindrical geometry in which the light beam is centered along the axis. Such cell can be made to operate either in the resonant mode or in the non-resonant mode. The pressure variations produced due to PA effect propagates radially outwards, perpendicular to the exciting beam. The hydrodynamic equation describing the time variation of pressure at a given point in the cell have been solved for cylindrical [137,140-142] and other [143] cell geometries. The pressure distribution P within a cylinder of length L and radius R is given by [137]

$$P(r, \phi, z, t) = \cos(m\phi) \cos\left(\frac{k\pi z}{L}\right) J_m\left(\frac{\alpha_{m,n}\pi r}{R}\right) \exp(-i\omega t) \quad (2.1)$$

where J_m is the Bessel function of the first kind of order m and the eigenvalues k , m and n relate to longitudinal

($k=1, m=n=0$), azimuthal ($m=1, k=n=0$) and radial ($n=1, k=m=0$) acoustic modes respectively. It is found that the cell exhibits a number of acoustic resonances. The resonance frequencies are given by [137]

$$f_{\text{res}} = \frac{C_0}{2} \sqrt{\left(\frac{k}{L}\right)^2 + \left(\frac{\alpha_{m,n}}{R}\right)^2} \quad (2.2)$$

where C_0 is the sound velocity in the gas and $\alpha_{m,n}$ is the n^{th} root of the equation $\left. \frac{dJ_m}{dr} \right|_{r=R} = 0$. Numerical values for the lowest order roots are $\alpha_{0,0} = 0$, $\alpha_{0,1} = 1.226$ and $\alpha_{1,0} = 0.589$. Cell resonances amplify the acoustic power at the resonance frequency. Cells with very high quality factor, which describes the degree of amplification or resonant quality of an acoustic cell, have been constructed [144,145]. Geometries other than cylindrical symmetries have also been employed in PA cell design. Ioli et al [146] used a configuration in which the light beam is directed transverse to the cylindrical axis in a cylindrical sample cell. This allows the excitation of a low frequency longitudinal resonance.

Another geometry for PA cell makes use of the Helmholtz resonator type configuration [147-149]. In this

case we have two volumes V_1 and V_2 , which form sample and microphone chambers respectively, connected by a narrow tube. The resonance frequency is given by [137]

$$2 \pi f_{\text{res}} = c_o \left(\frac{A}{l_c V_r} \right)^{\frac{1}{2}} \quad (2.3)$$

where

$$V_r = \frac{V_1 V_2}{V_1 + V_2} \quad (2.4)$$

A is the cross sectional area and l_c is the length of the channel. In this type of configuration the scattered light from the sample, sample holder and window on to the microphone is reduced. By using a sufficiently long connecting tube the sample chamber can be kept at a very cold or very hot temperature while the microphone is at room temperature [150,151].

The Brewster windows for minimum light scattering, multipassing for increased sensitivity, acoustic baffles for reduced effects due to window absorption etc., can be incorporated for improved performance. The effects of window heating can be eliminated by using a differential cell design [152].

2.1d Acoustic detectors

The PA signal produced in the cell can be detected by any sensitive microphone. A condenser microphone produces an electrical signal when a pressure wave is impinging on the diaphragm. Such microphones generally have flat frequency response upto ≈ 15 KHz, low distortion and are not sensitive to mechanical vibrations. Electret microphones [153], constructed using solid material of high dielectric constant which are electrically polarized, can also be used for detecting PA signals. No bias voltage is required for electret microphones and due to the large capacitance/area possible from electret materials they can be made into miniaturized microphones. Piezoelectric devices can also be used to sense the elastic waves generated in radiation absorbing solids and liquids [114,154, 155]. These devices offer much better acoustic impedance matching to the condensed samples and can detect high frequency signals.

2.1e Signal processing

In order to maximize the signal to noise ratio, the signal from the microphone preamplifier should be processed by an amplifier tuned to the chopping frequency. Using a phase sensitive lock-in amplifier [156] it is possible to measure the phase as well as the amplitude of the

signal. A lock-in amplifier is used also to eliminate noise from other sources. In a single-beam PA spectrometer the power spectrum of the light source for normalizing the PA signal is obtained either using a conventional power meter or using the PA spectrum obtained with a black absorber. In a double beam spectrometer [157] the monochromatized modulated beam is split into two. One of the beams falls on an optical detector or another PA cell containing carbon black while the second beam falls on the sample. The output from the sample cell is divided by that from the reference cell with a ratiometer and the normalized spectrum is directly recorded.

2.2 DETAILS OF OUR PHOTOACOUSTIC SPECTROMETER

We have assembled a single beam PA spectrometer for the investigations carried out in this work. The block diagram of this PA spectrometer is shown in Fig.2.2. It essentially contains the following components: (1) A 1 KW Xe arc lamp, (2) a grating monochromator, (3) light beam chopper, (4) PA cell with microphone, and (5) lock-in amplifier.

The light source we have used in the PA spectrometer is a 1 KW high pressure Xenon arc lamp (M/s. Spectroscopy Instruments, Model SVX 1000). It has got continuous

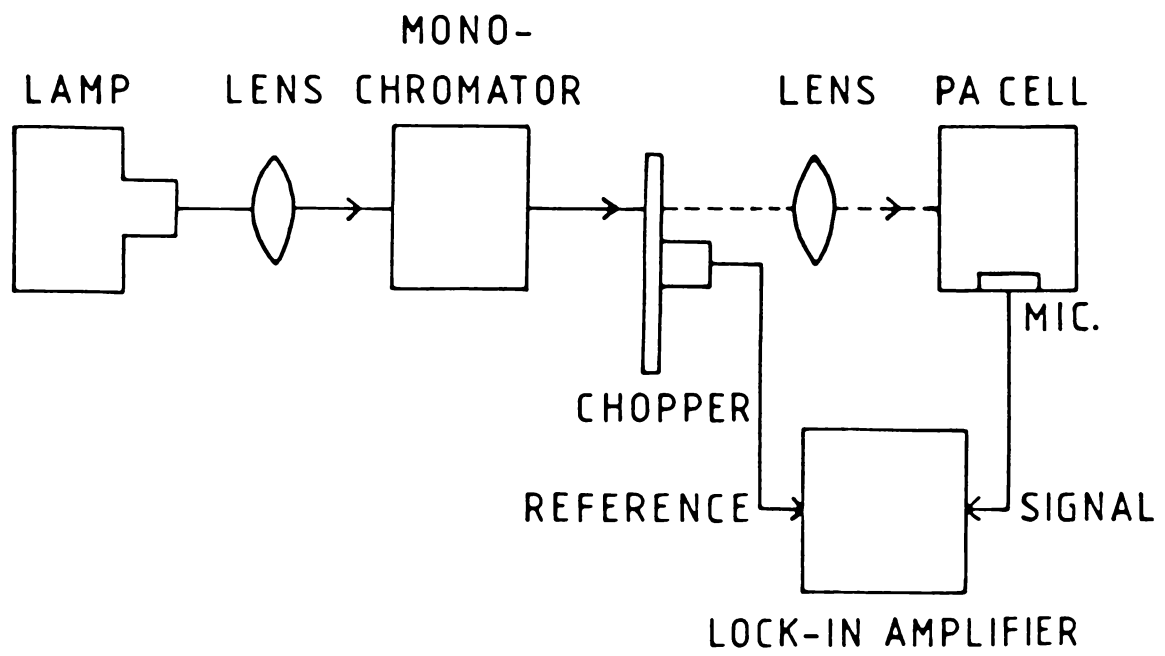


Fig.2.2 Block diagram of the PA spectrometer.

emission from 280 nm to 2500 nm with high intensity in the visible region and some intense lines between 800 nm and 1000 nm. The power supply constructed using the switching mode technology supplies constant current to the lamp which can be regulated in the 40 to 50 A range with a 10 turn potentiometer. The range of the operating voltage is 15 to 25V. The high pressure gas is capable of carrying a large current and dissipating large power in a small arc. This produces highly intense radiation lying in the visible as well as in ultraviolet and near infrared regions. The size and position of the reflected image of the arc can be adjusted with the micrometer screws provided for the purpose. The lamp house is also provided with focusing lens and cooling system.

For selecting the wavelength of the incident radiation from the Xe lamp we have used a source monochromator (Oriel, Model 7240). This monochromator can be used over a very wide range of wavelengths from 190 nm to 24 μm using appropriate gratings. A variable slit having adjustable width from 0 to 3.2 mm is used. This allows bandwidths of 0.8 to 20 nm in the visible region. The wavelength can be read in nm on a three digit mechanical counter. In order to scan the wavelength automatically over the selected range a monochromator drive controller

(Oriel, Model 78200), which is a bidirectional wavelength drive using a stepper motor, is used. The scan speed is adjustable and a six digit LED display shows wavelength in nm directly.

For intensity modulation of the incident light beam, a mechanical chopper (Photon Technology International, Model OC 4000) is used. With the two discs provided, a 5 sector disc and a 30 sector disc, chopping frequency can be varied continuously from 4 to 4000 Hz. The appropriate disc is mounted on the spindle of the chopper head. The motor speed, and thus the chopping frequency, can be varied using a 10 turn potentiometer. The reference signal for the lock-in amplifier, having frequency equal to the chopping frequency, is derived using a photodiode placed at the bottom of the chopper head. The chopping frequency can be directly read on the LED panel display of the unit.

The PA signal is processed using a lock-in amplifier (Stanford Research Systems, Model SR 510). The output of the microphone is fed into the lock-in amplifier for which the reference signal is provided by the chopper. The lock-in amplifier has a full scale sensitivity of 10 nV to 500 mV and an operating frequency range 0.5 Hz

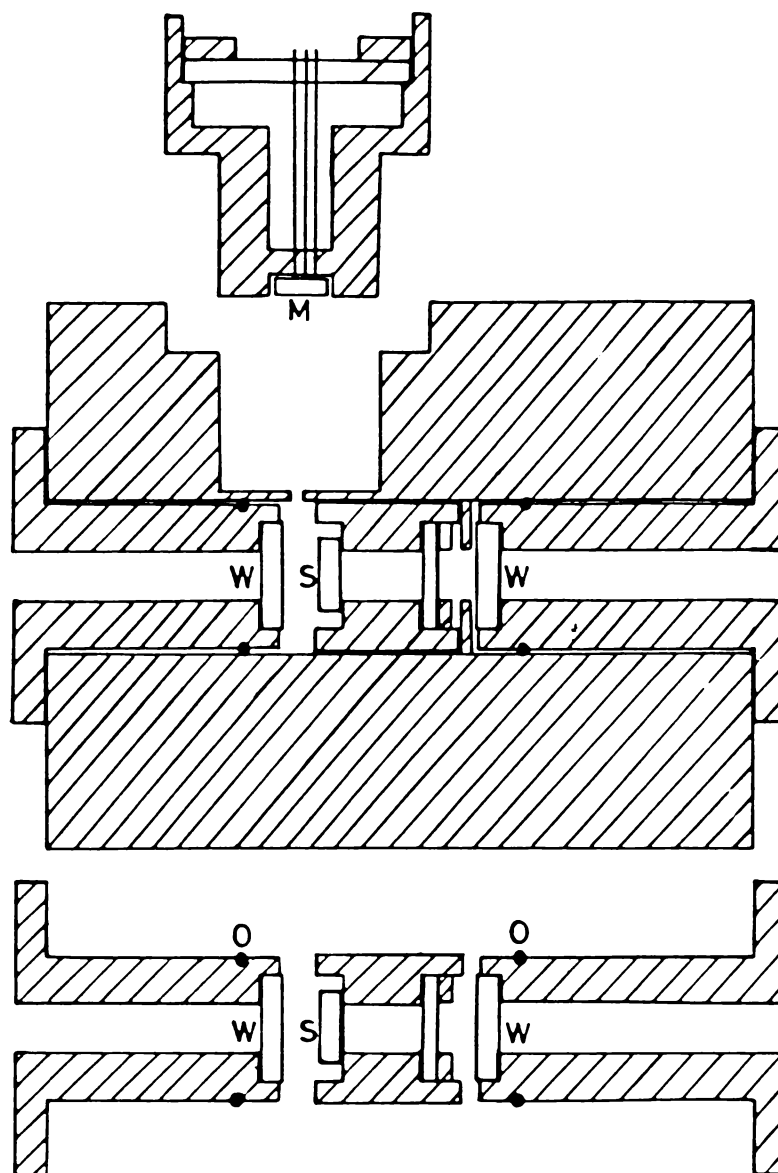
to 100 KHz. Phase can be controlled in large steps of 90° and fine steps of $.025^\circ$. Phase shift or frequency can be read from the four digit LCD display on the lock-in amplifier. The signal amplitude can be read either from the analogue meter or from the four digit auto-ranging LCD display.

2.3 DESIGN, FABRICATION AND CALIBRATION OF PHOTOACOUSTIC CELLS

The PA cell is the most important part of any PA spectrometer. We have constructed two PA cells; one for room temperature measurements and another for high temperatures. Description of these two cells are given below.

2.3a The room temperature PA cell

The small volume nonresonant cell used for room temperature measurements is made of aluminium. The cell with its various parts are shown in Fig.2.3. An axial bore of diameter 2.2 cm is made in a solid aluminium rod of diameter 10 cm and length 12 cm which constitutes the cell body. The sample holder, which is also made of aluminium, is placed in this bore. The construction of the



W- WINDOW
S- SAMPLE
M- MICROPHONE
O- 'O' RING

Fig.2.3 The room temperature PA cell. Microphone compartment, window holders and sample holder are shown separately.

sample holder is such that different backing materials can be used for the sample. Window holders and microphone compartment are also constructed out of aluminium. Two windows are provided, one on the front side and the other on the rear side, which enable to use both front and rear surface illumination of the sample. The cell volume is acoustically isolated from outside using 'O' rings on the window holders. The provision provided to change the backing material and to use the rear and front surface illuminations are important in the measurement of the thermal properties [158]. Also the replacement of the sample holder and windows and cleaning of the cell can easily be done. With this cell PA measurements on solids in bulk and thin film forms as well as on powders and liquid can be done.

The microphone used in the cell, for detecting the PA signal, is kept in a separate port which can be removed from the cell body. We have used a small size, high sensitive electret microphone (Knowles, Model BT 1759) having a built in FET preamplifier. It has got a flat frequency response in the frequency range 10 to 5000 Hz. The microphone output is taken using a BNC connector attached to the microphone port, and is fed to the lock-in amplifier. The minimum distance between the sample and window is 2 mm. This is very much greater than the thermal diffusion length of air which is 0.06 cm at a chopping frequency

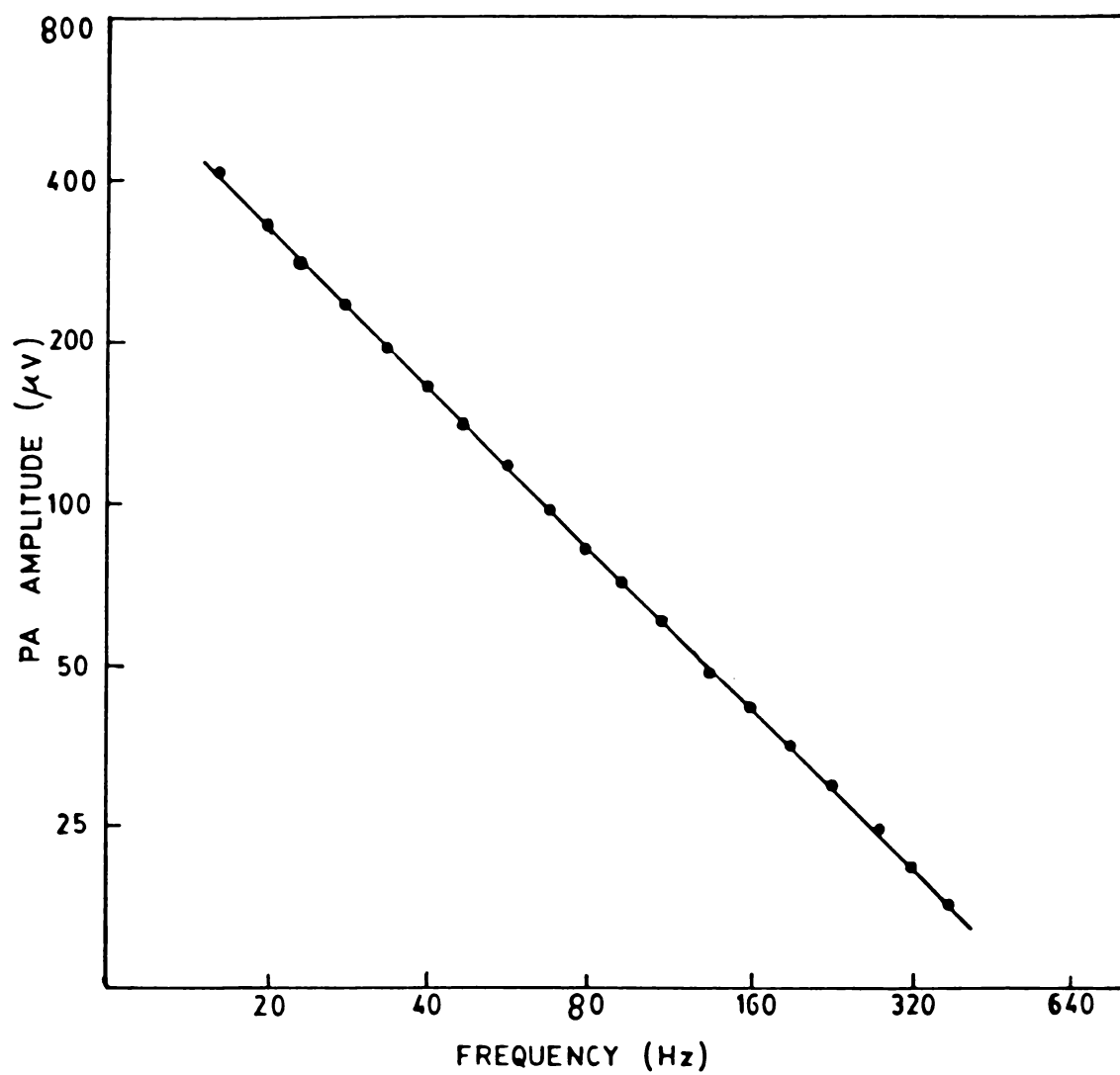


Fig.2.4 Log-log plot of the PA signal amplitude versus chopping frequency for carbon black sample.

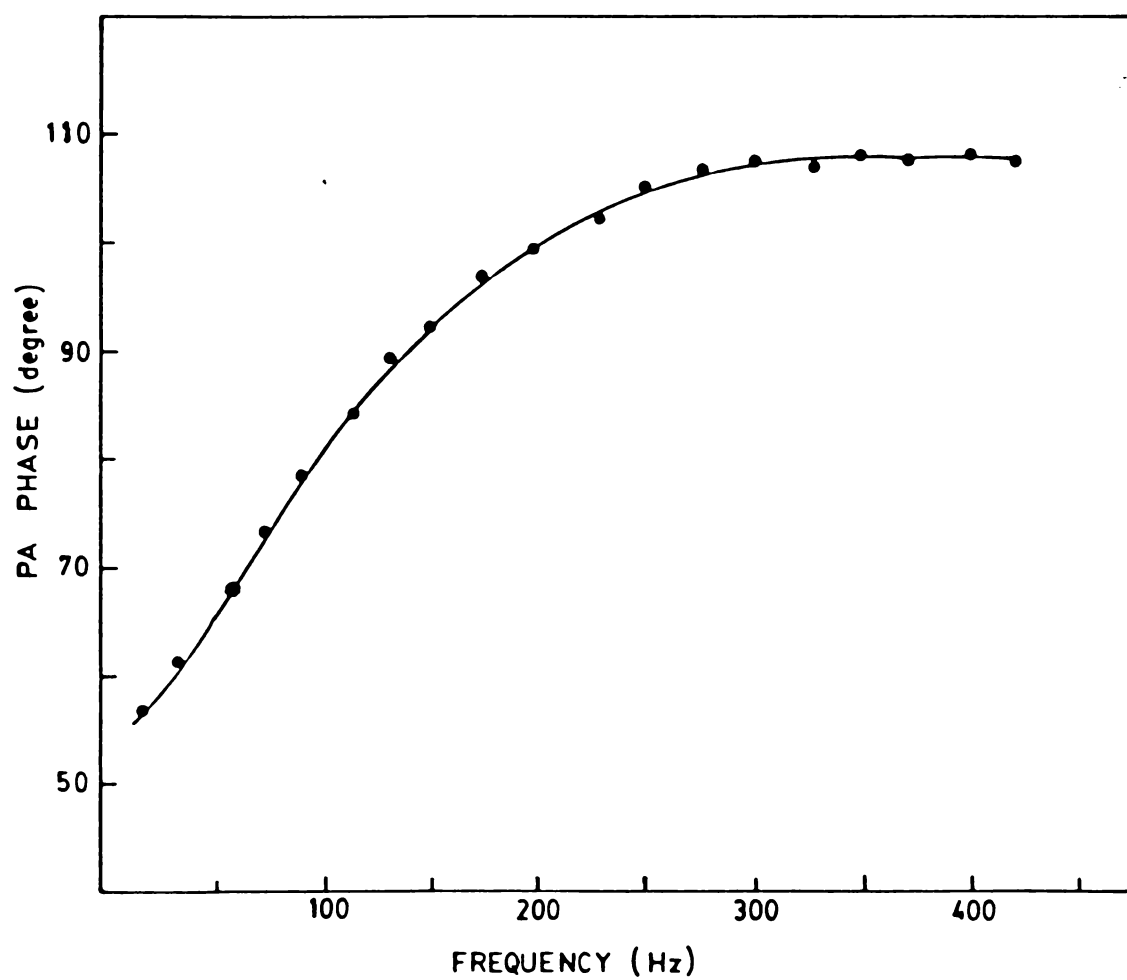


Fig.2.5 Variation of PA phase with chopping frequency for carbon black sample.

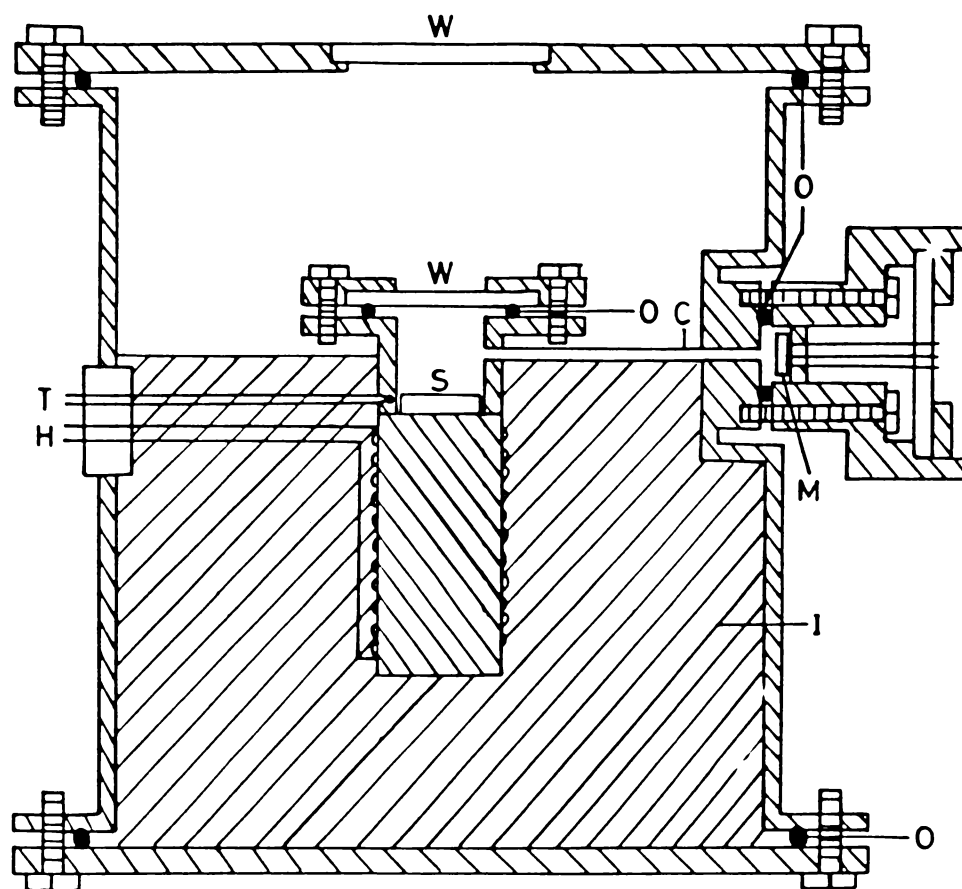
of 10 Hz. The minimum volume of the cell is ≈ 1 cc. The distance between the window and sample can be varied by moving the window holder. The resonance frequencies of the cell (longitudinal, radial and azimuthal) are very much above the operating frequency range of interest.

The cell has been calibrated using carbon black sample. For doing the calibration measurements chopped light beam is focused on the sample and PA signal amplitude and phase have been measured. The log-log plot of the PA signal amplitude versus chopping frequency with a carbon black sample is shown in Fig.2.4. This plot clearly shows the ω^{-1} dependence of the PA signal as predicted by the RG theory [95] for optically opaque materials. The corresponding variation in phase is shown in Fig.2.5. For a saturated PA signal the RG theory predicts the phase shift at the sample surface to be a constant, viz. $-\pi/2$ with respect to the modulated light beam. However, variations from this predicted phase can be caused by the system electronics and the frequency dependence of signal propagation in the gas.

2.3b High temperature PA cell

For high temperature measurements we have fabricated another PA cell with which measurements can be made

upto $\approx 250^{\circ}\text{C}$. This allows us to make PA studies on amorphous semiconductors in the vicinity of their glass transition temperatures. The high temperature PA cell employs Helmholtz resonator type configuration as shown in Fig.2.6. It has a sample compartment and a separate microphone compartment, both connected by a stainless steel tube of inner diameter 1.6 mm and length 7 cm. The sample compartment is made from a brass rod of diameter 2 cm and length 6 cm. Heating wires are wound on this rod to heat the sample to the desired temperature. One end of this rod is drilled to form a sample compartment of depth 1 cm and diameter 1 cm. At the top of this compartment a glass window is provided and this volume is sealed with a silicone 'O' ring. This is the volume where the PA signal is generated. The volume of the sample chamber can be slightly adjusted by putting metal discs of appropriate thickness. Also different backing materials can be used for the sample. This sample compartment is kept inside a metallic chamber of inner diameter 15 cm and wall thickness 6 mm. The microphone compartment is attached to this outer chamber using an 'O' ring for acoustic sealing. The acoustic signal generated in the sample compartment reaches the microphone compartment through the stainless steel connecting tube. The outer chamber is thermally



- W - WINDOW
 O - 'O' RING
 M - MICROPHONE
 S - SAMPLE
 I - INSULATING MATERIAL
 C - STEEL TUBE
 T - THERMOCOUPLE
 H - HEATER

Fig.2.6 The high temperature PA cell.

insulated from the sample compartment using suitable insulating materials. The sample temperature is measured using an iron-constantan thermocouple placed close to the sample. The electrical connections are taken through the walls of the outer chamber through teflon insulator. The thermocouple and the heating element can be connected to a temperature controller. With this design the heating of the microphone is completely avoided. The total volume of the sample cell is about 1 cc.

The initial calibration of this cell has also been done using carbon black sample. Frequency response of the cell has been studied over a wide chopping frequency range and temperature. In Fig.2.7 the variation of PA signal amplitude, for carbon black sample, with chopping frequency is plotted for two different temperatures. The corresponding variation in phase is plotted in Fig.2.8. The general behaviour is the same at the two temperatures except for a slight shift of the acoustic resonance frequency towards higher frequency side at higher temperature. For carbon black sample the PA signal is completely saturated and the PA signal amplitude should decrease with increase in chopping frequency [95]. This is the case for

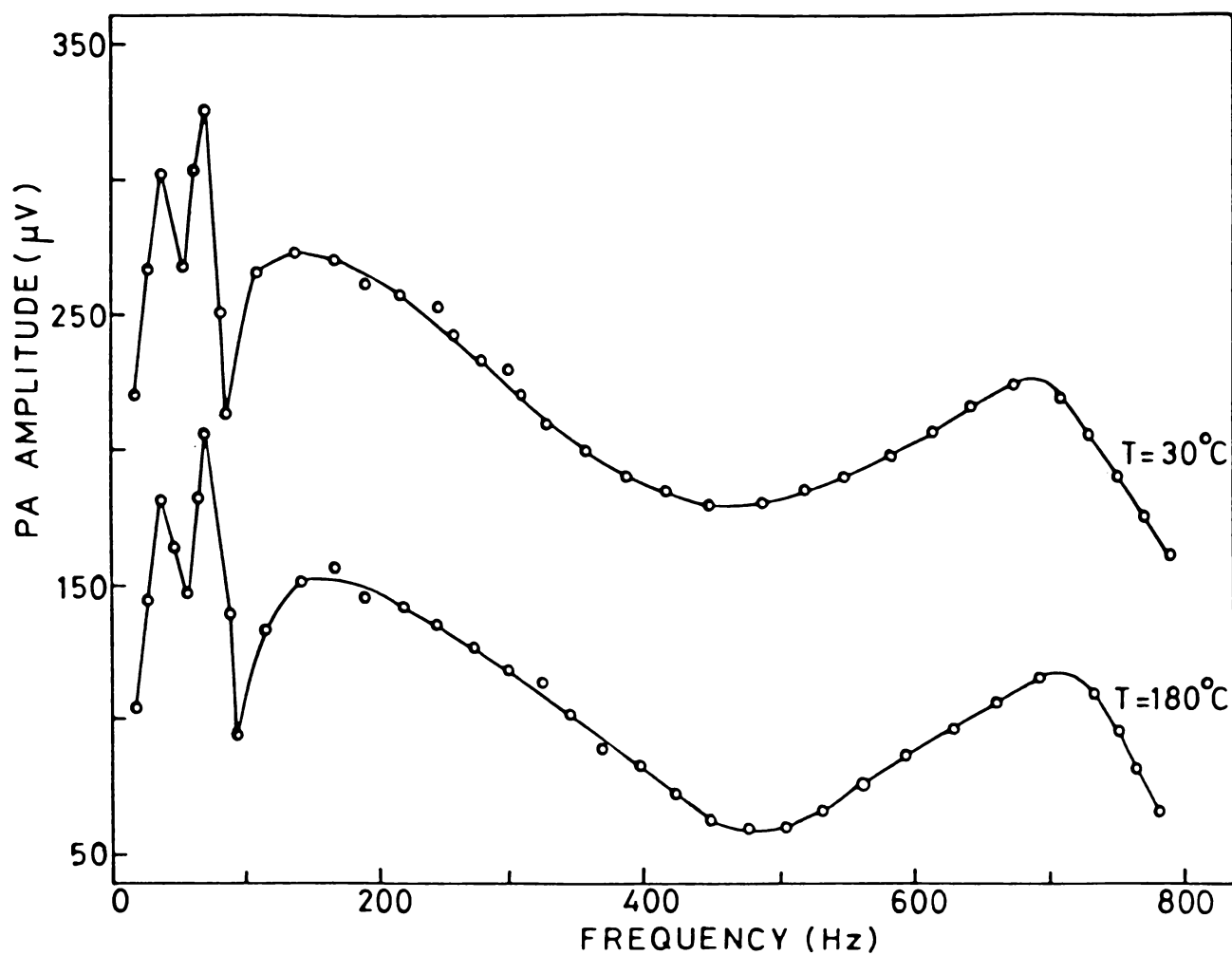


Fig.2.7 Variation of PA signal amplitude with chopping frequency for carbon black sample measured using high temperature PA cell.

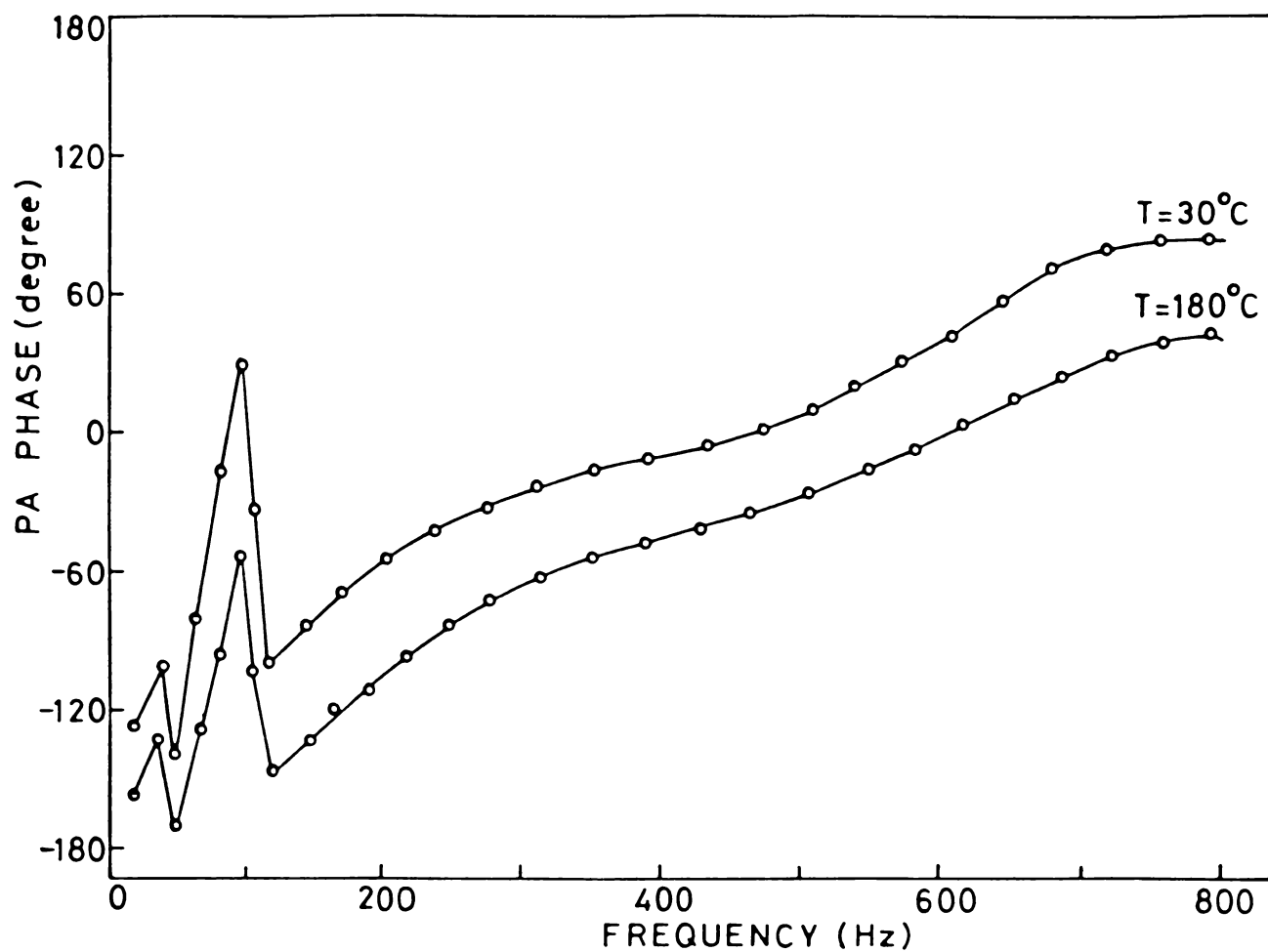


Fig.2.8 Variation of PA phase with chopping frequency for carbon black sample measured using high temperature PA cell.

intermediate frequencies in Fig.2.7. The fluctuations in the amplitude observed at lower frequencies can be attributed to acoustic damping in the sound transmitting channel. The resonance frequency of the cell calculated using eqn. (2.3) is 700 Hz which can be slightly varied by changing the cell volume. As can be seen in Fig.2.7 the amplitude versus frequency plot shows an enhancement of the PA signal amplitude around this frequency. The effect of the cell resonance is reflected also in the PA signal phase versus chopping frequency plot (shown in Fig.2.8). The temperature dependent variations of PA signal amplitude and phase for two different frequencies are shown in Fig.2.9 and Fig.2.10 respectively. As the temperature is increased the PA signal amplitude decreases and the phase shift increases. This is mainly due to the temperature dependence of the sample parameters and sound attenuation in the transmitting gas column.

The PA spectrometer, consisting of the modules described above has been set up on a sturdy table which helps to isolate building vibrations to a large extent. The performance of the PA spectrometer is found to be very good.

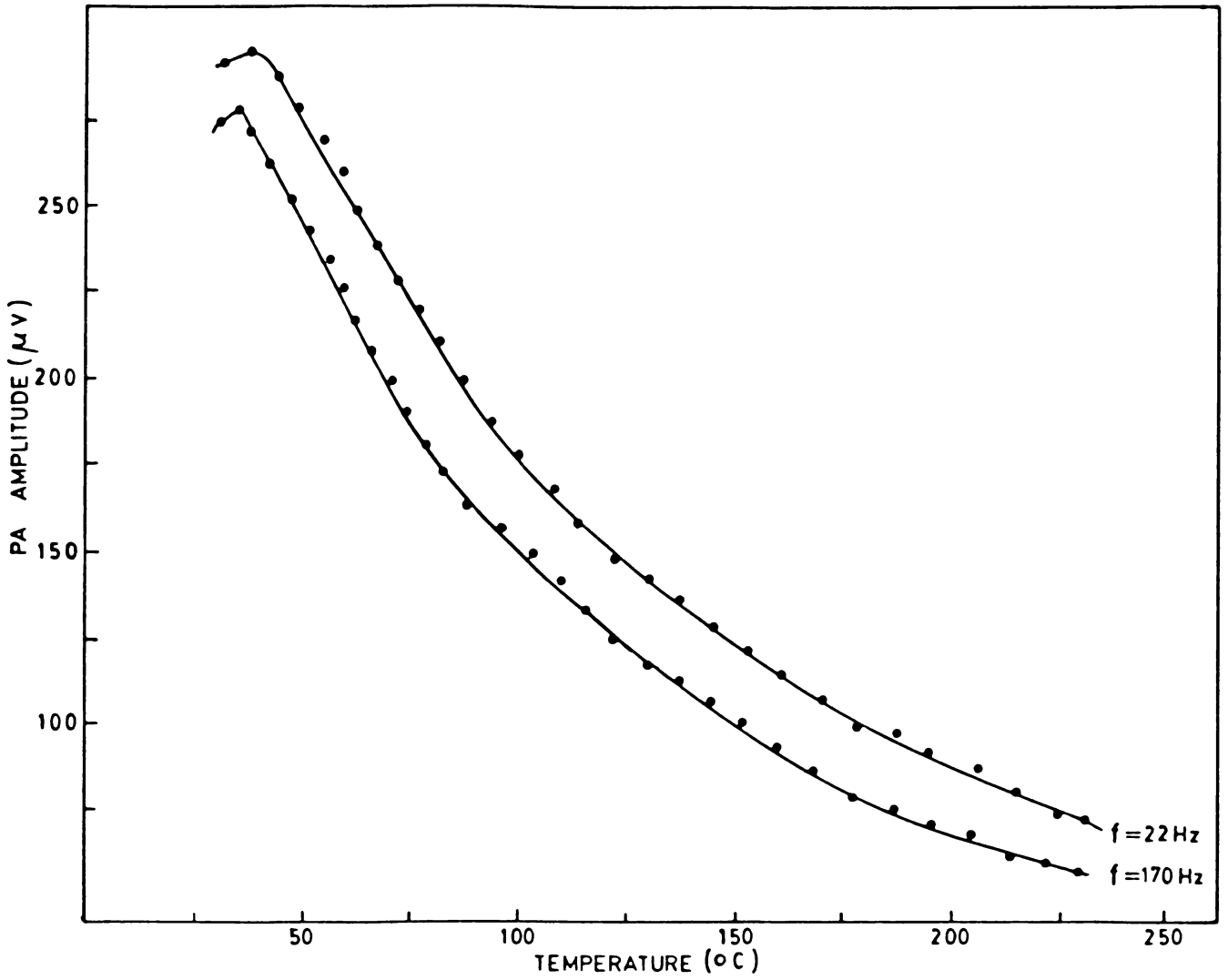


Fig.2.9 Variation of PA signal amplitude with temperature for carbon black sample.

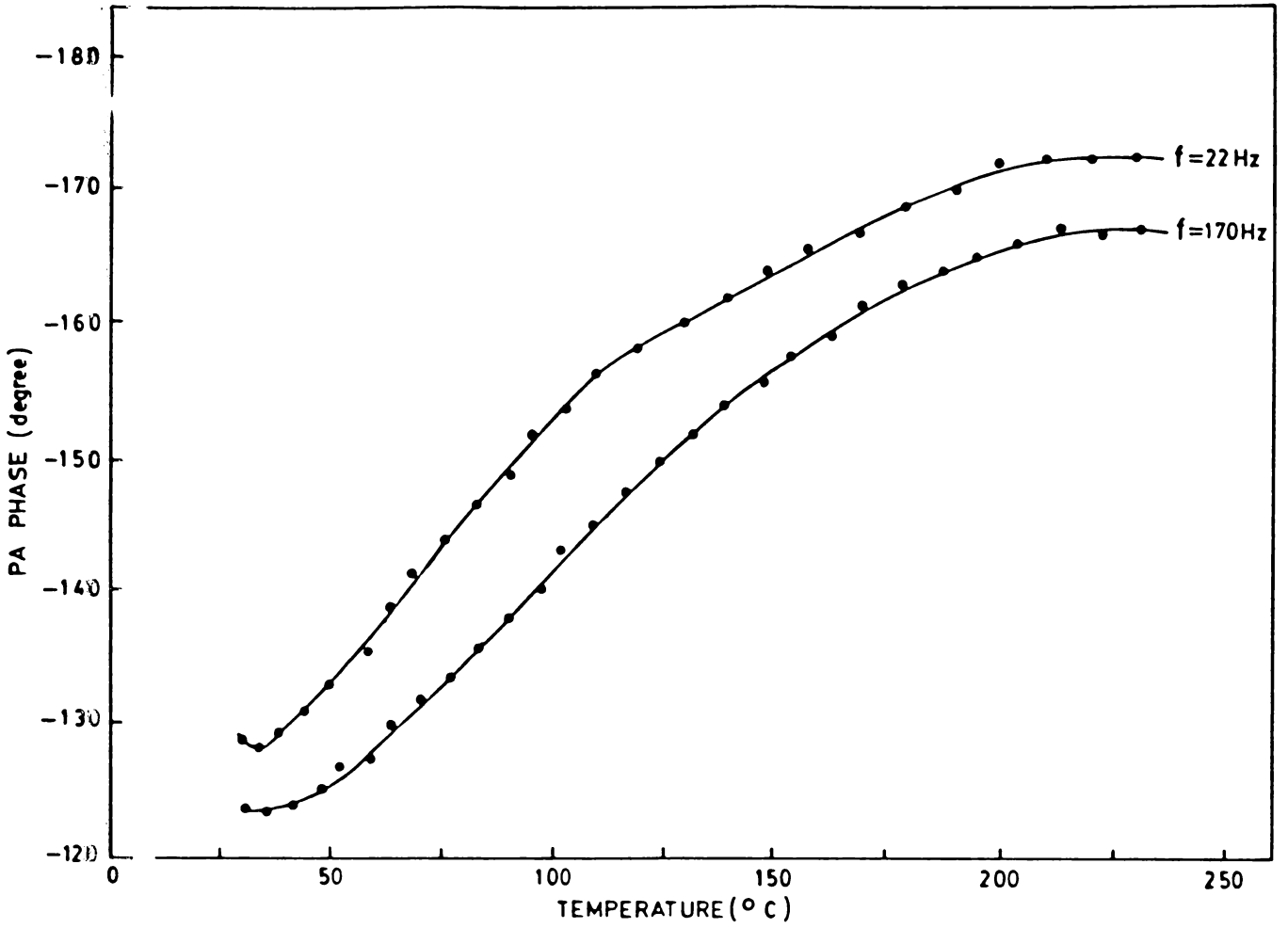


Fig. 2.10 Variation of PA phase with temperature for carbon black sample.

Chapter 3

COMPOSITION DEPENDENCE OF THE OPTICAL ENERGY GAP

IN A^{IV}B^{VI} GLASSES

3.1 INTRODUCTION

Chalcogenide glasses find extensive applications as materials for electronic and optoelectronic devices [39,159]. One advantage of these materials is that they can be prepared over a very wide composition range. Their physical properties do change with composition enabling composition dependent tunability of the physical properties. So an understanding of the composition dependence of their physical properties is necessary to select the proper composition for the desired application.

Germanium and silicon form good glasses with chalcogen elements such as selenium, tellurium, sulphur etc. over a reasonably wide composition range. Several of such glasses are found to exhibit interesting physical properties like electrical switching [24,160] and photo-structural transformations [161]. Of late, several workers have reported observation of anomalous behaviour in certain

physical properties at specific compositions. For the $A_x^{IV}B_{1-x}^{VI}$ system (A is a group IV element such as Ge or Si and B is a group VI element such as Se, Te or S) such anomalies have been observed at $x = 0.2$ and $x = 0.33$. Anomalies have been reported in density, coefficient of thermal expansion, infrared and Raman spectra, Mössbauer site intensities, photoluminescence intensity, crystallization behaviour, low to high conductivity transition pressure, electrical activation energy, refractive index etc. [162-172] at $x = 0.2$ or 0.33 . These results provide a great deal of information about the short range order, glass forming tendency, network stiffening etc. of these systems [173].

We have carried out a systematic investigation of the composition dependence of the optical energy gap E_o in bulk $A_x^{IV}B_{1-x}^{VI}$ glasses using PA technique. As has been discussed in chapter 1, PAS has proved to be a very effective method for the study of semiconducting samples, both crystalline and amorphous [132,174-177]. The advantages of PA technique over conventional spectroscopic techniques make it suitable for the study of glassy semiconductors. Since amorphous semiconductors are highly absorbing in the fundamental absorption region it is difficult

to use reflection or transmission type spectroscopies, especially for bulk samples. Also the PA technique is sensitive enough to probe the low absorption region. This is important in the case of amorphous semiconductors because the absorption in the low absorption coefficient region is associated with the disorder in the material.

In this chapter we describe the optical energy gap measurements done at room temperature on different glasses belonging to the $A^{IV}B^{VI}$ family. Measurements have been done on Ge_xSe_{1-x} , Ge_xTe_{1-x} and Si_xTe_{1-x} glasses. In each group measurements are reported on a number of compositions. Experimental details, results obtained and their discussion are given below.

3.2 EXPERIMENTAL DETAILS

Among the $A^{IV}B^{VI}$ class of chalcogenide glasses, PA investigations have been carried out on several compositions in the glass forming region of Ge_xTe_{1-x} ($0.15 \leq x \leq 0.28$), Si_xTe_{1-x} ($0.10 \leq x \leq 0.28$) and Ge_xSe_{1-x} ($0.10 \leq x \leq 0.38$) glasses.

3.2a Sample preparation

The samples are prepared using the conventional

melt quenching technique. Appropriate quantities of the constituent elements having 99.999% purity are sealed in evacuated quartz ampoule. Then the ampoule is kept in a furnace at about 1200 K for about 24 hours. The ampoule is periodically rotated at a speed of 10-12 rpm for homogeneous mixing of the constituents. The ampoule is subsequently quenched in ice water or NaOH + ice water mixture and then broken to take out the sample. The amorphous nature of the sample is confirmed by X-ray diffractometry. Properly shaped samples are placed in the PA cell for measurements. For recording the PA spectrum, powder samples are found to be good enough.

3.2b Photoacoustic measurements

The PA spectrometer already described in chapter 2 has been used for the present investigations. For recording the PA spectrum of a sample, first of all, the PA signal amplitude as a function of the wavelength of the exciting radiation is measured at a fixed chopping frequency. The chopping frequency used is 70 Hz. The power spectrum of the light source has initially been recorded as the variation of the PA signal amplitude for a carbon black sample as a function of wavelength at the same chopping frequency. The normalized PA signal is obtained by dividing the

measured signals from the sample by that from the carbon black sample at corresponding wavelengths. The PA spectrum of the sample is then obtained by plotting the normalized PA signal as a function of wavelength of the incident radiation.

3.3 PHOTOACOUSTIC SPECTRA OF $A_x^{IV}B_{1-x}^{VI}$ GLASSES

The PA spectra recorded for Ge_xTe_{1-x} ($x = 0.15, 0.17, 0.20, 0.22, 0.25, 0.28$), Si_xTe_{1-x} ($x = 0.10, 0.15, 0.17, 0.20, 0.22, 0.25, 0.28$) and Ge_xSe_{1-x} ($x = 0.10, 0.15, 0.20, 0.25, 0.28, 0.33, 0.38$) glasses are shown in Figs.3.1 to 3.6. These spectra give information about the optical absorption features of the samples. The normalized PA signal increases from the higher wavelength (lower photon energy) side and reaches a saturation level for photon energy $h\nu > E_o$, where E_o is the optical energy gap. As explained by Tauc [75] there are three different regions in the optical absorption curve for an amorphous semiconductor corresponding to three different ranges of the absorption coefficient β . A very high value of the absorption coefficient ($\beta \geq 10^4 \text{ cm}^{-1}$) characterises the region where the normalized PA signal gets saturated. RG theory [95] predicts this type of behaviour for highly absorbing

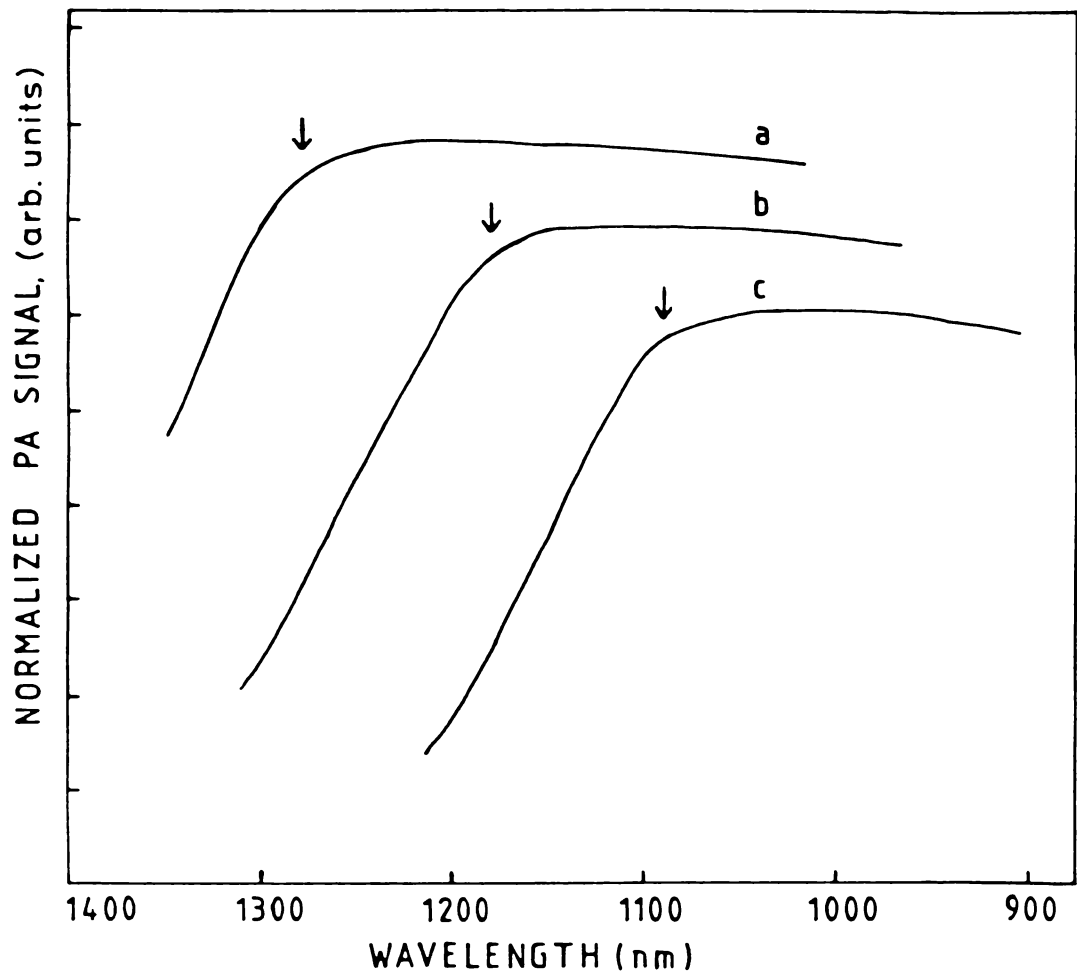


Fig.3.1 PA spectra of $\text{Ge}_x\text{Te}_{1-x}$ glasses. (a) $\text{Ge}_{0.15}\text{Te}_{0.85}$
(b) $\text{Ge}_{0.17}\text{Te}_{0.83}$, (c) $\text{Ge}_{0.20}\text{Te}_{0.80}$.

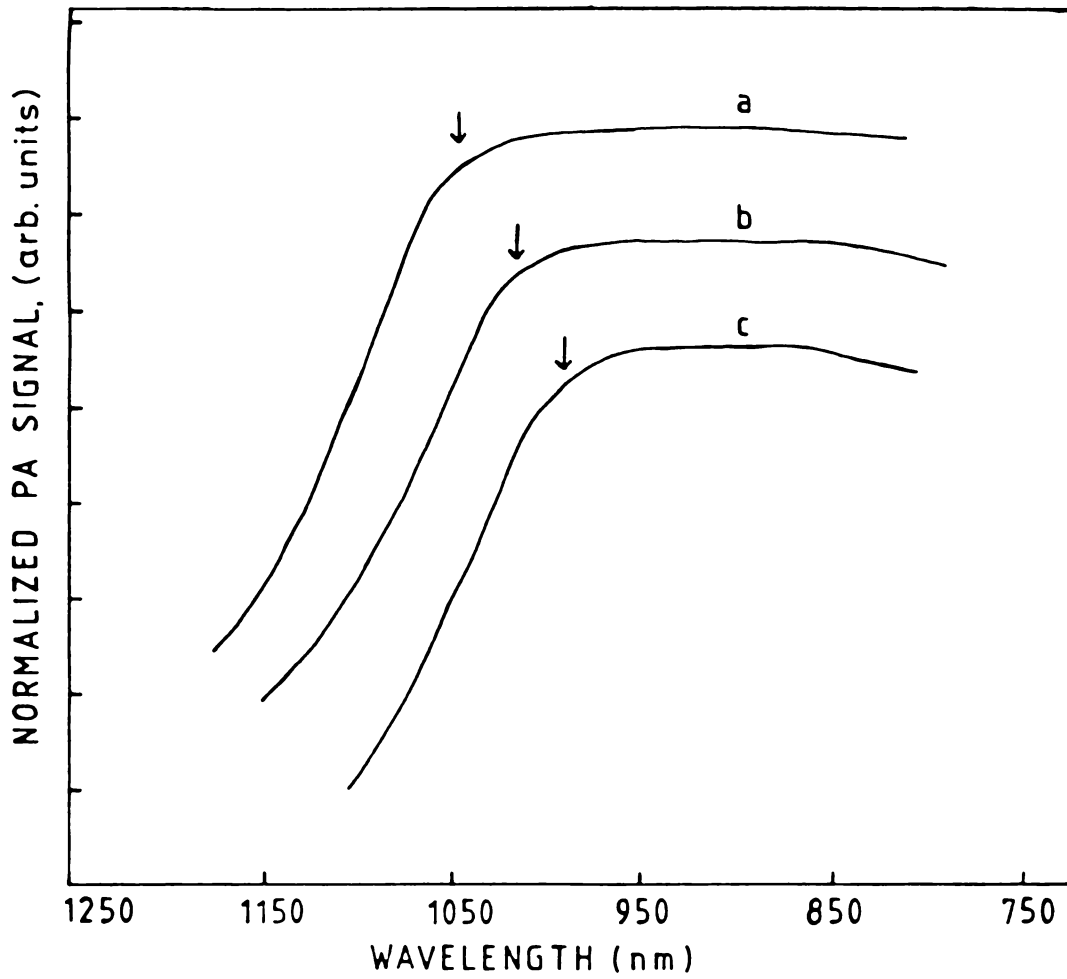


Fig.3.2 PA spectra of $\text{Ge}_x\text{Te}_{1-x}$ glasses. (a) $\text{Ge}_{0.22}\text{Te}_{0.78}$, $\text{Ge}_{0.25}\text{Te}_{0.75}$, (c) $\text{Ge}_{0.28}\text{Te}_{0.72}$.

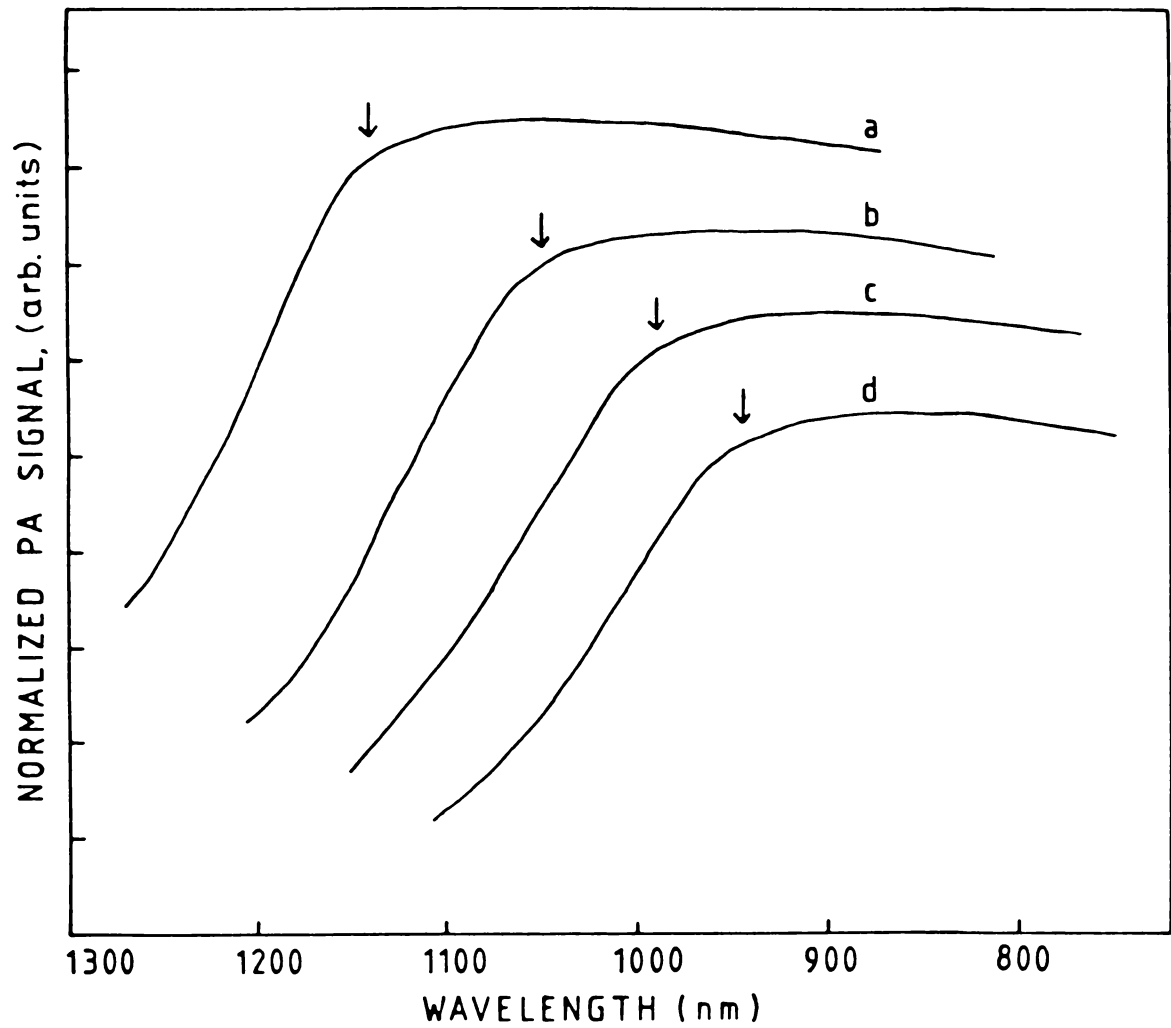


Fig.3.3 PA spectra of $\text{Si}_x\text{Te}_{1-x}$ glasses. (a) $\text{Si}_{0.10}\text{Te}_{0.90}$,
(b) $\text{Si}_{0.15}\text{Te}_{0.85}$, (c) $\text{Si}_{0.17}\text{Te}_{0.83}$, (d) $\text{Si}_{0.20}\text{Te}_{0.80}$.

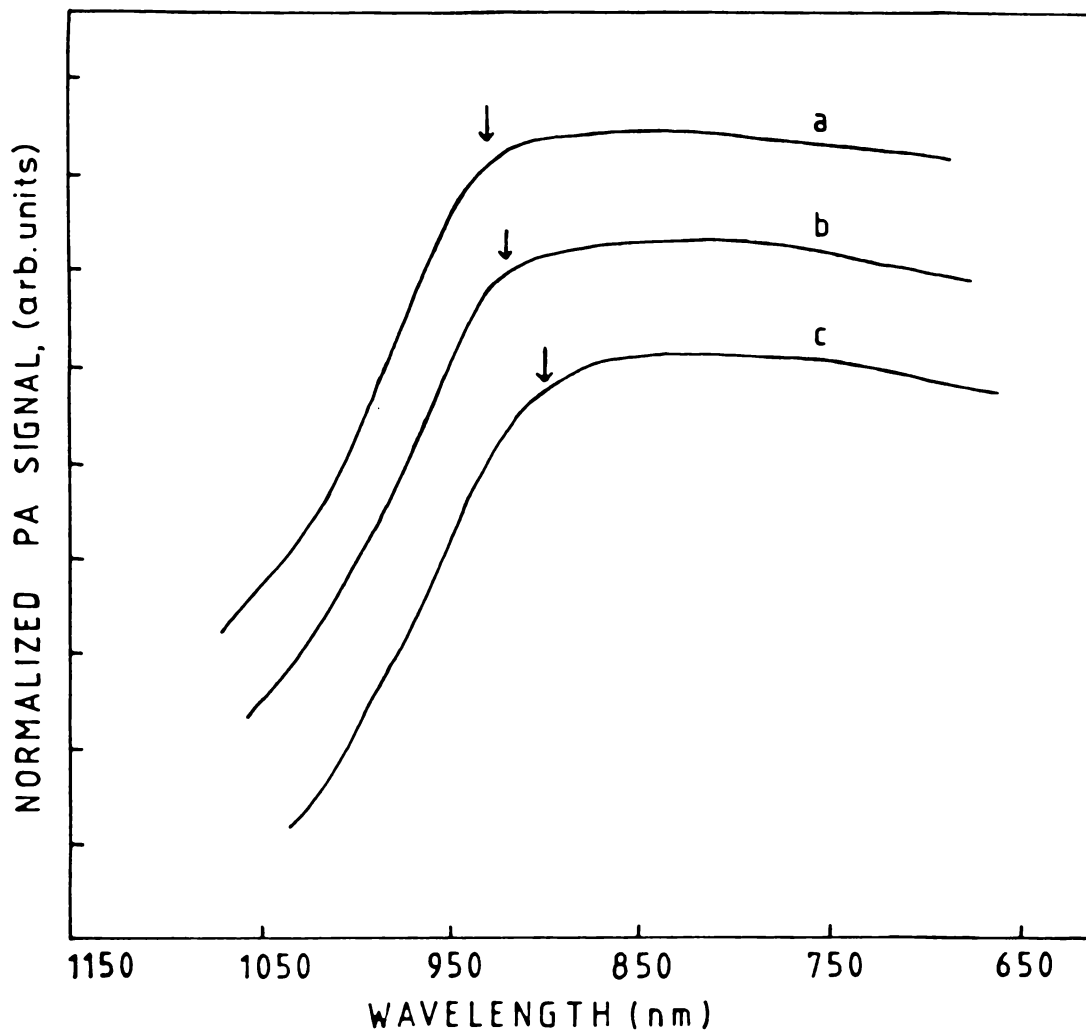


Fig.3.4 PA spectra of $\text{Si}_x\text{Te}_{1-x}$ glasses. (a) $\text{Si}_{0.22}\text{Te}_{0.78}$,
(b) $\text{Si}_{0.25}\text{Te}_{0.75}$, (c) $\text{Si}_{0.28}\text{Te}_{0.72}$.

-GATE-

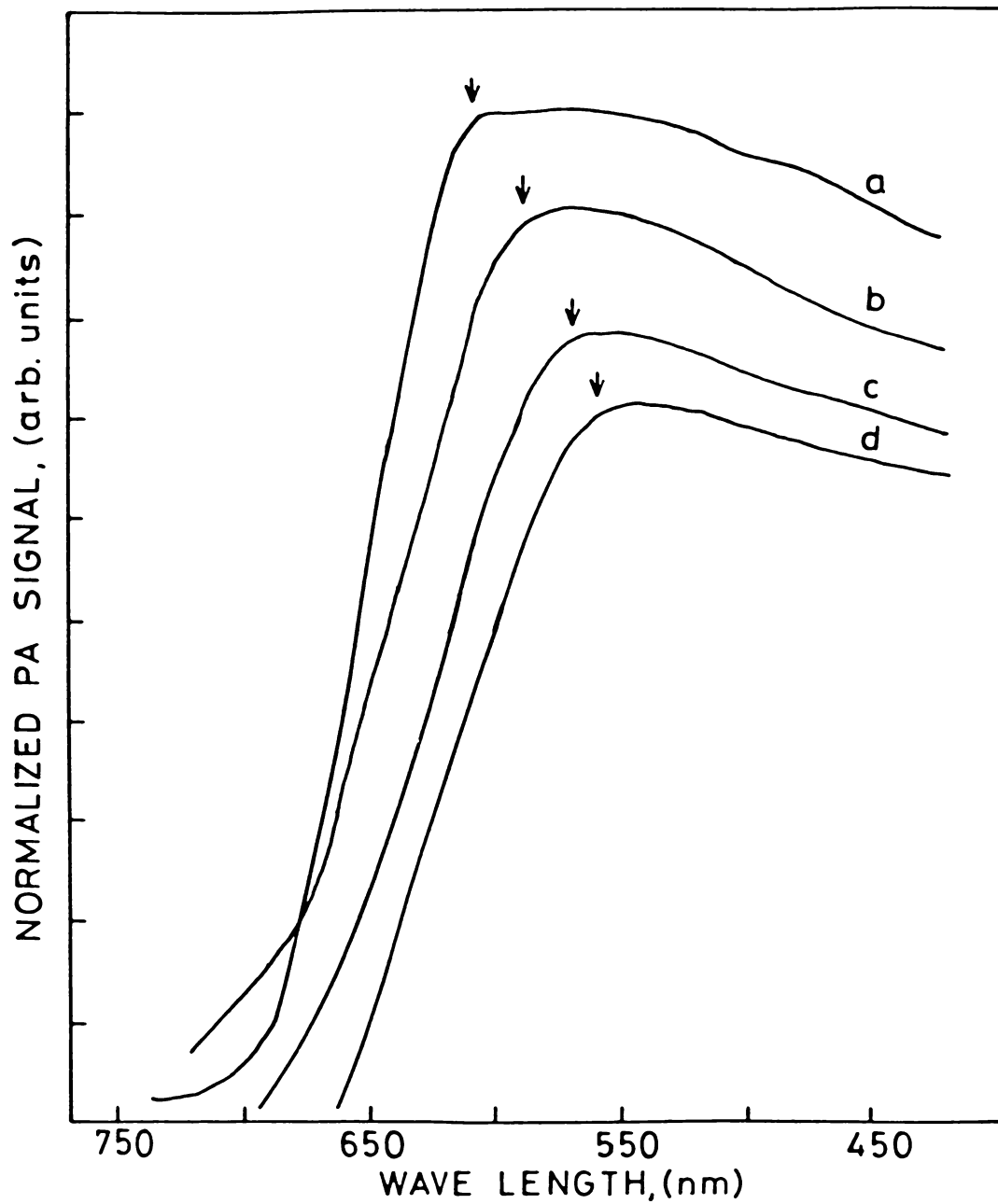


Fig. 3.5 PA spectra of $\text{Ge}_x\text{Se}_{1-x}$ glasses. (a) $\text{Ge}_{0.10}\text{Se}_{0.90}$, (b) $\text{Ge}_{0.15}\text{Se}_{0.85}$, (c) $\text{Ge}_{0.20}\text{Se}_{0.80}$, (d) $\text{Ge}_{0.25}\text{Se}_{0.75}$.

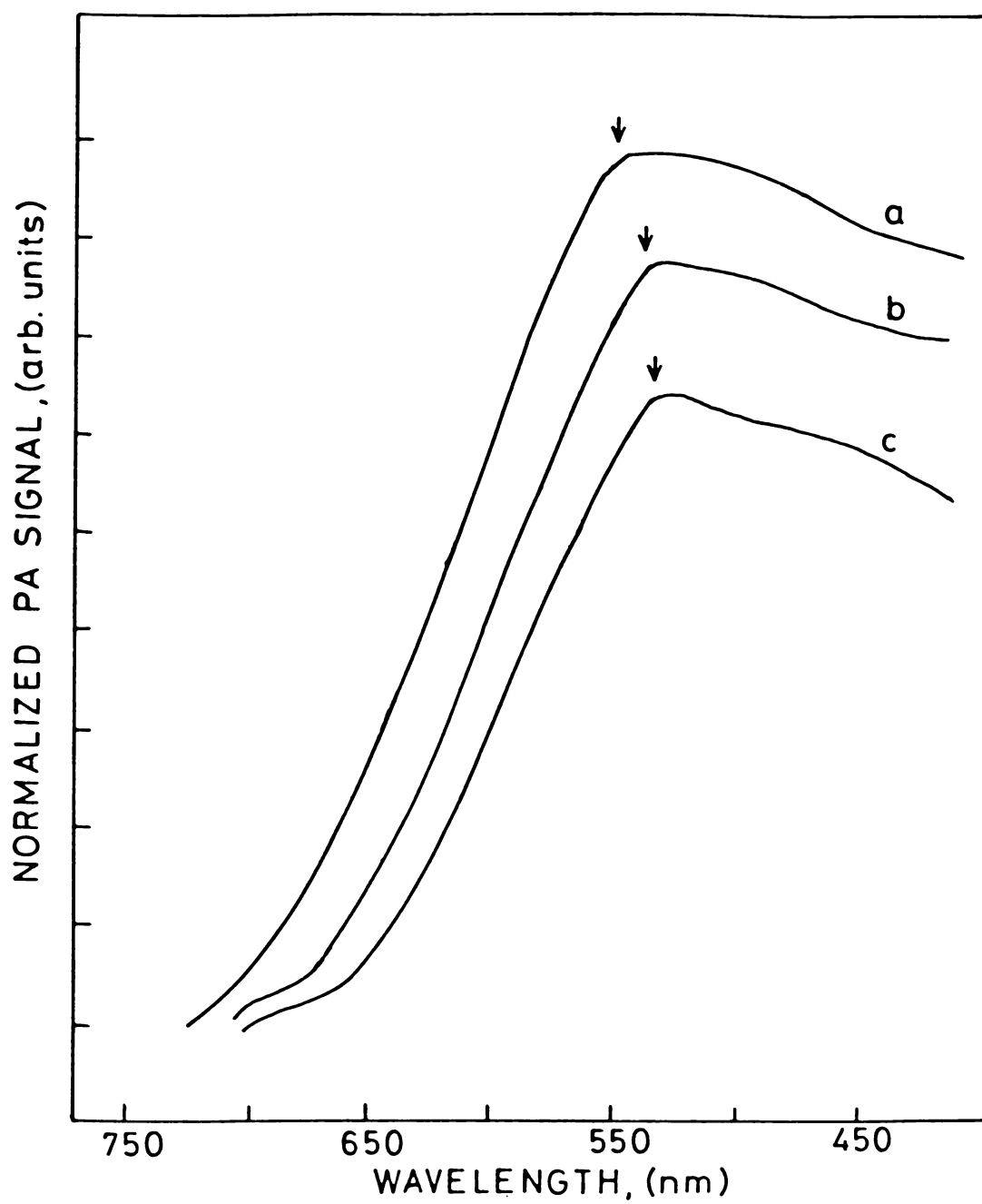


Fig.3.6 PA spectra of $\text{Ge}_x\text{Se}_{1-x}$ glasses. (a) $\text{Ge}_{0.28}\text{Se}_{0.72}$,
(b) $\text{Ge}_{0.38}\text{Se}_{0.62}$, (c) $\text{Ge}_{0.33}\text{Se}_{0.67}$.

samples with $l_{\beta} < l_s$ and $\mu_s > l_{\beta}$. This corresponds to the power law absorption region [75] and the absorption coefficient β has an energy dependence given by

$$h\nu\beta(h\nu) = B(h\nu - E_0)^2 \quad (3.1)$$

where B is a constant [24].

A slight decrease in the normalized PA signal in the saturation region has been observed in the case of Ge-Se samples which only indicates increased reflection of the incident light from the sample. This has been confirmed by recording the PA spectra in the saturation region for samples with roughened surface as well where the reflection is considerably reduced. Fig.3.7 shows PA spectrum for a representative sample ($\text{Ge}_{0.15}\text{Se}_{0.85}$) with smooth and roughened surfaces.

The absorption edge in amorphous semiconductors has an exponential part associated with disorder induced potential fluctuations which extends in the absorption coefficient range $1 \text{ cm}^{-1} \leq \beta \leq 10^4 \text{ cm}^{-1}$. The absorption in this region depends on the photon energy according to

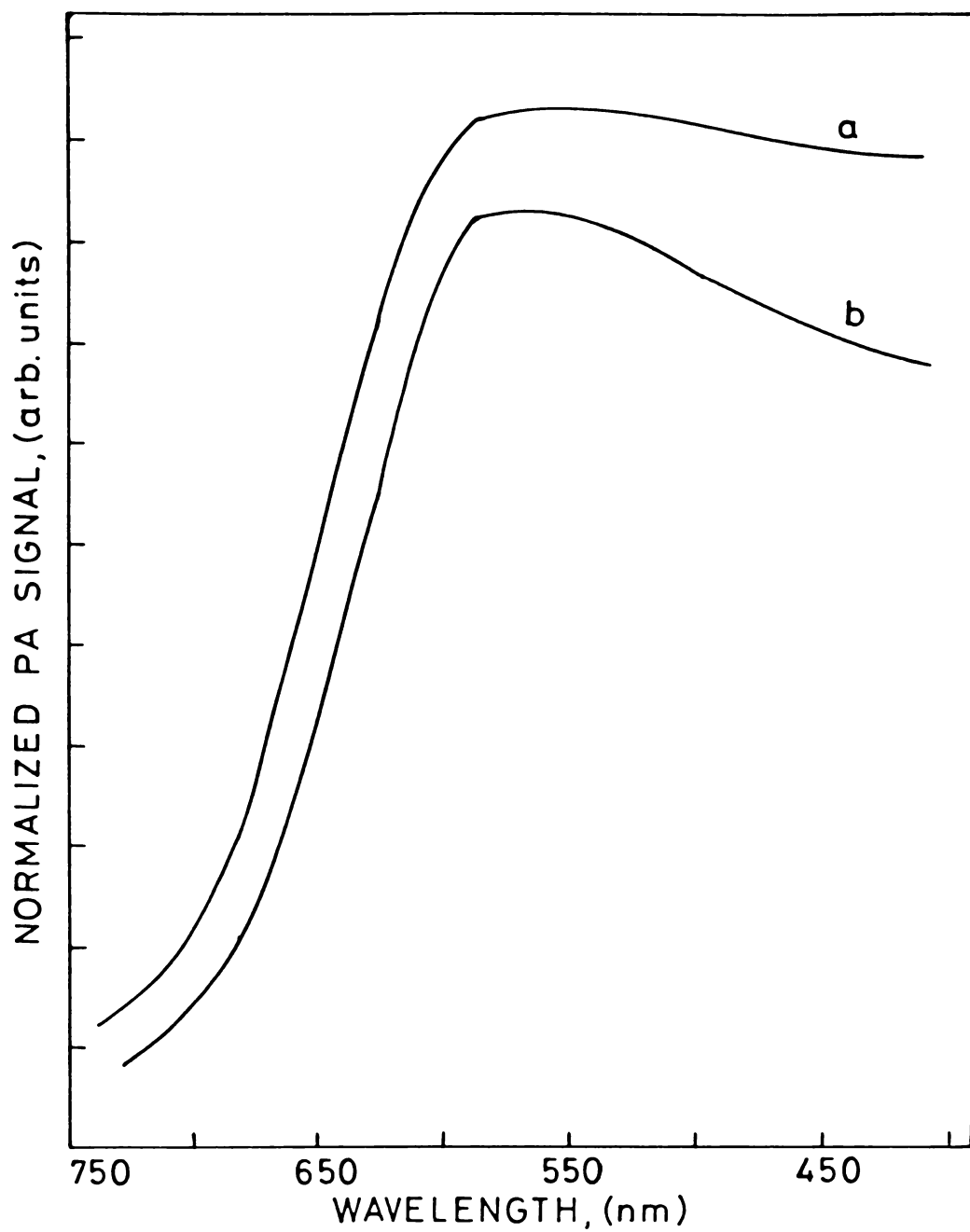


Fig.3.7 PA spectrum of $\text{Ge}_{0.15}\text{Se}_{0.85}$ sample.
(a) Roughened surface, (b) Smooth surface.

the relation [75]

$$\beta(h\nu) = \beta_0 \exp(h\nu/E) \quad (3.2)$$

where E characterises the slope of the exponential absorption region. In the PA spectra this corresponds to the region where the normalized PA signal increases with photon energy. In this region the normalized PA signal is proportional to the absorption coefficient as predicted by RG theory for the case of optically transparent solids [95]. The plot of the logarithm of the normalized PA signal versus the photon energy shows a straight line in this region. In Fig.3.8 such plots for a few representative samples ($\text{Ge}_{0.33}\text{Se}_{0.97}$, $\text{Ge}_{0.20}\text{Se}_{0.80}$ and $\text{Ge}_{0.10}\text{Se}_{0.90}$) are shown.

The weak absorption tail region with $\beta < 1 \text{ cm}^{-1}$, where the absorption depends upon the preparation, purity and thermal history of the material is not of much interest in the present studies and so is not discussed any further. A comparison between the PA spectrum and the conventional optical absorption spectrum [24,75] of the chalcogenide glasses shows that the two match very well

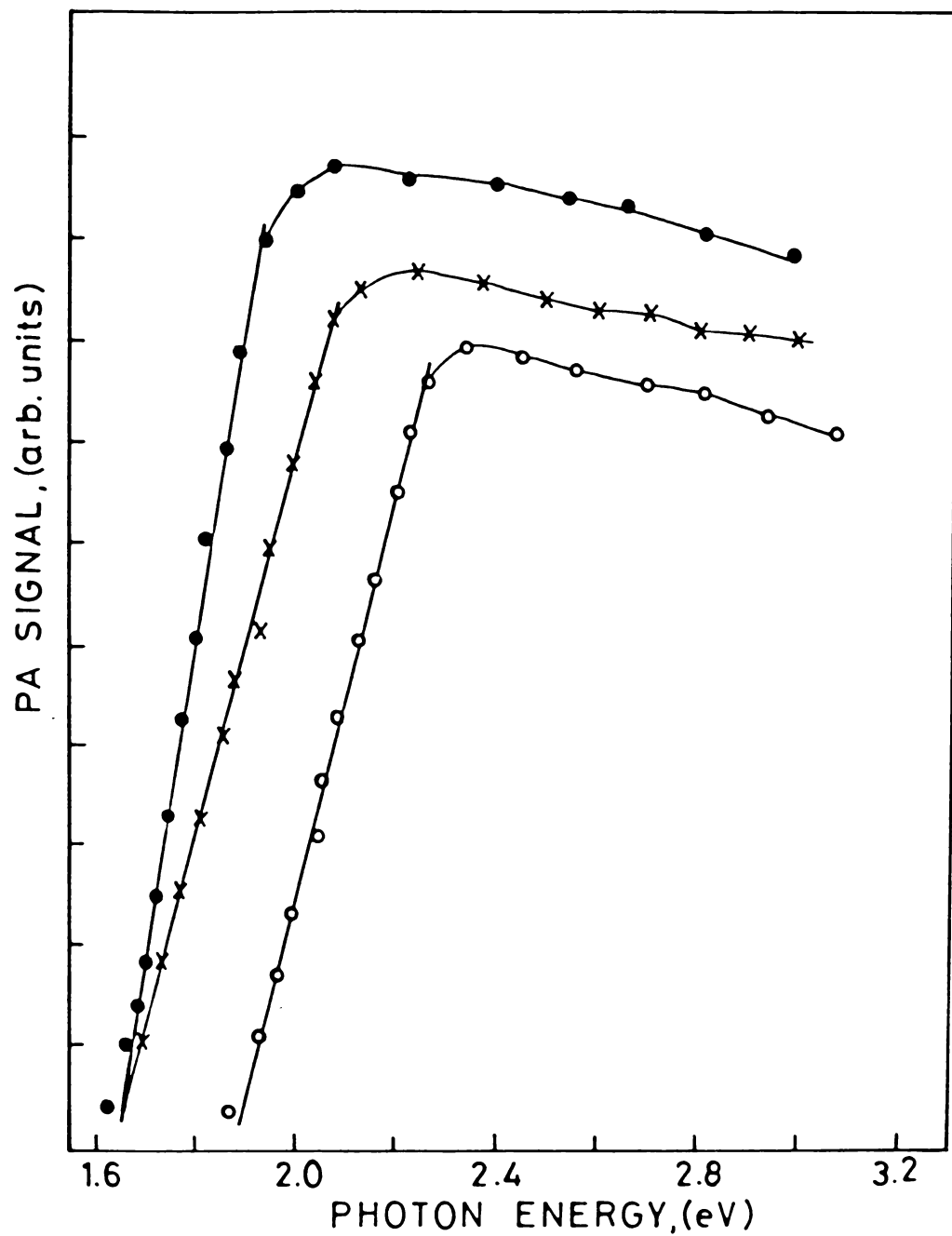


Fig.3.8 Plot of log PA amplitude versus incident photon energy. (○) $\text{Ge}_{0.33}\text{Se}_{0.67}$, (X) $\text{Ge}_{0.20}\text{Se}_{0.80}$, (●) $\text{Ge}_{0.10}\text{Se}_{0.90}$.

and the quantitative correlation between them is very good in the three regions. This has been verified by us and previously by Monahan and Nolle [103] in As_2S_3 powder samples by measuring the absorption coefficient β over a wide range from 10 cm^{-1} to more than 10^4 cm^{-1} using PA technique.

The optical energy gap E_o of all the samples investigated has been determined from the PA spectra. This has been done graphically by drawing the tangents to the wavelength versus PA signal plots at the PA saturation region and the region where absorption increases exponentially with photon energy [174]. The point where the two tangents meet corresponds to E_o . Thus the PA spectra provide valuable information about the optical absorption over a wide range of optical absorption coefficient and enable us to determine the optical energy gap.

3.4 OPTICAL ENERGY GAP OF A^{IV}B^{VI} SYSTEMS

3.4a $\text{Ge}_x\text{Te}_{1-x}$ and $\text{Si}_x\text{Te}_{1-x}$ glasses

A detailed study of the variation of the optical energy gap E_o with composition in bulk $\text{Ge}_x\text{Te}_{1-x}$ and $\text{Si}_x\text{Te}_{1-x}$ glasses has not been reported so far. However, the study of optical and electrical properties of amorphous thin

film Ge-Te samples done by Bahl and Chopra [178] and the studies on electrical, optical and structural properties of some compositions of Si-Te glasses done by Peterson et al [172] have revealed the difference between crystalline and amorphous samples. The optical energy gap E_o of Ge_xTe_{1-x} and Si_xTe_{1-x} glasses determined from the present investigations are tabulated in Table 3.1. The values plotted as a function of the composition parameter x are shown in Figs. 3.9 and 3.10 respectively. It can be seen that the value of E_o decreases when the Te content increases for these systems. But the rate at which this decrease takes place is higher for compositions with $x < 0.2$ than for those with $x > 0.2$ in both the systems. This change in slope in E_o versus x plot at $x = 0.2$ indicates that a change in the electronic properties do take place at this composition.

The observed behaviour can be explained on the basis of chemical bonding between the atoms and changes in the short range order taking place in the glass network when the Ge or Si concentration increases. Ever since Ioffe [179] pointed out that the basic electronic properties of a solid are determined primarily by the nature of the short range order, the chemical bond approach has been

Table 3.1: Values of the average coordination number m and optical energy gap E_o for Ge_xTe_{1-x} and Si_xTe_{1-x} glasses.

Composition	m	E_o (eV)
$Ge_{0.28}Te_{0.72}$	2.56	1.25
$Ge_{0.25}Te_{0.75}$	2.50	1.22
$Ge_{0.22}Te_{0.78}$	2.44	1.18
$Ge_{0.20}Te_{0.80}$	2.40	1.14
$Ge_{0.17}Te_{0.83}$	2.34	1.05
$Ge_{0.15}Te_{0.85}$	2.30	0.97

$Si_{0.28}Te_{0.72}$	2.56	1.38
$Si_{0.25}Te_{0.75}$	2.50	1.35
$Si_{0.22}Te_{0.78}$	2.44	1.33
$Si_{0.20}Te_{0.80}$	2.40	1.31
$Si_{0.17}Te_{0.83}$	2.34	1.25
$Si_{0.15}Te_{0.85}$	2.30	1.18
$Si_{0.10}Te_{0.90}$	2.20	1.09

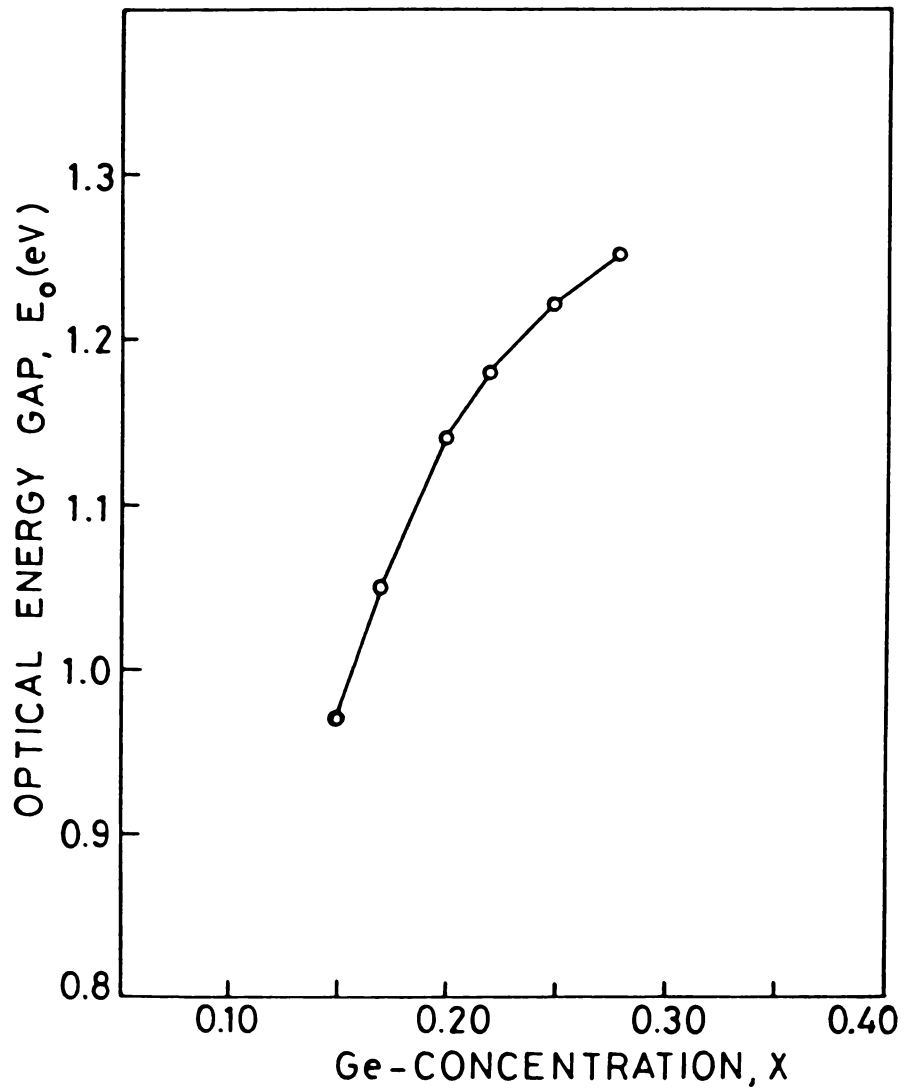


Fig.3.9 Variation of optical energy gap E_o with composition for $\text{Ge}_x\text{Te}_{1-x}$ glasses.

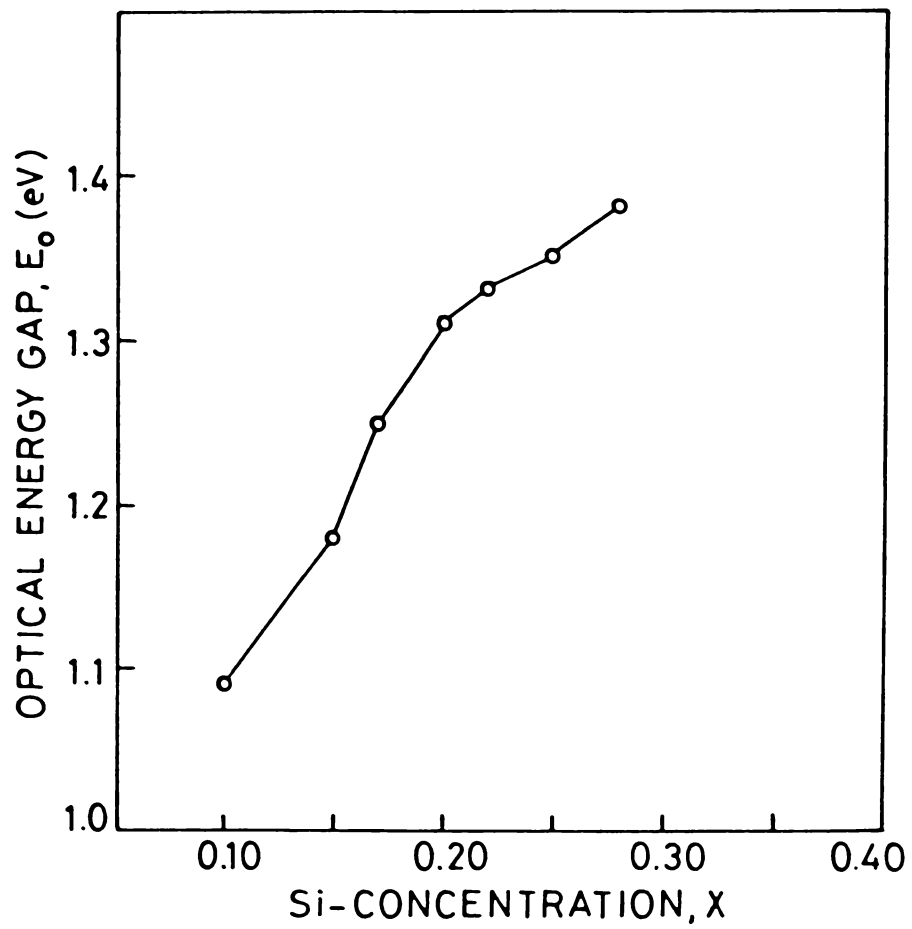


Fig.3.10 Variation of optical energy gap E_0 with composition for $\text{Si}_x\text{Te}_{1-x}$ glasses.

successfully used for predicting the properties of semiconductors [180,181]. Since noncrystalline solids lack long range order and their electronic properties are determined primarily by the nature of the short range order, the chemical bond approach is the right one to be adopted to explain their properties [182]. This approach has found to be useful in establishing relationships between the glass transition temperature T_g with energy band gap, atomization energy etc. [183-185]. In the following, relationship between the optical energy gap and chemical composition in chalcogenide glasses are examined based on chemical bonding aspects.

The electronic states in solids can be considered as the broadened superposition of the molecular orbital states of the constituent bonds. In chalcogenide glasses containing high concentration of chalcogen element the lone pair states associated with chalcogen atoms form the top of the valence band and the antibonding states form the conduction band [182,186,187]. The optical energy gap corresponds closely to the energy difference between the top of the valence band and the bottom of the conduction band. Therefore the variation of optical energy gap with

the composition parameter is directly related to the chemical bond energy.

For a binary alloy system A_xB_{1-x} , considering that the local atomic coordinations satisfy the 8-N rule for normal covalent bonding, there are two distinctively different ways to specify the distribution of the three bond types A-A, A-B and B-B. These are the random covalent network model [188] and chemically ordered network model [189,190]. The random covalent bonding description includes A-B, A-A and B-B bonds at all compositions other than $x = 0$ and $x = 1$. For explaining our results the chemically ordered network (CON) model is found to be more appropriate. The CON model for bond statistics emphasises the relative bond energies and is based on the assumption that the heteropolar A-B bonds are favoured at all compositions. At the stoichiometric compound composition with $x = x_c$ the system contains only A-B bonds. When $x > x_c$ the network contains A-B and A-A bonds whereas for $x < x_c$ it contains A-B and B-B bonds.

Variation of the optical energy gap in Ge_xTe_{1-x} and Si_xTe_{1-x} glasses is explained below based on the CON model. Taking the coordination numbers of Ge and Si as 4 and that of Te as 2 the compound composition corresponds

to $x_c = 0.33$. The composition range over which the investigations are carried out lies below x_c . Therefore in the chalcogen rich composition range of $\text{Ge}_x\text{Te}_{1-x}$ glasses, both Ge-Ge and Te-Te bonds are present. Similarly for $\text{Si}_x\text{Te}_{1-x}$ system in this range Si-Si and Te-Te bonds are present. The bond energy of Ge-Ge, Ge-Te, Te-Te, Si-Si and Si-Te bonds are 49.1, 40.86, 34, 53.4 and 51.3 KCal/mol respectively [191]. Therefore the increase in the number of Te-Te bonds, when x is decreased in the range of $0 < x < 0.33$ reduces the average bond energy in both the systems. This causes a corresponding decrease in the value of E_o when x is reduced in the chalcogen rich region, as can be seen in Figs.3.9 and 3.10. The increase in the number of Te-Te bonds in this composition range has the effect of widening the lone pair band, thus reducing the optical energy gap. Here the width of the lone pair band is governed by the overlap of the lone pair orbitals.

The average coordination number m , which can be used to characterise the electronic properties, is an important parameter to be considered in order to understand the variation of E_o with composition in chalcogenide glasses. The average coordination number m for the binary alloy system A_xB_{1-x} is given by [192]

$$m = xN_A + (1-x)N_B \quad (3.3)$$

where N_A and N_B are coordination numbers of the elements A and B respectively. Also it can be expected that the average heat of atomization [193], which is a measure of the cohesive energy and represents the relative bond strengths, is correlated to properties such as energy gap. The average heat of atomization of A_xB_{1-x} alloy is given by

$$\bar{H}_S = xH_A + (1-x)H_B \quad (3.4)$$

where H_A and H_B are heats of atomization of elements A and B respectively.

We now examine the optical energy gap of chalcogenide glasses based on the two parameters \bar{H}_S and m that are related to the chemical bonding properties of the elements in the alloy. The variation of E_0 and \bar{H}_S with m for Ge_xTe_{1-x} glasses is shown in Fig.3.11. The value of m is calculated using eqn.(3.3) with $m_{Ge} = 4$ and $m_{Te} = 2$ and the value of \bar{H}_S is calculated using eqn.(3.4) with $H_{Ge} = 90$ and $H_{Te} = 46$ KCal/gram-atom [193]. The variation of E_0 with m follows the same behaviour as E_0 with x . The value of m corresponding to $x = 0.2$, where the change in slope in the variation of E_0 takes place, is 2.4. However, \bar{H}_S increases with m linearly without

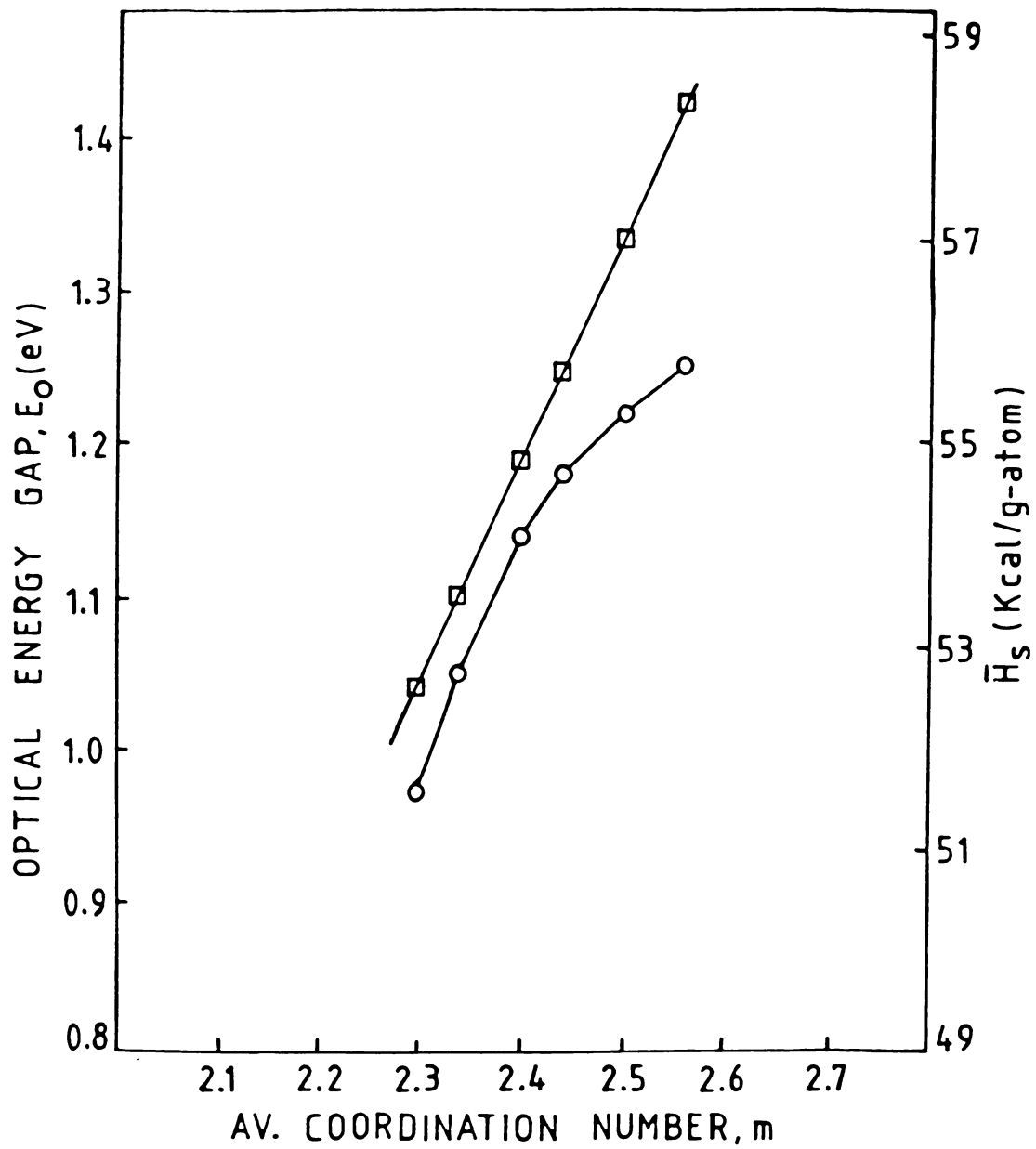


Fig.3.11 Variation of optical energy gap E_o and average heat of atomization H_s with average coordination number m . \square - H_s , \circ - E_o .

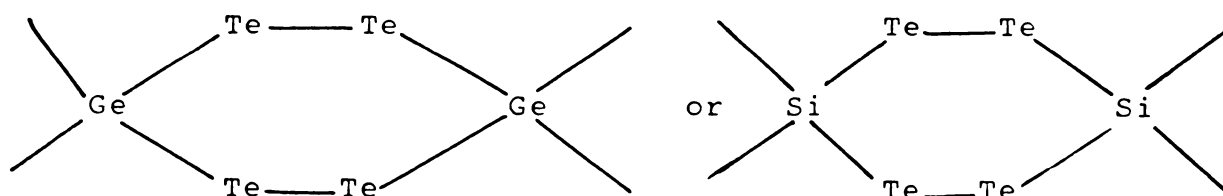
showing any change in slope. Using eqns.(3.3) and (3.4) and the values of heat of atomization and coordination number for Ge and Te, we can get the following relation for \bar{H}_s ,

$$\bar{H}_s = 22m + 2 \quad (3.5)$$

which represents a straight line as shown in Fig.3.11. The m values for various compositions of Ge-Te and Si-Te glasses are also tabulated in table 3.1.

The change in slope occurring at $m = 2.4$ (or $x = 0.2$) in $\text{Si}_x\text{Te}_{1-x}$ and $\text{Ge}_x\text{Te}_{1-x}$ glasses can be explained on the basis of the change taking place in the network when the concentration of group IV element is increased. For glasses with very low value of x the short range order is essentially one dimensional comprising of distorted Te chains. As the value of x increases the Te atom chain is increasingly interconnected by the four-fold coordinated group IV atoms. This leads to a continuous change in the one dimensional distorted chain short range order into a three dimensional tetrahedral network. At $x = 0.2$ stable structures based on GeTe_4 or SiTe_4 tetrahedral units are

formed as,



The effect of the formation of this type of structure gets reflected in the observed change in the variation of E_0 with x at $x = 0.2$.

3.4b $\text{Ge}_x\text{Se}_{1-x}$ glasses

Unlike Ge-Te and Si-Te, Ge-Se glasses can be prepared over a wider range of x . The E_0 values for various values of x for $\text{Ge}_x\text{Se}_{1-x}$ glasses are tabulated in table 3.2. In Fig.3.12 the variation of E_0 determined from the PA spectra is plotted as a function of the composition parameter x ($0.10 \leq x \leq 0.38$). The value of E_0 increases with increase in the Ge content upto $x = 0.33$. Using a molecular model such a variation for E_0 in Ge-Se system has been predicted by Lannoo and Bensoussan [194]. As in the case of Ge-Te and Si-Te glasses the rate of this increase is greater for samples with $x < 0.2$ than for $x > 0.2$. The average coordination number of m for $x = 0.2$ is 2.4. Around $x = 0.33$ ($m = 2.66$) composition,

Table 3.2: Values of the average coordination number m and optical energy gap E_o for Ge_xSe_{1-x} glasses.

Composition	m	E_o (eV)
$Ge_{0.38}Se_{0.62}$	2.76	2.29
$Ge_{0.33}Se_{0.67}$	2.66	2.32
$Ge_{0.28}Se_{0.72}$	2.56	2.24
$Ge_{0.25}Se_{0.75}$	2.50	2.21
$Ge_{0.20}Se_{0.80}$	2.40	2.17
$Ge_{0.15}Se_{0.85}$	2.30	2.10
$Ge_{0.10}Se_{0.90}$	2.20	2.03

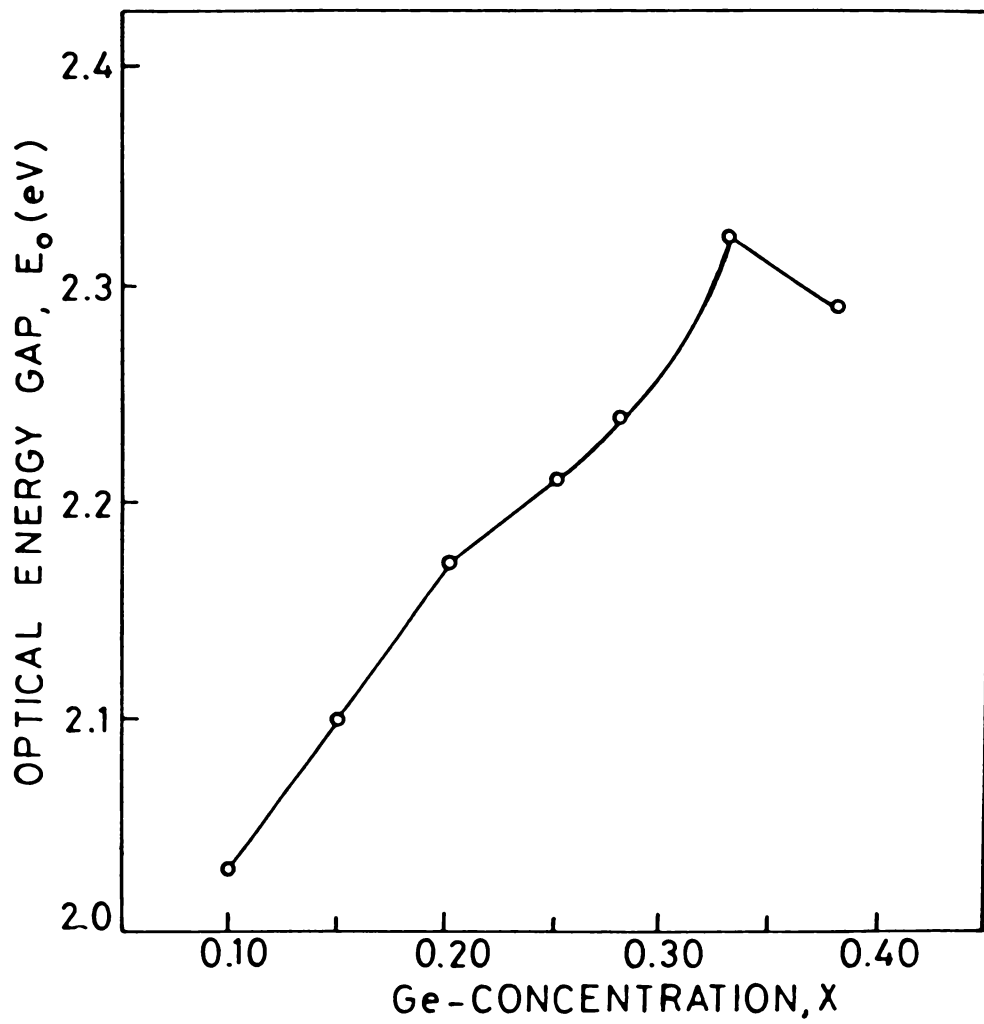


Fig.3.12 Variation of optical energy gap E_o with composition for Ge_xSe_{1-x} glasses.

E_0 is found to have a peak value. The value of m for different compositions of $\text{Ge}_x\text{Se}_{1-x}$ glasses are also given in Table 3.2.

In $\text{Ge}_x\text{Se}_{1-x}$ system of glasses the three possible types of bonds are Ge-Ge, Ge-Se and Se-Se with bond energies 49.1, 46.5 and 44 KCal/mole respectively [191]. According to CON model, for compositions with $x < 0.33$ the system contains Ge-Se and Se-Se bonds. At the stoichiometric composition $x = x_c = 0.33$ the system contains only Ge-Se bonds and for $x > 0.33$ both Ge-Se and Ge-Ge bonds are present. The bond counting statistics for $\text{Ge}_x\text{Se}_{1-x}$ system is shown in Fig.3.13 for two models, namely random covalent network and CON model [190]. Here, since the bond distribution is determined by chemical driving forces, the alloy is divided into two different regimes at the compound composition x_c . For $x < x_c$ each Ge atom has only Se type neighbours arranged in local molecular clusters of the form $\text{Ge}(\text{Se}_{\frac{1}{2}})_4$ and these clusters are connected through additional Se atoms. For $x > x_c$, since Ge-Ge bonds are also present the basic network forming units have different forms. The variation of E_0 with x can be explained on the basis of the distribution of different types of bonds and corresponding bond energies. Since the bond

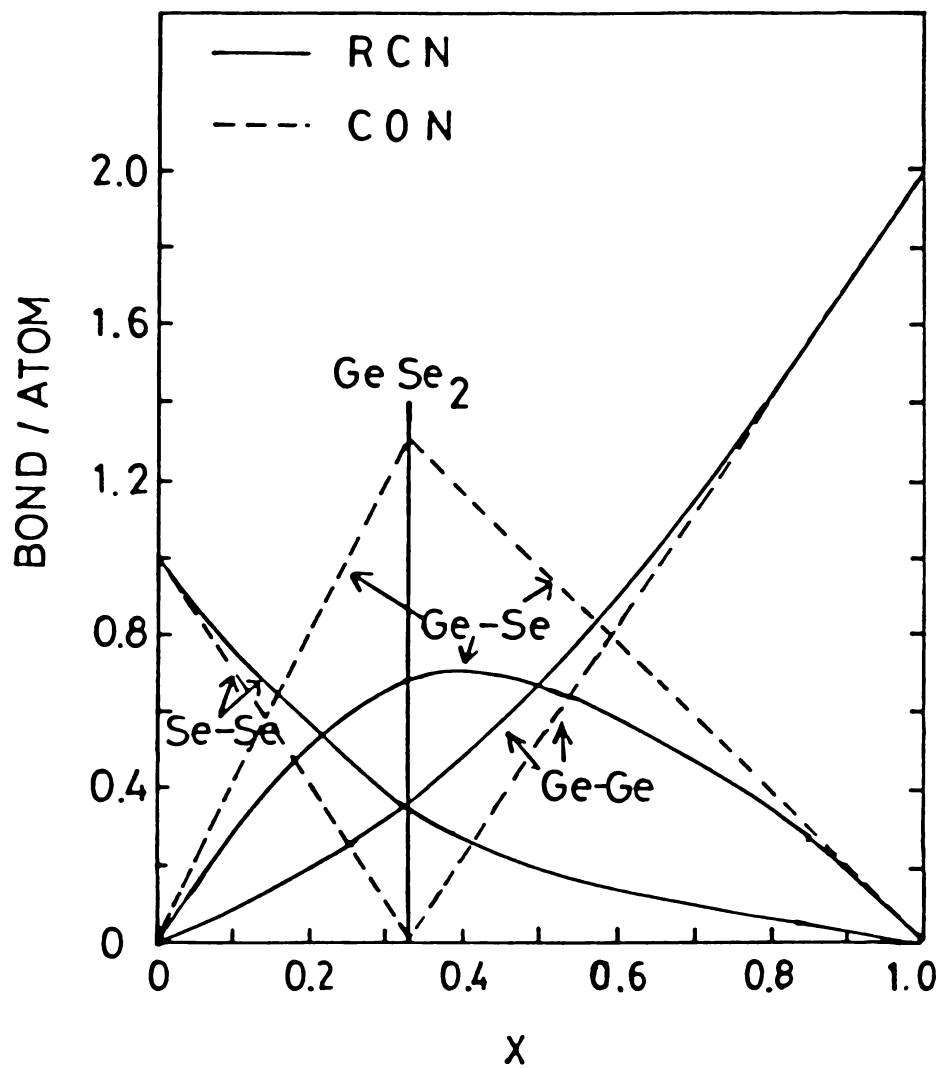


Fig.3.13 Bond counting statistics for $\text{Ge}_x\text{Se}_{1-x}$ glasses.
 ----- Chemically ordered network model.
 ——— Random covalent network model.

energy of Ge-Se bond is higher than that of Se-Se and Ge-Ge bonds, the antibonding band is at a higher energy for GeSe_2 ($x = 0.33$) sample compared to other compositions and correspondingly E_0 is maximum for this composition. The increase in the number of Se-Se bonds for compositions $x < 0.33$ and Ge-Ge bonds for $x > 0.33$ have the effect of reducing the average bond energy of the system and correspondingly the value of E_0 decreases on either side of the $x = 0.33$ composition. At $x = 0.2$ the glass network attains a stable structure consisting of GeSe_4 tetrahedral units. The network with very low concentration of Ge is constituted by one dimensional Se atom chains. As the concentration of Ge atoms increases, the Se atom chain is increasingly crosslinked by Ge atoms, thus changing the one dimensional chain to a three dimensional network consisting of GeSe_4 tetrahedral units at $x = 0.2$. The continuation of crosslinking leads to the formation of fully connected random network of tetrahedral $\text{Ge}(\text{Se}_{\frac{1}{2}})_4$ units at the stoichiometric composition.

In contrast to the random covalent network model and CON model, an alternative description of chalcogenide glasses has been proposed recently based on the formation of molecular cluster network [59,195,196]. This partially

polymerized cluster (PPC) model has been supported by experimental observations of strong companion A_1 line in the Raman spectra of GeSe_2 [170,197-199] and data from EXAFS [200] and Mössbauer [201,202] studies. According to this model the molecular clusters of GeSe_2 glass are described as a strongly associated mixture of large chalcogen rich outrigger rafts and small Ge rich ethane like units with the proportions adjusted to achieve overall stoichiometry. The chalcogen atoms on the edges of structural units are treated as surface atoms which have dimerized. The outrigger raft is a fragment of the high temperature form of crystalline GeSe_2 . The outrigger rafts of variable lateral dimensions tend towards layered structures in the glass phase. Layering is stabilized by weak inter-raft Van der Waals forces. In this molecular cluster model chemical ordering can possibly be intrinsically broken [60]. Unlike CON model, in PPC model the number of wrong bonds at the stoichiometric composition is not zero but it is much smaller than that in the random covalent network model.

Chapter 4

COMPOSITION DEPENDENCE OF ENERGY GAP IN As-Se GLASSES

4.1 INTRODUCTION

The incorporation of certain additives in pure amorphous selenium used for photographic drums [203] is found to improve the life time and sensitivity of the material. The common additives are 3 or 4 coordinated elements like As or Ge. This additives crosslink the Se chains and decrease the tendency of crystallization and increase the lifetime of pure Se drum [204]. It is interesting to study the role of additives on the width of the optical energy gap of glassy Se as well as its influence on other properties.

Of the glass forming alloys of the family $A_x^{V}B_{1-x}^{VI}$, As_xSe_{1-x} glasses are perhaps the most studied ones. A number of papers have appeared in literature reporting various properties of amorphous As-Se alloys both in the bulk and thin film forms [196,205-207]. Detailed analysis of the electrical, optical and structural properties of these materials have been presented by Mott and Davis [24]. Recent progress in the study of composition dependent

variation of properties of chalcogenide glasses has led to a better understanding of the physics of these materials [173]. Anomalous variations in the physical properties at certain specific compositions have attracted the attention of several workers. In As-Se system unusual variation in physical properties are expected for composition at which the stoichiometric crystalline compound forms. The critical composition corresponding to the stoichiometric compound is commonly known as the chemical threshold of the glass. In $\text{As}_x\text{Se}_{1-x}$ system such a chemical threshold occurs at $x = 0.4$. This has been experimentally established by observing the variation of several properties as a function of composition. A local minimum in the energy gap for $x = 0.4$ composition has been suggested by Hurst and Davis [208] who observed a conductivity maximum at this composition. The optical and dielectric properties of As-Se alloys are found to exhibit extrema at compound composition with a local coordination that satisfies the 8-N rule [206,207]. Evidence for a medium range order in As_2Se_3 has been obtained from the existence of a first sharp diffraction peak corresponding to formation of molecular clusters [209,210]. Raman shifts [196,205], glass transition temperature [211] and width of glass transition peak in the specific heat curve [212] are found to undergo anomalous variation at the compound composition. In order

to explain these results an approach based on chemical bonding and topology can be used because the atomic coordination, relative occurrence of homopolar and heteropolar bonds and the bonding topology determine the atomic structure of a binary alloy. As a representative of the $A^V B^{VI}$ alloys we have investigated the composition dependence of E_o in bulk $As_x Se_{1-x}$ glasses using PA technique.

4.2 PHOTOACOUSTIC SPECTRA OF $As_x Se_{1-x}$ GLASSES

$As_x Se_{1-x}$ glasses can be prepared easily over a wide range of composition. The crystallization process in this system is so slow as to allow preparation by cooling from melt at relatively low rate. For the present investigations bulk $As_x Se_{1-x}$ ($0.10 \leq x \leq 0.50$) glasses have been prepared by the usual melt quenching technique similar to that used for $A^{IV} B^{VI}$ alloys (see chapter 3). The amorphous nature of the samples are checked by X-ray diffractometry.

As described in chapter 3, the room temperature PA spectra have been recorded by plotting the variation of the normalized PA signal amplitude as a function of wavelength of the incident radiation. The PA spectra for $As_x Se_{1-x}$ samples so obtained are plotted in Figs.4.1, 4.2

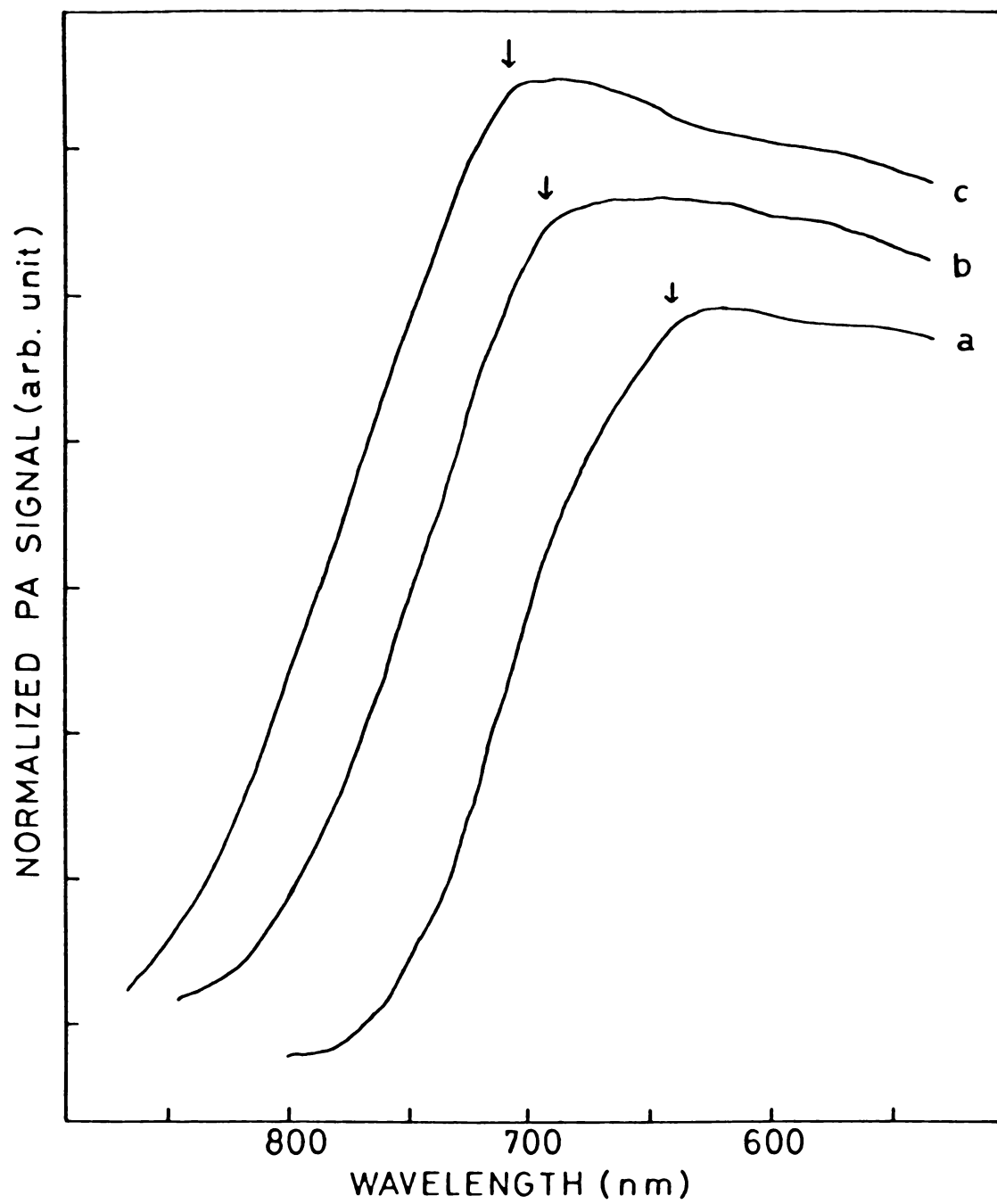


Fig.4.1 PA spectra of As_xSe_{1-x} glasses. (a) $As_{0.10}Se_{0.90}$
(b) $As_{0.50}Se_{0.50}$, (c) $As_{0.40}Se_{0.60}$.

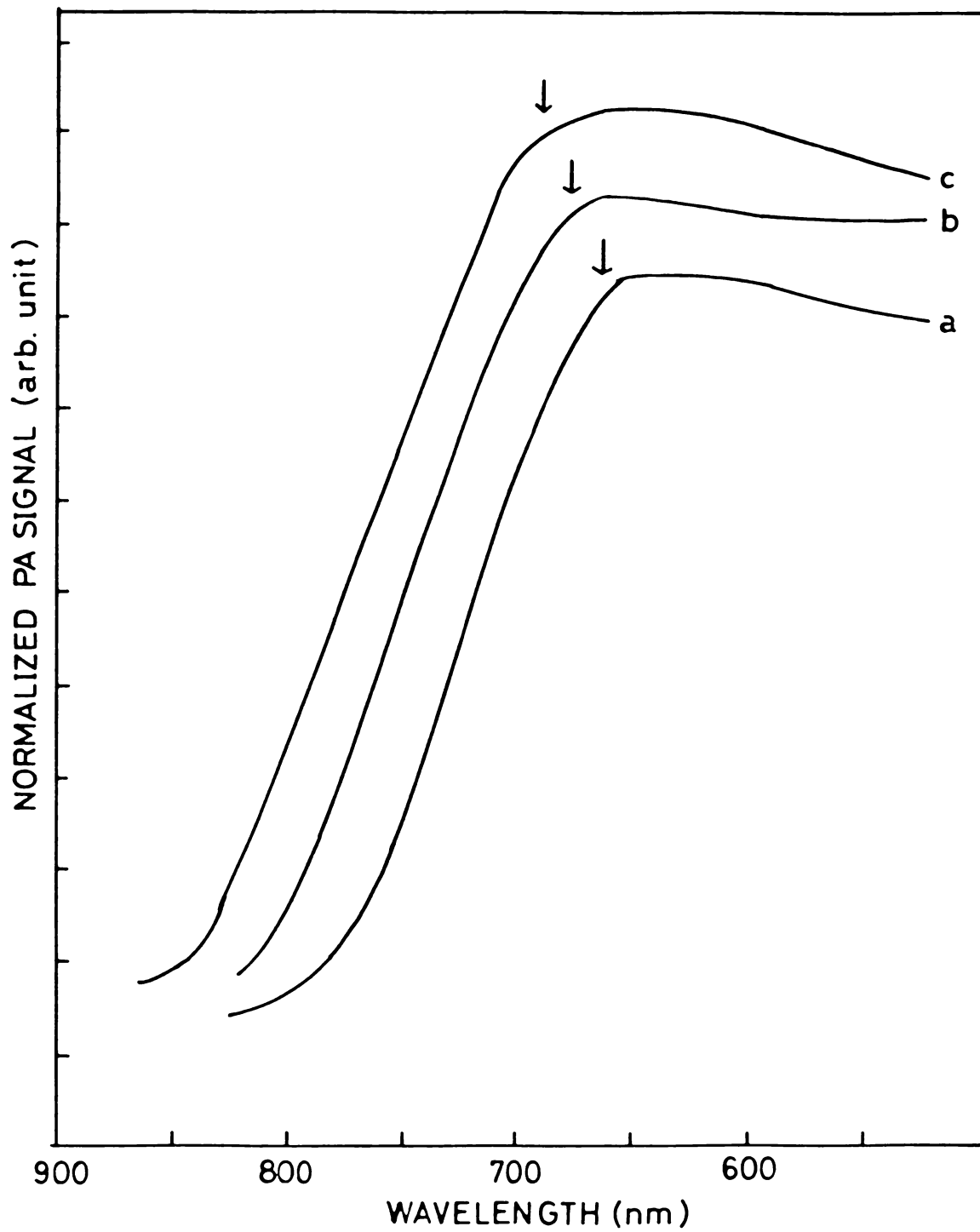


Fig.4.2 PA spectra of $\text{As}_x\text{Se}_{1-x}$ glasses. (a) $\text{As}_{0.20}\text{Se}_{0.80}$, (b) $\text{As}_{0.25}\text{Se}_{0.75}$, (c) $\text{As}_{0.30}\text{Se}_{0.70}$.

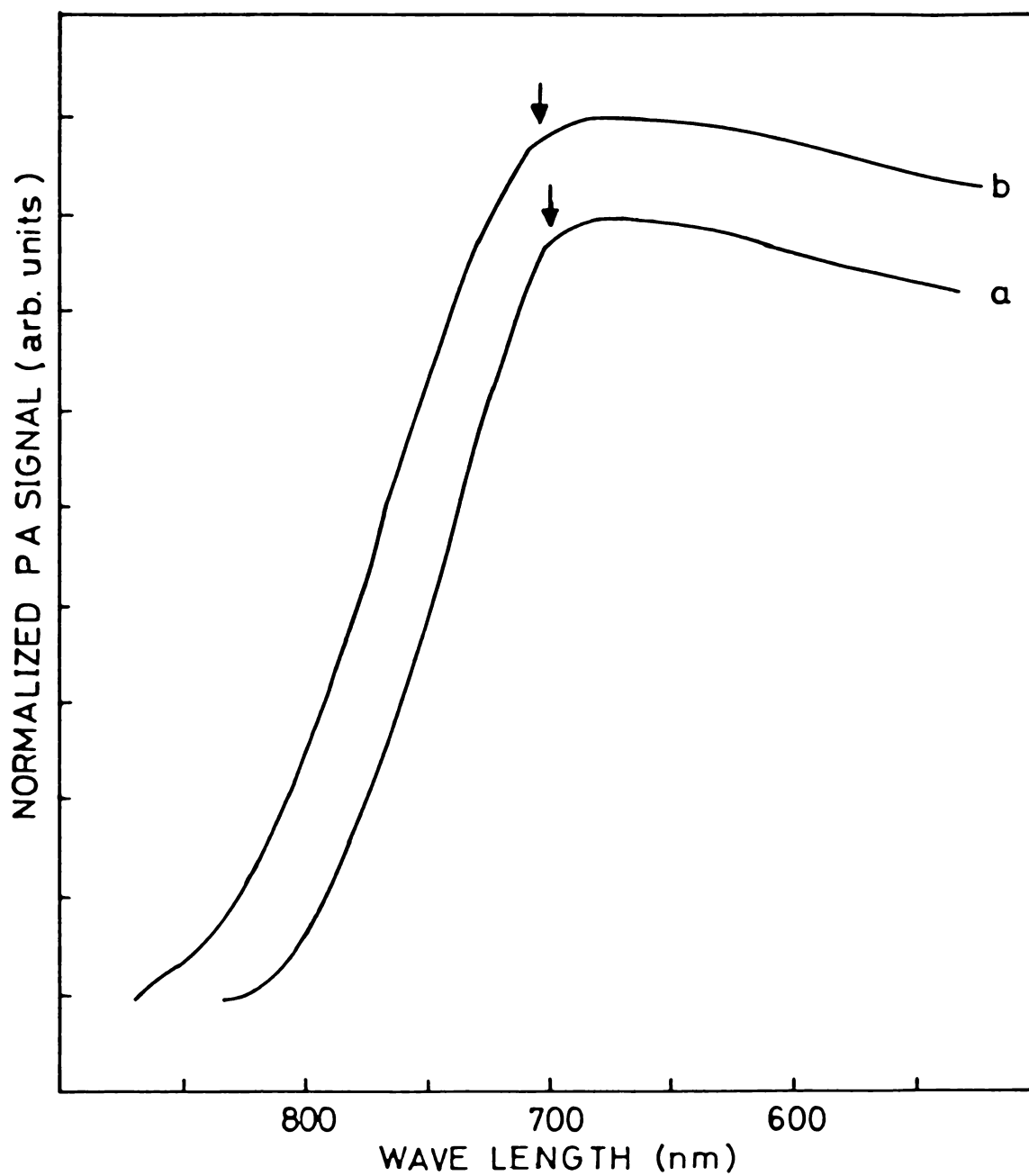


Fig.4.3 PA spectra of $\text{As}_x\text{Se}_{1-x}$ glasses. (a) $\text{As}_{0.35}\text{Se}_{0.65}$,
(b) $\text{As}_{0.45}\text{Se}_{0.55}$.

and 4.3. As has already been discussed in the previous chapter, these spectra give information about the optical absorption characteristics of the samples in the fundamental absorption edge region. The PA spectra saturate for photon energies $h\nu > E_0$ where E_0 is the optical energy gap. The slope of the exponential edge region of the spectra are not found to vary appreciably with composition over this fairly wide composition range.

4.3 VARIATION OF E_0 WITH COMPOSITION

The optical energy gap E_0 of each sample is determined from the PA spectrum as the photon energy above which the normalized PA signal amplitude saturates. The measured values are in good agreement with the results for those compositions on which the energy gap data are available [206]. The variation of E_0 with composition parameter x is shown in Fig.4.4. From this figure it can be seen that the value of E_0 is close to that of amorphous Se ($\approx 2\text{eV}$) for small concentrations of As and decreases as x increases. It has a minimum value at $x = 0.4 = x_c$ composition which corresponds to the formation of the stoichiometric compound As_2Se_3 . At this composition the network is formed by fully connected $\text{As}(\text{Se}_{\frac{1}{2}})_3$ pyramidal structural units with minimum number of homopolar bonds. For all

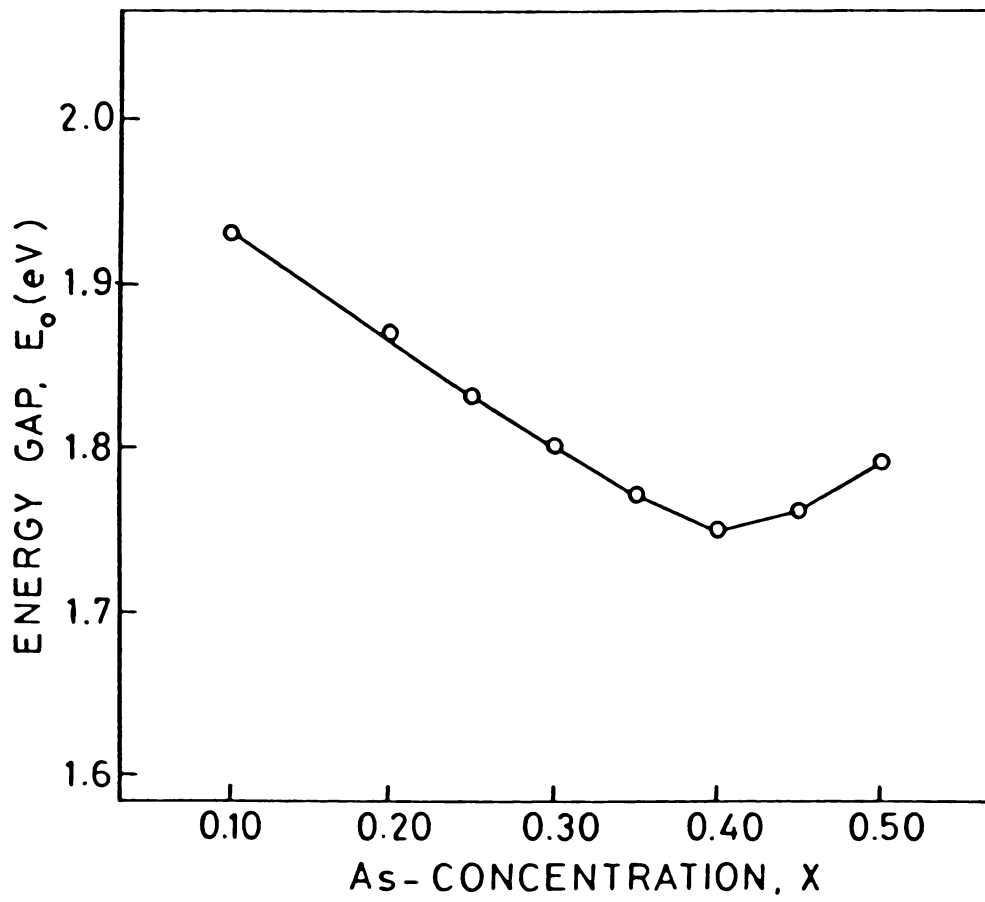


Fig.4.4 Variation of optical energy gap E_0 with composition for As_xSe_{1-x} glasses.

nonstoichiometric glasses, the short range order is related to that of the stoichiometric glasses with two-fold coordinated Se atoms and three-fold coordinated As atoms. For $x < x_c$ the chemical order is maintained for arsenic atoms, each of which is bonded to three Se atoms. The compositional variability is achieved by the Se atoms each of which is bonded to two Se atoms (as in a-Se) or to one Se and one As. For pure Se the network dimensionality is one and the structural elements are extended chains. Some rings of Se atoms interspersed between the chains may also be present. In Se rich glasses the network is dominated by Se atom chains and the introduction of three-fold coordinated As atoms produces branching or crosslinking between Se chains. With this crosslinking the topologically linear $(\text{Se})_n$ chains are interconnected at irregular intervals to form large and more highly connected structures. The connectivity changes with the concentration of crosslinking constituent and the number of disconnected individual molecular units drops sharply as the separate units link up. The crosslinking by three coordinated As atoms continue until $x = 0.4$ is reached where fully connected glass with $\text{As}(\text{Se}_{1/2})_3$ structural units are formed. Beyond this the network can contain other basic structural units like As_4Se_4 .

The energy gap and related optical properties are closely related to the nature of bonding between atoms and the short range order existing in the system because the electronic band structure is formed by the superposition of the molecular orbital states of the constituent bonds. In $\text{As}_x\text{Se}_{1-x}$, depending upon the composition, the valence band is constituted by the lone-pair band associated with Se or As and the antibonding band forms the conduction band. The variation of physical properties with composition and the topological aspects of the glass forming tendency [173] can be discussed in terms of the average coordination number m . Taking the coordination numbers of As and Se as three and two respectively, m values for all compositions are determined using eqn.(3.3). For the compositions we have studied, m lies in the range $2.1 \leq m \leq 2.5$ with $m = 2.4$ for $x = 0.4$ at which the As_2Se_3 glass is formed. The values of m and E_0 for various compositions of $\text{As}_x\text{Se}_{1-x}$ glasses are given in Table 4.1.

According to the chemically ordered network (CON) model the $\text{As}_x\text{Se}_{1-x}$ system contains only fully coordinated As-Se bonds at $x = x_c = 0.40$ [190]. For $x < x_c$ the system contains As-Se and Se-Se bonds whereas for $x > x_c$ As-Se and As-As bonds are present. The bond counting statistics

Table 4.1: Average coordination number and optical energy gap of $\text{As}_x\text{Se}_{1-x}$ glasses.

Composition	m	E_o (eV)
$\text{As}_{0.10}\text{Se}_{0.90}$	2.10	1.93
$\text{As}_{0.20}\text{Se}_{0.80}$	2.20	1.87
$\text{As}_{0.25}\text{Se}_{0.75}$	2.25	1.83
$\text{As}_{0.30}\text{Se}_{0.70}$	2.30	1.80
$\text{As}_{0.35}\text{Se}_{0.65}$	2.35	1.77
$\text{As}_{0.40}\text{Se}_{0.60}$	2.40	1.75
$\text{As}_{0.45}\text{Se}_{0.55}$	2.45	1.76
$\text{As}_{0.50}\text{Se}_{0.50}$	2.50	1.79

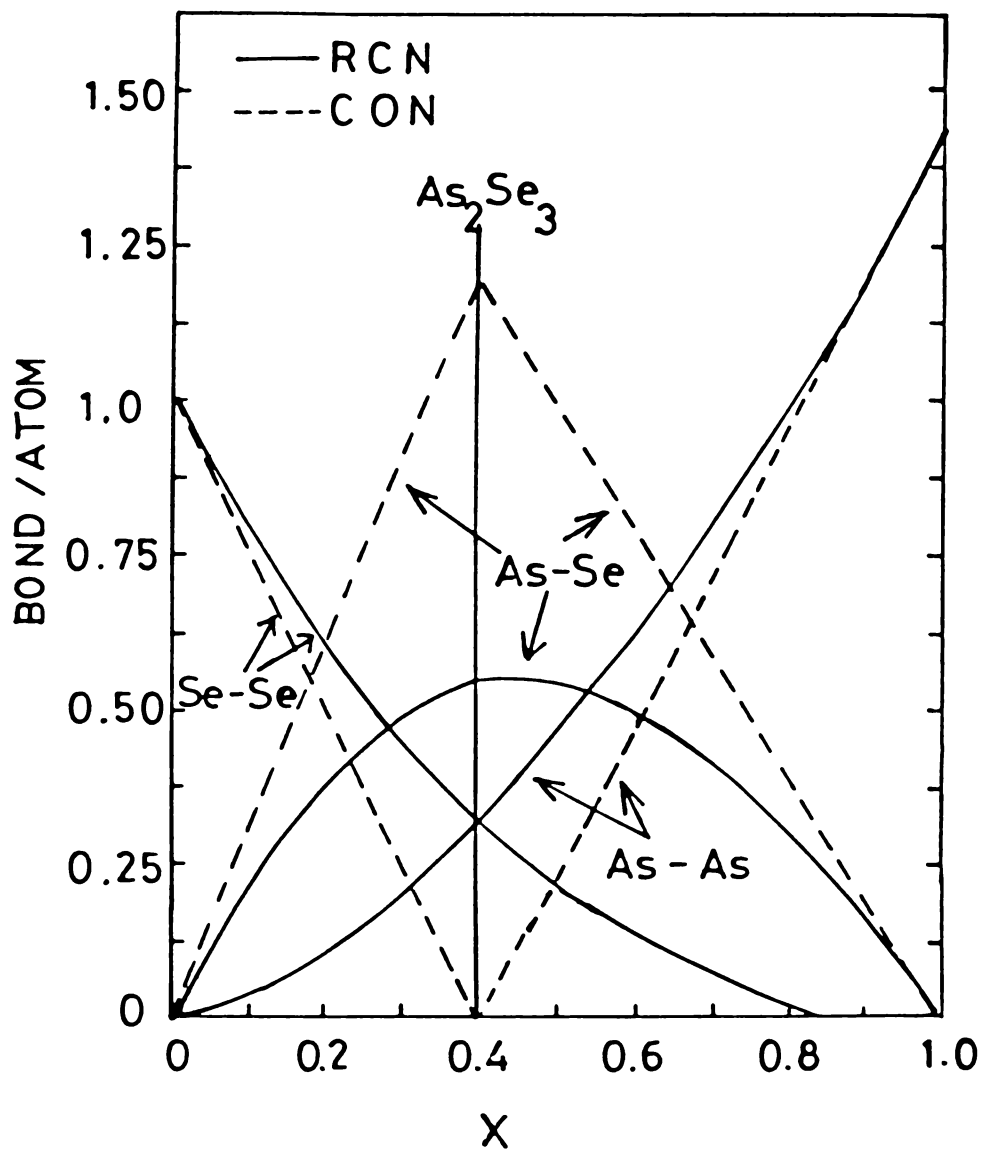


Fig.4.5 Bond counting statistics for $\text{As}_x\text{Se}_{1-x}$ glasses.

----- Chemically ordered network model.

————— Random covalent network model.

for CON model is given in Fig.4.5 [190]. However, certain amount of homopolar bonds are possible even at the stoichiometric composition. The bond energies of As-As, As-Se and Se-Se bonds are 43.4, 44.96 and 44 KCal/mole respectively [191]. Since these values are very close, it is rather difficult to explain the observed variation of E_o with x on the basis of CON model. It appears that the increase in network disorder associated with the deviation from stoichiometry has the effect of increasing E_o by pushing the mobility edge further into the bands.

White [213] has developed a random network model [55] for amorphous alloys which characterizes their band structure in terms of tight binding matrix elements [74] and applied this model to the As-Se system. The lone pair electrons play an important role in determining the properties of this system [182,186]. Unlike in $A^{IV}B^{VI}$ systems, where group IV atom does not have lone pair electrons, in As-Se both the constituents do have lone pair electrons. For As there are three bonding and one lone pair orbitals. Se atom has two bonding and two lone pair orbitals. The optical energy gap for As-Se glasses across the entire composition range will be associated with lone pair to antibonding transition. Therefore the variation of E_o with x is attributed to the interaction involving lone

pair electrons. Band structure calculation by White [213] using relatively small number of tight binding matrix elements for As-Se glasses yield a local minimum in the gap in the vicinity of the composition As_2Se_3 because the bottom of the conduction band is driven upward in energy at the Se-rich end due to the Se lone pair.

Molecular cluster model based on the formation of partially polymerized clusters [59] is found to be suitable for describing the structure of covalent network glasses. According to this the cluster surface plays an important role in determining the glass forming tendency and the final structure. The chemical order of the network is intrinsically broken while clusters are formed and the number of wrong bonds are not zero at the stoichiometric composition. In As-Se system the presence of wrong bonds at the stoichiometric composition may be reducing the average bond energy and this is reflected in the composition dependence of the energy gap.

Phillips et al [214] have constructed a molecular model for As_2Se_3 based on chemically ordered raft structure, similar to that of GeSe_2 , starting from basic ring of $\text{C-As}_2\text{Se}_3$ which is alternating As_6Se_6 units. In GeSe_2 the structure of the raft is conformationally unique while

in As_2Se_3 there are at least four distinct conformers whose statistical weights vary with pseudobinary alloying and temperature. This raft model explains well the anomalies in the temperature and pseudobinary alloying dependence of diffraction data, anomalies in Raman scattering etc. The strong inter cluster interactions present in the system are mediated by nonbonding lone pair electrons. The valence band spectra of As, Se and As_2Se_3 indicate that they have bonding electrons at low energies compared to the lone pair electrons. When the lone pair electrons are arranged in layers the nonbonding interaction is maximised. This increases the width of the lone pair band and reduces the effective energy gap.

Chapter 5

COMPOSITION DEPENDENCE OF THERMAL DIFFUSIVITY

IN $A_{x-1-x}^{IV} B_{1-x}^{VI}$ AND $A_{x-1-x}^V B_{1-x}^{VI}$ SYSTEMS

5.1 INTRODUCTION

Thermal diffusivity α_s , although a derived characteristic of a substance, is of direct importance in heat flow studies as it determines the rate of periodic or transient heat propagation through a medium. Because of its controlling effect and common occurrence in thermal conduction problems its determination is often necessary and a knowledge of the thermal diffusivity can be used to calculate the thermal conductivity. Thermal diffusivity is the ratio of the thermal conductivity to the specific heat and density of the material and has dimensions $(\text{length})^2 \times (\text{time})^{-1}$.

Experimental methods for determining the thermal transport properties of materials can be conveniently divided into three broad categories, steady state temperature methods, transitory temperature methods and periodic

temperature methods [215]. Although thermal conductivity and thermal diffusivity are directly related, the measurement of these two parameters are made by completely different experimental techniques. Thermal conductivity when measured directly by a steady state method, requires the measurement of a thermal flux and a temperature gradient. Thermal diffusivity requires the measurement of the time for a thermal disturbance to propagate to a known distance. This points out the importance of thermal diffusivity measurements because lengths and time intervals can be measured more easily and accurately than heat fluxes and temperature gradients. In the transient heat flow method an addition or removal of thermal energy from the sample will induce a transitory temperature change and α_s is determined from a measurement of the temperature as a function of time at one or more points along the sample. In periodic temperature methods the thermal energy supplied to the sample is modulated at a fixed period. Consequently the temperatures at all points in the sample vary with the same period and α_s is then determined from the measurements of the amplitude and phase of thermal wave in the sample.

The use of periodic method for measuring α_s has increased greatly in recent years due to the realization

of the advantages of nonsteady state methods. Most of the methods, used in time resolved temperature measurement techniques for determining α_s , are based on the original work carried out by Angström [216] and its modification by King [217] and Abeles et al [218]. Developments of time resolved methods for measuring thermal diffusivity have been reviewed by Touloukian et al [219]. In these methods the variation of sample temperature is usually sensed by thermocouples. The use of radiation whose amplitude varies sinusoidally with time to produce periodic heating at the front surface of a small plate has been proposed by Becker [220] for measuring α_s of semiconducting samples. Davis et al [221] irradiated GaAs sample with chopped light that contained wavelengths on both sides of the optical absorption edge for determining the thermal diffusivity.

The PA technique, which belongs to the periodic heat flow method, can effectively be used for studying the thermal properties such as thermal diffusivity, thermal conductivity, specific heat etc. of gases, liquids and solids. This is possible because the PA signal is directly related to the thermal diffusion processes in the sample, backing material and the gas medium and the consequent

dependence of the PA signal on the thermal properties of these materials. The method enables one to measure indirectly and with high sensitivity the surface temperature of the sample by noncontact means. This technique has been utilized for measuring the thermal diffusivity of a wide variety of samples ever since Rosencwaig and Gersho formulated their theory of PA effect [95] based on thermal diffusion characteristics. Adams and Kirkbright have used the PA method [133] to obtain the thermal diffusivity values of copper and glass using rear surface illumination technique in which an opaque surface is illuminated and the PA signal is transferred through a thin copper or glass layer to the gas within a gas-microphone PAS system. They also measured the thermal diffusivities of polymer films deposited on copper substrates [222]. In 1982 Charpentier et al [223] studied the theoretical and experimental problems which are encountered when PA technique is used. They presented a frequency analysis of the PA signal for the determination of thermal diffusivity by extending the RG theory. An account of the mechanical vibrations of the sample due to its periodic dilation (drum effect) has also been discussed by these authors. Yamashita et al [224] used PA technique to obtain the thermal conductivity

and thermal diffusivity of CdIn_2S_4 semiconductor and Zammit et al [225] reported the determination of optical and thermal parameters in ion implanted Si and GaAs layers as a function of implantation dose. An approach which uses a lateral heating source for the sample was proposed for PA determination of α_s of solids by Cesar et al [226]. PA measurements of the thermal diffusivity and thermal conductivity of thin film optical coatings are described by Swimm [227]. The thermal properties of bulk polymers have also been determined using this technique [158,228]. Lachaine [229] made an extensive study of the variation of PA signal phase with different sample thickness and could obtain the thermal parameters of lead samples.

5.2 OUTLINE OF THE THEORY

The RG theory of the PA effect [95] and the later refinements to this theory [106,230] show that the pressure variations produced in the PA cell in the case of an optically opaque sample depends on the thermal diffusivity α_s of the sample. According to RG theory the complex envelope of the sinusoidal pressure variations in the PA cell can be written as (chapter 1)

$$\Delta P = |\Delta P| \exp(-i\phi) \quad (5.1)$$

The explicit formula for ΔP is

$$\Delta P = \frac{\beta I_0 \gamma P_0}{2\sqrt{2} T_0 k_s l_g a_g (\beta^2 - \sigma_s^2)} \left[\frac{(\gamma-1)(b+1)e^{\sigma_s l_s} - (\gamma+1)(b-1)e^{-\sigma_s l_s} + 2(b-\gamma)e^{-\sigma_s l_s}}{(g+1)(b+1)e^{\sigma_s l_s} - (g-1)(b-1)e^{-\sigma_s l_s}} \right] \quad (5.2)$$

where β is the optical absorption coefficient, I_0 is the incident light flux, γ is the ratio of specific heats of air, P_0 is the ambient pressure, T_0 is the ambient temperature, k_s is the thermal conductivity of the sample, l_g is the length of the air column in the PA cell, a_g is the thermal diffusion coefficient of air and l_s is the sample thickness.

Also,

$$b = \frac{k_b a_b}{k_s a_s} \quad (5.3)$$

$$g = \frac{k_g a_g}{k_s a_s} \quad (5.4)$$

$$\gamma = (1-i)\frac{\beta}{2a_s} = (1-i)\frac{\beta \mu_s}{2} \quad (5.5)$$

$$\sigma_s = (1+i)a_s = (1+i)\frac{1}{\mu_s} \quad (5.6)$$

k_b and k_g are the thermal conductivities of backing material and air respectively and a_b and a_g are the corresponding thermal diffusion coefficients. Thermal diffusion length μ_s of the sample is given by

$$\mu_s = \left(\frac{2\alpha_s}{\omega} \right)^{1/2} = \left(\frac{\alpha_s}{\pi f} \right)^{1/2} = \frac{1}{a_s} \quad (5.7)$$

where f is the chopping frequency.

$$\text{Now,} \quad \sigma_s l_s = (1+i) \frac{l_s}{\mu_s} \quad (5.8)$$

$$\text{and} \quad \beta = \gamma \sigma_s \quad (5.9)$$

Starting from RG theory the amplitude and phase with respect to a thermally thick reference for an optically opaque sample under front surface illumination geometry has been expressed in a different form by Charpentier et al [223] and Bennett and Patty [231]. Expression for ΔP in eqn. (5.2) can be rewritten as

$$\Delta P = \frac{\beta I_0 \gamma P_0}{2\sqrt{2} T_0 k_s l_g a_g (\beta^2 - \sigma_s^2)} \left\{ \frac{\left[1 - \frac{(\gamma+1)(b-1)e^{-\sigma_s l_s}}{(\gamma-1)(b+1)e^{\sigma_s l_s}} + \frac{2(b-\gamma)e^{-\beta l_s}}{(\gamma-1)(b+1)e^{\sigma_s l_s}} \right]}{\left[\frac{(\gamma+1)(b+1)e^{\sigma_s l_s}}{(\gamma-1)(b+1)e^{\sigma_s l_s}} - \frac{(\gamma-1)(b-1)e^{-\sigma_s l_s}}{(\gamma-1)(b+1)e^{\sigma_s l_s}} \right]} \right\}$$

$$(5.10)$$

Substituting for r , b , $\sigma_s l_s$ etc. and rearranging, one can rewrite above equation as

$$\Delta P = \frac{A}{x^2} \frac{[1 - R^2 e^{-4x} + 2R e^{-2x} \cos(2x)]}{[(1 - R^2 e^{-4x})^2 + 4R^2 e^{-4x} \sin^2(2x)]^{1/2}} \quad (5.11)$$

where

$$A = \frac{\rho_0 \gamma I_0 l_s^2 \sqrt{\alpha_g}}{l_g T_0 k_s \sqrt{\alpha_s}} \quad (5.12)$$

$$x = \frac{l_s}{\mu_s} = \left(\frac{\pi f}{f_c} \right)^{1/2} \quad (5.13)$$

and the thermal wave reflection coefficient R is given by

$$R = \frac{1-d}{1+d} \quad (5.14)$$

Here d is the ratio of the effusivities of the backing material e_b and the sample e_s given by

$$d = \frac{e_b}{e_s} = \left[\frac{k_b \rho_b c_b}{k_s \rho_s c_s} \right]^{1/2} \quad (5.15)$$

where ρ_s and C_s are density and specific heat of the sample and ρ_b and C_b are those of the backing material. The corresponding expression for the phase $\Delta\phi$ (with respect to a thermally thick reference) is given by

$$\tan(\Delta\phi) = \frac{2R \sin(2x)}{e^{2x} - R^2 e^{-2x}} \quad (5.16)$$

Since

$$\alpha_s = \frac{k_s}{\rho_s C_s}, \quad (5.17)$$

d can be written as

$$d = \frac{k_b}{k_s} \frac{\sqrt{\alpha_s}}{\sqrt{\alpha_b}} \quad (5.18)$$

The signal depends upon the modulation frequency through the product $\sigma_s l_s$ which can be written using eqn.(5.7) and (5.8) as

$$\sigma_s l_s = (1+i) \sqrt{\kappa t / f_c} \quad (5.19)$$

where the characteristic frequency f_c is defined by

$$f_c = \alpha_s / l_s^2 \quad (5.20)$$

Therefore by determining the characteristic frequency f_c , the thermal diffusivity α_s of the sample can easily be calculated.

5.3 EXPERIMENTAL PROCEDURE

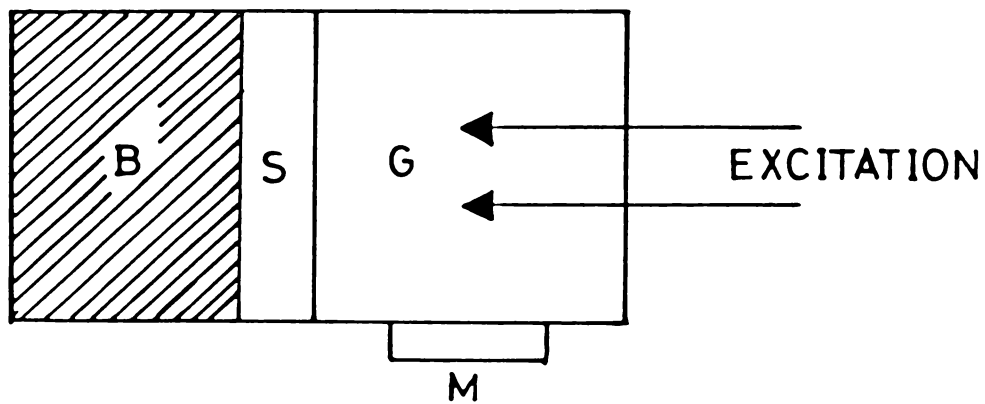
The theoretical formulations presented above account for the chopping frequency dependence and the effect of the backing material on the PA signal phase and amplitude. For a thermally thick sample the thermal diffusion length is confined within the sample for the entire chopping frequency range. Consequently the thermal wave reflection coefficient $R = 0$. However, when the sample is thermally thin the heat generated in the sample is propagated through the sample into the backing material which is thermally thick. Since thermal diffusion length μ_s decreases as the chopping frequency increases, by properly choosing the sample thickness l_s it is possible to find out the characteristic frequency f_c , above which the PA signal is independent of the effect of backing material.

The details of the measurement of thermal diffusivity of chalcogenide glasses at room temperature are presented below.

We have measured the thermal diffusivity in several compositions of $\text{Ge}_x\text{Te}_{1-x}$ ($0.15 \leq x \leq 0.28$), $\text{Si}_x\text{Te}_{1-x}$ ($0.10 \leq x \leq 0.28$) and $\text{Ge}_x\text{Se}_{1-x}$ ($0.10 \leq x \leq 0.38$) samples belonging to the $\text{A}_x^{\text{IV}}\text{B}_{1-x}^{\text{VI}}$ family and in $\text{As}_x\text{Se}_{1-x}$ ($0.10 \leq x \leq 0.50$) and $\text{As}_x\text{Te}_{1-x}$ ($0.25 \leq x \leq 0.55$) samples belonging to the $\text{A}_x^{\text{V}}\text{B}_{1-x}^{\text{VI}}$ family. The samples are prepared by melt quenching technique. The experimental set up used for these measurements is same as that described in Chapter 2. Since the wavelength of the light beam is so chosen that $h\nu > E_0$, the sample can be considered as optically opaque. For these measurements disc type samples having appropriate thickness are prepared by hand lapping and polishing such that the characteristic frequency at which a crossover from a thermally thin to a thermally thick regime takes place as the chopping frequency is increased, lies well within the operation frequency range of our spectrometer. Typical sample thickness is in the range 100-300 μm . The thickness of each sample used for measurements is tabulated in Tables 5.1 and 5.2. The prepared sample is fixed on a thermally thick backing material which is either copper or aluminium

disc in our experiments, ensuring proper thermal contact and is placed in the room temperature PA cell for measurements using front surface illumination. The front surface illumination geometry used in the experiment is shown in Fig.5.1.

The characteristic frequency f_c is determined by measuring the variation of PA signal amplitude and phase with chopping frequency. For this first of all the amplitude of the PA signal for a thermally thick reference sample (thickness ≈ 1 mm) is measured as a function of the chopping frequency f . This reference sample is thermally thick in the entire chopping frequency range used in the measurements. Then the variation of PA amplitude with f for the experimental sample of appropriate thickness is measured. The log-log plot of the PA amplitude versus chopping frequency for all the $\text{Ge}_x\text{Te}_{1-x}$, $\text{Si}_x\text{Te}_{1-x}$, $\text{Ge}_x\text{Se}_{1-x}$, $\text{As}_x\text{Se}_{1-x}$ and $\text{As}_x\text{Te}_{1-x}$ samples are given in Figs.5.2 to 5.11. The corresponding plots for thermally thick reference samples are also given in these figures. From the figures it can be seen that the plots for the reference sample are straight lines with slope ≈ -1 . This is in agreement with the RG theory [95] for an optically opaque ($l_p \ll l_s$) and



B — Backing material

S — Sample

G — Gas medium

M — Microphone

Fig.5.1 The front surface illumination geometry used in the experiment.

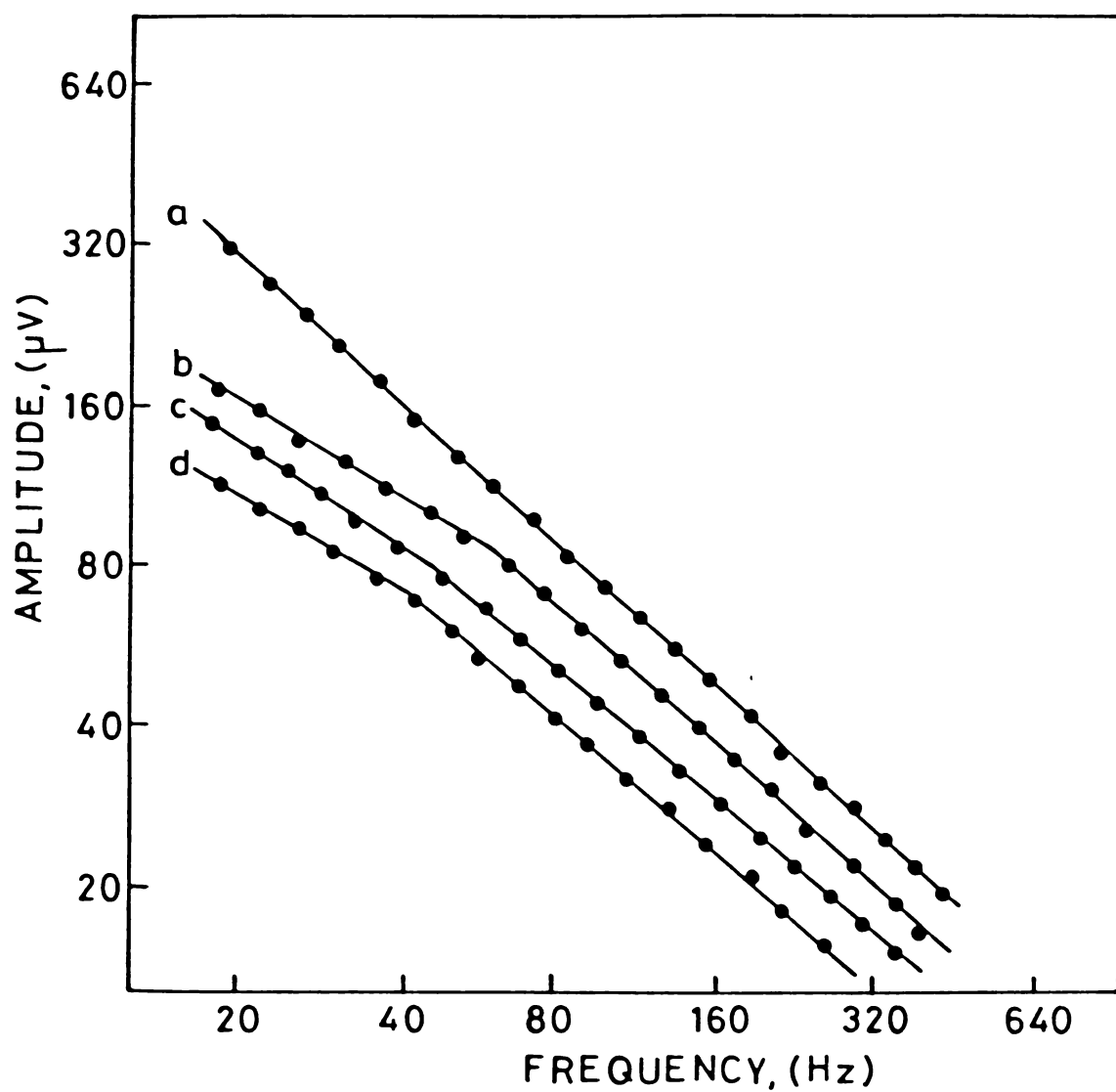


Fig.5.2 Log-log plots of variation of PA signal amplitude with chopping frequency for $\text{Ge}_x\text{Te}_{1-x}$ glasses.

(a) Reference sample, (b) $\text{Ge}_{0.20}\text{Te}_{0.80}$,

(c) $\text{Ge}_{0.17}\text{Te}_{0.83}$, (d) $\text{Ge}_{0.15}\text{Te}_{0.85}$.

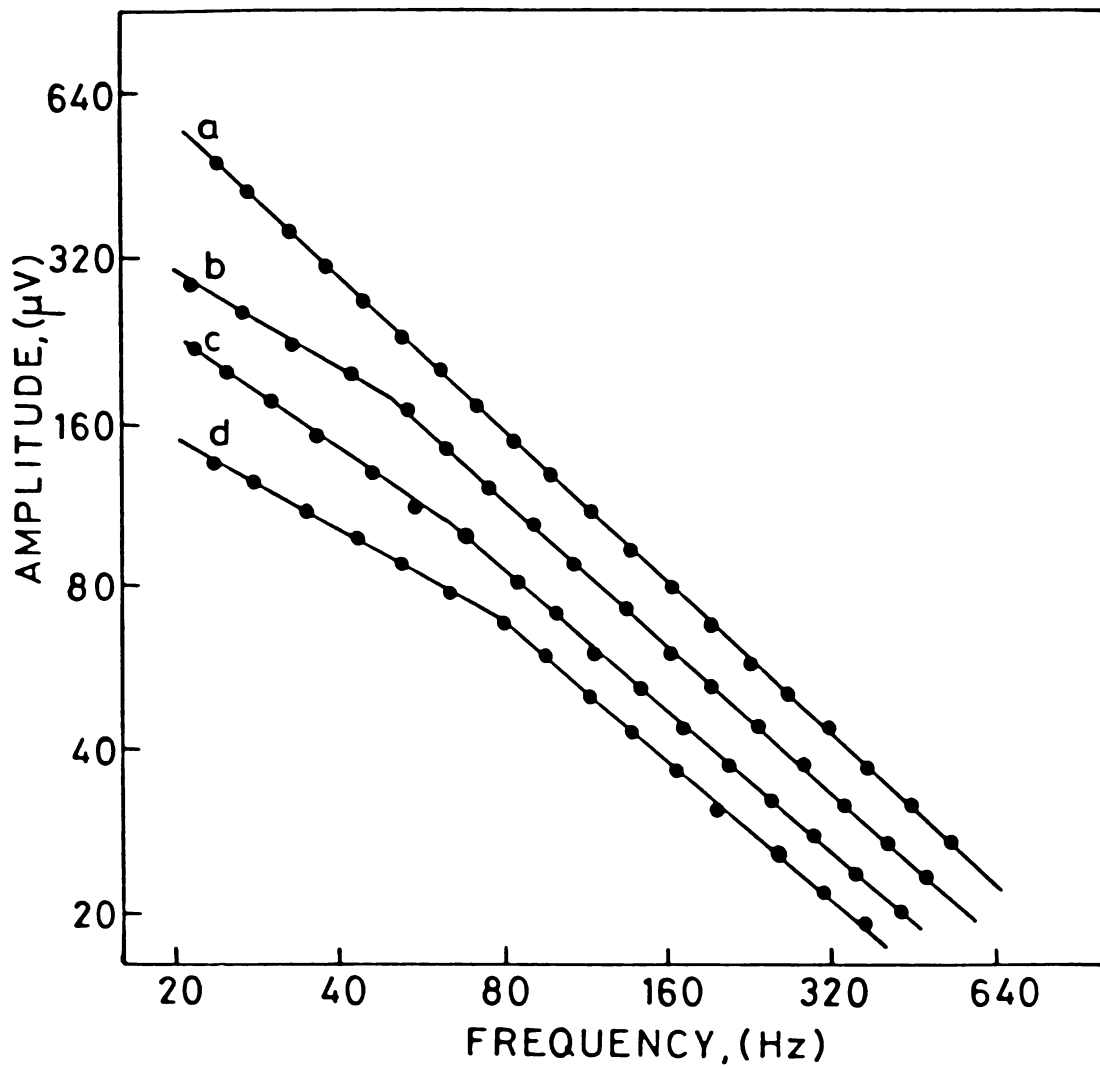


Fig.5.3 Log-log plots of variation of PA signal amplitude with chopping frequency for $\text{Ge}_x\text{Te}_{1-x}$ glasses.

(a) Reference sample, (b) $\text{Ge}_{0.28}\text{Te}_{0.72}$,

(c) $\text{Ge}_{0.25}\text{Te}_{0.75}$, (d) $\text{Ge}_{0.22}\text{Te}_{0.78}$.

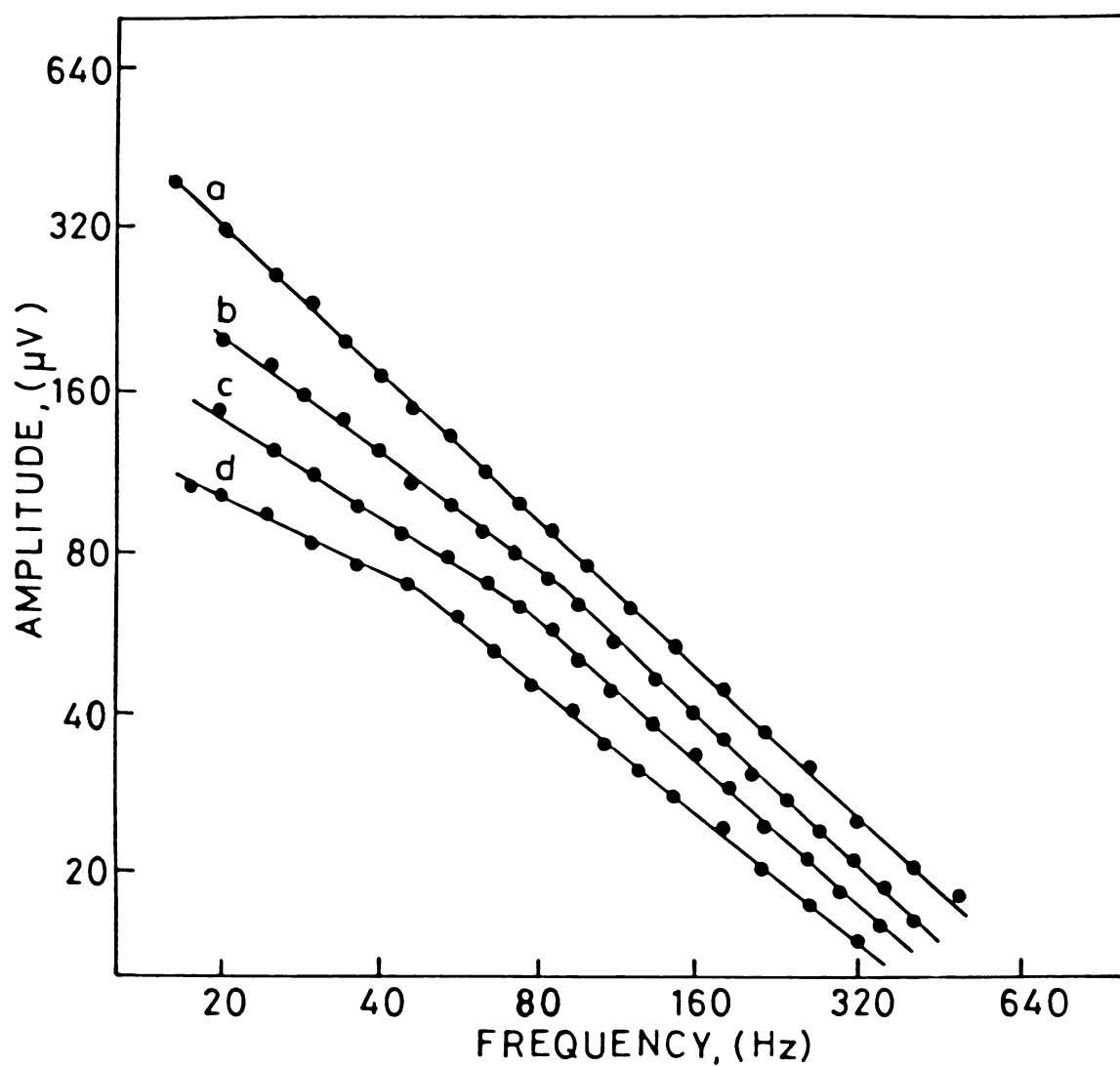


Fig.5.4 Log-log plots of variation of PA signal amplitude with chopping frequency for $\text{Si}_x\text{Te}_{1-x}$ glasses.

(a) Reference sample, (b) $\text{Si}_{0.17}\text{Te}_{0.83}$,

(c) $\text{Si}_{0.15}\text{Te}_{0.85}$, (d) $\text{Si}_{0.10}\text{Te}_{0.90}$.

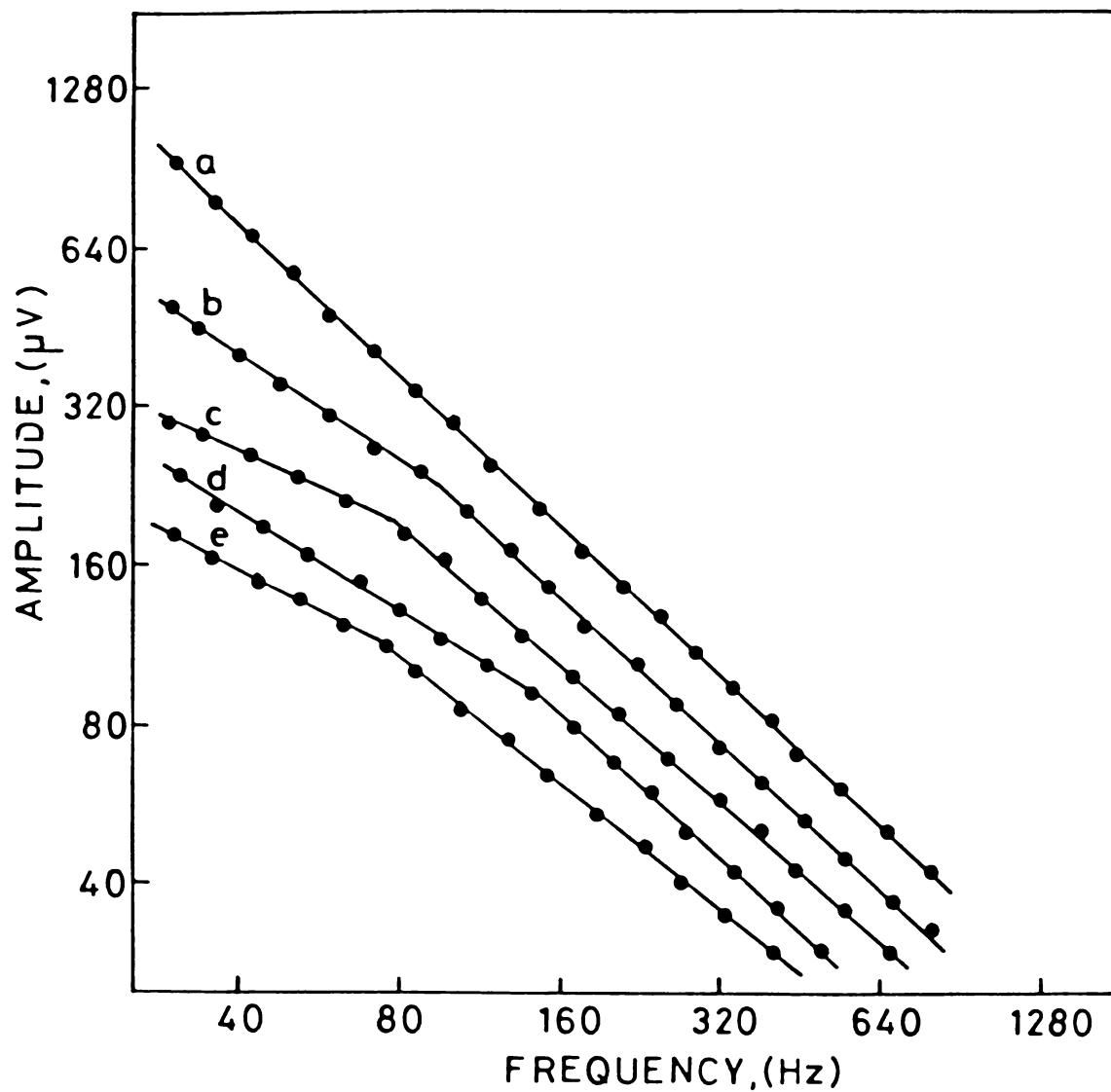


Fig.5.5 Log-log plots of variation of PA signal amplitude with chopping frequency for $\text{Si}_x\text{Te}_{1-x}$ glasses.

(a) Reference sample, (c) $\text{Si}_{0.28}\text{Te}_{0.72}$,

(c) $\text{Si}_{0.25}\text{Te}_{0.75}$, (d) $\text{Si}_{0.22}\text{Te}_{0.78}$, (e) $\text{Si}_{0.20}\text{Te}_{0.80}$.

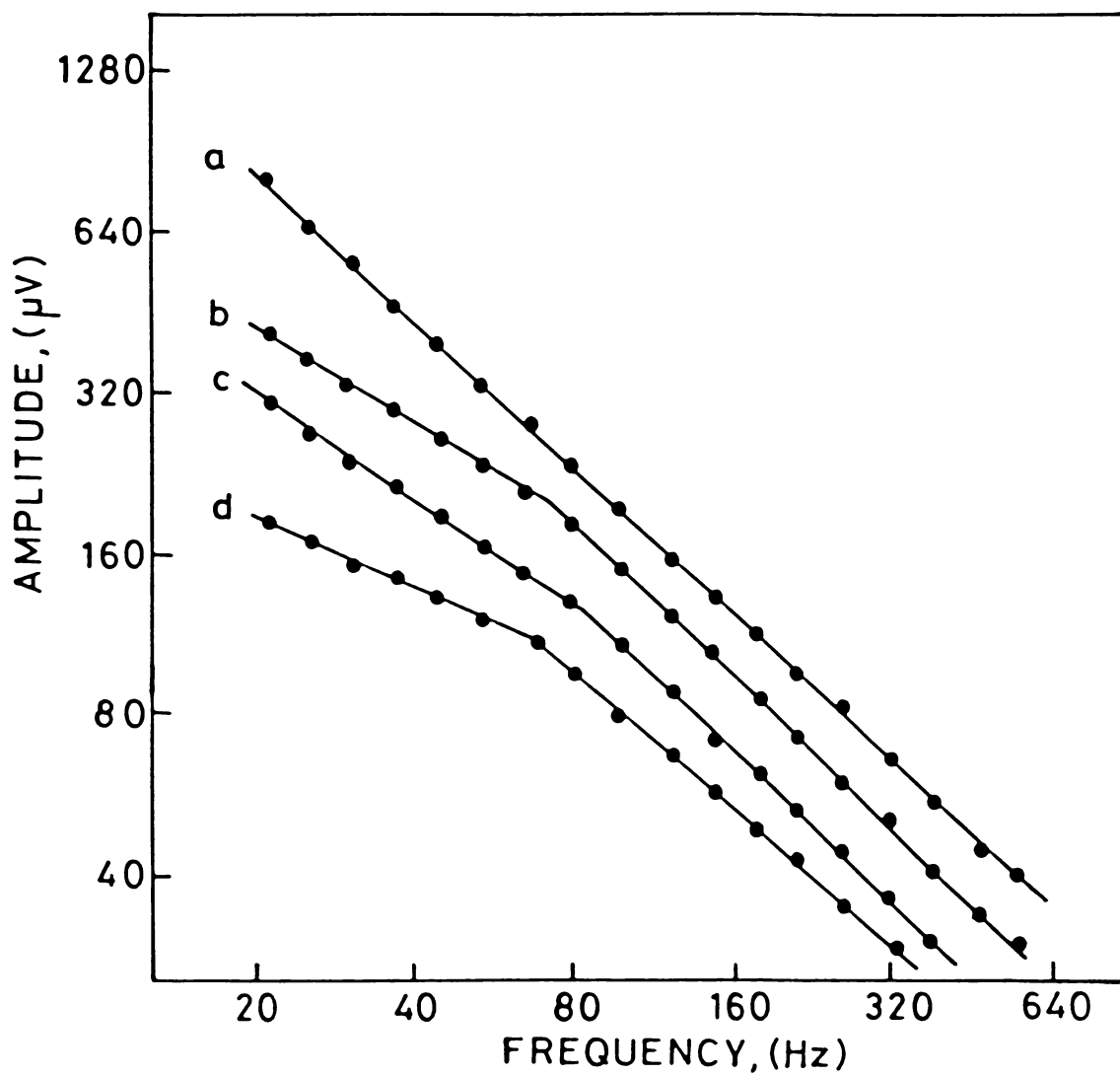


Fig.5.6 Log-log plots of variation of PA signal amplitude with chopping frequency for $\text{Ge}_x\text{Se}_{1-x}$ glasses.

(a) Reference sample, (b) $\text{Ge}_{0.10}\text{Se}_{0.90}$,
 (c) $\text{Ge}_{0.15}\text{Se}_{0.85}$, (d) $\text{Ge}_{0.20}\text{Se}_{0.80}$.

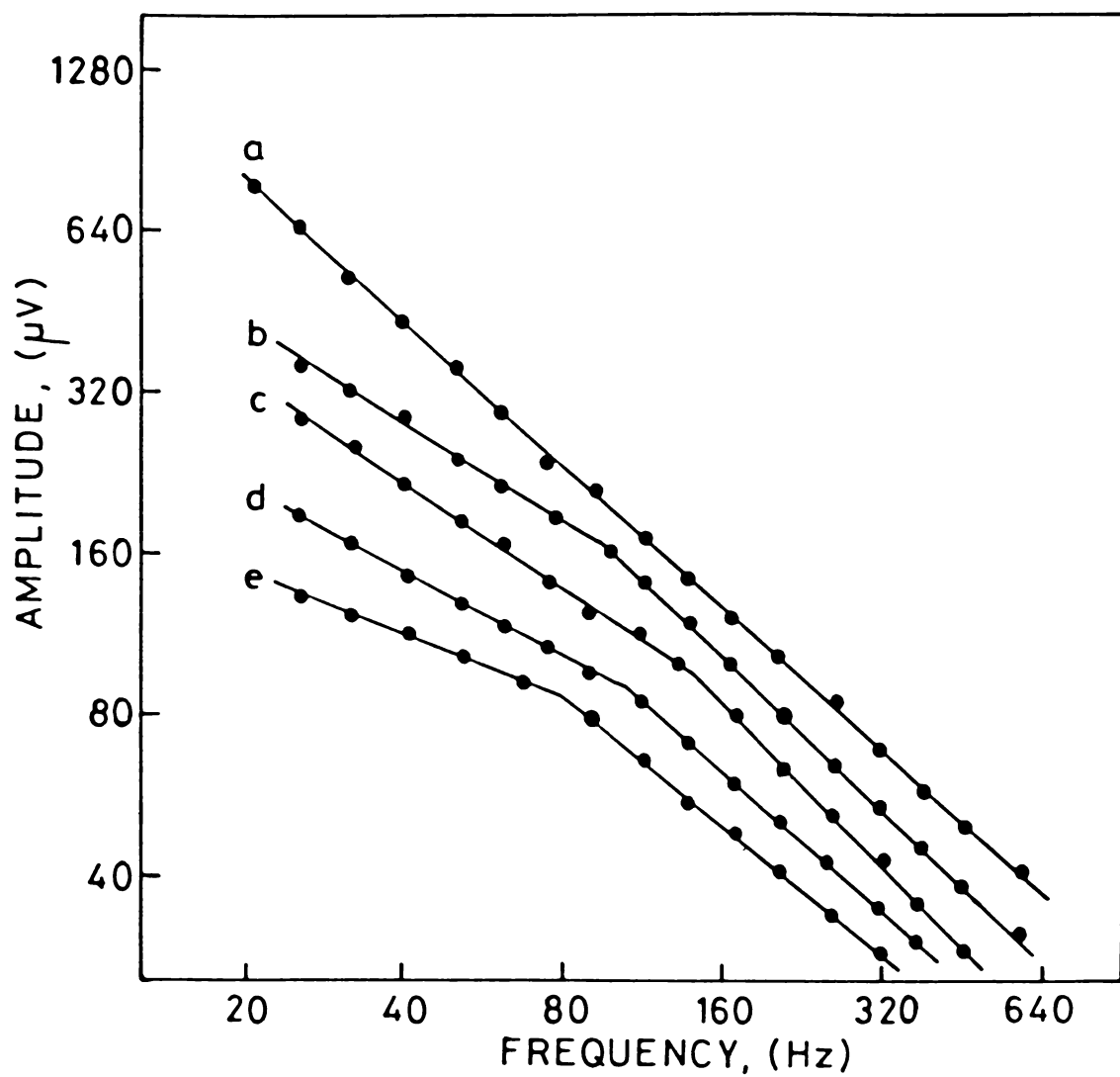


Fig.5.7 Log-log plots of variation of PA signal amplitude with chopping frequency for $\text{Ge}_x\text{Se}_{1-x}$ glasses.

(a) Reference sample, (b) $\text{Ge}_{0.25}\text{Se}_{0.75}$,

(c) $\text{Ge}_{0.28}\text{Se}_{0.72}$, (d) $\text{Ge}_{0.33}\text{Se}_{0.67}$, (e) $\text{Ge}_{0.38}\text{Se}_{0.62}$.

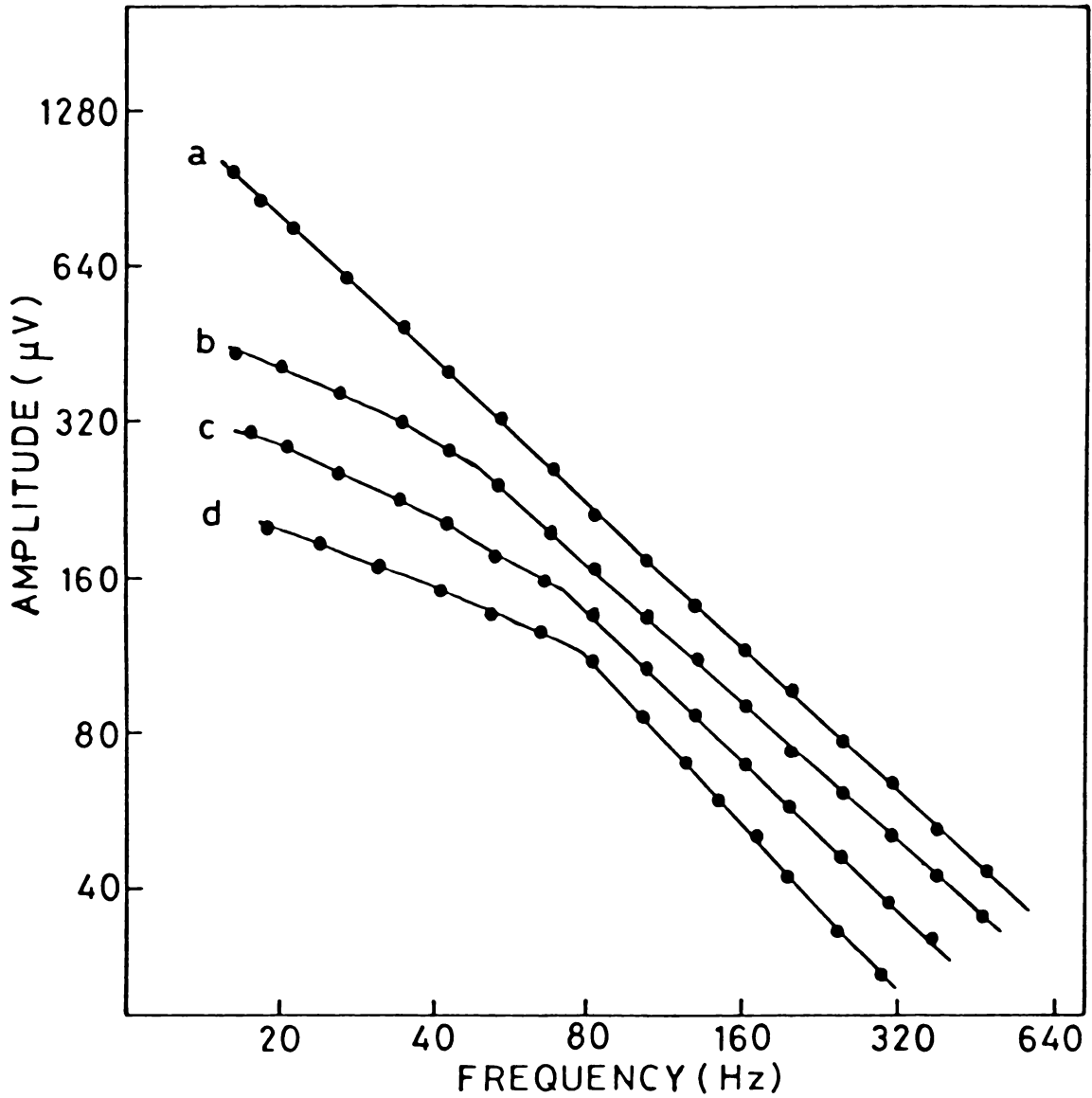


Fig.5.8 Log-log plots of variation of PA signal amplitude with chopping frequency for $\text{As}_x\text{Se}_{1-x}$ glasses.

- (a) Reference sample, (b) $\text{As}_{0.10}\text{Se}_{0.90}$,
 (c) $\text{As}_{0.40}\text{Se}_{0.60}$, (d) $\text{As}_{0.50}\text{Se}_{0.50}$.

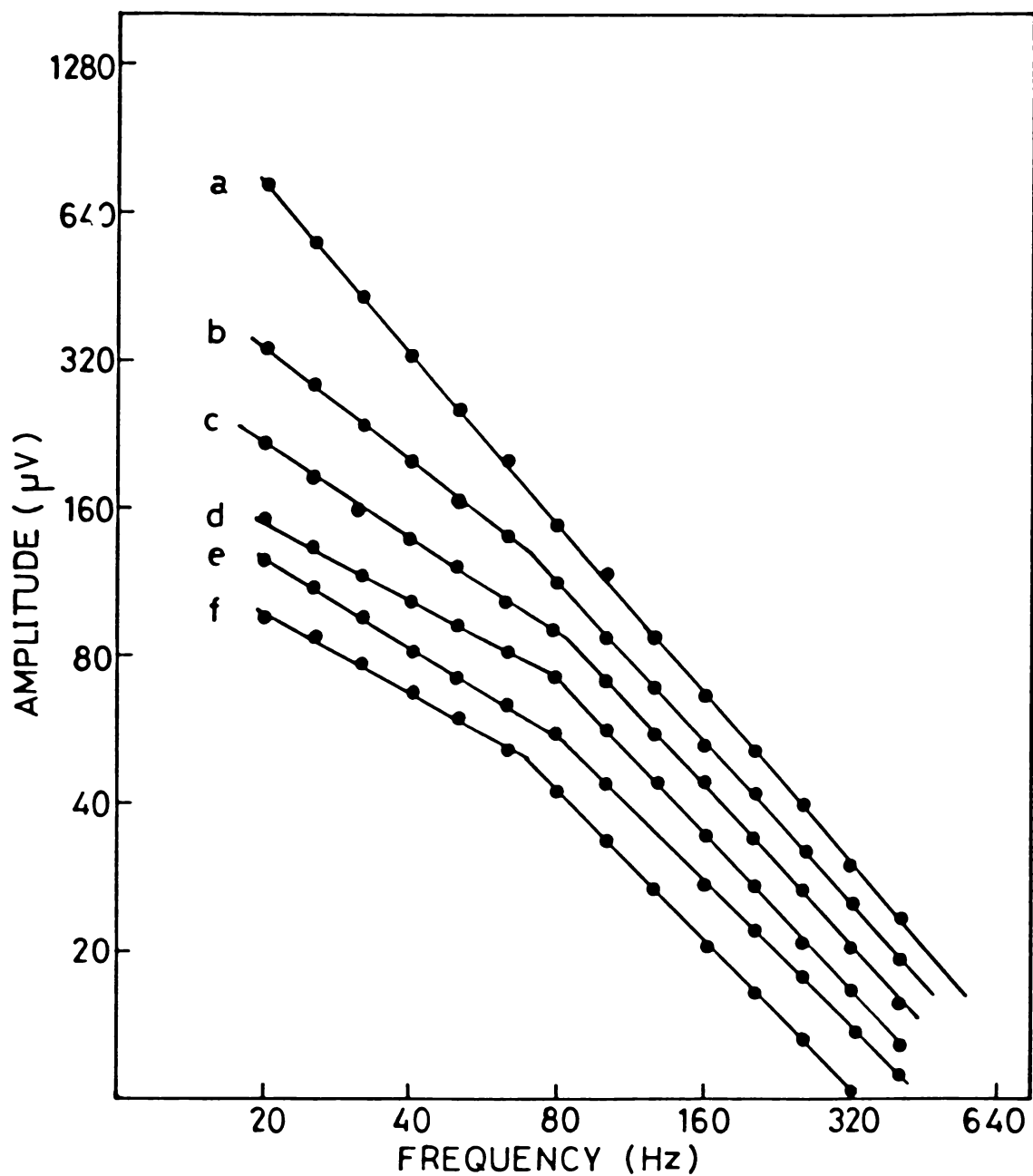


Fig.5.9 Log-log plots of variation of PA signal amplitude with chopping frequency for $\text{As}_x\text{Se}_{1-x}$ glasses.

(a) Reference sample, (b) $\text{As}_{0.20}\text{Se}_{0.80}$,

(c) $\text{As}_{0.25}\text{Se}_{0.75}$, (d) $\text{As}_{0.30}\text{Se}_{0.70}$,

(e) $\text{As}_{0.35}\text{Se}_{0.65}$, (f) $\text{As}_{0.45}\text{Se}_{0.55}$.

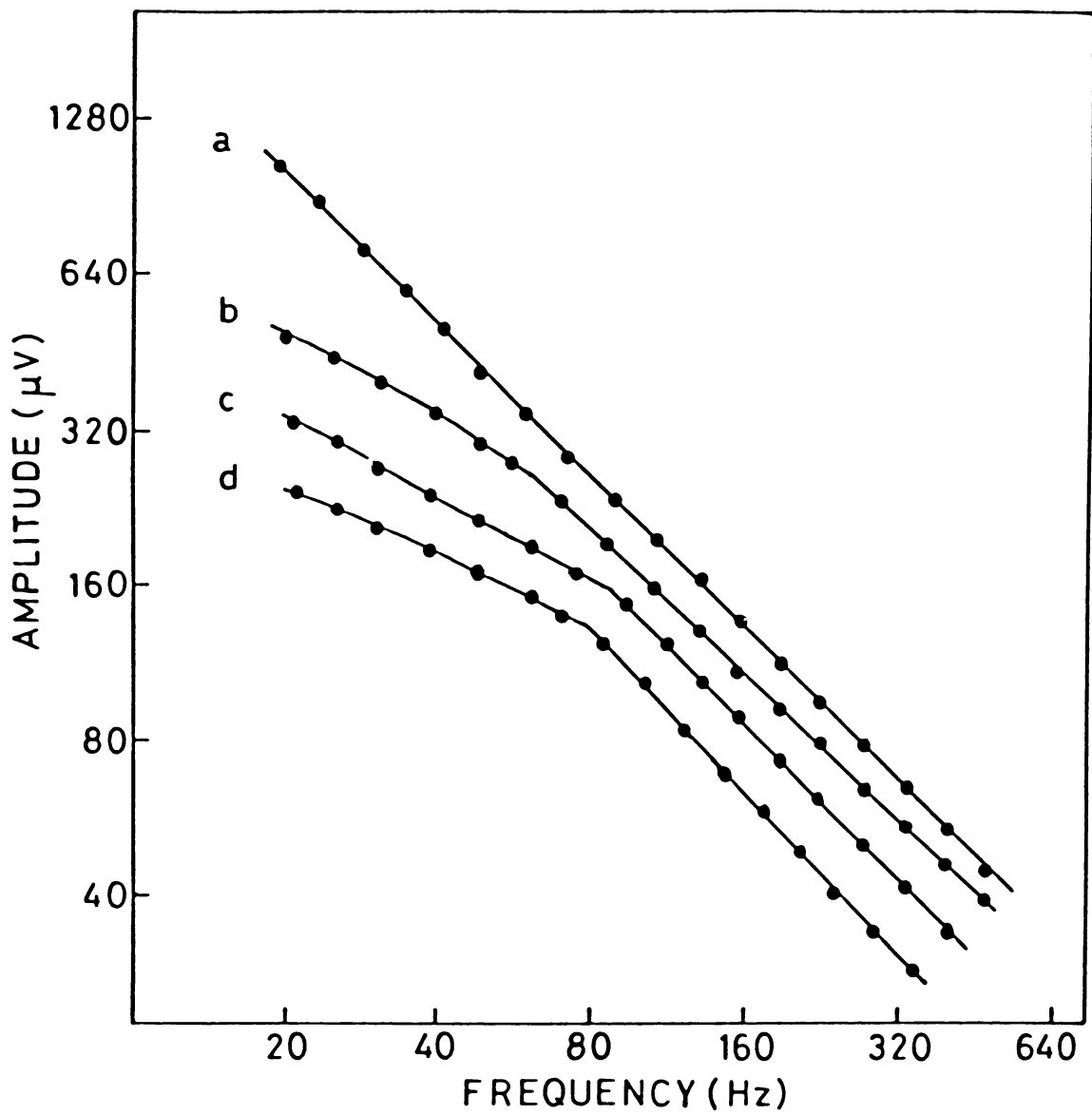


Fig.5.10 Log-log plots of variation of PA signal amplitude with chopping frequency for $\text{As}_x\text{Te}_{1-x}$ glasses.

(a) Reference sample, (b) $\text{As}_{0.25}\text{Te}_{0.75}$,

(c) $\text{As}_{0.30}\text{Te}_{0.70}$, (d) $\text{As}_{0.35}\text{Te}_{0.65}$.

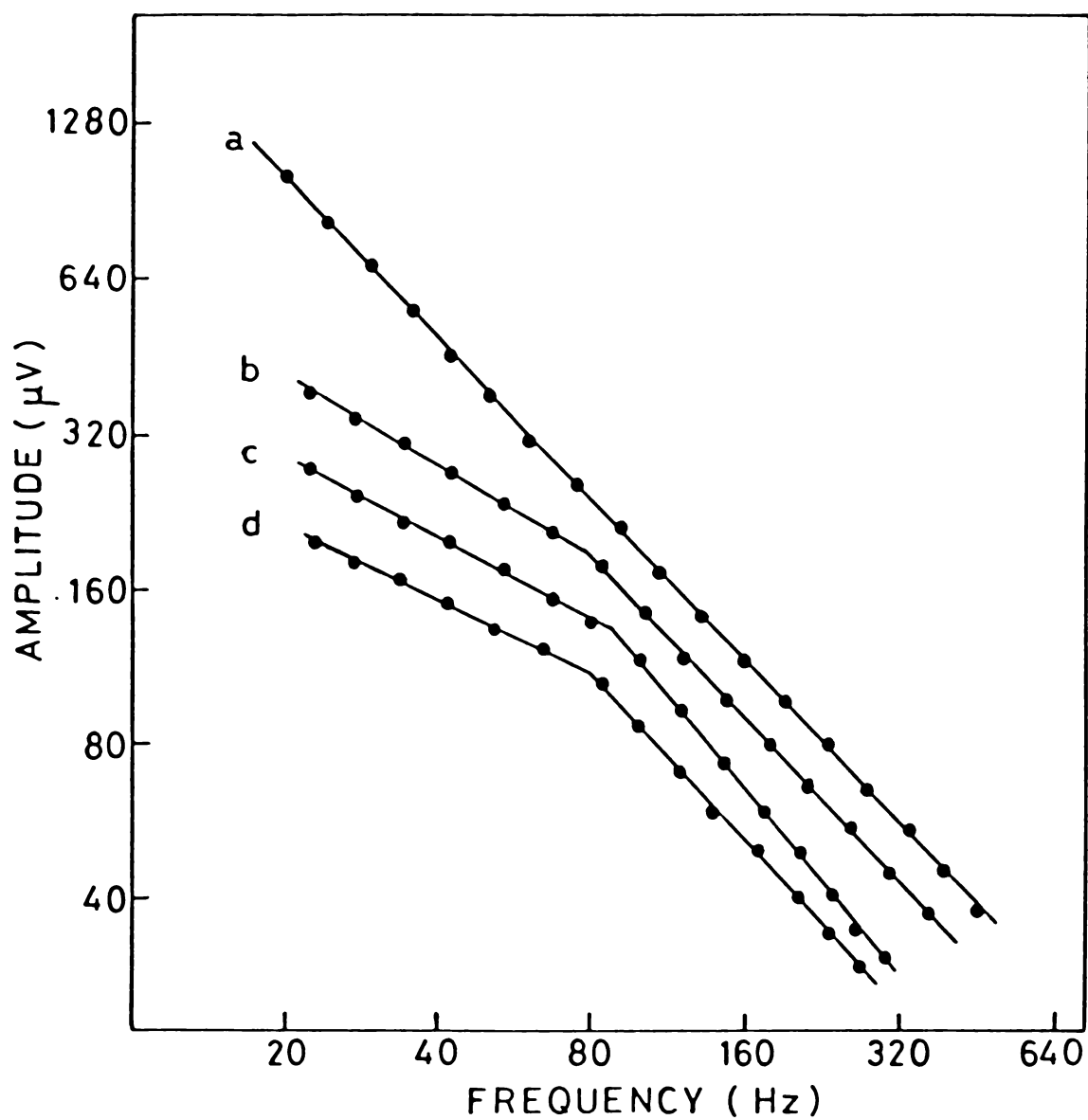


Fig.5.11 Log-log plots of variation of PA signal amplitude with chopping frequency for $\text{As}_x\text{Te}_{1-x}$ glasses.

(a) Reference sample, (b) $\text{As}_{0.40}\text{Te}_{0.60}$,

(c) $\text{As}_{0.45}\text{Te}_{0.55}$, (d) $\text{As}_{0.55}\text{Te}_{0.45}$.

thermally thick ($\mu_s < l_s; \mu_s > l_\beta$) sample. In the case of thin samples the slope of the amplitude versus chopping frequency plot changes from that of the reference sample at the characteristic frequency. Thus the determination of f_c from the amplitude versus frequency plots can easily be done. For $f > f_c$ the thermal diffusion length is confined within the sample itself and thus the amplitude versus chopping frequency plot is similar to that of the reference sample. For $f < f_c$ the sample is thermally thin and heat flow takes place to the backing material. The effect of the backing material produces a change in slope. Once f_c is determined the thermal diffusivity can be calculated using the formula $\alpha_s = f_c l_s^2$.

Characteristic frequency can also be determined from the variation of the phase of PA signal with chopping frequency. In order to eliminate nonsample parasite phase variations, the phase (ϕ_1) as a function of frequency for a thermally thick reference sample ($R = 0$) is measured. The sample phases (ϕ_2) are then subtracted from these phases to obtain $\Delta\phi$ as $\Delta\phi = \phi_1 - \phi_2$. $\Delta\phi$ becomes zero for $f > f_c$. The values of f_c determined in this way agrees well with those obtained from amplitude measurement.

The sample thickness, characteristic frequency, thermal diffusivity and average coordination number for all the $A_x^{IV}B_{1-x}^{VI}$ glasses and $A_x^VB_{1-x}^{VI}$ glasses studied are given in Tables 5.1 and 5.2 respectively.

5.4 VARIATION OF THERMAL DIFFUSIVITY WITH COMPOSITION

The variation of thermal diffusivity α_s as a function of the composition parameter x for three systems of glasses namely, Ge_xTe_{1-x} ($0.15 \leq x \leq 0.28$), Si_xTe_{1-x} ($0.10 \leq x \leq 0.28$) and Ge_xSe_{1-x} ($0.10 \leq x \leq 0.38$) are given in Figs. 5.12, 5.13 and 5.14 respectively. For the Ge_xTe_{1-x} and Si_xTe_{1-x} glasses, in the range of compositions studied, it is found that α_s has a maximum value at $x = 0.20$. For Ge_xSe_{1-x} glasses in which measurements are taken upto $x = 0.33$, α_s shows a peak value at the stoichiometric composition $x = 0.38$ while a discontinuous change is observed around $x = 0.2$. The variations in α_s with x can be related to the changes in the short range order taking place in the glass network with the increase in the concentration of group IV element as described in Chapter 3. The stable structure based on the AB_4 tetrahedral units formed at $x = 0.2$ in these systems offers relatively small resistance to the propagating thermal waves, since the system contains small amount of disorder at this composition compared to other compositions. In

Table 5.1: The average coordination number m , sample thickness l_s , characteristic frequency f_c and thermal diffusivity α_s of various compositions of $\text{Ge}_x\text{Te}_{1-x}$, $\text{Si}_x\text{Te}_{1-x}$ and $\text{Ge}_x\text{Se}_{1-x}$ glasses.

Composition	m	l_s (μm)	f_c (Hz)	$\alpha_s \times 10^{-2} \text{ cm}^2 / \text{sec.}$
$\text{Ge}_{0.28}\text{Te}_{0.72}$	2.56	200	49	1.96
$\text{Ge}_{0.25}\text{Te}_{0.75}$	2.50	200	63	2.52
$\text{Ge}_{0.22}\text{Te}_{0.78}$	2.44	200	78	3.12
$\text{Ge}_{0.20}\text{Te}_{0.80}$	2.40	250	61	3.81
$\text{Ge}_{0.17}\text{Te}_{0.83}$	2.34	200	45	1.80
$\text{Ge}_{0.15}\text{Te}_{0.85}$	2.30	150	42	0.95
$\text{Si}_{0.28}\text{Te}_{0.72}$	2.56	200	95	3.8
$\text{Si}_{0.25}\text{Te}_{0.75}$	2.50	250	78	4.9
$\text{Si}_{0.22}\text{Te}_{0.78}$	2.44	200	143	5.7
$\text{Si}_{0.20}\text{Te}_{0.80}$	2.40	300	72	6.5
$\text{Si}_{0.17}\text{Te}_{0.83}$	2.34	250	90	5.6
$\text{Si}_{0.15}\text{Te}_{0.85}$	2.30	250	74	4.6
$\text{Si}_{0.10}\text{Te}_{0.90}$	2.20	250	47	2.9
$\text{Ge}_{0.38}\text{Se}_{0.62}$	2.76	120	76	1.1
$\text{Ge}_{0.33}\text{Se}_{0.67}$	2.66	120	104	1.5
$\text{Ge}_{0.28}\text{Se}_{0.72}$	2.56	80	140	0.90
$\text{Ge}_{0.25}\text{Se}_{0.75}$	2.50	100	92	0.92
$\text{Ge}_{0.20}\text{Se}_{0.80}$	2.40	120	67	0.96
$\text{Ge}_{0.15}\text{Se}_{0.85}$	2.30	100	82	0.82
$\text{Ge}_{0.10}\text{Se}_{0.90}$	2.20	100	71	0.71

Table 5.2: The average coordination number m , sample thickness l_s , characteristic frequency f_c and thermal diffusivity α_s of various compositions of As_xSe_{1-x} and As_xTe_{1-x} glasses.

Composition	m	l_s (m)	f_c (Hz)	$\alpha_s \times 10^{-2} \text{ cm}^2 / \text{sec.}$
$As_{0.10}Se_{0.90}$	2.10	90	47	0.38
$As_{0.20}Se_{0.80}$	2.20	90	70	0.57
$As_{0.25}Se_{0.75}$	2.25	90	84	0.68
$As_{0.30}Se_{0.70}$	2.30	100	76	0.76
$As_{0.35}Se_{0.65}$	2.35	100	82	0.82
$As_{0.40}Se_{0.60}$	2.40	110	70	0.84
$As_{0.45}Se_{0.55}$	2.45	110	67	0.81
$As_{0.50}Se_{0.50}$	2.50	110	77	0.77
$As_{0.25}Te_{0.75}$	2.25	110	60	0.72
$As_{0.30}Te_{0.70}$	2.30	100	85	0.85
$As_{0.35}Te_{0.65}$	2.35	110	77	0.93
$As_{0.40}Te_{0.60}$	2.40	120	75	1.08
$As_{0.45}Te_{0.55}$	2.45	110	86	1.04
$As_{0.55}Te_{0.45}$	2.55	110	79	0.96

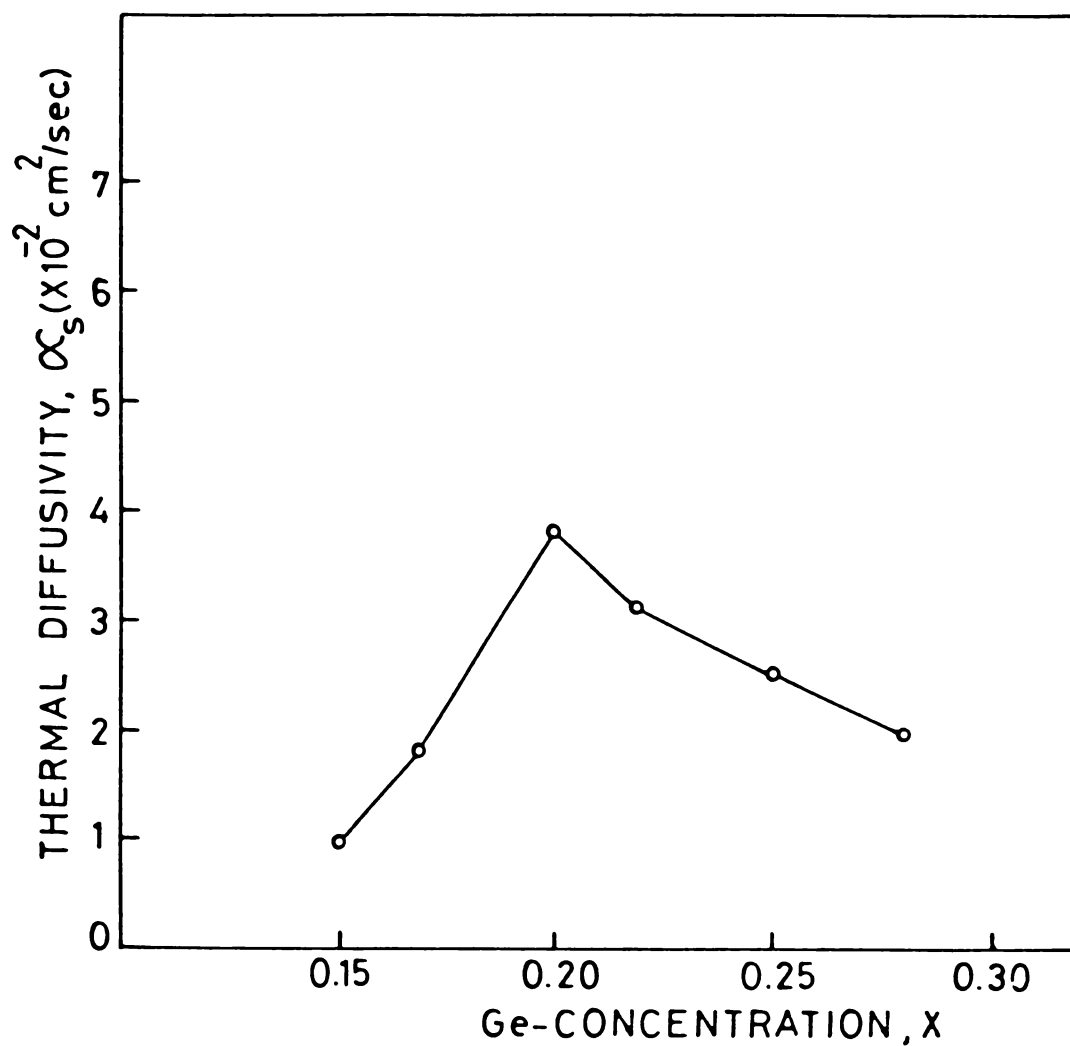


Fig.5.12 Variation of thermal diffusivity with composition for $\text{Ge}_x\text{Te}_{1-x}$ glasses.

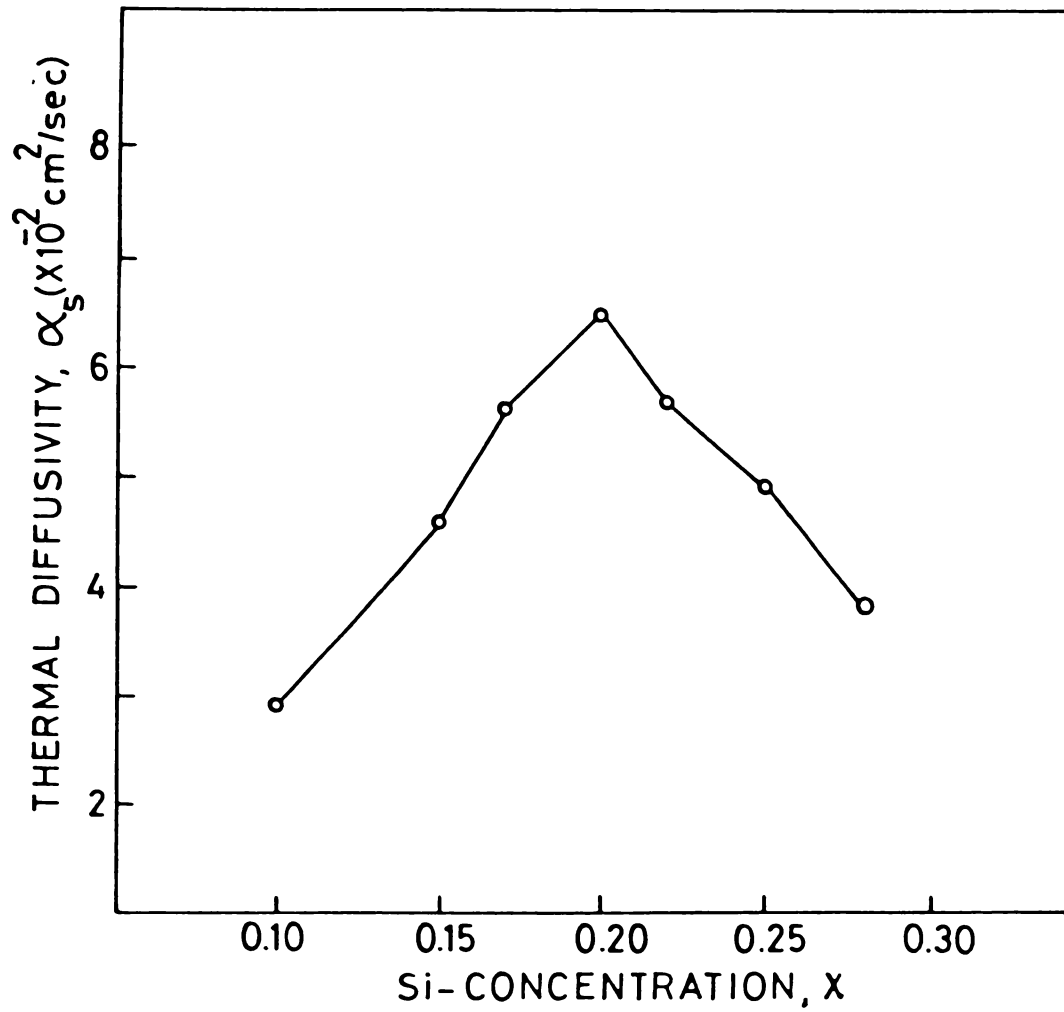


Fig.5.13 Variation of thermal diffusivity with composition for Si_xTe_{1-x} glasses.

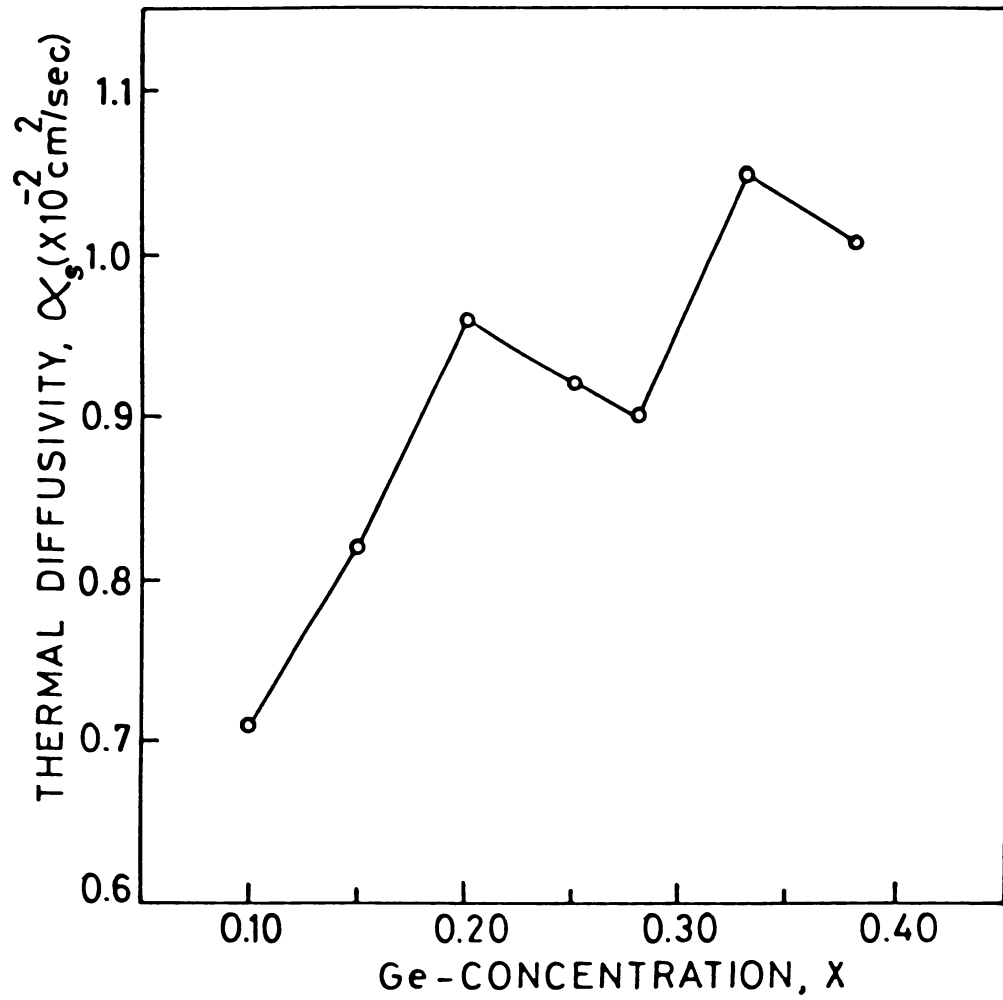


Fig.5.14 Variation of thermal diffusivity with composition for $\text{Ge}_x\text{Se}_{1-x}$ glasses.

the case of $\text{Ge}_x\text{Se}_{1-x}$ glasses the maximum in α_s occurs at $x = 0.33$ which corresponds to chemical threshold for this system.

The variation of α_s for $\text{As}_x\text{Se}_{1-x}$ ($0.10 \leq x \leq 0.50$) and $\text{As}_x\text{Te}_{1-x}$ ($0.25 \leq x \leq 0.55$) samples with the composition parameter x are given in Fig.5.15 and 5.16 respectively. In both these systems α_s has a maximum value at $x = 0.4$ at which the stoichiometric compound $\text{A}_2^{\text{V}}\text{B}_3^{\text{VI}}$ is formed as described in chapter 4. The disorder which causes the scattering of thermal phonons is minimum at this composition in these glasses. Disorder in the network increases as the value of x is varied from that corresponding to the compound composition, thus decreasing the thermal diffusivity.

In the next chapter a more rigorous discussion on the variation of α_s with x , which shows maxima at compositions having average coordination $m = 2.4$ ($x = 0.2$ for $\text{A}_x^{\text{IV}}\text{B}_{1-x}^{\text{VI}}$ systems and $x = 0.4$ for $\text{A}_x^{\text{V}}\text{B}_{1-x}^{\text{VI}}$ systems) for all the five groups of samples are presented based on the constraints theory and the idea of rigidity percolation in these random networks.

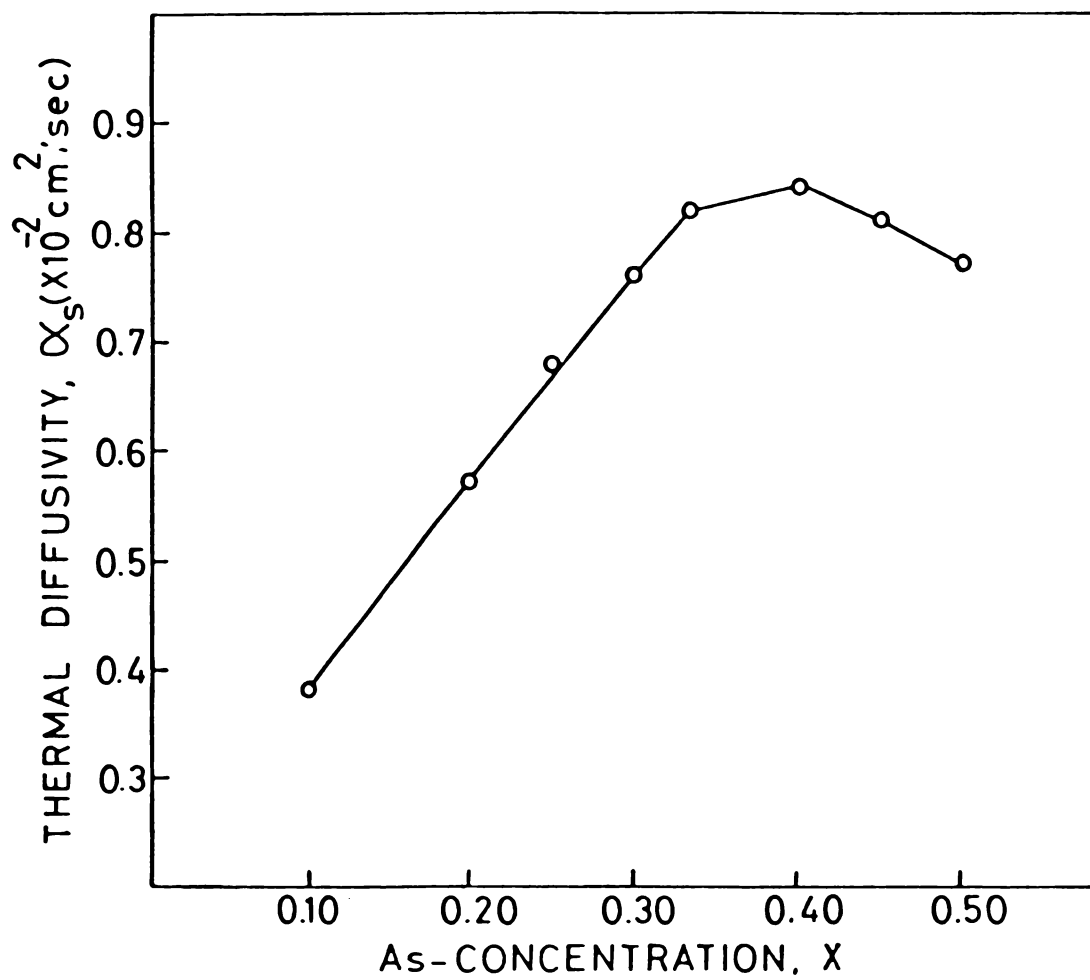


Fig.5.15 Variation of thermal diffusivity with composition for $\text{As}_x\text{Se}_{1-x}$ glasses.

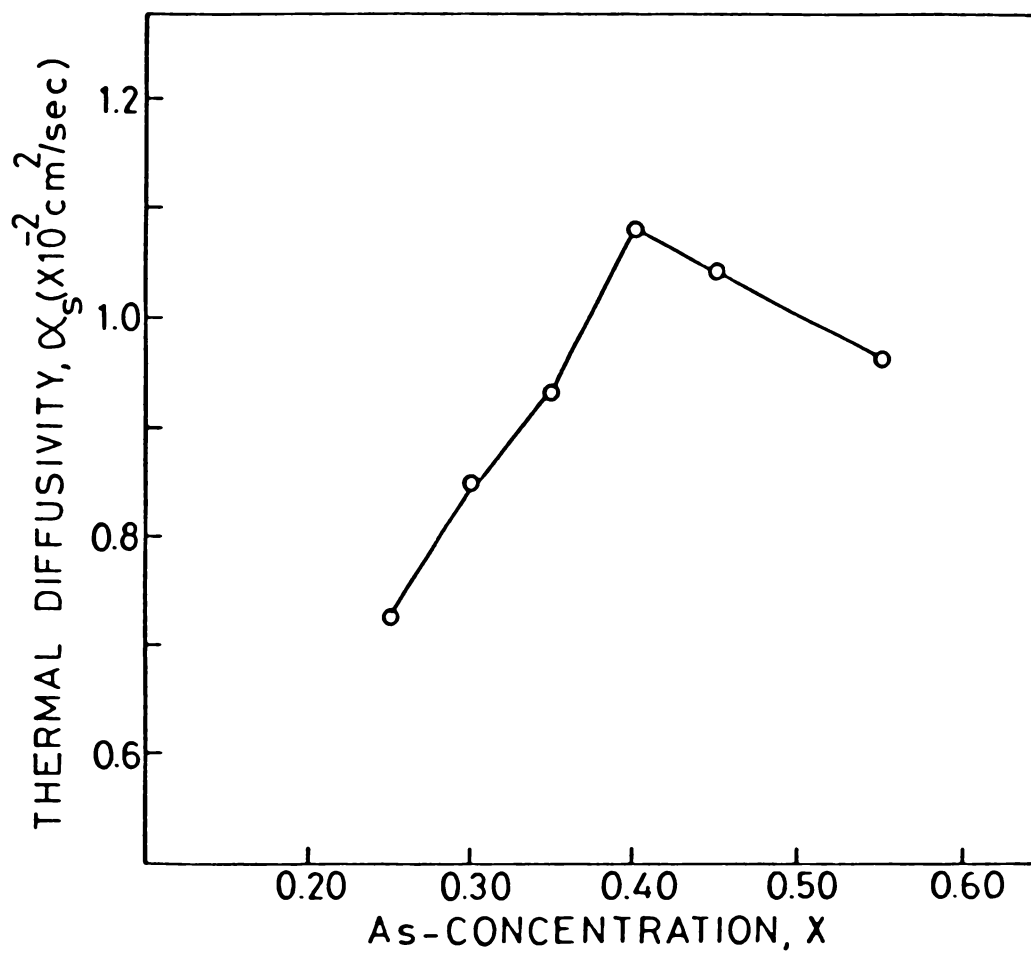


Fig.5.16 Variation of thermal diffusivity with composition for $\text{As}_x\text{Te}_{1-x}$ glasses.

Chapter 6

RIGIDITY PERCOLATION AND THRESHOLD THERMAL CONDUCTION IN BINARY CHALCOGENIDE RANDOM NETWORKS

6.1 INTRODUCTION

Percolation ideas have been applied to several different physical phenomena [232]. In recent years there has been a great deal of interest in the elastic and vibrational properties of random percolating systems [233-238]. These studies deal with problems related to elastic properties of random networks near percolation transitions. Kantor and Webman [234] studied the macroscopic elastic moduli of an elastic percolating network in the critical region using a microscopic elastic Hamiltonian which contains the bending energy term and concluded that the elastic behaviour of a percolating network with local bending elasticity is characterized by a different critical exponent than that of the related conductivity problem. Bond percolation on elastic networks involving nearest neighbour forces studied by numerical simulations by Feng and Sen [233] also indicate a value for the elastic critical exponent higher than that of the corresponding electrical

conductivity exponent. They pointed out that the percolation threshold for central forces p_{α} is much larger than p_c , the threshold for scalar percolation such as charge percolation. For nearest neighbour central forces, Feng, Thorpe and Garboczi [235] showed, using effective medium theory, that

$$p_{\alpha} = dp_c \quad (6.1)$$

where d is the dimensionality of the space in which the network is embedded. Similar effective medium theories for scalar problems have shown that [239]

$$p_c = \frac{2}{z} \quad (6.2)$$

so that,

$$p_{\alpha} = \frac{2d}{z} \quad (6.3)$$

where z is the coordination number. The vector percolation threshold is much larger than the scalar one because many connections in the network produce zero elastic restoring forces.

According to Phillips theory [173,196,240] of non-equilibrium network glass formation, the glass forming composition is optimized mechanically by equating the number

of force field constraints which are intact at glass transition to the number of atomic degrees of freedom. Later Thorpe [241] showed that in the range of glass forming compositions the system contains both rigid and floppy regions, the later being associated with soft vibrational modes stabilized only by broken or ineffective force field constraints such as Van der Waals forces between chains. A linear increase in the elastic constants in glass alloys with increase in the number of force field constraints has been predicted by several workers [235,242].

A clear understanding of the mechanical critical behaviour in a system close to configurational equilibrium depends on the experimental evidence for the same. There has been a number of experimental evidences for the existence of a critical composition at an average coordination m_c in several chalcogenide glasses. The experimental evidences for vibrational thresholds near critical average coordination in alloy network glasses has been reviewed and discussed previously by Phillips [236]. The composition dependence of acoustic attenuation and velocity in Ge_xSe_{1-x} and Ge_xS_{1-x} glasses measured by Gilroy and Phillips [243] exhibit a low temperature peak in the attenuation for $x = 0.2$ and 0.33 . The composition dependence of several narrow Raman bands in Ge_xSe_{1-x} glass alloys have been

measured by Murase et al [244]. They have reported a discontinuity near $x = 0.2$ composition corresponding to a Raman shift of $\delta\omega \approx 3 \text{ cm}^{-1}$. The infrared transverse and longitudinal optic spectra of $\text{Ge}_x\text{Se}_{1-x}$ glasses reported by Murase and Fukunaga [245] indicate a softening of the LO peak with a threshold at $x = 0.2$. Since the LO mode involves long range Coulomb interactions it is more sensitive to network stiffening than other modes. The high pressure electrical resistivity measurements reported by Asokan et al [166] on $\text{Si}_x\text{Te}_{1-x}$ glasses show that they undergo discontinuous changes in electrical resistivity, transition pressure and activation energy again at the $x = 0.2$ composition. The As-Se alloys are mechanically most stable at $x = 0.4$ which is evident from the deep minimum in the glass transition width at this composition in the specific heat curves of these alloys [212,246,247]. The width of the specific heat peak at $x = 0.4$ is twice as narrow as at $x = 0.30$ or 0.50 . The composition dependence of the glass transition temperature [211] and optical properties [207] in this system also indicate the existence of critical composition at $x = 0.4$. The results on the thermal diffusivity measurements on $\text{A}_x^{\text{IV}}\text{B}_{1-x}^{\text{VI}}$ and $\text{A}_x^{\text{V}}\text{B}_{1-x}^{\text{VI}}$ glasses presented in the previous chapter also give a clear experimental evidence for the critical behaviour in these systems, as is demonstrated in this chapter.

The constraints theory [173] and the ideas of rigidity percolation [241] have been used to explain the existence of critical composition in chalcogenide network glasses. Even though the percolation models stress only acoustic mode thresholds, experiments seem to indicate that related thresholds are present in Raman active optic modes as well. Pressure dependence of the A_1 modes [245] suggests that application of external pressure to an over-constrained network at first compresses only the floppy regions, but then at a critical pressure it begins to convert the floppy regions into rigid ones.

6.2 TOPOLOGICAL DESCRIPTION OF THE GLASS NETWORK

Phillips [173] introduced an atomic model which considered the glass transition as a network phenomenon, governed by topological considerations, to predict the glass forming tendency as a function of composition. It has been shown that compositional dependence of the glass forming tendency in chalcogenide alloys depends primarily on short range order which is determined by the bond stretching and bond bending interactions. The interactions function as mechanical constraints in the system and the ideal glass is formed when these constraints are equal to the number of degrees of freedom at a critical average

coordination number m_c . When the average coordination number $m < m_c$, the network is underconstrained and tends to disintegrate into nonpolymerized fragments. For small positive values of $(m_c - m)$ the fragments retain their three dimensional character, but further increase in $(m_c - m)$ produces dimensional contraction, first to quasi planar crossed chains and finally to quasi linear chain bundles. When $m > m_c$ the network is overconstrained. Then the interatomic interactions can be separated into intact and broken constraints. The transition from the intact constraints to broken constraints can be explained on the basis of molecular cluster formation [240].

Thorpe [241] described the glassy network in terms of its rigidity. He pointed out that a network consisting of long polymer chains is different from a network describing an amorphous solid as far as its rigidity is concerned. The former can be deformed easily whereas the later is rigid. The number of ways M_0 in which the network can be continuously deformed with no cost in energy is equivalent to the number of zero frequency modes. For low average coordination number m the network is a polymeric glass in which the rigid regions are isolated. As the mean coordination increases, these rigid regions increase

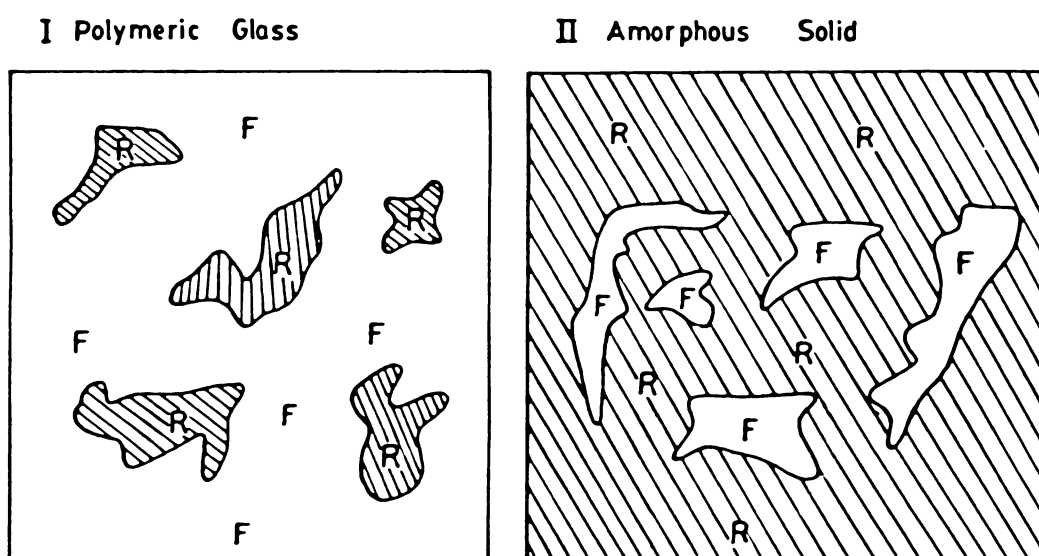


Fig.6.1 Rigid and floppy regions in networks of polymeric glass and amorphous solid.

in volume until at $m = m_c$ a percolation transition takes place to a rigid network or amorphous solid. This is shown schematically in Fig.6.1. It is the percolation of rigidity that drives the transition. Mean field theory predicts that such a transition takes place at $m = m_c = 2.4$ [241]. In general the number of zero frequency modes M_0 is given by the difference between the number of degrees of freedom and the number of linearly independent constraints. Considering linearly independent bond bending and bond stretching constraints Thorpe showed that M_0 tends to zero at $m = m_c = 2.4$.

6.3 THRESHOLD BEHAVIOUR AND CONSTRAINTS IN THE GLASS NETWORK

Threshold behaviour in thermal conduction exhibited by the $A_x^{IV}B_{1-x}^{VI}$ and $A_x^V B_{1-x}^{VI}$ glasses can be attributed to the mechanical stiffening of the glass network at the critical composition x_c due to the threshold percolation of rigidity and the corresponding threshold in the internal stress. Because of the random nature of the network, it can be thought of as a two phase material with floppy and rigid regions. If N_{CON} is the number of interatomic force field constraints per atom and N_d the number of vector degrees of freedom per atom, the material will be rigid

if $N_{\text{CON}} > N_d$ which corresponds to the rigidity percolation. Within the framework of the effective medium theory [235, 241] the number of cyclical zero frequency modes per atom is given by

$$\begin{aligned} f &= N_d - N_{\text{CON}} \quad \text{if } N_d > N_{\text{CON}} \\ &= 0 \quad \quad \quad \text{if } N_d < N_{\text{CON}} \end{aligned} \quad (6.4)$$

If p is the bond occupation probability and p_α the percolation threshold of p for central forces, then for $N_{\text{CON}} > N_d$, the elastic constants C scale with $p - p_\alpha$ as

$$C \sim (p - p_\alpha)^{f_\alpha} \quad (6.5)$$

with $f_\alpha = 1.0$. If we include both central bond stretching and rotationally invariant bond bending forces, the constraints theory can be used to derive expression for the corresponding threshold in bond occupation probability $p_{\alpha\beta}$ as follows.

The number of constraints associated with the α bond stretching and β bond bending forces can be written as

$$N_{\text{CON}} = N^\alpha + N^\beta \quad (6.6)$$

If z is the coordination number, then

$$N^{\alpha}(z) = \frac{1}{2} z \quad (6.7)$$

and $N^{\beta}(dz) = \frac{1}{2}(d-1)(2z-d)$

where d is the dimensionality of the lattice. Obviously all atoms with $z \leq d-2$ must be eliminated which only means that the dangling bonds must not be considered in the evaluation of force constants in a three dimensional glass network. When each bond is present with probability p then

$$N_{\text{CON}}(p) = N^{\alpha}(pz) + N^{\beta}(d,pz) \quad (6.8)$$

and Phillips glass forming condition [173] which determines $p_{\alpha\beta}$ in mean field theory becomes

$$p_{\alpha\beta} z + (d-1)(2p_{\alpha\beta} z - d) = 2d \quad (6.9)$$

However, when only the bond stretching forces are considered we will get

$$p_{\alpha} z = 2d \quad (6.10)$$

Phillips and Thorpe [242] have computed $p_{\alpha\beta}$ for a number of well known lattices. A striking feature of relation (6.9) is that the threshold positions are independent of the strengths of α and β . This means that as $\beta \rightarrow 0$, $C(p)$ consists of two parts given by

$$C(p) = \beta C_1 (p - p_{\alpha\beta})^{f_{\alpha\beta}} + \alpha C_2 (p - p_{\alpha})^{f_{\alpha}} \quad (6.11)$$

with $f_{\alpha} \simeq 1.0$. Numerical simulations [233,248,249] show that $f_{\alpha\beta}$ is greater than 2 in two dimensions.

The value of $p_{\alpha\beta}$ in a percolative model of a noncrystalline alloy is rather straight forward [173,240]. Assume that the binary alloy $A_x B_{1-x}$ have coordination number z_A and z_B and that the network contains fractions f_{AA} , f_{AB} and $2f_{AB}$ (with $f_{AA} + f_{BB} + 2f_{AB} = 1$) of chemical bonds arranged consistent with x , z_A and z_B in such a way as to maximize f_{AB} , i.e. to maximize the chemical order. If the fractions of occupied bonds are p_{AA} , p_{BB} and $p_{AB} = \{p\}$ and if both α and β forces are present for all three types of bonds then a linear superposition in mean field theory gives

$$N_{CON}(x, \{p\}) = x N_{CON}^A(\{p\}) + (1-x) N_{CON}^B(\{p\}) \quad (6.12)$$

with

$$N_{\text{CON}}^A(\{p\}) = N^\alpha(\tilde{z}_A) + N^\beta(d, \tilde{z}_A) \quad (6.13)$$

and a similar expression holding good for N_{CON}^B with N^α and N^β given by (6.7)

Here

$$\tilde{z}_A = \frac{z_A [f_{AA} p_{AA} + f_{AB} p_{AB}]}{[f_{AA} + f_{AB}]} \quad (6.14)$$

and a similar expression for \tilde{z}_B . Putting $N_{\text{CON}} = d$ we obtain

$$x\tilde{z}_A + (1-x)\tilde{z}_B = z_{\alpha\beta}(d) \quad (6.15)$$

For a three dimensional network one obtains

$$z_{\alpha\beta}(3) = 2.4 \quad (6.16)$$

For $A_x^{IV} B_{1-x}^{VI}$ and $A_x^V B_{1-x}^{VI}$ alloys the average coordination number m can be determined knowing the coordination numbers z_A and z_B of elements A and B respectively using the expression [192]

$$m = xz_A + (1-x)z_B \quad (6.17)$$

The values of m for various compositions of all the glasses belonging to the five groups of alloys described in chapter 5 have been calculated. The average coordination number m is 2.4 corresponding to the composition at which threshold maxima in thermal diffusivity occur in all these systems. See figures 5.12, 5.13 and 5.14 for the Ge-Te, Si-Te and Ge-Se systems and figures 5.15 and 5.16 for the As-Se and As-Te systems respectively. This value of m is the same as the value of $z_{\alpha\beta}$ for a three dimensional network. The value of x corresponding to the critical average coordination is 0.2 for $A_x^{IV}B_{1-x}^{VI}$ glasses and 0.4 for $A_x^V B_{1-x}^{VI}$ glasses. The composition for which $x = 0.2$ corresponds to the formation of stable AB_4 tetrahedra for $A_x^{IV}B_{1-x}^{VI}$ glasses whereas in the case of $A_x^V B_{1-x}^{VI}$ glasses at $x = 0.4$ stable structure based on pyramidal $A(B_{\frac{1}{2}})_3$ is formed. It is for these compositions we get the threshold peak in the thermal diffusivity/conductivity values. The surprisingly good agreement of the observed behaviour with the percolation model leads us to believe that the observed behaviour is a consequence of the threshold percolation of rigidity in the glass network.

The rigidity of the glass forming network can most usefully be described in terms of the mechanical

constraints. An ideal glass is one in which the total number of constraints imposed by the valence forces is equal to the number of degrees of freedom i.e. $N_{\text{CON}} = N_d$. The two types of short range order bonding interactions described by valence force fields (VFF) are, two body central force α associated with bond stretching and three body noncentral forces β associated with bond bending. In the VFF model, considering an average coordination number $m = z_A + (1-x)z_B$ for a binary alloy $A_x B_{1-x}$ where z_A and z_B are coordination numbers of A and B respectively, the number of constraints per atom as a function of the average coordination number m is given by

$$N_{\text{CON}}(m) = \frac{m}{2} + \frac{m}{2}(m-1) \quad (6.18)$$

Here the first term on the right hand side is associated with α forces and the second term with β forces. Now considering the ideal glass forming conditions $N_{\text{CON}} = N_d$, for $N_d = 3$ we get the critical average coordination $m_c = 2.45$. For the case of $As_x Se_{1-x}$ glasses Phillips' constraints counting arguments lead to critical composition and mean

coordination number as $x_c = 0.4$ and $m_c = 2.4$ respectively. The corresponding values of x_c and m_c for $\text{Ge}_x\text{Se}_{1-x}$ glasses are 0.16 and 2.33 respectively. However, Gilroy and Phillips [243] pointed out that the number of independent bond angles is the relevant quantity and for coordination number m this is $(2m-3)$ rather than $m(m-1)$. With this modification the ideal glass composition occurs at $x = 0.2$ in $\text{Ge}_x\text{Se}_{1-x}$ system. In $\text{As}_x\text{Se}_{1-x}$ glasses the mechanical and chemical thresholds coincide at $x = 0.4$ whereas in $\text{Ge}_x\text{Se}_{1-x}$ glasses the mechanical thresholds occur at $x = 0.2$ and chemical thresholds at $x = 0.33$. Our results seem to be a very good manifestation of the threshold behaviour exhibited by both $\text{A}_x^{\text{IV}}\text{B}_{1-x}^{\text{VI}}$ and $\text{A}_x^{\text{V}}\text{B}_{1-x}^{\text{VI}}$ glasses. The ideal glass formed at $m = 2.4$ in these systems offer minimum resistance to thermal waves or the corresponding phonons and this is consistent with our observations.

According to the mean field model when the network is slightly underconstrained corresponding to $x < x_c$, cyclical zero frequency vibrational modes are present with their number going to zero at $x = x_c$ [241]. When fluctuations and cluster internal surface effects are included a small number of cyclical modes would be present even at $x = x_c$. These modes tend to be much more delocalized than modes

with $\omega^2 > 0$ [250]. In any case the number of such modes would be minimum at $x = x_c$. In the polymeric glass with the floppy regions dominating compared to rigid ones, the number of zero frequency modes increases as we go away from m_c towards lower m values. As the mean coordination m increases, rigid regions increase in volume until at $m = m_c$ a percolation transition takes place to a rigid network. In the amorphous solid with rigid regions dominating finite frequency modes begin to appear as we move away from m_c towards higher side. There seems to be good agreement between our observations and predictions based on ideas of rigidity percolation.

Chapter 7

GLASS TRANSITION AND TEMPERATURE DEPENDENCE OF THERMAL

DIFFUSIVITY AND ENERGY GAP IN SELECTED $A_x^{IV} B_{1-x}^{VI}$ AND

$A_x^V B_{1-x}^{VI}$ GLASSES INVESTIGATED USING

PHOTOACOUSTIC TECHNIQUE

7.1 INTRODUCTION

Even 56 years after Zachariassen published his classic diffraction paper [53] on the radial distribution probability in SiO_2 glass, our understanding of the glassy state of solid matter still remains far from complete. A clear picture of the mechanism of glass transition is yet to evolve even though substantial amount of experimental data have accumulated during the past three decades. A lot more experimentation and proper interpretation of data seem to be necessary to answer several questions connected with glass transition and the microscopic glass forming tendency of certain materials.

A liquid undergoes a glass transition into a state with thermodynamic and elastic properties characteristic of a solid when it is supercooled sufficiently fast

and far below its equilibrium freezing temperature without crystallizing. When the cooling rate is high enough, the freezing temperature T_f is bypassed and the liquid phase persists until lower temperature T_g is reached. The liquid \rightarrow glass transition occurs in a narrow temperature interval near T_g , the glass transition temperature. As the temperature is lowered below T_g , the molecular relaxation time τ becomes very high so that material loses its ability to rearrange its atomic configuration. The atoms get frozen into well defined positions which corresponds to the configuration they had at T_g .

The process of glass transition involves both thermodynamical and dynamical features. This is confirmed by the experimental observations of a jump in specific heat, viscosity, compressibility, thermal expansion coefficient etc. [30]. As has been discussed in chapter 6, substantial progress has been made in recent years in relating the microscopic glass forming tendency with experimental results on several systems [173,240,241].

The characteristic properties of glass transition closely resemble a second order thermodynamic transition [30]. While the volume $V(T)$ is continuous through the vicinity of T_g , thermal expansion coefficient $\alpha(T)$ and

specific heat $C_p(T)$ step up from a low value characteristic of the glass to a high value characteristic of the liquid, upon passing through this region. However, these changes are diffuse, occurring over a small temperature interval rather than a single sharply definable temperature as in the case of a true second order transition. Differential scanning calorimetry (DSC) is one of the useful technique for studying the process of glass formation. DSC traces show small step at T_g .

The study of the various physical parameters near the glass transition temperature T_g is very important to understand the process of glass transition. In this chapter we demonstrate that PA technique can be effectively used for studying the optical and thermal properties over a wide range of temperature including T_g . Even though the use of the PA effect for studying first and second order phase transitions have been demonstrated by several authors before [134,251-253], not much work on probing the features of glass transition using this technique has been reported in literature. Due to the dependence of the PA signal on the thermal properties such as specific heat, thermal expansion and thermal conductivity of the sample, on going through a phase transition, the PA response

essentially reflects the thermodynamic changes that are taking place in the sample. Therefore PA studies will give information about the changes in the thermal properties of samples at the glass transition temperature, which in turn can provide valuable information about the mechanism of this transition. We have used the PA technique to locate the glass transition temperature T_g in selected chalcogenide glasses belonging to the $A_x^{IV}B_{1-x}^{VI}$ and $A_x^VB_{1-x}^{VI}$ systems and determined the temperature dependence of the thermal diffusivity and optical absorption in them upto temperatures above their T_g . The details of the high temperature PA cell and the PA set up used for the high temperature studies have been discussed already in Chapter 2. For the high temperature studies we have chosen Ge_xSe_{1-x} ($0.10 \leq x \leq 0.38$) and As_xSe_{1-x} ($0.10 \leq x \leq 0.55$) glasses as representatives of the $A_x^{IV}B_{1-x}^{VI}$ and $A_x^VB_{1-x}^{VI}$ systems respectively.

7.2 DETERMINATION OF GLASS TRANSITION TEMPERATURE

Initially the variation of the PA signal amplitude and phase from the samples have been measured as a function of temperature with white light from the Xe lamp chopped at a frequency of 22 Hz with the intention of studying their variations near the glass transition temperature T_g . The samples used are thermally thick at this chopping

frequency so that the thermal properties of the backing medium do not affect the PA signal.

The temperature dependence measurements have been done at intervals of $\approx 2^\circ\text{C}$. A temperature controller was used to aid accurate measurements. The heating rate used is $\approx 1^\circ\text{C}/\text{min}$.

The variation of the PA amplitude with temperature for various compositions of $\text{As}_x\text{Se}_{1-x}$ and $\text{Ge}_x\text{Se}_{1-x}$ glasses are drawn in Figs.7.1 and 7.2 respectively. The glass transition temperatures of all these glasses are already known from calorimetric measurements. It can be seen from these curves that the amplitude starts falling significantly before the glass transition temperature T_g and shows a minimum value at T_g . The temperatures at which minima in PA amplitude occurs coincide with the known T_g values for all the samples investigated. Therefore we find that it is possible to locate the T_g from these plots very easily.

The variations of the PA phase with temperature for $\text{As}_x\text{Se}_{1-x}$ and $\text{Ge}_x\text{Se}_{1-x}$ glasses are drawn in Figs.7.3 and 7.4 respectively. The PA phase has a critical maximum value again at T_g . The agreement between the T_g values

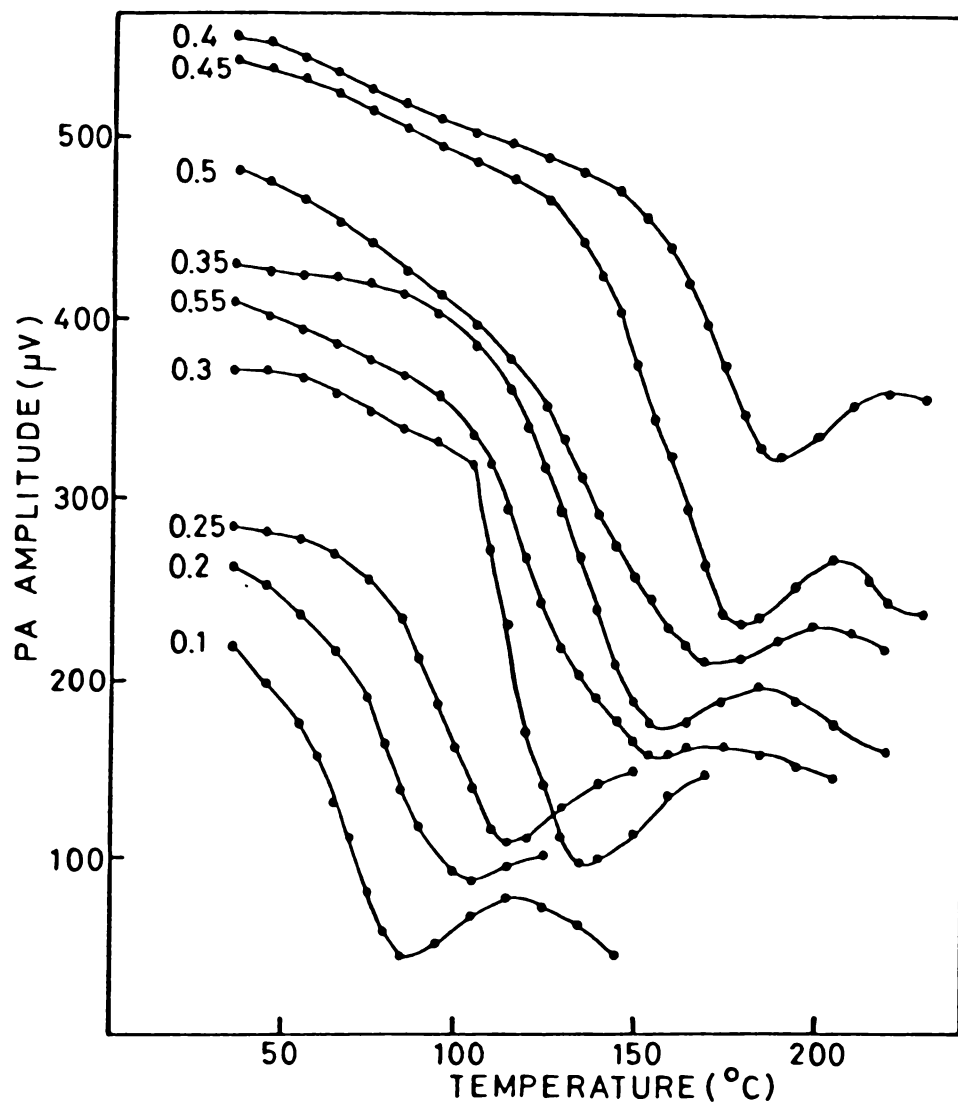


Fig.7.1 Variation of PA amplitude with temperature for As_xSe_{1-x} glasses. The x values are noted on the curves.

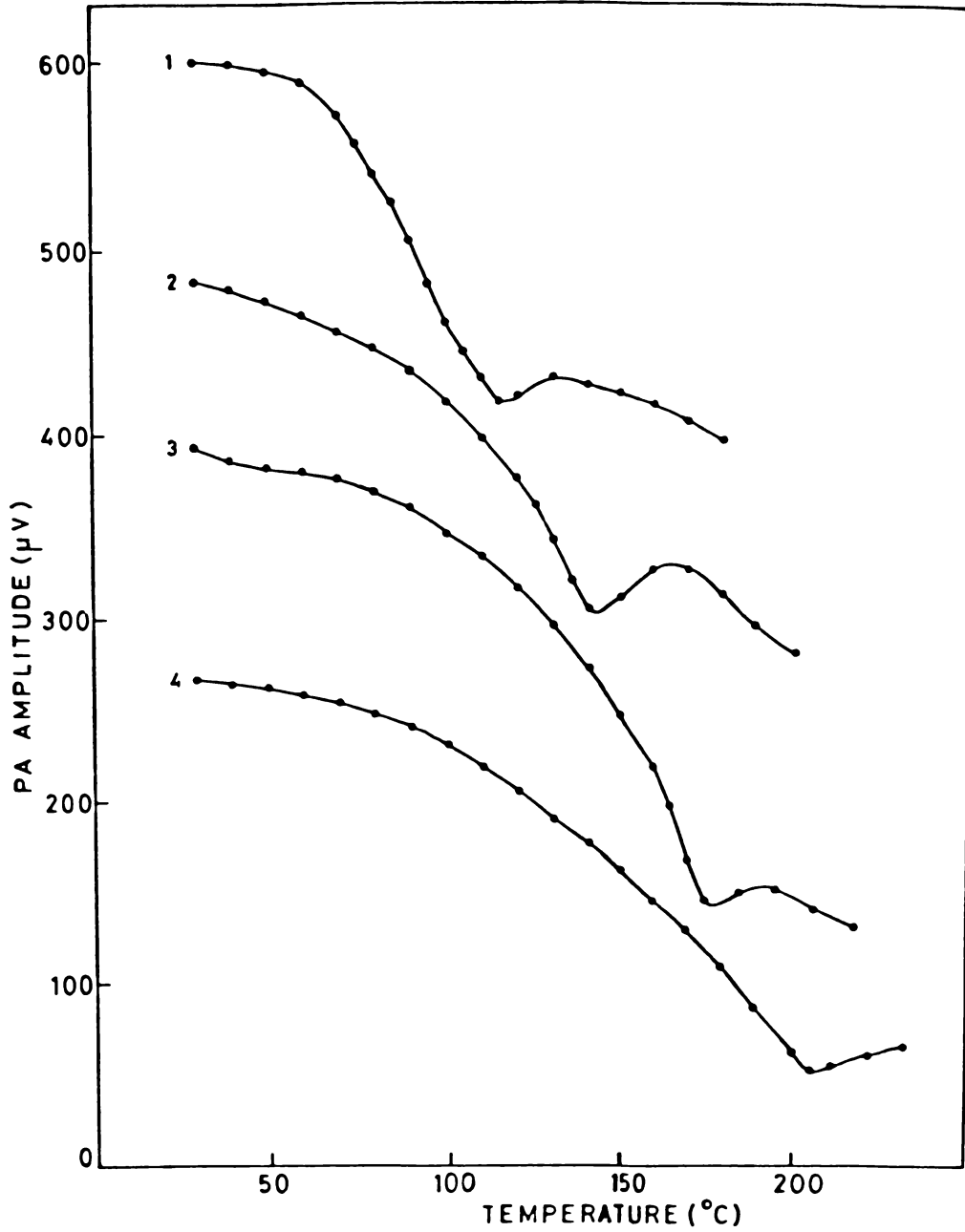


Fig.7.2 Variation of PA amplitude with temperature for $\text{Ge}_x\text{Se}_{1-x}$ glasses.

- (1) $\text{Ge}_{0.10}\text{Se}_{0.90}$, (2) $\text{Ge}_{0.15}\text{Se}_{0.85}$,
 (3) $\text{Ge}_{0.20}\text{Se}_{0.80}$, (4) $\text{Ge}_{0.25}\text{Se}_{0.75}$.

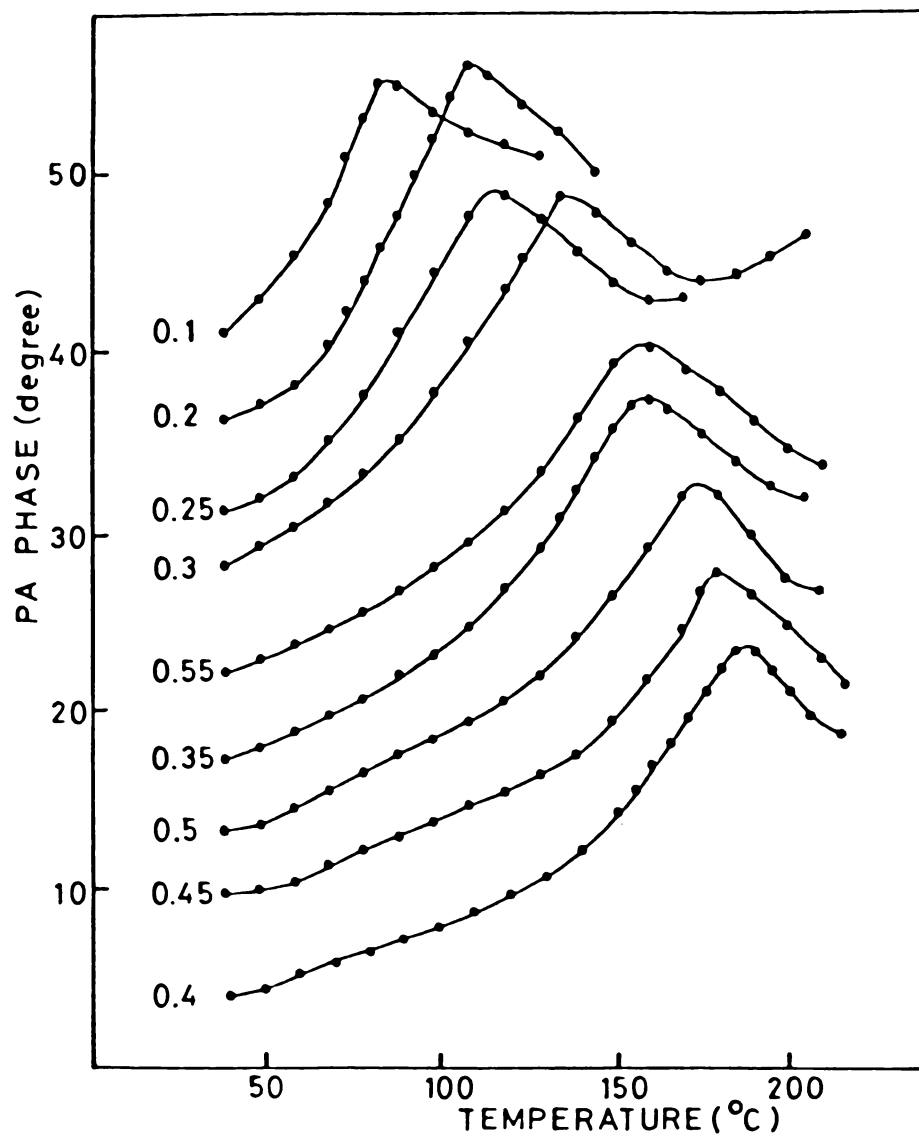


Fig.7.3 Variation of PA phase with temperature for As_xSe_{1-x} glasses. The x values are noted on the curves.

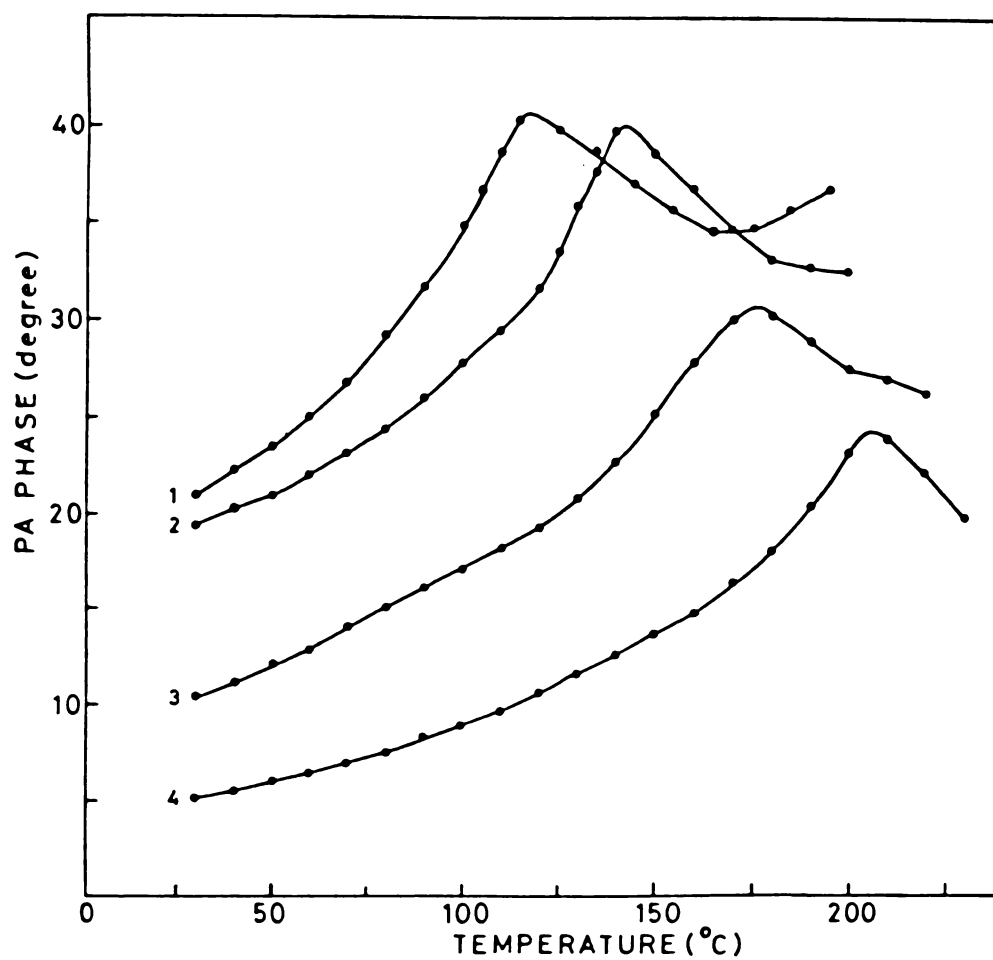


Fig.7.4 Variation of PA phase with temperature for $\text{Ge}_x\text{Se}_{1-x}$ glasses.

(1) $\text{Ge}_{0.10}\text{Se}_{0.90}$, (2) $\text{Ge}_{0.15}\text{Se}_{0.85}$,

(3) $\text{Ge}_{0.20}\text{Se}_{0.80}$, (4) $\text{Ge}_{0.25}\text{Se}_{0.75}$.

at which the amplitude exhibits minimum and phase exhibits maximum is excellent in all the samples. The T_g values determined in this way do agree very well with the values determined from calorimetric measurements. The fact that PA amplitude has a critical minimum value at T_g shows that the sample has minimum thermal diffusivity or maximum thermal resistance at T_g . Consequently it takes longer time for the generated thermal waves to travel through the sample and get converted into pressure waves so that the phase delay is maximum at T_g . As far as we know this is the first time it is demonstrated that PA technique can be used to locate glass transition temperatures in glassy solids.

The composition dependence of T_g in As_xSe_{1-x} glasses determined using PA technique is drawn in Fig.7.5. The same plot obtained from calorimetric measurements and reported by Myers and Felty [211] is reproduced in the same figure for comparison. The glass transition temperature is found to be maximum for the $As_{0.4}Se_{0.6}$ composition which is the stable composition mechanically and chemically in As-Se system. The T_g values of Ge_xSe_{1-x} glasses with $0.10 \leq x \leq 0.25$ determined from PA studies are plotted as a function of composition in Fig.7.6. This does not show any anomalous change at $x = 0.2$ which is the mechanical

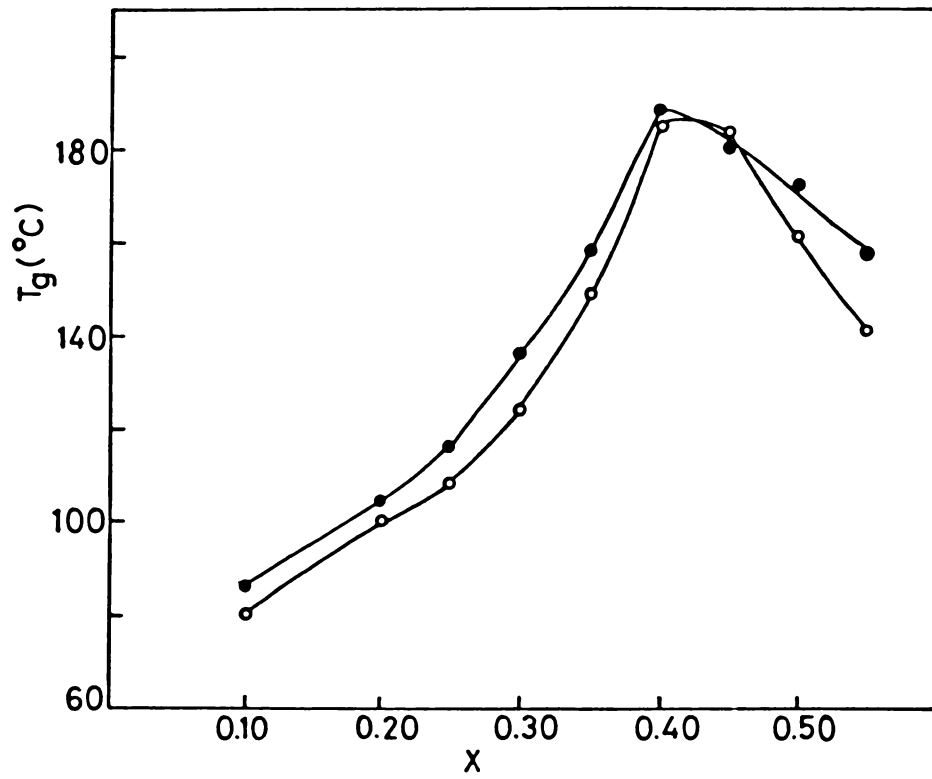


Fig.7.5 Variation of glass transition temperature with composition for As_xSe_{1-x} glasses. (●) Present data, (○) Data reproduced from Ref.211.

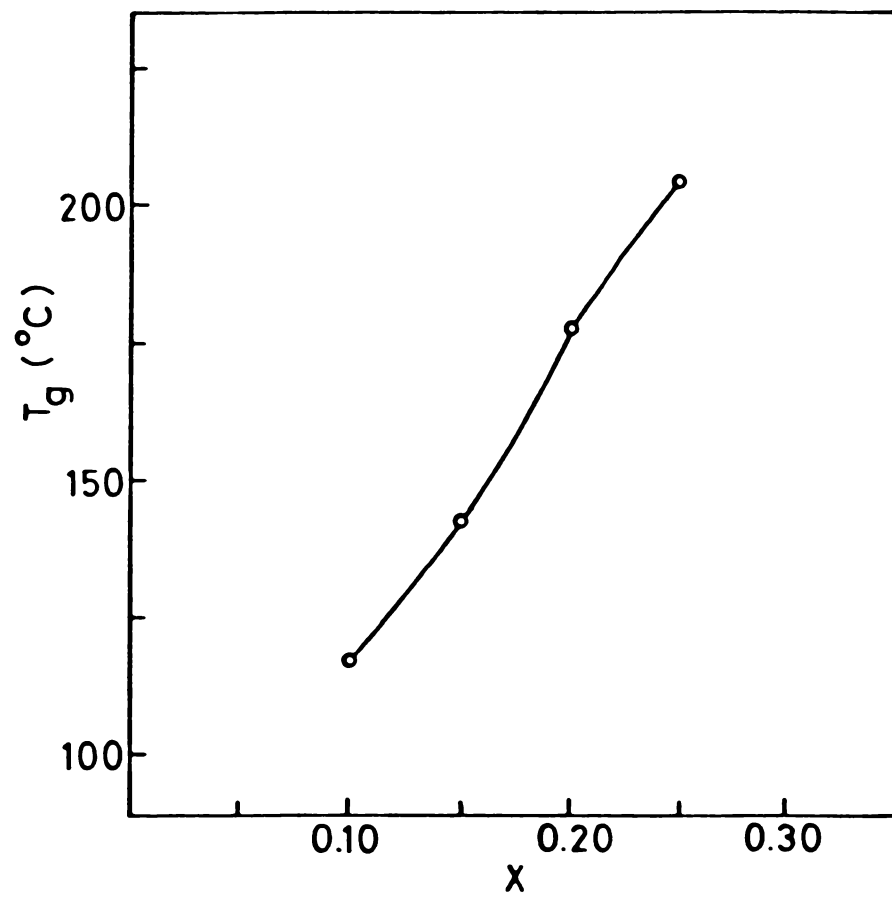


Fig.7.6 Variation of glass transition temperature with composition for $\text{Ge}_x\text{Se}_{1-x}$ glasses.

threshold for this system. Here also the T_g values determined by the present technique agree well with the reported data from calorimetric measurements which also does not exhibit any anomaly at $x = 0.2$ [167].

From the investigations on the variation of PA amplitude and phase as a function of temperature at different chopping frequencies, it is found that the T_g measurement by the PA method depend slightly on the chopping frequency. The temperature-amplitude plots taken at three different chopping frequencies on $As_{0.3}Se_{0.7}$ sample are shown in Fig.7.7. The corresponding phase plots are drawn in Fig.7.8. These plots indicate that T_g shows lower values at lower chopping frequencies. The T_g values shift slightly to higher values as the chopping frequency is increased. Even though these measurements have been carried out on other samples as well, all the curves are not shown here as the nature of all of them is about the same. The slight frequency dependence for the observed T_g values indicates that the opto-thermal-acoustic conversion mechanism in PA effect is directly related to the relaxation occurring at T_g [30] and is getting affected by the repetition rate of the input radiation.

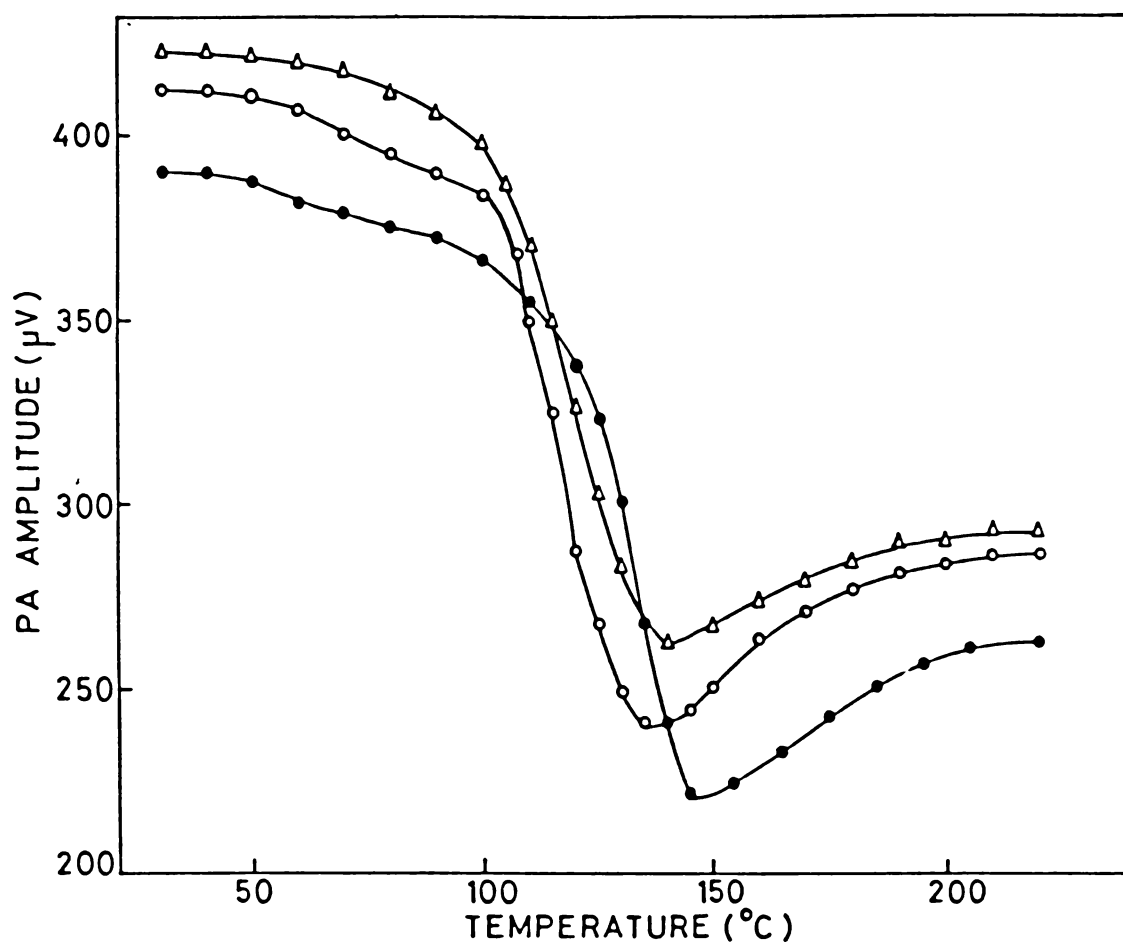


Fig.7.7 PA amplitude as a function of temperature for $\text{As}_{0.30}\text{Se}_{0.70}$ sample at three different chopping frequencies.

(○) 22 Hz, (Δ) 70 Hz, (●) 320 Hz.

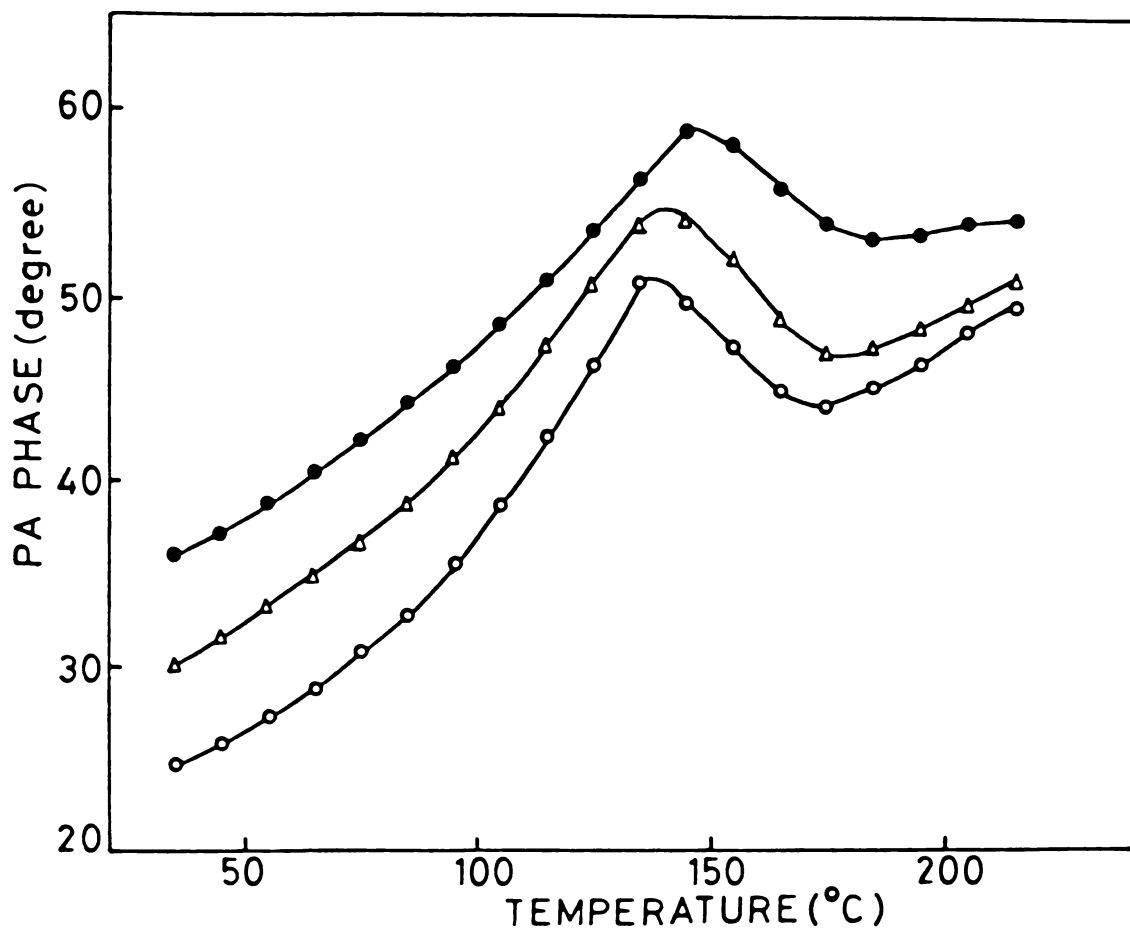


Fig.7.8 PA phase as a function of temperature for $\text{As}_{0.30}\text{Se}_{0.70}$ sample at three different chopping frequencies.

(○) 22 Hz, (Δ) 70 Hz, (●) 320 Hz.

7.3 VARIATION OF THERMAL DIFFUSIVITY WITH TEMPERATURE

A systematic measurement of the temperature dependence of the thermal diffusivity in various compositions of the $\text{As}_x\text{Se}_{1-x}$ and the $\text{Ge}_x\text{Se}_{1-x}$ glasses have been carried out using PA technique. The results are presented for temperatures upto and above glass transition temperature T_g to bring out the features near T_g . As has been described in Chapter 5, thermal diffusivity α_s is determined by measuring the variation of the PA signal amplitude and phase as a function of chopping frequency. The samples are shaped and thinned down to thickness of the order of 0.1 mm by hand lapping and polishing to make them suitable for determining the characteristic frequency f_c above which the PA signal is independent of the effect of the backing material. For these measurements the samples are fixed on a brass disc which acts as a thermally thick backing medium. For determining f_c the PA phase of a thermally thick reference sample (thickness ≈ 1 mm) and that of the experimental sample are measured as a function of the chopping frequency. Then f_c is obtained as the frequency at which the difference between these two phases $\Delta\phi$ tend to zero.

The characteristic frequency has also been determined from the frequency-amplitude plot as the frequency at which a clear change in its slope takes place. Then the thermal diffusivity α_s is given by $\alpha_s = f_c l_s^2$ where l_s is the sample thickness. In this way the thermal diffusivities of different compositions of As_xSe_{1-x} and Ge_xSe_{1-x} glasses are determined at various fixed temperatures upto $T > T_g$. The temperature has been controlled with the help of a heater wound around the sample chamber and powered by a control circuit. The $\Delta\phi$ versus chopping frequency plots at various temperatures for two representative samples $As_{0.25}Se_{0.75}$ and $Ge_{0.20}Se_{0.80}$ are shown in Fig.7.9 and Fig. 7.10 respectively.

The corresponding amplitude plots for the same two samples are shown in Fig.7.11 and 7.12. Similar plots have been obtained for all the compositions of the two systems. But all of them are not reproduced here to avoid repetition. The thermal diffusivity values obtained by this method are tabulated in Table 7.1.

The variation of the thermal diffusivity as a function of temperature determined as described above for As_xSe_{1-x} glasses are shown in Fig.7.13. It is found that thermal diffusivity decreases with increase in the

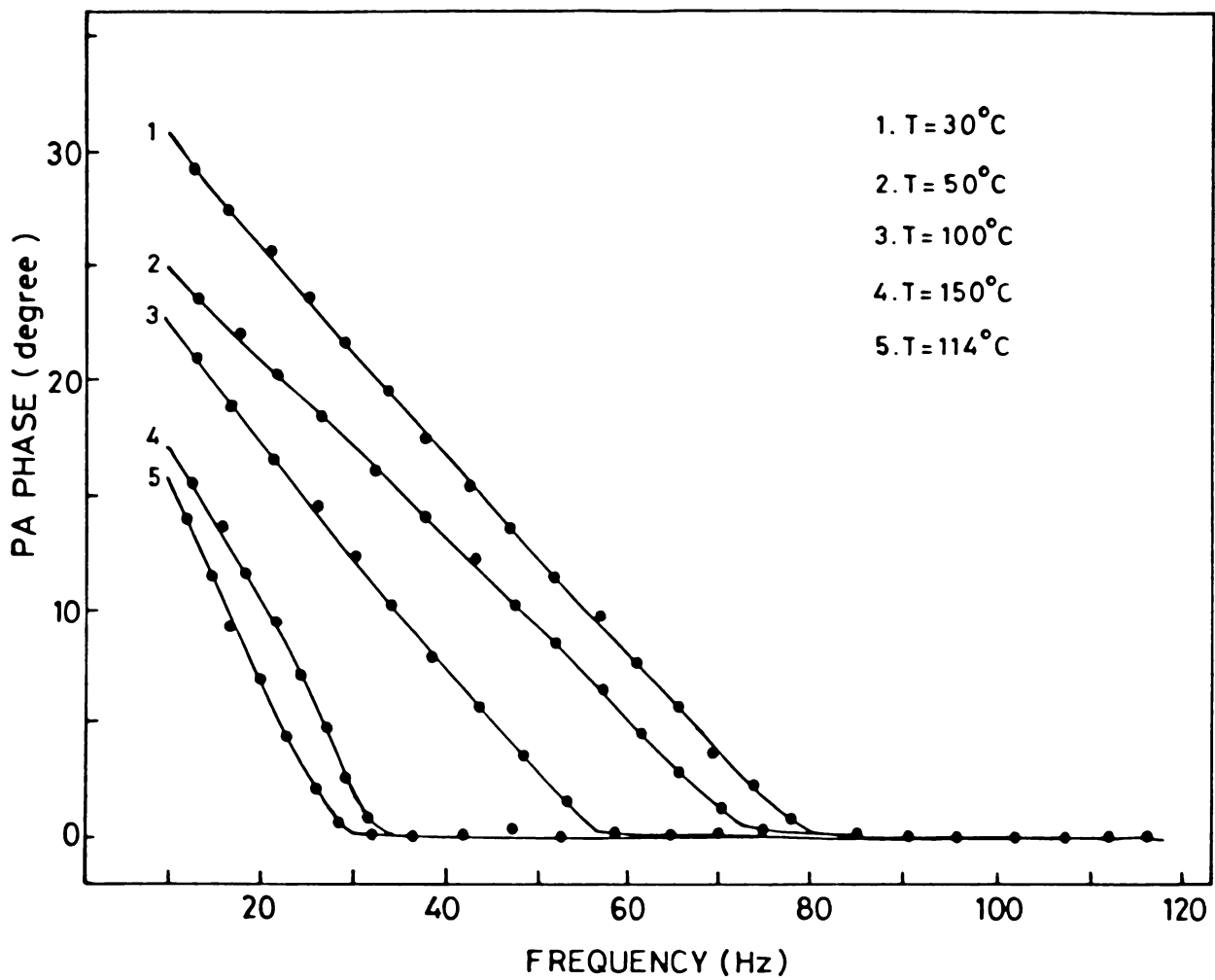


Fig.7.9 PA phase $\Delta\phi$ versus chopping frequency plots for $\text{As}_{0.25}\text{Se}_{0.75}$ sample at different temperatures.

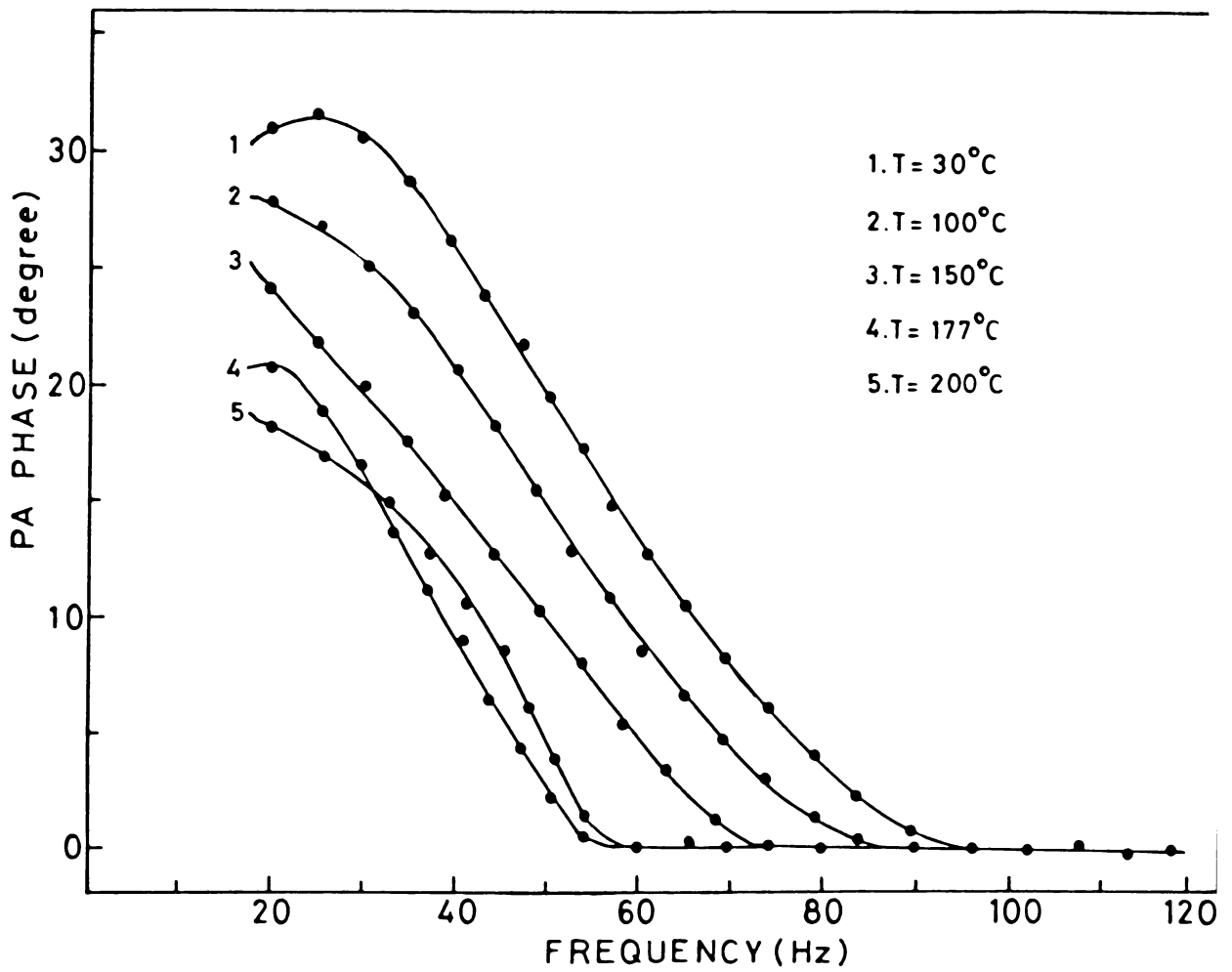


Fig.7.10 PA phase $\Delta\phi$ versus chopping frequency plots for $\text{Ge}_{0.20}\text{Se}_{0.80}$ sample at different temperatures.

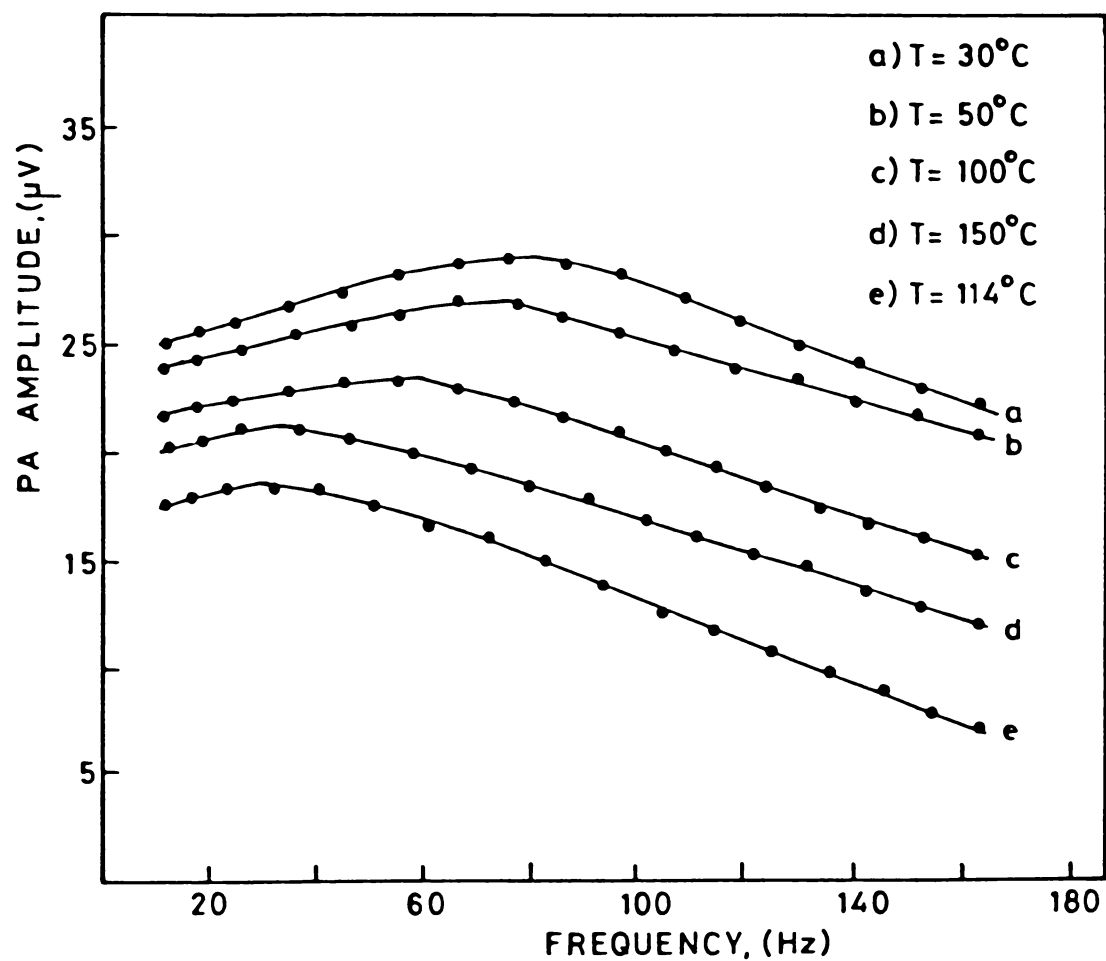


Fig.7.11 Difference between PA amplitudes of reference sample and experimental sample plotted as a function of chopping frequency at different temperatures for $\text{As}_{0.25}\text{Se}_{0.75}$ sample.

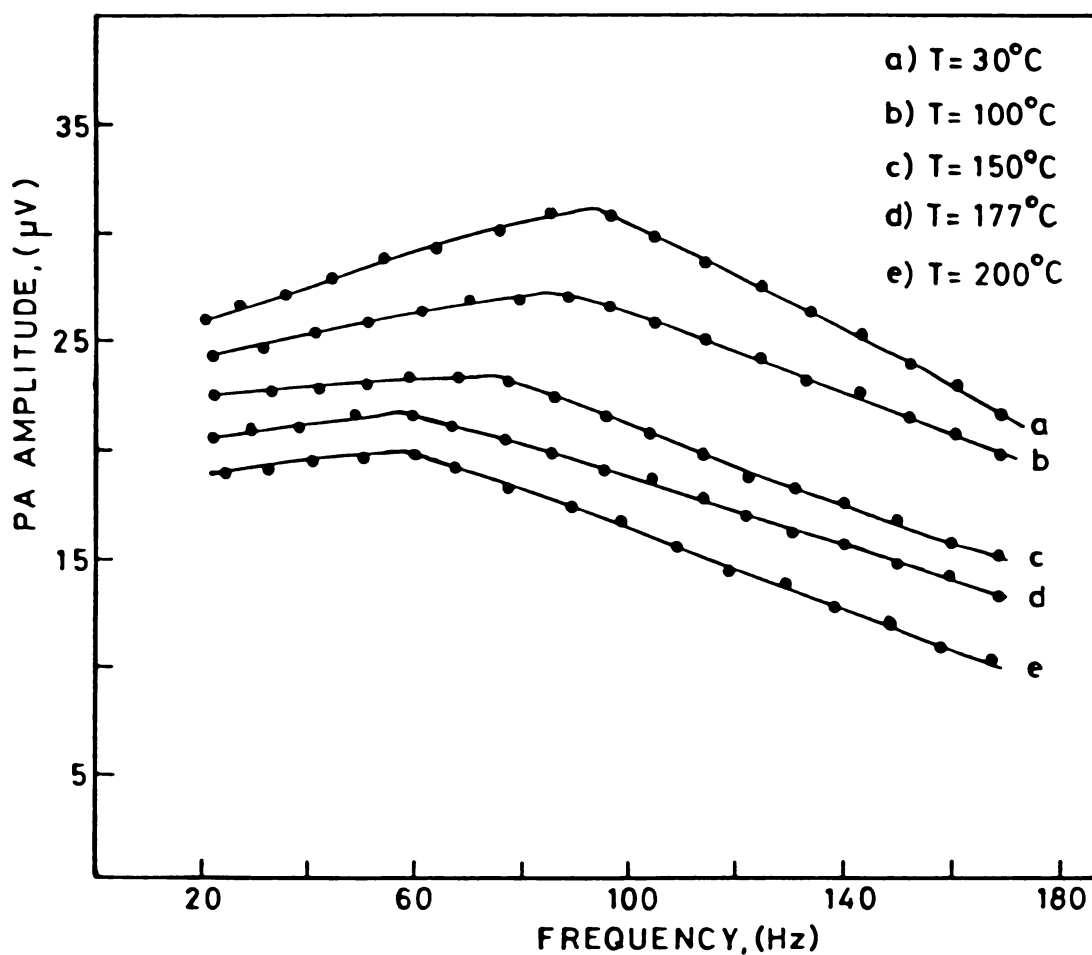


Fig.7.12 Difference between PA amplitudes of reference sample and experimental sample plotted as a function of chopping frequency at different temperatures for $\text{Ge}_{0.20}\text{Se}_{0.80}$ sample.

Table 7.1: Variation of thermal diffusivity α_s with temperature T for As-Se and Ge-Se glasses.

α_s in 10^{-3} cm²/sec.

T in °C

	T	30	100	150	170	188	200	220
As _{0.40} Se _{0.60}	α_s	8.6	7.9	7.1	6.1	4.8	5.1	5.2
	T	30	50	100	114	130	150	
As _{0.25} Se _{0.75}	α_s	6.5	6.1	4.6	2.9	3.1	3.3	
	T	30	70	110	136	150	160	
As _{0.30} Se _{0.70}	α_s	7.4	6.4	5.3	3.6	3.7	3.6	
	T	30	80	100	140	172	190	
As _{0.50} Se _{0.50}	α_s	7.5	6.4	6.0	4.6	3.6	3.5	
	T	30	85	100	150	180	190	
As _{0.45} Se _{0.55}	α_s	8.0	6.7	6.5	4.7	4.0	4.1	
	T	30	60	100	158	170	180	
As _{0.35} Se _{0.65}	α_s	8.3	7.9	7.3	4.6	4.6	4.5	
	T	30	100	150	177	200		
Ge _{0.20} Se _{0.80}	α_s	9.3	8.4	7.2	5.6	5.8		
	T	30	70	110	142	160		
Ge _{0.15} Se _{0.85}	α_s	8.4	7.9	6.7	4.05	4.05		
	T	30	50	100	117	130	140	
Ge _{0.10} Se _{0.90}	α_s	7.3	7.0	4.5	3.2	3.3	3.3	

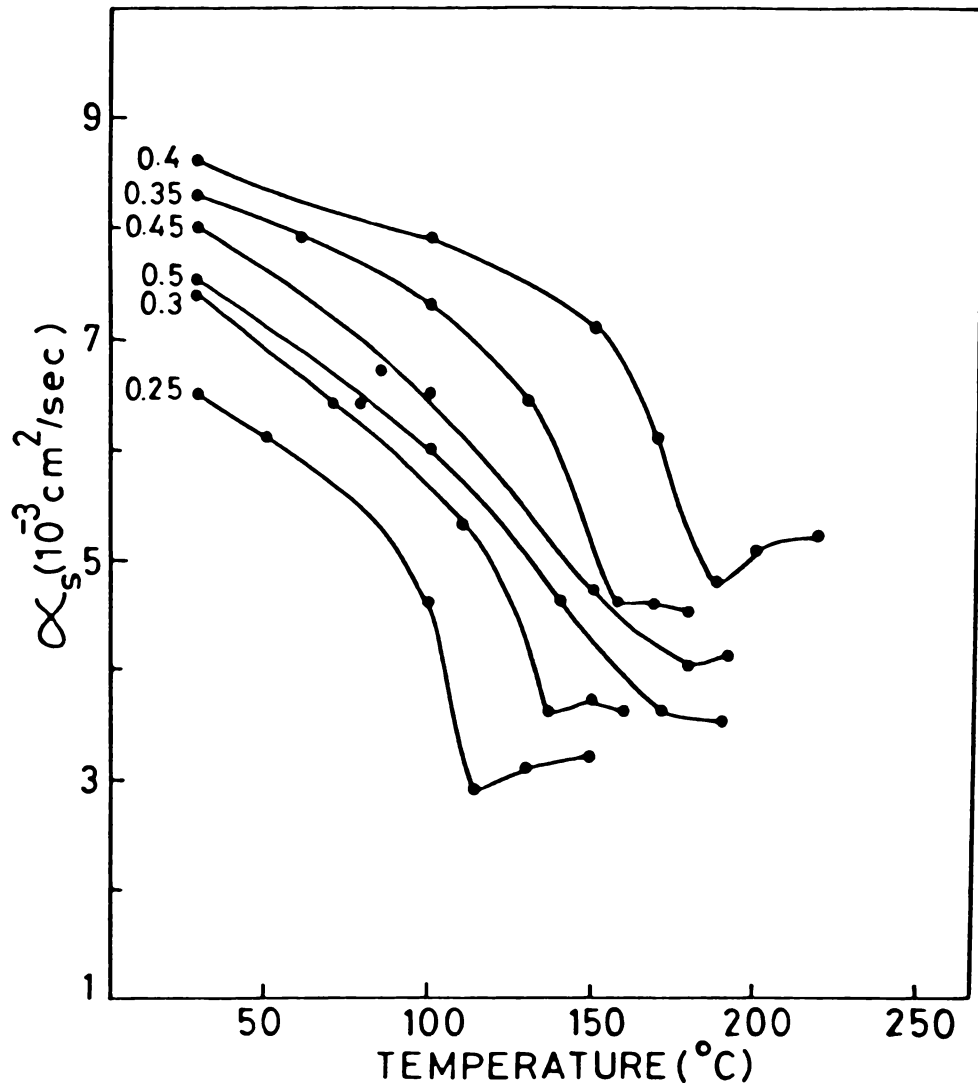


Fig.7.13 Thermal diffusivity plotted as a function of temperature for $\text{As}_x\text{Se}_{1-x}$ glasses. The x values are noted on the curves.

temperature and shows a critical minimum value at T_g in all the samples. A comparison of the composition dependence of α_s with that of T_g shows that they are quite similar for any composition. The ratio α_s/T_g turns out to have the same value of 0.0025 for all the compositions. Another important point to be noted in Fig.7.13 is that at T_g also the thermal diffusivity is maximum for the stoichiometric composition $As_{0.4}Se_{0.6}$. This is more evident in Fig.7.14 where we have plotted the thermal diffusivity values at T_g , namely α_{T_g} , against the composition parameter x for As_xSe_{1-x} glasses. This plot has nearly the same shape as at any other temperature below T_g . At all temperatures $T \leq T_g$, α_s has a threshold maximum value for the stoichiometric composition with $x = 0.4$ at which the formation of stable As_2Se_3 compound takes place. This suggests that the arguments presented in the previous chapter based on the percolation model is valid for all temperatures below T_g .

In Fig.7.15 the variation of the thermal diffusivity as a function of temperature for three compositions with $x = 0.10, 0.15$ and 0.20 of Ge_xSe_{1-x} glasses are shown. Here also we find that thermal diffusivity has a minimum value at T_g for all the compositions studied.

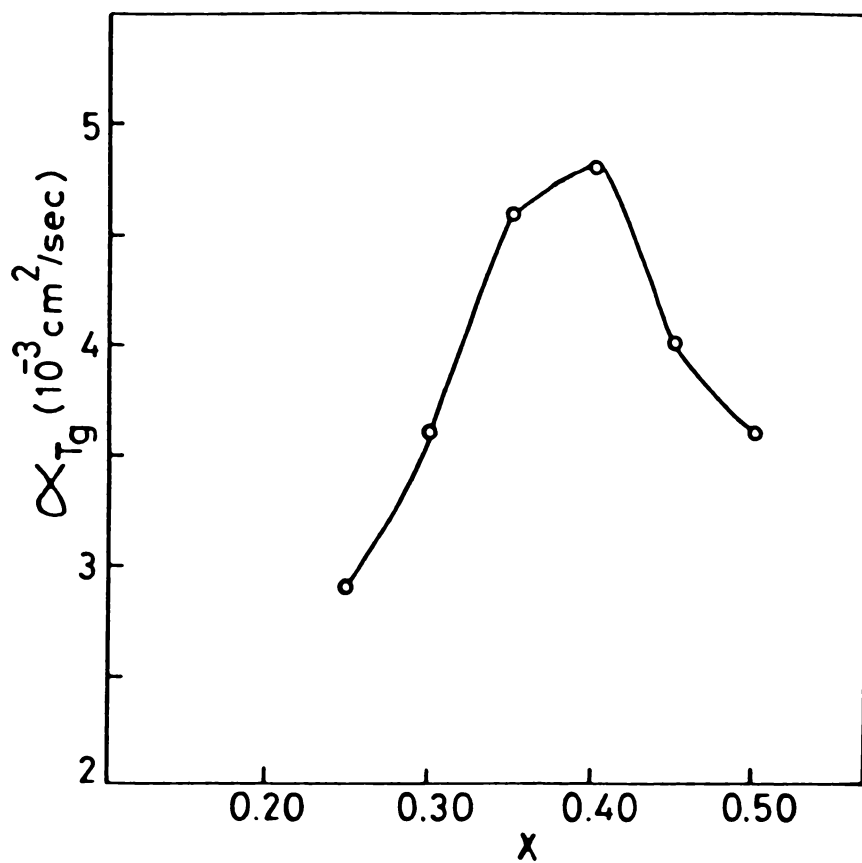


Fig.7.14 Variation of thermal diffusivity at glass transition temperature with composition for $\text{As}_x\text{Se}_{1-x}$ glasses.

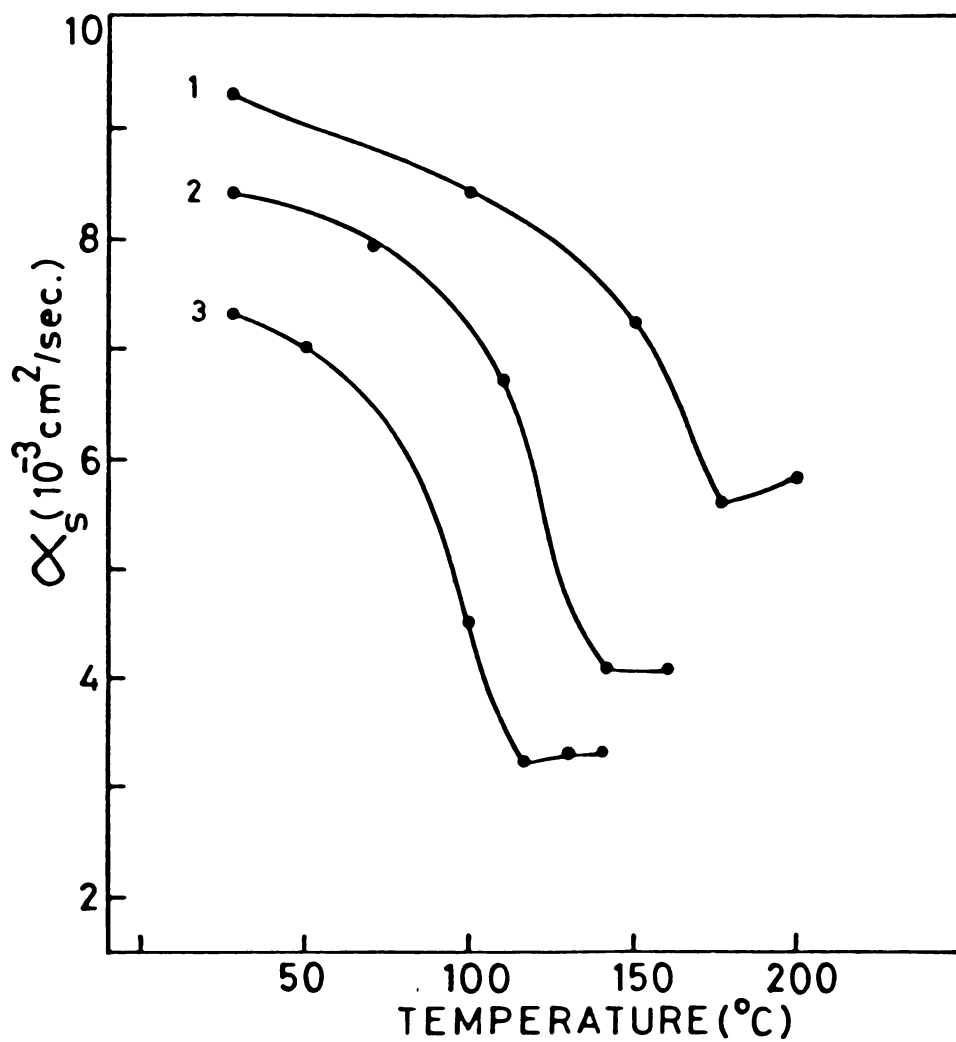


Fig.7.15 Variation of thermal diffusivity with temperature for $\text{Ge}_x\text{Se}_{1-x}$ glasses. (1) $\text{Ge}_{0.20}\text{Se}_{0.80}$, (2) $\text{Ge}_{0.15}\text{Se}_{0.85}$, (3) $\text{Ge}_{0.10}\text{Se}_{0.90}$.

RG theory predicts that the PA signal for optically opaque ($l_p \ll l_s$) and thermally thick ($\mu_s < l_s$; $\mu_s > l_p$) samples where l_s is the sample thickness and l_p is the optical absorption length of the sample, is proportional to the thermal diffusion length μ_s of the sample given by

$$\mu_s = \left(\frac{\alpha_s}{\pi f} \right)^{1/2} = \left(\frac{k_s}{\pi \rho c_p f} \right)^{1/2} \quad (7.1)$$

Here k_s is the thermal conductivity, ρ is the density, c_p is the specific heat, f is the chopping frequency and $\alpha_s = \frac{k_s}{\rho c_p}$. The fact that PA amplitude has minimum value at T_g indicates that the sample has minimum thermal diffusivity. As the temperature increases there will be a decrease in the mean free path due to increase in phonon collision rates. This in turn reduces the thermal conductivity. As T_g , which is the softening temperature, is approached the mean free path is decreased substantially which retards the thermal transport to the maximum extent as is evident from Figs. 7.13 and 7.15 for As-Se and Ge-Se glasses respectively. The anomalous increase in specific heat taking place at T_g will also be contributing to effect a corresponding decrease in thermal diffusivity. Both these effects, in fact, work in the same direction to make thermal diffusivity minimum at T_g .

7.4 VARIATION OF OPTICAL ENERGY GAP WITH TEMPERATURE

We have recorded the PA spectra of $\text{As}_x\text{Se}_{1-x}$ and $\text{Ge}_x\text{Se}_{1-x}$ glasses at various fixed temperatures by plotting the normalized PA signal amplitude as a function of the incident wavelength at these temperatures. Spectra have been recorded for temperatures upto $T > T_g$. The PA spectra recorded for $\text{As}_{0.25}\text{Se}_{0.75}$ and $\text{Ge}_{0.10}\text{Se}_{0.90}$ samples are shown in Figs.7.16 and 7.17 respectively. Similar spectra have been recorded for other samples as well. It is observed that the exponential absorption edge region of the spectrum broadens as the temperature is increased and the rate of this broadening is more for temperatures larger than T_g . It can be inferred that the disorder induced potential fluctuations increase as temperature increases and this is getting reflected in the PA spectra. The optical energy gap E_o at various temperatures has been determined for $\text{As}_x\text{Se}_{1-x}$ and $\text{Ge}_x\text{Se}_{1-x}$ glasses from the PA spectra as the photon energy above which the spectra saturate. The variations of E_o with temperature for $\text{As}_x\text{Se}_{1-x}$ and $\text{Ge}_x\text{Se}_{1-x}$ glasses are shown in Figs.7.18 and 7.19 respectively. For all these samples E_o decreases with increase in temperature and the rate of this decrease is larger for temperature $T > T_g$. This agrees with the results published by previous workers [24,254]. The absence of

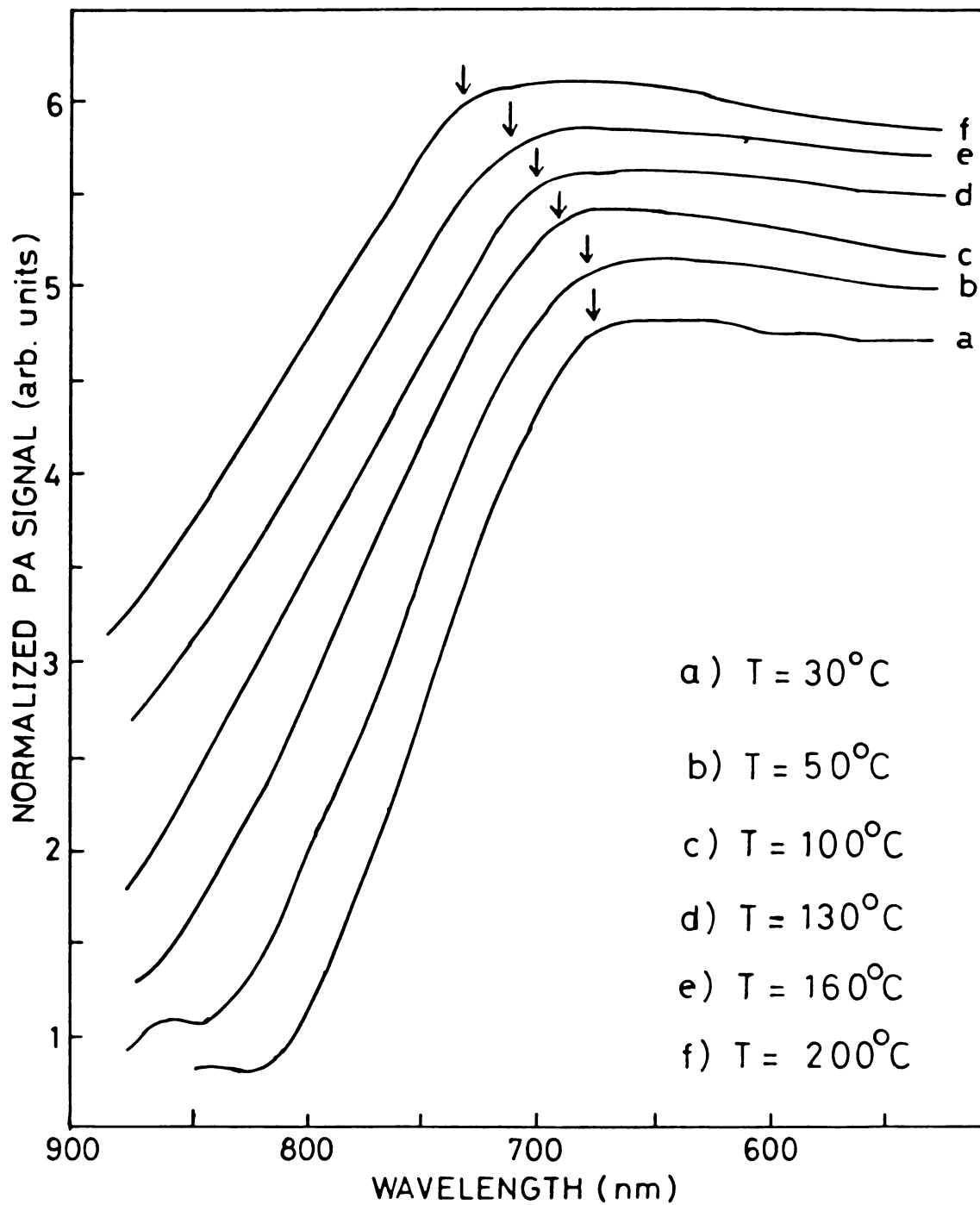


Fig.7.16 PA spectra of $\text{As}_{0.25}\text{Se}_{0.75}$ sample recorded at different temperatures.

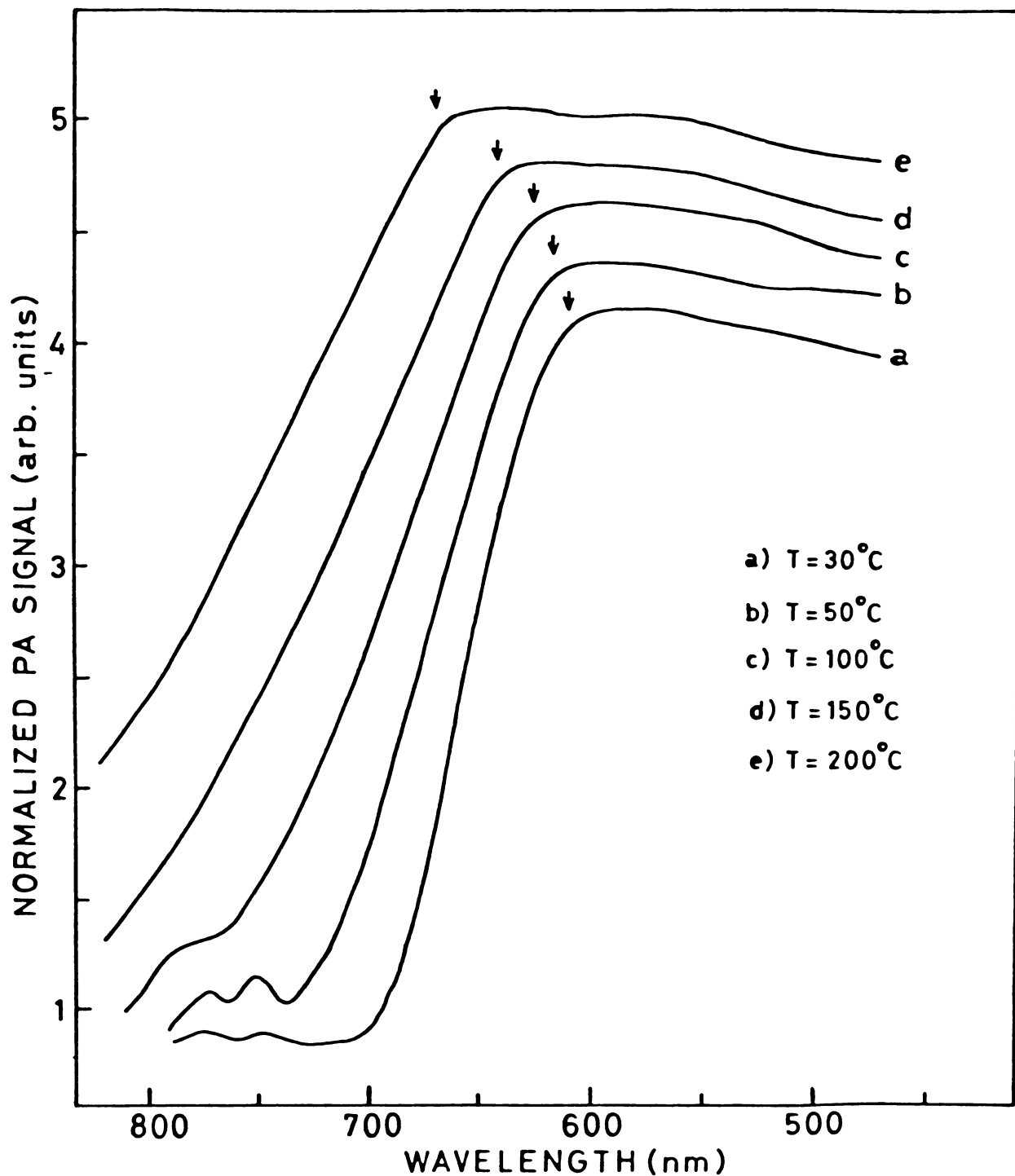


Fig.7.17 PA spectra of $\text{Ge}_{0.10}\text{Se}_{0.90}$ sample recorded at different temperatures.

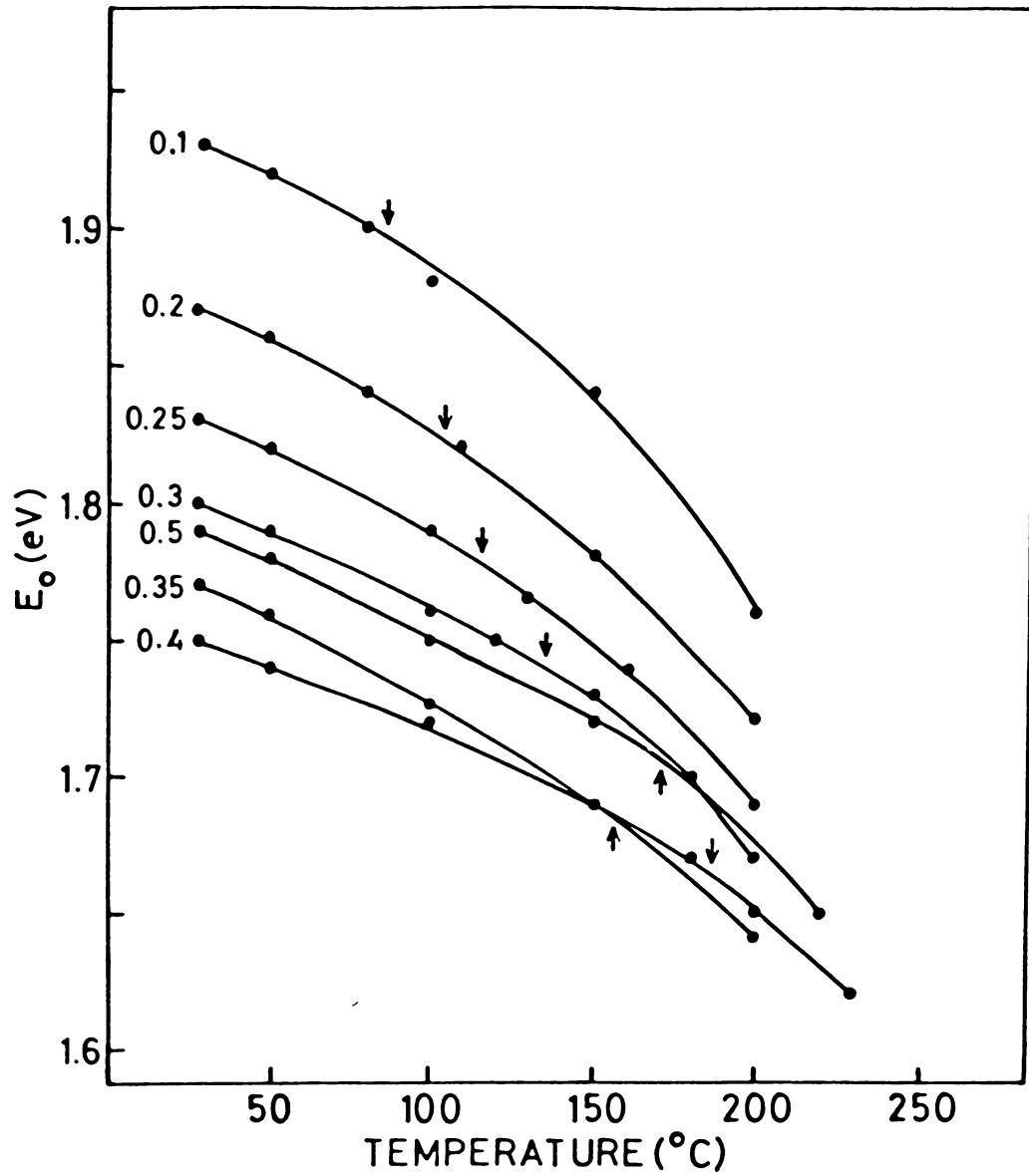


Fig.7.18 Variation of optical energy gap E_0 with temperature for As_xSe_{1-x} glass. The x values are noted on the curves. ¹ Arrow indicates glass transition temperature.

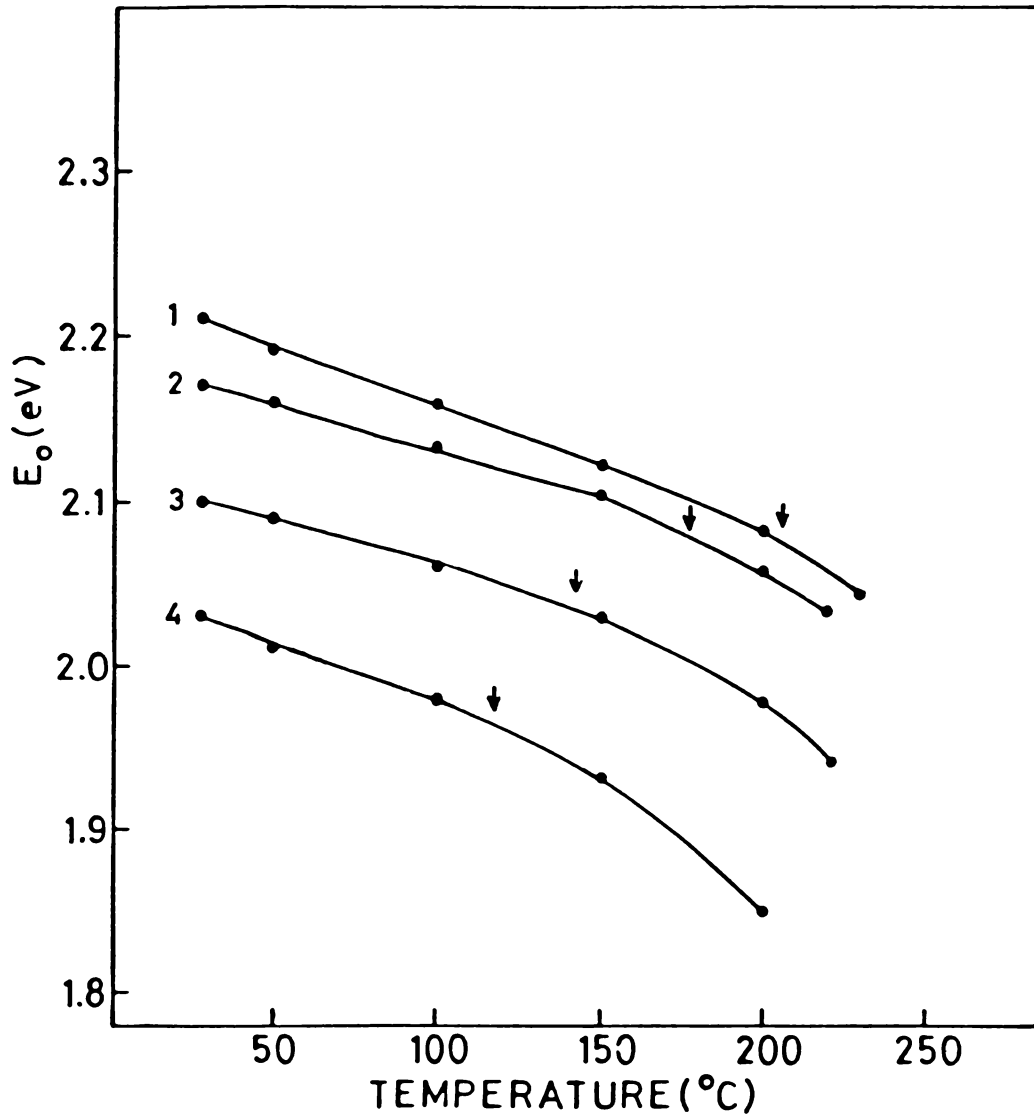


Fig.7.19 Variation of optical energy gap E_o with temperature for Ge_xSe_{1-x} glasses. Arrow \circ indicates glass transition temperature.
 (1) $Ge_{0.25}Se_{0.75}$, (2) $Ge_{0.20}Se_{0.80}$, (3) $Ge_{0.15}Se_{0.85}$,
 (4) $Ge_{0.10}Se_{0.90}$.

any sharp change in E_0 at T_g indicates that at glass transition no drastic change in the electronic properties or band structure do take place.

Dow and Redfield [77] proposed that exponential edges are due to the electric field induced ionization of the excitons. The electric field can be caused by ionized impurities, phonons or by potential fluctuations. For larger average electric fields the exponential slope of the edge is smaller and the edge is broader. At higher temperatures, phonon induced electric fields will dominate and the slope of the edge will be temperature dependent. Thus the electron-phonon interactions play a major role in determining the temperature dependent variation of optical absorption.

The observed decrease in E_0 with temperature can be explained on the basis of the chemically ordered network model. For As-Se glasses one can calculate the average bond energy from the individual bond energies of Se-Se, As-Se and As-As bonds, which are 44.0, 44.5 and 43.4 KCal/mole respectively. So E_0 , the energy gap, will be higher when Se concentration is larger. When temperature increases, the average bond energy decreases and

correspondingly E_0 decreases. The above argument cannot fully be taken for granted because other effects namely temperature dependence of other parameters such as thermal expansion, Debye-Waller factor, Debye temperature etc. also do contribute to the temperature dependence of the energy gap. The argument based on the CON model gives the correct sign for the effect.

Chapter 8

SUMMARY AND CONCLUSIONS

This thesis work has mainly concentrated on the investigation of the optical and thermal properties of binary semiconducting chalcogenide glasses belonging to the $A_x^{IV}B_{1-x}^{VI}$ and $A_x^VB_{1-x}^{VI}$ families. The technique used for these studies is a relatively new one namely, the photoacoustic (PA) technique. This technique is based on the detection of an acoustic signal produced in an enclosed volume when the sample is irradiated by an intensity modulated radiation. The signal produced depends upon the optical properties of the sample, and the thermal properties of the sample, backing material and the surrounding gas.

For the present studies an efficient signal beam gas-microphone PA spectrometer, consisting of a high power Xenon lamp, monochromator, light beam chopper, PA cell with microphone and lock-in amplifier, has been set up. Two PA cells have been fabricated; one for room temperature measurements and another for measurements at high temperatures. With the high temperature PA cell measurements can be taken upto $\approx 250^\circ\text{C}$. Provisions are incorporated

in both the cells to change the volume and to use different backing materials for the sample. The cells have been calibrated by measuring the frequency response of the cells using carbon black as the sample.

The PA spectra of several compositions of $\text{Ge}_x\text{Te}_{1-x}$ ($0.15 \leq x \leq 0.28$), $\text{Si}_x\text{Te}_{1-x}$ ($0.10 \leq x \leq 0.28$), $\text{Ge}_x\text{Se}_{1-x}$ ($0.10 \leq x \leq 0.38$) and $\text{As}_x\text{Se}_{1-x}$ ($0.10 \leq x \leq 0.50$) glasses, prepared by melt quenching technique, have been recorded in the fundamental absorption edge region using the PA spectrometer. These spectra give information about the features of optical absorption. The three regions of absorption coefficient namely, the power law absorption region, exponential absorption region and weak absorption region are clearly seen in the PA spectra. The PA technique is found to be very effective for the study of optical absorption of bulk semiconducting glasses. The optical energy gap E_0 of the samples have been determined from the PA spectra as the photon energy above which the spectra saturate. The variation of E_0 as a function of composition for all the groups of samples have been studied. In the case of $\text{A}_x^{\text{IV}}\text{B}_{1-x}^{\text{VI}}$ glasses the value of E_0 increases with

increase in the concentration of the group IV element. But the rate of the increase is small when $x > 0.2$ and thus there is a change in slope at this composition. The average coordination number m corresponding to $x = 0.2$ for these systems of glasses is 2.4. The results provide evidence for the existence of stable structures at this composition based on the formation of AB_4 tetrahedral units. For Ge_xSe_{1-x} glasses the values of E_o is found to have a maximum value at $x = 0.33$ composition which corresponds to the stoichiometric composition of this system. From the variation of E_o with x for As_xSe_{1-x} glasses it is found that E_o has a minimum value at $x = 0.4$ which again corresponds to the stoichiometric compound composition where the stable As_2Se_3 glass is formed. The average coordination number for this composition is also 2.4. These results on the variation of E_o with x for $A_x^{IV}B_{1-x}^{VI}$ and $A_x^{V}B_{1-x}^{VI}$ glasses have been explained on the basis of the chemical bonding and the change in short range order taking place when the composition is varied.

The thermal diffusivity α_s of Ge_xTe_{1-x} , Si_xTe_{1-x} and Ge_xSe_{1-x} glasses belonging to the $A_x^{IV}B_{1-x}^{VI}$ family and As_xSe_{1-x} and As_xTe_{1-x} glasses belonging to the $A_x^{V}B_{1-x}^{VI}$ family have

been measured again using PA technique. The method involves the determination of the characteristic frequency f_c above which the sample is thermally thick, by measuring the variation of PA signal amplitude and phase with chopping frequency. The measurements are done with samples of appropriate thickness l_s . Then the thermal diffusivity is given by $\alpha_s = f_c l_s^2$. Thus the PA technique provides a simple and very effective method for determining thermal properties of bulk semiconducting glasses. The variation of α_s as a function of the composition parameter has been studied for all five groups of samples. For $A_x^{IV}B_{1-x}^{VI}$ glasses this variation shows a threshold maximum value at $x = 0.2$ ($m = 2.4$) composition. For Ge_xSe_{1-x} glasses the value of α_s shows a maximum value again at $x = 0.33$. In the case of $A_x^VB_{1-x}^{VI}$ glasses α_s is found to have a peak value around the $x = 0.4$ ($m = 2.4$) composition. These results suggests that a stable structure with minimum disorder is formed when $m = 2.4$ for these glasses. The glass network offers minimum resistance to the propagating thermal waves at this composition. These results on thermal diffusivity measurements provides a clear evidence for the existence of critical composition in binary chalcogenide glasses.

An explanation for the observed behaviour of thermal diffusivity has been presented on the basis of constraints theory and the ideas of rigidity percolation in random networks. The glass forming composition is optimized mechanically by equating the number of force field constraints which are intact at the glass transition temperature to the number of atomic degrees of freedom. In the glass forming region the system contains both floppy and rigid regions. The threshold behaviour in thermal conduction exhibited by $A_x^{IV}B_{1-x}^{VI}$ and $A_x^V B_{1-x}^{VI}$ glasses is attributed to the mechanical stiffening of the glass network at the critical composition as a result of the threshold percolation of rigidity. Considering central bond-stretching and rotationally invariant bond-bending forces for a binary alloy system $A_x B_{1-x}$, based on ideas of rigidity percolation and effective medium theory, the critical average coordination number m works out to be 2.4 for a three dimensional random network. This agrees well with our experimental observations which provide evidence for the existence of critical composition at $x = 0.20$ for $A_x^{IV}B_{1-x}^{VI}$ and at $x = 0.4$ for $A_x^V B_{1-x}^{VI}$ glasses. The value of the average coordination number turns out to be 2.4 at these critical compositions for both the systems.

The use of PA technique for the study of glass transition has been demonstrated, probably for the first time. The glass transition temperature T_g of As_xSe_{1-x} and Ge_xSe_{1-x} glasses have been determined from the variation of the PA signal amplitude and phase with temperature. At T_g the PA amplitude shows a minimum and phase shows a critical maximum. The glass transition temperature determined in this way compare well with results from calorimetric measurements. The dependence of glass transition temperature on the chopping frequency seems to provide information about the relaxation process in the glass. The variation of α_s and E_o as a function of temperature have been presented. A significant decrease in α_s is found to occur at T_g in all the samples studied. The variation of α_s with x has the same general behaviour for all temperatures $T \leq T_g$ as that at room temperature. Such studies have not been reported earlier. The results indicate that the critical composition remains the same and the network rigidity is kept intact at all temperatures below the glass transition temperature. The optical absorption is also found to depend on temperature. The value of E_o decreases with increase in temperature. The rate of decrease is found to be larger for temperatures $T > T_g$.

We have made use of the PA technique, which has become a powerful analytical technique during the last

10-15 years, for a systematic study of optical and thermal properties of bulk semiconducting chalcogenide glasses. It is somewhat difficult to get such informations using conventional techniques. The fact that several physical properties related to optical and thermal properties characteristic of the material can be studied, makes it one of the most versatile techniques. The informations obtained from the present studies on the composition and temperature dependence of optical and thermal properties of chalcogenide glasses provide significant insight into the physics of these materials. Along with conventional calorimetric methods PA technique can be effectively used to get more information about the process of glass transition.

REFERENCES

1. B.T.Kolomiets, Proc.Int.Conf. on Semiconductor Physics, Prague 1960, (Czechoslovak Academy of Sciences, 1961) p.884; Phys.Stat.Solidi 7 359,713 (1964).
2. W.E.Spear, Proc.Phys.Soc. (London), 870 1139 (1957); 76 826 (1960).
3. J.Tauc, R.Grigorovici and A.Vancu, Phys.Stat.Solidi 15 627 (1966).
4. S.R.Ovshinsky, Phys.Rev.Lett. 21 1450 (1968).
5. H.F.Sterling and R.C.G.Swann, Solid State Electron. 8 653 (1965).
6. R.C.Chittick, J.H.Alexander and H.F.Sterling, J.Electrochemn.Soc. 116 77 (1969).
7. W.E.Spear and P.G.Lecomber, Solid State Commun. 17 1193 (1975); Phil.Mag. 33 935 (1976).
8. W.E.Spear, P.G.Lecomber, S.Kinmond and M.H.Brodsky, Appl.Phys.Lett. 28 105 (1976).
9. D.E.Carlson and C.R.Wronski, Appl.Phys.Lett. 29 602 (1976).

10. W.E.Spear and P.G.Lecomber, in *The Physics of Hydrogenated Amorphous Silicon I*, ed: J.D.Joannopoulos and G.Lucovsky (Springer-Verlag, Berlin, 1984) p.63.
11. F.Bloch, *Z.Physik.* **52** 555 (1928).
12. A.H.Wilson, *Theory of Metals* (Cambridge University Press, NY, 1936).
13. P.W.Anderson, *Phys.Rev.* **109** 1492 (1958).
14. K.Ishii, *Suppl.Prog.Theor.Phys.* **53** 77 (1973).
15. D.J.Thouless, *J.Phys.C* **3** 1559 (1970).
16. D.C.Licciardello and E.N.Economou, *Phys.Rev.B* **11** 3697 (1975).
17. D.C.Licciardello and D.J.Thouless, *J.Phys.C* **8** 4157 (1975); *J.Phys.C* **11** 935 (1977).
18. D.Weaire and V.Srivastava, *Solid State Commun.* **23** 863 (1977).
19. K.Tsujino, A.Tokunaga, M.Yamamoto and F.Yonezawa, *Solid State Commun.* **30** 531 (1979).
20. E.N.Economou and P.D.Antoniou, *Solid State Commun.* **21** 28 (1977).

21. A.Abrahams, P.W.Anderson, D.C.Licciardello and T.V. Ramakrishnan, Phys.Rev.Lett. **42** 673 (1979).
22. P.A.Lee and T.V.Ramakrishnan, Rev.Mod.Phys. **57** 287 (1985).
23. D.J.Thouless, in Ill Condensed Matter, ed: R.Balian, R.Maynard and G.Toulouse (North-Holland, Amsterdam, 1978) p.5.
24. N.F.Mott and E.A.Davis, Electronic Processes in Non-Crystalline Materials (Clarendon Press, 1971).
25. A.F.Ioffe and A.R.Regel, Prog.in Semiconductors, ed: A.F.Gibson (Wiley, New York, 1960) Vol.4, p.237.
26. R.R.Reitz, Solid State Phys. **1** 1 (1955).
27. N.F.Mott, Phil.Mag. **22** 7 (1970).
28. M.H.Cohen, H.Fritzsche and S.R.Ovshinsky, Phys.Rev.Lett. **22** 1065 (1969).
29. E.A.Davis and N.F.Mott, Phil.Mag. **22** 903 (1970).
30. R.Zallen, The Physics of Amorphous Solids (Wiley, New York, 1983).
31. K.L.Chopra, Thin Film Phenomena (McGraw-Hill, New York, 1969).

32. J.C.Phillips, Comments Solid State Phys. 4 9 (1971).
33. P.W.Anderson, Phys.Rev.Lett. 34 953 (1975).
34. D.Adler, Phys.Rev.Lett. 41 1755 (1978).
35. D.Adler, Solar Cells 2 199 (1980).
36. R.A.Street and N.F.Mott, Phys.Rev.Lett. 35 1293 (1975).
37. N.F.Mott, E.A.Davis and R.A.Street, Phil.Mag. 32 961 (1975).
38. R.A.Street, Phys.Rev.B 17 3984 (1978).
39. M.Kastner, D.Adler and H.Fritzsche, Phys.Rev.Lett. 37 1504 (1976).
40. M.Kastner and H.Fritzsche, Phil.Mag. 37 199 (1978).
41. T.D.Moustakas, Solid State Commun. 35 745 (1980).
42. W.B.Jackson, N.M.Amer, A.C.Boccaro and D.Fournier, Appl. Opt. 20 1333 (1981).
43. C.Y.Huang, S.Guha and S.J.Hudgens, Phys.Rev.B 27 7460 (1983).
44. A.Madan, Solar Cells 2 277 (1980).
45. D.V.Lang, J.D.Cohen and J.P.Harbison, Phys.Rev.B 25 5285 (1982).

46. I.Balberg, Phys.Rev.B 22 3853 (1980).
47. H.Okushi, Y.Tokumaru, S.Yamasaki, H.Oheda and K.Tanaka, Phys.Rev.B 25 4313 (1982).
48. I.Balberg, E.Gal and B.Pratt, J.Non-Cryst.Solids, 59-60 277 (1983).
49. N.M.Johnson, J.Non-Cryst.Solids 59-60 265 (1983).
50. K.P.Chik, C.K.Yu, P.K.Lim, B.Y.Tong, S.K.Wong and P.K. John, J.Non-Cryst.Solids 59-60 285 (1983).
51. J.Dijon, Solid State Commun. 48 79 (1983).
52. A.C.Write and A.J.Leadbetter, Phys.Chem.Glass 17 122 (1976).
53. W.H.Zachariasen, J.Amer.Chem.Soc. 54 3841 (1932).
54. N.F.Mott, Adv.Phys. 16 49 (1967).
55. D.E.Polk, J.Non-Cryst.Solids 5 365 (1971).
56. G.N.Greaves and E.A.Davis, Phil.Mag. 29 1201 (1974).
57. M.Long, P.Galiron, R.Alben and G.A.N.Connel, Phys.Rev.B 13 1821 (1976).
58. J.C.Phillips, Phys.Rev.B 21 5724 (1980).

59. J.E.Griffiths, G.P.Espinosa, J.P.Remeika and J.C.Phillips, Solid State Commun. **40** 1077 (1981); Phys.Rev.B **25** 1272 (1982).
60. P.Boalchand, J.Grothaus, W.J.Bresser and P.Suranyi, Phys.Rev.B **25** 2975 (1982).
61. J.C.Phillips, J.Non-Cryst.Solids **35-36** 1157 (1980).
62. J.C.Phillips, C.A.Beevers and S.E.B.Gould, Phys.Rev.B **21** 5724 (1980).
63. R.Grigorovici, J.Non-Cryst.Solids **1** 303 (1969).
64. G.Lucovsky, in Physical Properties of Amorphous Materials, ed: D.Adler, B.B.Schwartz and M.C.Steele (Plenum Press, New York, 1985) p.277.
65. L.Ley, M.Cardona and R.A.Pollak, in Photoemission in Solids II (Springer-Verlag, Berlin, 1979) Vol.27, p.11.
66. P.P.Seregin, A.R.Regel, A.A.Andreev and F.S.Nasredinov, Phys.Stat.Solidi **74a** 373 (1982).
67. P.J.Bray, F.Bucholtz, A.E.Geissberger and I.A.Harris, Nucl.Instrum.Methods **199** 1 (1982).
68. E.A.Stern, in Physical Properties of Amorphous Materials, ed: D.Adler, B.B.Schwartz and M.C.Steele (Plenum Press, New York, 1985) p.201.

69. R.C.Mackenzie, in *Differential Thermal Analysis*, ed: R.C.Mackenzie (Academic Press, New York, 1970).
70. N.F.Mott, *Phil.Mag.* **19** 835 (1969).
71. I.G.Austin and N.F.Mott, *Adv.Phys.* **18** 41 (1969).
72. P.Nagels, in *Amorphous Semiconductors* ed:M.H.Brodsky (Springer-Verlag, Berlin, 1979) p.113.
73. H.Scher and E.W.Montroll, *Phys.Rev.B* **12** 2455 (1975).
74. D.Weaire and M.F.Thorpe, *Phys.Rev.B* **4** 2508, 3518 (1971).
75. J.Tauc, in *Amorphous and Liquid Semiconductors* ed: J.Tauc (Plenum Press, New York, 1974) p.159.
76. J.Tauc, *Mat.Res.Bull.* **5** 721 (1970).
77. J.D.Dow and D.Redfield, *Phys.Rev.B* **5** 594 (1972).
78. R.A.Street, *Solid State Commun.* **24** 363 (1977).
79. A.Vaško, D.Ležal and I.Srb, *J.Non-Cryst.Solids* **4** 311 (1970).
80. R.C.Zeller and R.O.Pohl, *Phys.Rev.B* **4** 2029 (1971).
81. S.Alexander, O.E.Wohlman and R.Orbach, *Phys.Rev.B* **34** 2726 (1986).

82. W.W.Wendlandt and H.G.Hecht, Reflection Spectroscopy (Wiley, New York, 1966).
83. P.A.Walks Jr. and T.Hirschfeld, Appl.Spectrosc.Rev. 1 99 (1968).
84. G.B.Wright (ed.), Light Scattering in Solids (Springer-Verlag, Berlin, 1969).
85. A.G.Bell, Amer.J.Sci. 20 305 (1880).
86. A.G.Bell, Phil.Mag. 11 510 (1881).
87. M.L.Viengerov, Dokl.Akad.Nauk SSSR 19 687 (1938).
88. A.H.Pfund, Science 90 326 (1939).
89. K.F.Luft, Z.Tech.Phys.24 97 (1943).
90. M.L.Viengerov, Dokl.Akad.Nauk SSSR 46 182 (1945).
91. G.Gorelik, Dokl.Akad.Nauk SSSR 54 779 (1946).
92. P.V.Slobodskaya, Izv.Akad.Nauk SSSR, Ser.Fiz. 12 656 (1948).
93. A.Rosencwaig, Opt.Comm. 7 305 (1973).
94. A.Rosencwaig, Anal.Chem. 47 592A (1975).

95. A.Rosencwaig and A.Gersho, *J.Appl.Phys.* **47** 64 (1976).
96. A.Rosencwaig, in *Advances in Electronics and Electron Physics*, ed: L.Morton (Academic Press, New York, 1978) Vol.**46**, p.207.
97. Lord Rayleigh, *Nature* **23** 274 (1881).
98. J.G.Parker, *Appl.Opt.***12** 2974 (1973).
99. A.Rosencwaig and A.Gersho, *Science* **190** 556 (1975).
100. M.J.Adams, G.F.Kirkbright and K.R.Menon, *Anal.Chem.* **51** 508 (1979).
101. J.F.McClelland and R.N.Kniseley, *Appl.Phys.Lett.* **28** 467 (1976).
102. G.C.Wetsel Jr. and F.A.McDonald, *Appl.Phys.Lett.* **30** 252 (1977).
103. E.M.Monahan Jr. and A.W.Nolle, *J.Appl.Phys.* **48** 3519 (1977).
104. H.S.Bennett and R.A.Forman, *Appl.Opt.* **15** 2405 (1976).
105. L.C.Aamodt, J.C.Murphy and J.G.Parker, *J.Appl.Phys.* **48** 927 (1977).
106. F.A.McDonald and G.C.Wetsel Jr., *J.Appl.Phys.* **49** 2313 (1978).

107. F.A.McDonald, *Appl.Opt.* **18** 1363 (1979).
108. C.K.N.Patel and R.J.Kerl, *Appl.Phys.Lett.* **30** 578 (1977).
109. R.G.Bray and M.J.Berry, *J.Chem.Phys.* **71** 4909 (1979).
110. G.Stella, J.Gelfand and W.H.Smith, *Chem.Phys.Lett.* **39**
146 (1976).
111. C.K.N.Patel, *Science* **220** 157 (1978).
112. T.H.Vansteenkiste, F.R.Faxvog and D.M.Roessler, *Appl.*
Spectrosc. **35** 194 (1981).
113. P.C.Claspy, C.Ha and Y.H.Pao, *Appl.Opt.* **16** 2972 (1977).
114. A.Hordvik and H.Schlossberg, *Appl.Opt.* **16** 101 (1977).
115. A.Rosencwaig, *Phys.Today* **28** 23 (1975).
116. T.Ikari, S.Shigetomi, Y.Koga, S.Shigetomi, N.Nishimura
and H.Suzuki, *J.Phys.C* **19** 2633 (1986).
117. P.Rochon and T.J.Racey, *J.Photoacoust.* **1** 475 (1983).
118. W.Lahman and H.J.Ludewig, *Chem.Phys.Lett.* **45** 177 (1977).
- 119 M.J.Adams, J.G.Highfield and G.F.Kirkbright, *Anal.Chem.*
49 1850 (1977).
120. J.C.Murphy and L.C.Aamodt, *J.Appl.Phys.* **48** 3502 (1977).

121. R.S.Quimby and W.M.Yen, *Opt.Lett.* **3** 181 (1978).
122. C.D.Merkle and R.C.Powell, *Chem.Phys.Lett.* **46** 303 (1977).
123. R.G.Peterson and R.C.Powell, *Chem.Phys.Lett.* **53** 366 (1978).
124. D.Cahen, *Appl.Phys.Lett.* **33** 810 (1978).
125. A.C.Tam, *Appl.Phys.Lett.* **37** 978 (1980).
126. W.Thielemann and H.Neumann, *Phys.Stat.Solidi* **A61** K123 (1980).
127. K.Wasa, K.Tsubuchi and N.Mikoshiba, *Jpn.J.Appl.Phys.* **19** L653 (1980).
128. H.Tokumoto, M.Tokumoto and T.Ishiguro, *J.Phys.Soc.Jpn.* **50** 602 (1981).
129. J.F.McClelland and R.N.Kniseley, *Appl.Phys.Lett.* **35** 121 (1979).
130. J.F.McClelland and R.N.Kniseley, *Appl.Phys.Lett.* **35** 585 (1979).
131. V.A.Sablikov and V.B.Sandomirskii, *Sov.Phys.Semicond.* **17** 50 (1983).
132. A.Mandelis and E.K.M.Siu, *Phy.Rev.B* **34** 7209 (1986);
Phys.Rev.B **34** 7222 (1986).

133. M.J.Adams and G.F.Kirkbright, *Analyst* **102** 281 (1977).
134. T.Somasundaram, P.Ganguly and C.N.R.Rao, *J.Phys.C* **19** 2137 (1986).
135. F.P.Schäfer (ed.), *Dye Lasers* (Springer-Verlag, Berlin, 1977).
136. A.C.Tam, in *Ultrasensitive Laser Spectroscopy*, ed: D.Klinger (Academic Press, N.Y. 1983) p.1.
137. A.Rosencwaig, *Photoacoustics and Photoacoustic Spectroscopy* (Wiley, New York, 1980).
138. L.G.Rosengren, *Appl.Opt.* **14** 1960 (1975).
139. C.F.Dewey, in *Optoacoustic Spectroscopy and Detection*, ed: Y.H.Pao (Academic Press, New York, 1977) p.47.
140. P.M.Morse, *Vibration and Sound* (McGraw-Hill, New York, 1948).
141. L.A.Farrow and R.E.Richton, *J.Appl.Phys.* **48** 4962 (1977).
142. C.F.Dewey Jr., R.D.Kamm and C.E.Hackett, *Appl.Phys.Lett.* **23** 633 (1973).
143. E.Kritchman, S.S.Shtrikman and M.Slatkine, *J.Opt.Soc.Amer.* **68** 1257 (1978).

144. L.D.Thomas III, M.J.Kelley and N.M.Amer, Appl.Phys.Lett. 32 736 (1978).
145. E.Nodov, Appl.Opt. 17 1110 (1978).
146. N.Ioli, P.Violino and M.Meucci, J.Phys.E 12 168 (1979).
147. N.C.Fernelius and T.W.Haas, Appl.Opt. 17 3348 (1978).
148. N.C.Fernelius, Appl.Opt. 18 1784 (1979).
149. R.S.Quimby, P.M.Selzer and W.M.Yen, Appl.Opt. 16 2630 (1977).
150. L.C.Aamodt and J.C.Murphy, J.Appl.Phys. 48 3502 (1977).
151. P.A.Bechthold, M.Campagna and J.Chatzipetros, Opt.Comm. 36 369 (1981).
152. T.F.Deaton, D.A.Dapatie and T.W.Walker, Appl.Phys.Lett. 26 300 (1975).
153. G.M.Sessler and J.E.West, J.Acoust.Soc.Amer. 53 1589 (1973).
154. C.K.N.Patel and A.C.Tam, Appl.Phys.Lett. 34 467 (1979).
155. C.L.Sam and M.L.Shand, Opt.Comm. 31 174 (1979).
156. M.L.Meade, Lock-in Amplifiers: Principles and Applications (Peter Peregrinus Ltd., London, 1983).

157. D.Cahen, E.I.Lerner and A.Auerback, Rev.Sci.Instrum. **49** 1206 (1978).
158. K.N.Madhusoodanan, M.R.Thomas and J.Philip, J.Appl.Phys. **62** 1162 (1987).
159. D.Adler, Sci.Amer. **236** 36 (1977).
160. S.R.Ovshinsky, in Physical Properties of Amorphous Materials, ed: D.Adler, B.B.Schwartz and M.C.Steele (Plenum Press, New York, 1985) p.105.
161. A.E.Owen, A.P.Firth and P.J.S.Ewen, Phil.Mag.B **52** 347 (1985).
162. R.Azoulay, H.Thibierge and A.Brenac, J.Non-Cryst.Solids, **18** 33 (1975).
163. M.Bensoussan, Rev.Phys.Appl. **12** 753 (1977).
164. R.Ota, T.Yamate, N.Soga and M.Kunugi, J.Non-Cryst.Solids **29** 67 (1978).
165. A.Deneuville, J.P.Kerade, P.Gerrard and A.Mini, Solid State Commun. **17** 109 (1979).
166. S.Asokan, G.Parthasarathy and E.S.R.Gopal, J.Non-Cryst. Solids **86** 48 (1986).
167. A.Feltz, H.Aust and A.Blayer, J.Non-Cryst. Solids **55** 179 (1983).

168. R.W.Johnson, S.Susman, J.McMillan and K.J.Volin, Mater. Res.Bull. 21 41 (1986).
169. W.Bresser, P.Boolchand and P.Suranyi, Phys.Rev.Lett. 56 2493 (1986).
170. K.Murase, K.Yakushiji and T.Fukunaga, J.Non-Cryst.Solids, 59-60 855 (1983).
171. V.A.Vassilyev, K.Koos and I.K.Somogyi, Phil.Mag.B 39 333 (1979).
172. K.E.Peterson, U.Birkholtz and D.Adler, Phys.Rev.B 8 1453 (1973).
173. J.C.Phillips, J.Non-Cryst.Solids 34 153 (1979).
174. A.K.Bhatnagar and S.V.Subrahmanyam, Solid State Commun. 42 81 (1982).
175. Y.Yamasaki, Phil.Mag.B 56 79 (1987).
176. K.Nagata, Y.Miyamoto, H.Nishimura, H.Suzuki and S.Yamasaki, Jpn.J.Appl.Phys. 24 L858 (1985).
177. M.Kitamura, T.Ogawa and T.Arai, J.Non-Cryst.Solids 59-60 Pt.2 917 (1983).
178. S.K.Bahl and K.L.Chopra, J.Appl.Phys. 40 4940 (1969); J.Appl.Phys. 41 2196 (1970).

179. A.F.Ioffe, *Bull.Acad.Sci. USSR* **15** 477 (1951).
180. J.C.Phillips, *Rev.Mod.Phys.* **49** 317 (1970).
181. J.C.Phillips, *Bonds and Bands in Semiconductors* (Academic Press, New York, 1973).
182. M.Kastner, *Phys.Rev.B* **7** 5237 (1973).
183. M.Nunoshita and H.Arai, *Solid State Commun.* **11** 213 (1972).
184. A.Feltz, H.J.Buttner, F.J.Lippmann and W.Maul, *J.Non-Cryst.Solids* **8-10** 64 (1972).
185. J.P.DeNeufville and H.K.Rockstad, in *Amorphous and Liquid Semiconductors*, ed: J.Stuke and W.Brenig (Taylor and Francis Ltd., London, 1974) p.419.
186. M.Kastner, *Phys.Rev.Lett.* **28** 355 (1972).
187. D.W.Bullet, *Phys.Rev.B* **14** 1683 (1976).
188. F.Betts, A.Bienenstock and S.R.Ovshinsky, *J.Non-Cryst. Solids* **4** 554 (1970).
189. G.Lucovsky, F.L.Galeener, R.H.Geils and R.C.Keezer, in *The Structure of Non-Crystalline Materials*, ed: P.H.Gaskell (Taylor and Francis, London, 1977) p.12.

190. G.Lucovsky and G.M.Hayes, in *Amorphous Semiconductors*, ed: M.H.Brodsky (Springer-Verlag, Berlin, 1979) p.215.
191. R.T.Sanderson, *Chemical Bonds and Bond Energy* (Academic Press, New York, 1971).
192. H.Fritzsche, in *Fundamental Physics of Amorphous Semiconductors*, ed: F.Yonezawa (Springer-Verlag, Berlin, 1981) p.1.
193. L.Brewer, in *Electronic Structure and Alloy Chemistry of Transition Elements*, ed: P.A.Beek (Interscience, New York, 1963) p.222.
194. M.Lannoo and M.Bensoussan, *Phys.Rev.B* **16** 3546 (1977).
195. P.M.Bridenbaugh, G.P.Espinosa, J.E.Griffiths, J.C. Phillips and J.P.Remeika, *Phys.Rev.B* **20** 4140 (1979).
196. J.C.Phillips, *J.Non-Cryst.Solids* **43** 37 (1981).
197. P. Tronc, M.Bensoussan, A.Brenac and C.Sebenne, *Phys. Rev.B* **8** 5947 (1973).
198. S.Sugai, *Phys.Rev.B* **35** 1345 (1987).
199. R.J.Nemanich, S.A.Solin and G.Lucovsky, *Solid State Commun.* **27** 273 (1977).

200. P.H.Puoss, P.Eisenberger, W.K.Warbuston and A.Bienenstock, Phys.Rev.Lett. **46** 1537 (1981).
201. W.J.Bresser, P.Boolchand, P.Suranyi and J.D.DeNeufville, Phys.Rev.Lett. **46** 1689 (1981).
202. M.Stevens, P.Boolchand and J.G.Hernandez, Phys.Rev.B **37** 981 (1985).
203. G.Pfister, J.Elect.Mat. **8** 789 (1979).
204. E.A.Marseglia and E.A.Davis, J.Non-Cryst.Solids **50** 13 (1982).
205. R.J.Nemanich, G.A.N.Connell, T.M.Hayes and R.A.Street, Phys.Rev.B **18** 6900 (1978).
206. R.A.Street, R.J.Nemanich and G.A.N.Connell, Phys.Rev.B **18** 6915 (1978).
207. G.Lucovsky, R.H.Geils and R.C.Keezer, in The Physics of Non-Crystalline Solids, ed: G.H.Firschat (Trans Tech, Switzerland, 1977) p.299.
208. C.H.Hurst and E.A.Davis, Presented at the Int.Conf. on Amorphous and Liquid Semiconductors, Garmisch, September 1973.
209. A.A.Vaipolin and E.N.P.Koshits, Sov.Phys.Solid State **5** 186 (1963).

210. A.L.Renninger and B.C.Auerbach, *Phys.Rev.B* **8** 1507 (1973).
211. M.B.Myers and E.J.Felty, *Mater Res.Bull.* **2** 535 (1967).
212. J.C.Phillips, *Phys. Today* **35** 27 (1982).
213. R.M.White, *J.Non-Cryst.Solids* **16** 387 (1974).
214. J.C.Phillips, C.A.Beevers and S.E.B.Gould, *Phys.Rev.B* **21** 5724 (1980).
215. R.P.Tye, *Thermal Conductivity* (Academic Press, New York), Vols.1 and 2.
216. A.J.Angström, *Phil.Mag.* **26** 161 (1863).
217. R.W.King, *Phys.Rev.* **6** 437 (1915).
218. B.Abeles, G.D.Cody and D.S.J.Beers, *J.Appl.Phys.* **31** 1585 (1960).
219. Y.S.Touloukian, P.W.Powell, C.Y.Ho and M.C.Nicolasu, *Thermal Diffusivity* (IFI/Plenum Press, New York, 1973).
220. J.H.Becker, *J.Appl.Phys.* **31** 612 (1960).
221. P.W.Davis, A.B.Timberlake and T.S.Shilliday, *J.Appl. Phys.* **33** 765 (1962).
222. M.J.Adams and G.F.Kirkbright, *Analyst* **102** 678 (1977).

223. P.Charpentier, F.Lepoutre and L.Bertrand, *J.Appl.Phys.* **53** 608 (1982).
224. K.Yamashita, H.Kasahara, K.Yamamoto and K.Abe, *Jpn.J. Appl.Phys.* **21** Suppl.21-3 107 (1982).
225. U.Zammit, M.Marinelli, F.Scudieri and S.Martellucci, *High Temp.- High Pressures* **18** 551 (1986).
226. C.C.Cesar, H.Vargas, J.M.Filho and L.C.M.Miranda, *Appl. Phys.Lett.* **43** 551 (1983).
227. R.T.Swimm, *Appl.Phys.Lett.* **42** 955 (1983).
228. A.Lachaine and P.Poulet, *Appl.Phys.Lett.* **45** 953 (1984).
229. A.Lachaine, *J.Appl.Phys.* **57** 5075 (1985).
230. F.A.McDonald, *Appl.Phys.Lett.* **36** 123 (1980).
231. C.A.Bennett Jr. and R.R.Patty, *Appl.Opt.* **21** 49 (1982).
232. R.Zallen, in *Percolation Structure and Processes*, ed: G.Deutscher, R.Zallen and J.Adler, *Annals of the Israel Physical Society*, Vol.5 (Hilger, Bristol, 1983) p.3.
233. S.Feng and P.N.Sen, *Phys.Rev.Lett.* **52** 216 (1984).
234. Y.Kantor and I.Webman, *Phys.Rev.Lett.* **52** 189 (1984).
235. S.Feng, M.F.Thorpe and E.Garboczi, *Phys.Rev.B* **31** 276 (1985).

236. J.C.Phillips, Phys.Rev.B 31 8157 (1985).
237. M.Sahimi and J.D.Goddard, Phys.Rev.B 32 1869 (1985).
238. L.M.Schwartz, S.Feng, M.F.Thorpe and P.N.Sen, Phys.Rev.B 32 4607 (1985).
239. S.Kirkpatric, Rev.Mod.Phys. 45 574 (1973).
240. J.C.Phillips, Phys.Stat.Solidi B 101 473 (1980).
241. M.F.Thorpe, J.Non-Cryst.Solids 37 355 (1983).
242. J.C.Phillips and M.F.Thorpe, Solid State Commun. 53 699 (1985).
243. K.S.Gilroy and W.A.Phillips, Phil.Mag.B 47 655 (1983).
244. K.Murase, T.Fukunaga, K.Yakushiji, T.Yoshimi and I.Yunoki, J.Non-Cryst.Solids 59-60 885 (1983).
245. K.Murase and T.Fukunaga, in Optical Effects in Amorphous Semiconductors, ed: P.C.Taylor and S.G.Bishop (AIP, New York, 1984) p.449.
246. P.Chaudhuri, P.Beardmore and M.B.Bever, Phys.Chem.Glasses 7 157 (1966).
247. R.Blachnik and A.Hoppe, J.Non-Cryst.Solids 34 191 (1979).

248. S. Feng, B.I.Halperin and C.J.Lob, Phys.Rev.B 30 5386 (1984).
249. D.Bergman, Y.Kantor and I.Webman, Phys.Rev.Lett. 52 1891 (1984).
250. J.A.Aronovitz, J.R.Banavar, M.A.Marcus and J.C.Phillips, Phys.Rev.B 28 4454 (1983).
251. P.S.Bechthold, M.Campagna and T.Schober, Solid State Commun. 36 225 (1980).
252. J.Etxebarria, S.Uriarte, J.Fernandez, M.J.Tello and A.G.Cuevas, J.Phys.C 17 6601 (1984).
253. P.Korpiun and R.Tilgner, J.Appl.Phys. 51 6115 (1980).
254. J.T.Edmond, Br.J.Appl.Phys. 17 979 (1966).